The Early to Late Ordovician rock record of the Oppdal area, Scandinavian Caledonides: Explosive volcanism, element recycling and basin infill during closure of the Iapetus Ocean

Bjørgunn Heggem Dalslåen

Department of Geosciences

Faculty of Mathematics and Natural Sciences

University of Oslo

Dissertation for the degree of Philosophiae Doctor (PhD)

Series of dissertations submitted to the
Faculty of Mathematics and Natural Sciences, University of Oslo
No. 2458

ISSN 1501-7710

Cover: Hanne Baadsgaard Utigard.
Print production: Reprosentralen, University of Oslo.

“Mountains seem to answer an increasing imaginative need in the West. More and more people are discovering a desire for them, and a powerful solace in them. At bottom, mountains, like all wildernesses, challenge our complacent conviction - so easy to lapse into - that the world has been made for humans by humans. Most of us exist for most of the time in worlds which are humanly arranged, themed and controlled. One forgets that there are environments which do not respond to the flick of a switch or the twist of a dial, and which have their own rhythms and orders of existence. Mountains correct this amnesia. By speaking of greater forces than we can possibly invoke, and by confronting us with greater spans of time than we can possibly envisage, mountains refute our excessive trust in the man-made. They pose profound questions about our durability and the importance of our schemes. They induce, I suppose, a modesty in us.”

Robert MacFarlane, Mountains of the Mind: Adventures in Reaching the Summit

Preface

In agreement with the dissertation requirements for the degree of Philosophiae Doctor, this thesis was submitted to the Faculty of Mathematics and Natural Sciences at the University of Oslo. The project was mainly funded by the Department of Geosciences, UiO, with support for fieldwork and geochemical analyses from the Geological Survey of Norway (NGU). The candidate was enrolled as a PhD research fellow at the Department of Geosciences from September 2013 to June 2019 under the supervision of Professor Arild Andresen (UiO), Deta Gasser (NGU, HVL) and Tor Grenne (NGU). One year was assigned for duty work, mainly as teaching a BSc level course in interpretation and making of geological maps, followed by a field course. The candidate was teaching this course for three semesters.

The thesis presented herein aims to shed light on the Cambrian to Silurian evolution of the southern part of the Trondheim Nappe Complex, a little studied and understood part of the central Norwegian Caledonides, through mapping, geochronology and geochemistry. Fieldwork was carried out over three field seasons (2014, 2015 and 2017) and an area of approximately 600 km^2 was covered, with more than 2500 localities visited. This thesis consists of an introduction, three papers, and a brief synthesis. In addition a folded map that shows the geology of the study area in detail, with all the sample localities, is enclosed inside the back cover. This larger scale map makes it easier to follow the descriptions and discussions in this volume, and to understand relationships between the various components.

All papers are a result of collaboration between the co-authors. The papers focus on three different rock units within the area, and are presented in the order they were written:

Dalslåen, B.H., Gasser, D., Grenne, T., Augland, L.E. and Corfu, F., 2020. **Ordovician shoshonitic to ultrapotassic volcanism in the central Norwegian Caledonides: The result of sediment subduction, mantle metasomatism and mantle partial melting.** Lithos, 356. https://doi.org/10.1016/j.lithos.2020.105372

Dalslåen, B.H., Gasser, D., Grenne, T., Augland, L.E. and Andresen, A., 2020. **Early to Middle Ordovician sedimentation and bimodal volcanism at the margin of Iapetus: The Trollhøtta–Kinna basin of the Central Norwegian Caledonides.** *In*: Murphy, J.B., Strachan, R. & Quesada, C. (eds) *Pannotia to Pangaea: Neoproterozoic and Paleozoic Orogenic Cycles in the Circum-Atlantic Region.* Geological Society, London, Special Publications, 503. https://doi.org/10.1144/SP503-2020-37

Dalslåen, B.H., Gasser, D., Grenne, T., Ganerød, M. and Andresen, A. **The Skuggliberga unit of the Oppdal area, central Scandinavian Caledonides: calc-alkaline andesitic pyroclastic volcanism in a fluvial to shallow marine basin following mid-Ordovician tectonism.** Accepted for publication in Norwegian Journal of Geology.

Acknowledgements

First, I would like to thank my supervisors, Deta Gasser, Tor Grenne and Arild Andresen for their guidance, advice, support and patience during my PhD. I would also like to thank Lars Eivind Augland and Fernando Corfu for their contribution to TIMS zircon dating and their helpful and interesting discussions. Discussions with Tom Andersen and Johan Petter Nystuen have also been of great value. I am grateful for the help from Magnus Kristoffersen, Siri Simonsen, Gunborg Fjeld Bye, Salah Akhavan and Muriel Erambert at the University of Oslo (UiO) for their assistance with LA-ICPMS, SEM, mineral separation, thin section preparation and microprobe analysis. Morgan Ganerød at the Norwegian Geological Survey (NGU) is thanked for performing the Ar-Ar biotite dating, and the lab staff at NGU (Torkil S. Røhr, Jasmin Schönenberger, Ann Elisabeth Karlsen and Øyvind Skår) for the geochemical analyses. I would also like to thank office mates, fellow PhD students and colleagues at UiO for their company, and Ella W. Stokke for her assistance and company in the field. A big thank you goes to the University of Oslo for funding my PhD position, TIMS and LA-ICPMS analyses, and to NGU for funding field work and geochemical analyses.

I would like to thank family and friends for joining me on the longest hikes in the remote parts of my field area and for (more or less) volunteering to help carry rock samples, and my mother for the accommodation during fieldwork. A special thank you to my husband for his financial support after I reached the end of the university funding. My son is thanked for giving the best hugs.

It has been a great privilege to do this PhD work in an area that means a lot to me. This is where my family has its roots, and my interest in geology started in these mountains. A big thank you to my mother and late father who let me collect all the rocks I wanted, and always encouraged my curiosity.

Gråurdfjellet, Oppdal, 1992

Table of Contents

Abstract 1

1. Introduction 3

1.1 Subduction zone processes 4

1.2 Geological framework of the Caledonide Orogen 11

1.3 The geology of the central Scandinavian Caledonides 14

2 Objectives of the project 19

3 Approach and methods 20

4 Summary of results 21

4.1 Paper I 21

4.2 Paper II 22

4.3 Paper III 23

4.4 Results not published elsewhere: The transition to the Gula Nappe 25

5 Synthesis 29

5.1 Key findings 29

5.2 The evolution of the Cambrian – Silurian units preserved in the Oppdal area 31

5.3 Relation to similarly aged rocks in the Caledonian-Appalachian system 33

5.4 Extremely enriched magmatism along the Iapetus margin 35

5.5 A note on the use of detrital zircon ages and maximum depositional age 36

6 Concluding remarks and recommendations for future research 37

7 Other contributions 39

7.1 Co-author papers 39

7.2 Conference proceedings 39

7.3 Public outreach 39

8 References 41

Paper I I

Paper II II

Paper III III

Supplementary material A: Stokke et al., 2018 IV

Supplementary material B: Detrital zircon data from the Trollhøtta unit (Paper II) V

Supplementary material C: Detrital zircon data from the Skuggliberga unit (Paper III) VI

Supplementary material D: Detrital zircon data not published elsewhere VII

Abstract

Continent–continent collision zones form when oceanic basins close. Studying the remnants of oceanic crust, island arcs, and the associated sedimentary cover successions trapped and preserved in collision zones allows us to better reconstruct and understand the processes that are active during closure of an ocean. The Scandinavian Caledonides record the closure of the Iapetus Ocean, where the Silurian continental collision between Laurentia, Baltica and Avalonia led to formation of a Himalaya-scale mountain range, and included stacking large thrust sheets upon the Baltican basement. Units derived from within the Iapetus Ocean are preserved in the upper part of the nappe stack along large parts of the orogen. This thesis focuses on the Iapetus-related units preserved in the Oppdal area, central Norwegian Caledonides. This area has not previously been studied in detail, earlier work is related to a 1:250 000 bedrock map sheet (Nilsen and Wolff, 1989) and local studies focussing on a large intrusion in the area.

My co-authors and I have investigated peculiar, highly enriched volcanic rocks (Paper I), an extensional volcano-sedimentary basin (Paper II) and a basin with sedimentary and volcanic rocks which lies unconformably on the other units (Paper III). The 474–470 Ma volcanic rocks of the Kinna and Storgruvpiken units in Paper I have a very unusual chemical composition; they are Mg- and Cr-rich which indicates that they are mantle derived, but are also extremely enriched in elements such as K, Th and U; elements that usually are associated with a source in the continental crust. By analogy with geochemically similar volcanic rocks from younger orogenic belts we interpret these rocks as the result of partial melting of a mantle source metasomatised by crustal-derived material, possibly as a result of subduction of continentally-derived material during obduction of the Løkken–Vassfjellet–Bymarka ophiolite.

In Paper II we describe the Trollhøtta basin, an extensional basin with MORB-like metabasaltic rocks and deep marine sediments and minor highly enriched volcanic rocks, which formed at c. 475–470 Ma. This unit is probably a southward continuation of the Støren metabasalts in the classic Trondheim region, and interfingers with the Kinna volcanic succession to the south.

Paper III focuses on a newly defined late Ordovician unit, the Skuggliberga unit, which rests unconformably on the Trollhøtta and Skarvatnet units. This unit has previously been mapped as a greywacke. We show that it consists of sandstone and an andesitic calc-alkaline, arc-related volcanic deposit. Detrital zircon data suggest that the sandstone-dominated lower part of the Skuggliberga unit was probably deposited around 460–445 Ma, and was then overlain by the Skuggliberga volcanic rocks, and later intruded by the Innset massif at c. 435 Ma. Such late Ordovician, arc-related volcanic rocks are rare elsewhere in the Scandinavian Caledonides. We

also provide an Ar-Ar biotite age of 416 Ma for the metamorphism in the area, a metamorphic event which is likely to have affected the detrital zircon ages.

Our results give a previously unknown detailed reconstruction of the formation of a 475–470 Ma basin with mid-ocean ridge basalts (MORB) and extremely enriched volcanism, represented by a unique tectono-magmatic-sedimentary phase along the Caledonian orogen, a subsequent accretion phase, followed by a regional-scale unconformity and new deposition combined with arc-related volcanism.

1. Introduction

In 1966, Tuzo Wilson published a paper where he suggested that the Atlantic Ocean closed and re-opened. This idea of how continents rift apart and become separated by oceans, followed by subduction and continent collision is known as a Wilson cycle. Although this model must be regarded as conceptual, it is a useful introduction to how oceans and continents evolve through time. When the continental crust extends and thins, this produces accommodation space for deposition of sediments, and the decrease in pressure exerted on the mantle by the continental crust can cause decompression melting of the asthenospheric mantle. Extended continental margins, also known as passive margins, are therefore commonly associated with thick sedimentary successions often intruded by mafic rocks (e.g. Jakob et al., 2019; Kjøll et al., 2019).

If the continental crust is even more stretched, the mantle rocks might be exposed and juxtaposed with sedimentary rocks (Andersen et al., 2012). During extension, fragments of the continental crust are often rifted off and become separate microcontinents. Finally, extension can develop into active spreading and the formation of oceanic crust. Subduction and destruction of the oceanic crust can be initiated in a variety of settings, either spontaneously, for instance along zones of crustal weakness where the lateral buoyancy contrast is large, or induced by changes in plate motion (e.g. Stern and Gerya, 2018). Arc and back-arc related rocks form above the subduction zones; these rocks are generally too buoyant to subduct into the denser mantle, and can be obducted or accreted to continental crust. Subduction can eventually lead to continent–continent collision, which is characterised by large-scale stacking of thrust sheets, high-pressure metamorphism, and mountain building. Both the extended, passive margins and the areas above subduction zones are very complex, and to reconstruct the history of events within a closing ocean is not a straightforward task.

Different rock types are commonly associated with specific tectonic settings, for instance igneous rocks that are formed above subduction zones are commonly calc-alkaline with an intermediate to high content of silica, in contrast to the commonly low silica content of rocks that have formed at ocean spreading centres. Thus, the geochemical signature (especially the trace elements) can be used to infer the conditions under which the rocks formed, and the metamorphic and structural overprint combined with age constraints give us clues to the history of the rocks and the evolution of an area**.** Since the oceanic crust commonly is subducted and consumed when oceans close, the history of the large, lost oceans can mainly be assessed by studying the preserved remnants of the oceanic-derived rocks; namely the supra-subduction zone arc and back-arc complexes which are accreted or obducted onto continental crust and become part of the continents.

The rock record in the Scandinavian Caledonides contains the remnants of a large, lost oceanic basin: the Iapetus Ocean. Rocks formed within this oceanic basin are a major constituent of the Köli Nappe Complex and correlated units, which can be found along much of the orogen. The Köli Nappe Complex is part of a sequence of allochthonous nappes that was thrust eastward over Baltica during the Caledonian orogeny, an early Silurian (c. 430–400 Ma) event of continent–continent collision and Himalaya-scale mountain building (e.g. Roberts and Gee, 1985; Corfu et al., 2014). The main collisional phase of the Caledonian orogeny was preceded by the Late Cambrian to early Silurian subduction and closure of the Iapetus ocean; a process which included several events of subduction initiation, island arc/back-arc formation and obduction within the narrowing Iapetus ocean. Although the general narrative of this Cambrian–Silurian period of Iapetus closure is widely accepted, many details of the complex and at least 60 myr long series of accretionary events are unknown. In particular, many Cambrian–Silurian volcano-sedimentary units have unknown eruptive and/or depositional age and poorly resolved geological history. This thesis reports field observations, and geochemical and geochronological data, from the Oppdal area of central Norway, where such units are preserved. Here an Early–Middle Ordovician (c. 480–470 Ma) volcano-sedimentary basin with a highly unusual bimodal volcanism, with combined mid-ocean ridge basalt (MORB) and basaltic to rhyolitic rocks with an extreme enrichment in elements like U, Th, Pb, K and LREE is preserved. Such elements are commonly associated with a crustal source, but the rocks also have a high content of the mantle-derived elements Mg, Cr and Ni. Analogy with younger rocks with similar geochemical traits (e.g. Foley, 1992; Peccerillo, 1999; Conticelli et al., 2009; Förster et al., 2017) suggests a mantle source previously metasomatised by crustal material transferred from a subducted slab. These peculiar rocks are unconformably overlain by Late Ordovician–Early Silurian sandstone, and andesitic volcanic rocks with a typical arc signature.

1.1 Subduction zone processes

In the late 60s and early 70s at the dawn of the discovery of plate tectonics**,** the spatial relationship between subduction zones, volcanic arcs and typical rocks for this setting (trondhjemite, tonalite, granodiorite (the TTG-suite) and andesite, dacite and rhyolite) was established, but the processes responsible for generating such rock types were not fully understood (e.g. Dickinson, 1970; Kushiro, 1973). Some workers suggested that the subducted, basaltic oceanic crust was subject to partial melting, where the slab-derived melts could to some extent react with the overlying mantle (Green and Ringwood, 1968; Wyllie and Sekine, 1982). However, the subducted slabs were considered too cold to melt under normal thermal gradients (e.g. Peacock, 1996), but melting of young and hot slabs was considered a feasible mechanism (Defant and Drummond, 1990). The other suggested mechanism for arc magma generation was that the slab dehydration process transfers volatiles to the mantle wedge, which lowers the

melting point of the mantle rocks and leads to partial melting (Kushiro, 1973; Tatsumi, 1989) This is an important mechanism, but the processes involved are much more complex. What kinds of fluids are transferred? What is their composition? What happens to the subducted sediments? What are the stability fields of minerals that control the element budget, especially the trace element rich accessory minerals? In a broad sense, the subduction system can be considered a reaction zone with large differences in chemical and physical properties between the slab and the mantle wedge.

Subduction zones can be regarded as "conveyor belts" where eroded continental material is recycled back into the mantle, but subduction zones are also the locus of crustal growth through geological time, by subduction related volcanism and accretion of island arcs (e.g. Reymer and Schubert, 1984; Draut et al., 2009). The global magma production in arcs is between 2.5 and 3.5 km^3 per year, approximately the same as the volume of material recycled back into the mantle (Clift et al., 2009). Subduction zone processes are crucial for both crust forming events and the chemical evolution of the mantle. Supra-subduction zone magmas cover the whole range from basalt to rhyolite. Broadly speaking, basalts are formed in the back-arc region (also known as marginal basin), while the basaltic, andesitic and rhyolitic magma are characteristic for the arc region. Supra-subduction zone magmas are commonly hydrous, oversaturated in silica, are subalkaline, and belong to the volumetrically most important calc-alkaline or tholeiitic series, together with the less common boninitic and shoshonitic series, whereas the calc-alkaline magmas are generally restricted to subduction zones. Magmas can also be subdivided into low-K (often tholeiitic), intermediate-K and high-K magmas (commonly calc-alkaline), and shoshonitic rocks which are even more enriched in K and other incompatible elements (e.g. Stern, 2002).

Despite the great variation, subduction-related magmatism has some common features, which are evident if one compares arc magma to mid-ocean ridge basalt (MORB). In a MORB-normalised multi-element diagram (Fig. 1A), the MORB obviously has a flat pattern, but MORB formed from mantle sources that previously have undergone partial melting are commonly depleted in the most incompatible elements, the Large Ion Lithophile Elements (LILE; e.g. Gale et al., 2013). Arc rocks are enriched in the LILEs, but are quite depleted in High Field Strength Elements (HFSE) and consequently have a high LILE/HFSE ratio (Fig. 1A). LILE are fluid-mobile, and the LILE-enrichment in arc magmas indicates that volatiles are involved in the transport of elements from the slab to the mantle. In chondrite-normalised multi-element plots MORB has a relative depletion in the LREE, and a flat HREE-pattern (Fig. 1B). Arc rocks are enriched in LREE, they have a flat HREE pattern (Fig. 1B), or negative slope among the HREE if garnet is present in the residual. In general, arc rocks have a relative enrichment in incompatible and/or fluid mobile elements like LREE, LILE, and other elements like U and Pb compared to other mantle melts

(Hawkesworth et al., 1993). The negative Nb-Ta anomaly is also a characteristic feature of subduction-related magma, and is caused by residual rutile which holds Nb and Ta back from entering the melt (e.g. Hermann and Rubatto, 2009).

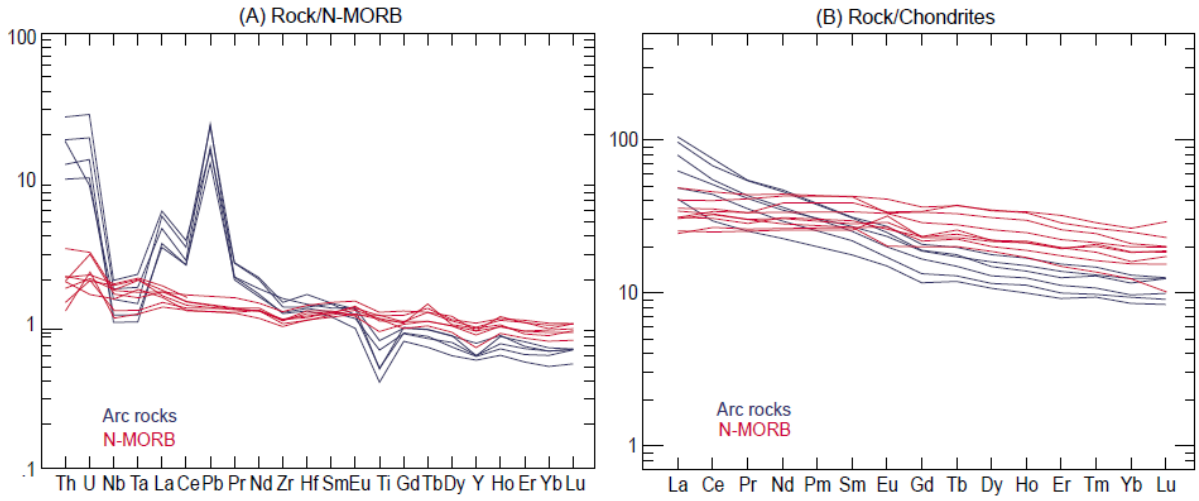

Fig. 1: Examples of typical trace element signatures of arc rocks (blue) and MORB (red). The data are from Papers II and III. **(A)** Data normalised to MORB values of Gale et al. (2013). **(B)** Data normalised to chondrite (Sun and McDonough, 1989).

The subduction zone input is mainly oceanic crust and lithosphere, sediments and volatiles, and more rarely continental crust. The oceanic crust is hydrothermally altered, particularly in the upper part (c. 500 m), and enriched in volatiles (H_2O, CO_2, Cl, S), and trace elements like K, Rb, Cs, U, Pb, Sr, As and B (e.g. Spandler and Pirard, 2013). During subduction the oceanic crust and overlying sediments undergo greenschist or blueschist, and eventually eclogite facies metamorphism. The upper part of the lithospheric mantle can be partly serpentinised and enriched in H_2O, halogens, Li, B, As, and Sb (e.g. Spandler and Pirard, 2013). Arc lavas have isotopic and trace element compositions that require input from fluids derived from serpentinised mantle, such as a high proportion of the heavy ^{11}B isotope. Hydrous minerals in serpentinites like white mica and talc can be stable to sub-arc depths in the mantle, and serpentinites can cycle volatiles into the deep mantle (Tatsumi, 1989).

Subducted sediment is also an important contributor to the chemical composition of arc magmas. The composition of the global subducting sediment (GLOSS) is comparable to the chemical signature of the continental crust, and is estimated to consist of 17% biogenic material (carbonate and biogenic silica), 76% terrigeneous sediments; the rest is mineral-bound H_2O (Plank and Langmuir, 1998). Pelitic and turbiditic sediments dominate and are enriched in LILE, Li, B, Pb, C, N and Sr, and are an important carrier of H_2O as pore fluid and in hydrous minerals.

One of the best evidences of sediment contribution to arc magmas comes from ^{10}Be isotopes in young volcanic rocks. ^{10}Be is a cosmogenic isotope with a half-life of approximately 1.5 Ma, which does not exist naturally in the mantle. In their classic paper Tera et al. (1986) showed that many subduction related magmas have substantially higher concentrations of ^{10}Be than are found in MORB and OIB, and that the concentration is higher in arcs where a large proportion of the subducted sediment is young. The occurrence of ^{10}Be in arc lava demonstrates that the cycle of deposition, subduction, transfer to the mantle and volcanic activity must happen within 10 million years to be detectable. More evidence of sediment contribution comes from the Rb/Sr and Sm/Nd isotope systems (e.g. Faure and Mensing, 2005): Radiogenic ^{87}Sr forms by β+ decay of ^{87}Rb. Rb is enriched relative to Sr in the melt, and consequently is the parent of ^{87}Sr that is concentrated in the crust while stable ^{86}Sr is retained in the mantle. Over time this increases the ^{87}Sr/^{86}Sr ratio of crustal rocks. The Sm/Nd system works in the opposite direction; ^{143}Nd forms by α-decay of ^{147}Sm, and since Sm is more compatible than Nd, the mantle is enriched in the parent isotope, but depleted in the daughter isotope, over time increasing the ^{143}Nd/^{144}Nd ratio. The crust and mantle therefore evolve toward different isotopic signatures, and a crustal signature in arc magmas indicates involvement of subducted sediments.

Fluids are an essential component in metamorphic and metasomatic reactions, transfer of elements, and melting in the mantle. Under the pressures and temperatures that prevail in the subduction zone the term “fluid” includes aqueous fluids, hydrous melts and supercritical liquids; fluid states with different physical and chemical properties (e.g. Hermann and Rubatto, 2009; Spandler and Pirard, 2013). Supercritical liquids can carry high concentrations of LILE, Pb, Th, U, Sr and LREE (Kessel et al., 2005). However, since supercritical liquids only exist over a rather limited Pressure–Temperature–Composition range such liquids are probably incapable of transporting sufficient volumes from subducting slab to overlying mantle wedge (Manning, 2004). High-pressure aqueous fluids are relatively dilute and can hold only 5–15 wt% solute, but are enriched in Si, Al, and alkali elements (Hermann and Rubatto, 2009). Contribution from aqueous fluids alone is insufficient to produce the arc trace element signature, because several elements are retained in phases like phengite, rutile, zircon and allanite/monazite, that do not easily dissolve. Hermann and Rubatto (2009) also point out that increased flux of aqueous fluid will lead to more extensive mantle melting, which will dilute the slab component rather than enrich it. Transport of incompatible elements from the subducting slab into the overlying mantle wedge is more efficient by partial melts (including supercritical fluids), than by aqueous fluids released during dehydration (e.g. Hermann and Rubatto, 2009).

Thermal models and field data from exhumed subduction zones suggest that the slab is mechanically coupled to the convecting mantle, and that flow processes in the mantle wedge

provide influx of hot magma to heat the slab. In a hot slab, melting of water-bearing crustal rocks is possible, particularly in metapelitic rocks which are close to their wet solidus under such conditions (approximately 600 °C at ca 80 km depth; e.g. Syracuse et al., 2010). It is therefore likely that partial melting of subducted material happens, and that melt is an important transport agent from the slab to the overlying mantle wedge. During hydrous melting of the slab, the trace element distribution is controlled by chemical equilibrium with solid phases. According to e.g. Spandler and Pirard (2013), garnet, zoisite and allanite are the most important REE-controlling minerals, zircon runs the Zr and Hf budget, pyroxenes and amphibole control Li and Be and, together with zoisite and allanite, also control Cr and V. Rutile controls Ti, Nb and Ta, and apatite is the main source for P, but also contributes to the LREE and MREE. Phengite and paragonite is important for Rb, Cs, Ba, B, and to a lesser extent Cr, V, Li and Be. The various degrees of involvement of these minerals to supra-subduction zone magmatism is reflected in the large variation found especially in arc magmas, but the slab signature is also common in marginal basin magmas (Pearce and Stern, 2006; Dilek and Furnes, 2011).

Accordingly there is evidence that the subducted slab (particularly the sediments) undergoes partial melting, and that fluids or melt react with the mantle above, but how does transfer to the mantle wedge take place? There are several models: metasomatism of the mantle either by porous flow or concentrated in veins, via metasomatism of subduction zone melange, or melange plumes that partially melt as they rise (Spandler and Pirard, 2013). Melange consists of variously sheared metasediments, fragments of the oceanic crust and partly serpentinised mantle fragments, which form along the subduction interface. Such rocks are known from many (ultra)high-pressure (HP) terranes and represent exhumed fossil subduction zones (Bebout and Penniston-Dorland, 2016), and act as natural laboratories for subduction zone studies.

Melanges might have enough buoyancy to disconnect from the descending slab and rise as a plume through the mantle wedge, as suggested by e.g. Marschall and Schumacher (2012). This melange-plume will also dehydrate, and may thus cause melting of a mantle that is enriched in the fluid-mobile elements; alternatively it may itself partially melt due to the rapid heating, and the melt will leave the plume and react with the mantle (Fig. 2). The plume dehydration model also points to another important aspect; that dehydration reactions that happen at depths shallower than 80–90 km (meaning below the fore-arc region where the mantle is too cold to melt) can still be important, since mantle flow processes can drag the hydrous mantle down to parts of the mantle warm enough to induce melting (Marschall and Schumacher, 2012).

Another model for transport of elements from the slab to the mantle is porous flow (e.g. Manning, 2004), where dehydration of subducted crust and serpentinite provide fluids that can

percolate into the mantle and produce phlogopite by metasomatism (Fig. 3). Mantle flow processes bring material deeper into the mantle where sequential dehydration/mineral forming events transfer the slab components to the mantle before mantle melt with a slab signature is produced. However, if this percolation is slow, the process of transport and melt generation cannot preserve the observed disequilibrium in isotope systems with short lived isotopes.

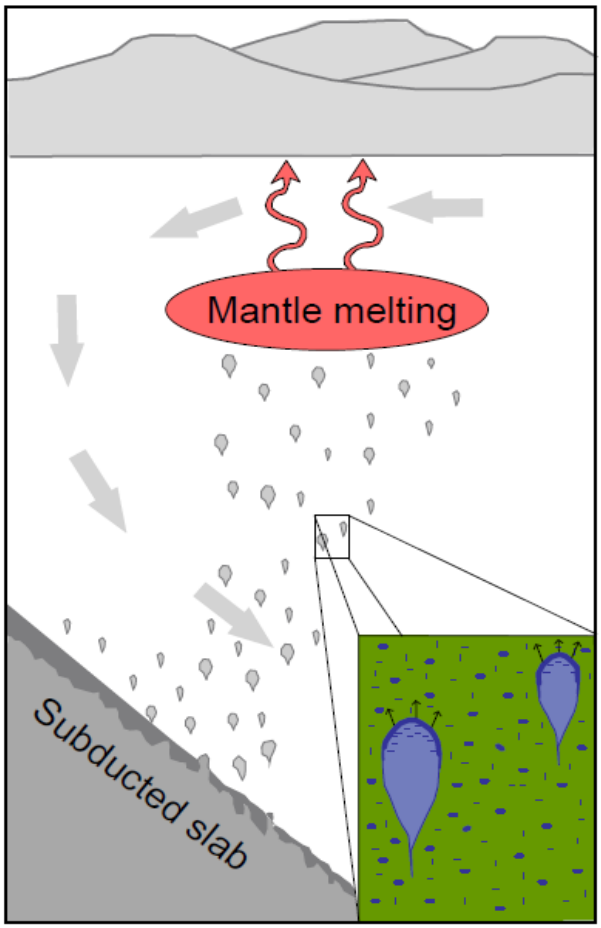

Fig. 2: Schematic model for rise and partial melting of detached melange plumes, redrawn from Spandler and Pirard (2013). The grey arrows represent the direction of asthenospheric flow in the mantle.

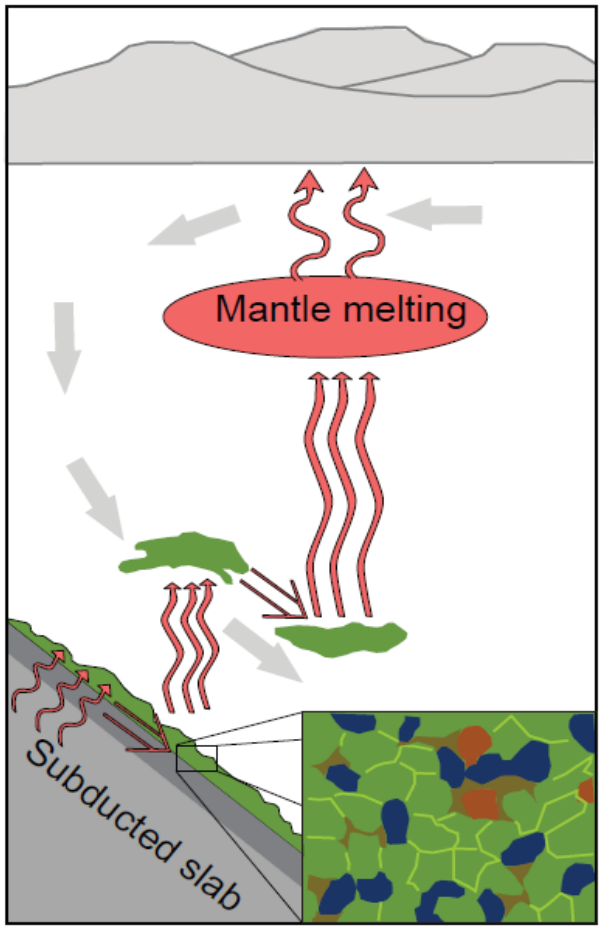

Fig. 3: Schematic model for porous flow, where fluids from the slab percolate into the mantle, where metasomatic reactions produce e.g. phlogopite (brown). Redrawn from Spandler and Pirard (2013). Grey arrows represent the dirction of asthenospheric flow.

Spandler and Pirard (2013) consider the most probable scenarios for generation of slab-derived melts are either melting of the slab top (particularly the sediments) from fluxing fluids from the serpentinised mantle, or *in situ* melange melting along the slab–mantle interface. Focused flow of such potassium-rich melts derived from slabs into the mantle, and subsequent metasomatic reaction with mantle peridotite, can produce networks of altered veins (Fig. 4). This slab to

mantle transport mechanism with formation of incompatible element enriched veins, which probably consist of clinopyroxene and mica (probably phlogopite), was first proposed by Foley (1992).

Melting of such veins together with various amounts of unaltered mantle peridotite can account for the large compositional variation above subduction zones, and for the transfer of the slab component to the overlying mantle and finally to the arc magmas (e.g. Spandler and Pirard, 2013). This mechanism is particularly important during formation of shoshonitic and ultrapotassic rocks. Highly LREE-enriched (ultra)potassic and shohonitic rocks within e.g. the Alpine-Himalayan orogenic belt and the Variscan orogen have received considerable attention and are generally attributed to recycling of subducted continental material, metasomatic reaction with the mantle and partial melting of heterogeneous mantle domains (Conticelli and Peccerillo, 1992; Peccerillo, 1999; Gao et al., 2007; Prelević et al., 2013; Förster et al., 2017; Soder and Romer, 2018). The petrogenesis of this peculiar rock suite requires a line of events; subduction and partial melting of crustal-derived material, a metasomatic reaction with the mantle wedge where the crustal signature is preserved in clinopyroxene- and mica-rich veins, and preferential melting of these altered mantle domains in a setting with some degree of extension. Such anomalous rocks are rare on a global scale and have not previously been described from the Scandinavian Caledonides, but are documented in this thesis.

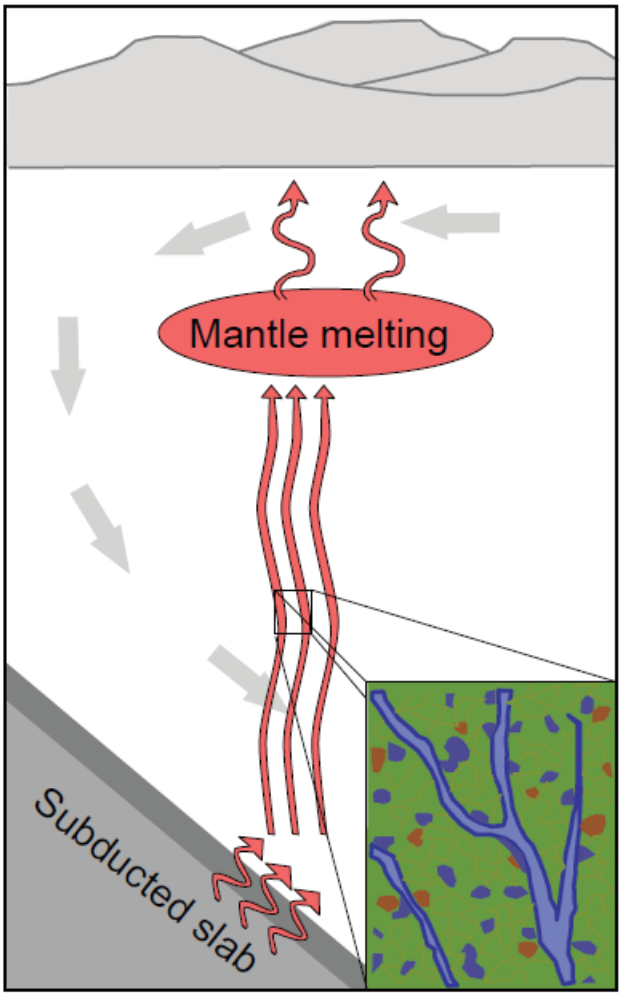

Fig. 4: Focused flow of partial melt (light blue) from the slab which reacts with the mantle peridotite, and form veins with a contact zone dominated by pyroxene and mica (dark blue). These zones are enriched in incompatible elements, a feature reflected in magmas sourced from such veined mantle domains. Grey arrows represent the flow direction in the asthenospheric mantle. Redrawn from Spandler and Pirard (2013).

1.2 Geological framework of the Caledonide Orogen

Roughly 900 million years ago all major continental blocks were amalgamated into one large landmass, the Rodinia supercontinent (e.g. Li et al., 2008). In most reconstructions Laurentia and Baltica were connected at the margins which presently face each other. Extension and rift basin formation started around 850 Ma (Nystuen et al., 2008); the 605-616 Ma dyke swarms preserved in the nappe stack and in the basement of southern Norway are interpreted as marking the break-up between Laurentia and Baltica, and the initial formation of Iapetus oceanic crust (Bingen and Demaiffe, 1999; Kjøll et al., 2019). Convergence between these two continents began in the early Ordovician (e.g. Domeier, 2016) and is recorded in the ophiolite- and arc successions now preserved in Scandinavia, the British Isles and in the Appalachians (Fig. 5A).

The development of subduction systems within the Iapetus Ocean started with subduction in the Taconic Seaway between Laurentia and a microcontinent; closure of this seaway was followed by west-dipping (present co-ordinates) subduction of the Iapetus oceanic crust, several phases of arc magmatism, marginal basin formation and ophiolite obduction along the Laurentian margin (e.g. van Staal et al., 2009). Many of the ophiolite and arc-related successions in the Scandinavian Caledonides were formed in this setting, accreted to the Laurentian margin or associated microcontinents shortly after formation, and later transferred to the Baltic plate during the main, Scandian phase of the Caledonian orogeny. The evolution along the Baltica margin is not well understood, but local ultra-high pressure metamorphic rocks imply early (late Cambrian/Early to Late Ordovician) subduction of the Baltica margin (e.g. Klonowska et al., 2014). Subduction of the Iapetus ocean was also active to the south, under the Gondwana margin, causing back-arc extension and several microcontinents (e.g. East and West Avalonia, Ganderia) to rift off during the latest Cambrian/Early Ordovician, opening the Rheic Ocean (e.g. Domeier, 2016). East Avalonia docked to the present southern margin of Baltica at the end of the Ordovician, an event which marks the closure of the Tornquist Ocean (Fig. 5A; e.g. Domeier, 2016). A phase of mafic and bimodal intrusions aged 438–434 Ma was confined to the tectonic units with an inferred oceanic or Laurentian affinity. Slagstad and Kirkland (2018) suggested that this formed in a continental extension setting in the upper plate during initial contact between Laurentia and Baltica, and thus delineates the Scandian collisional suture zone.

The convergence terminated in the early Silurian (c. 430 Ma) when the amalgamated Baltica and East Avalonia plate finally collided with Laurentia in the Scandian phase of the orogeny, creating a Himalaya-scale mountain chain known as the Caledonides in Europe and the Appalachians in North America (Roberts and Gee, 1985; Labrousse et al., 2010; Corfu et al., 2014). During this collision event, nappes or allochthons were telescoped eastward over Baltica (e.g. Roberts and

Gee, 1985; Corfu et al., 2014), and correlatable tectonic units can be traced along substantial parts of the orogen. The Scandinavian Caledonides have traditionally been separated into Lower, Middle, Upper and Uppermost Allochthons (Fig. 5B); groups of nappes which from the bottom and upwards have inferred origins at increasing distances from Baltica (e.g. Roberts and Gee, 1985). Although the traditional classification has by many been superceded now, and should be avoided (for several reasons as discussed in Corfu et al., 2014), it forms the stratigraphic framework in the classic literature and provides a useful scheme to introduce the geology of the Scandinavian Caledonides. It is therefore used in this introductory chapter but is avoided in the more detailed chapters as well as in the papers. In the following the general units are described from the base and upwards.

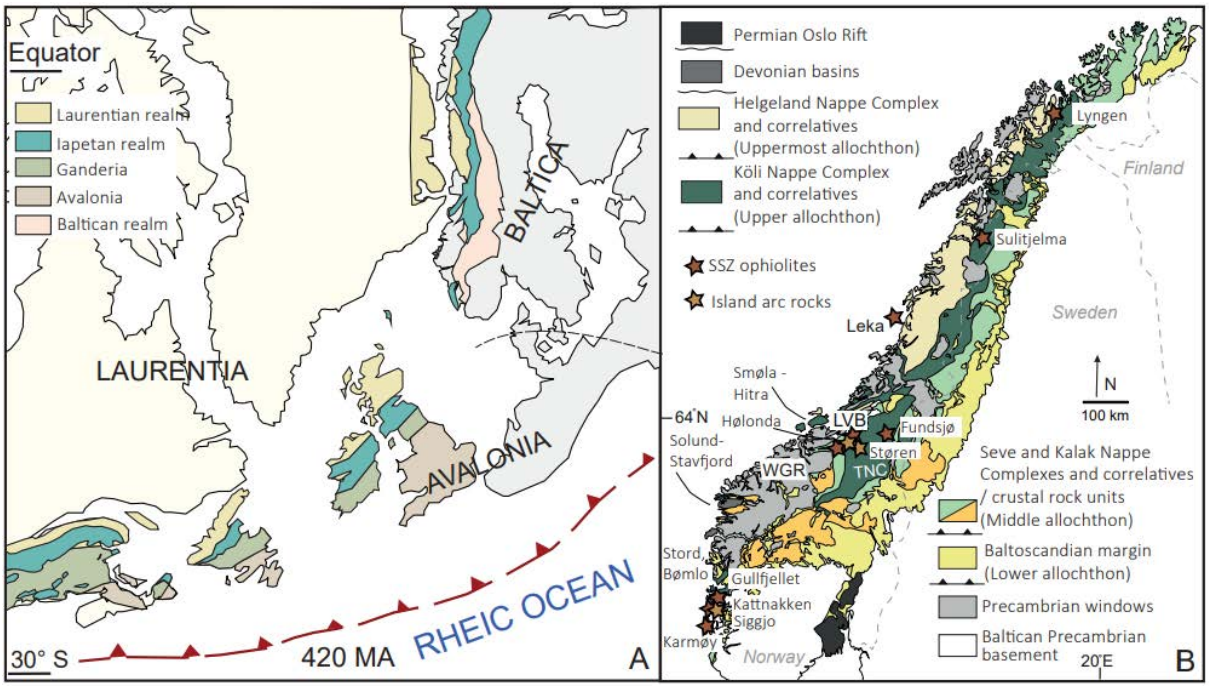

Fig. 5: (A) Tectonic reconstruction at 420 Ma, redrawn from Domeier (2016). The stippled line between Baltica and Avalonia is the approximate Tornquist Ocean suture zone. **(B)** Overview map of the Scandinavian Caledonides.

The basement rocks of Baltica range in age from Archean to Neoproterozoic; generally with the oldest rocks in the northeast and progressively younger rocks southwards. Except for some imbrication the basement is largely unaffected by the Caledonian deformation in the south and east. In the Western Gneiss Region (WGR, also known as the Western Gneiss Complex) in western Norway (Fig. 5B) the basement rocks record ultra-high pressure (UHP) metamorphism and are interpreted to have been subducted down to depth conditions of >2.8 GPa during peak Scandian collision (Hacker et al., 2010), and educted as a coherent slab (Andersen et al., 1991). The Lower allochthon (Fig. 5B) is para-autochthonous and consists of the sedimentary cover to

the Baltican basement rocks, mainly deposited in the Neoproterozoic (e.g. Nystuen et al., 2008). The Middle allochthon (Fig. 5B) is dominated by crystalline basement rocks, mainly of Palaeo-to Mesoproterozoic age, and various sedimentary rocks. In the southern part of the Scandinavian Caledonides, an extensional mélange zone with peridotites is commonly observed below the crystalline rocks. This zone was interpret by Andersen et al. (2012) to represent a hyperextended, pre-Caledonian margin, with the crystalline rocks representing rifted crustal fragments or microcontinents. Comparable rocks are found within the Seve Nappe in the central Scandinavian Caledonides (Fig. 5B) and in the Kalak Nappe in northern Scandinavia (Andréasson et al., 1998), but it is unclear if the units with solitary peridotites are correlateable (Jakob et al., 2019).

The Upper allochthon is dominated by ophiolitic fragments, arc rocks and cover successions; such rocks can be found along major parts of the Scandinavian Caledonides (Fig. 5B). These units are also known as the Köli Nappe Complex and correlatives. The preserved record of ophiolite formation indicates that intra-oceanic subduction and suprasubduction-zone magmatism had started around 497 Ma (Leka ophiolite (Fig. 5B); Dunning and Pedersen, 1988). The ophiolite fragments in southwestern Norway are relatively well studied and record several phases of magmatic activity: ophiolite formation (>494 ± 2 Ma to 489 ± 3 Ma), followed by immature arc magmatism around 485-482 Ma, renewed MORB magmatism and finally mature arc magmatism around 475-470 Ma (Fig. 5B; Dunning and Pedersen, 1988; Pedersen and Dunning, 1997). A similar evolution has been proposed for the central Norwegian ophiolite fragments which are of comparable age (Slagstad et al., 2014), this is further elaborated in section 1.3. In Northern Norway, the >494 Ma Lyngen (Fig. 5B; Slagstad et al., 2020) and Gratangseidet igneous complexes represent Early Ordovician ophiolite complexes formed close to the Laurentian margin (Augland et al., 2014), and record magmatic activity spanning approximately 20 million years (Slagstad et al., 2020).

The majority of ophiolitic and arc successions in southwestern Norway and the Trondheim region are considered by most workers to have originated somewhere close to Laurentia or its related microcontinents, based on faunal evidence, ages of inherited zircons in arc-related plutons, palaeomagnetism or geochemistry (e.g. Bruton and Bockelie, 1980; Pedersen and Furnes, 1991; Slagstad et al., 2014; Domeier, 2016). In the Köli Nappe Complex (Fig. 5B), the Lower Köli Nappe is commonly placed in a setting proximal to Baltica, with the Upper Köli Nappe closer to Laurentia; the position of the Middle Köli Nappe is more uncertain (e.g. Stephens, 2020). The majority of ophiolites preserved in the Scandinavian Caledonides formed over a time span of 30-40 million years during the late Cambrian to earliest Ordovician, possibly in separate basins (Slagstad et al., 2020). These events was followed by a younger phase which include formation of the 443 ± 3 Ma Solund-Stavfjord ophiolite (Fig. 5B) in a short-lived

marginal basin proximal to the Laurentian margin (Furnes et al., 2012), and the 437 ± 2 Ma Sulitjelma ophiolite (Fig. 5B; Pedersen et al., 1991).

In central Scandinavia and northwards, rocks with an inferred origin along the Laurentian continental margin commonly overlie the clearly oceanic rocks of the Upper allochthon, and are traditionally assigned to the Uppermost allochthon (Fig. 5B). These rocks include mainly Neoproterozoic to Ordovician clastic and calcareous passive margin deposits intruded by numerous Early to Middle Ordovician and Silurian arc-related plutons (e.g. Yoshinobu et al., 2002; Barnes et al., 2007; Barnes et al., 2011; Augland et al., 2012; Hollocher et al., 2016). Such magmatism is largely absent in the underlying tectonic units.

1.3 The geology of the central Scandinavian Caledonides

This section focuses on the area between the Grong-Olden basement window in the north, the Western Gneiss Region, and the autochthonous basement rocks in the east and southeast (Fig. 6). The area provides a transect from the undeformed, autochthonous basement in the east, through the preserved stack of nappes which generally thins westward, to the reworked high-pressure metamorphic basement in the west; a transect which allows for detailed studies of the relation between the nappes and the evolution of the Caledonides. The area hosts several large

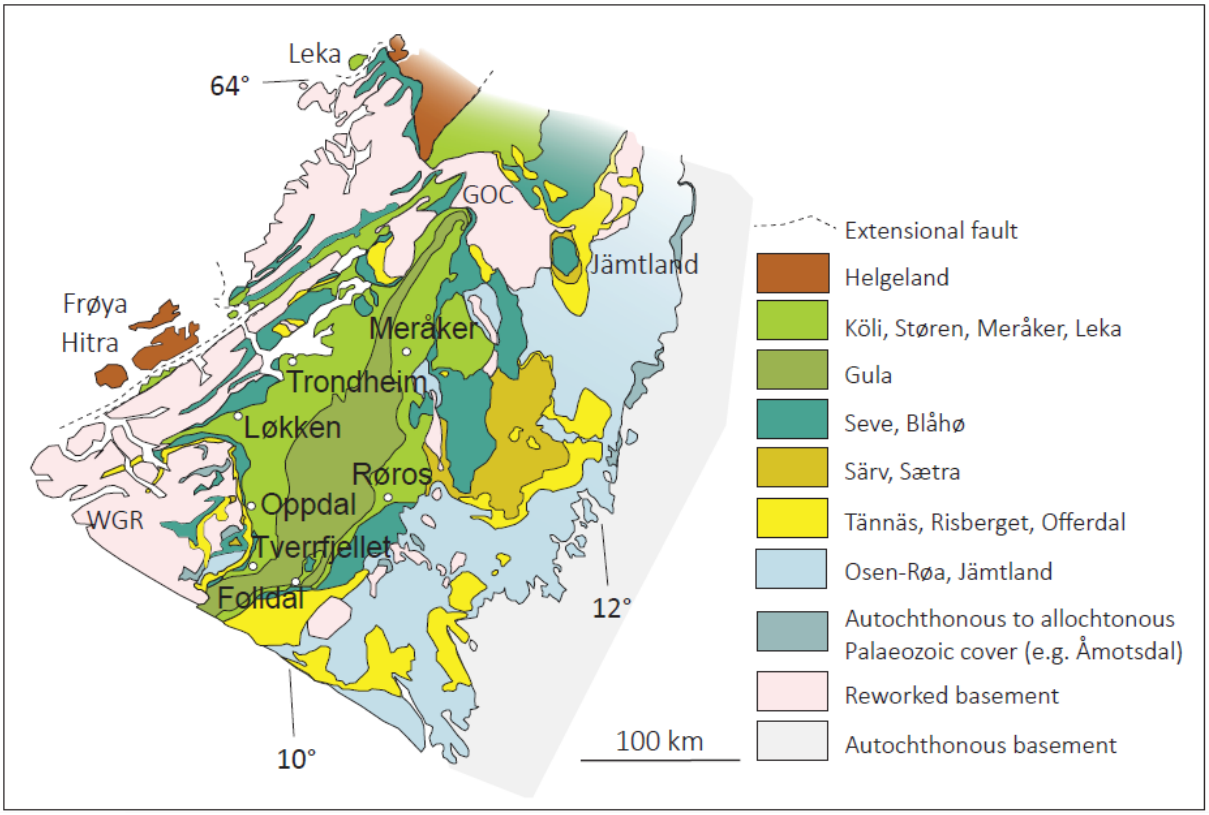

Fig. 6: Map of the Scandinavian Caledonides, modified from Corfu et al. (2014). WGR = Western Gneiss Region, GOC = Grong-Olden basement culmination.

and numerous smaller Cu–Zn deposits, where the abandoned Løkken, Tverrfjellet, Røros and Folldal mines (Fig. 6) were the most important, and all the deposits are interpreted to have been formed in back-arc settings or associated with mafic intrusions during initial collision (Grenne et al., 1999).

The central Scandinavian Caledonides (Fig. 6) are comprised, from base upwards, of a (para)autochthonous Proterozoic cover, known as the Åmotsdal Nappe in the Oppdal area (Fig. 6), which locally are overridden by the Osen-Røa Nappe Neoproterozoic sedimentary succession (Nystuen et al., 2008) and the Ordovician to Lower Silurian foreland basin deposits of the Jämtland nappes (Gee, 1975). Such foreland deposits are absent in the Oppdal region. These rocks are tectonically overlain by nappes dominated by augen gneiss, for instance the Tännäs Nappe in Sweden and Risberget Nappe in the Oppdal area. The Risberget Nappe mainly consists of coarse augen gneiss, with minor gabbro, anorthosite and rapakivi granite, where the augen gneisses gave U–Pb ages at 1650-1640 Ma and 1190-1180 Ma (Handke et al., 1995). Together with the tectonically overlying feldspathic sandstones known as the Särv Nappe in Sweden and Sætra Nappe (quarried for the "Oppdalskifer" flagstone) in Oppdal; these rocks traditionally constitute the Middle allochthon (Fig. 6). The Sætra and Särv nappes are interpreted to have been deposited in a fluvial to shallow marine setting along the extended continental margin of Baltica. The detrital zircon population is dominated by late Palaeoproterozoic to early Mesoproterozoic grains, with the youngest grains ranging from c. 890 to 960 Ma (Be'eri-Shlevin et al., 2011). The sedimentary rocks of the Sætra and Särv nappes are intruded by dolerite dykes, in Sætra mainly occuring as amphibolitic bands in the flagstone. The age data on these dykes are sparse, but correlatable rocks further north have been dated to c. 605 Ma (Kjøll et al., 2019). The overlying unit, known as the Seve Nappe in Sweden and the Blåhø Nappe in the Oppdal area (Fig. 6), consists mainly of pelitic and psammitic schists, gneisses, amphibolites, and minor marble, peridotite lenses and orthogneisses; these are generally of higher metamorphic grade compared to over- and underlying units. Several parts of the Seve Nappe record (ultra)high-pressure metamorphism predating the continent-continent collision, for instance in the Jämtland area northeast of our study area, where Root and Corfu (2012) report a U-Pb zircon age of 446 Ma for the eclogite facies metamorphism. Similar but older (U)HP events are described further north in the Seve nappe (c. 482 Ma; Root and Corfu, 2012). The significance of these early metamorphic events is not fully understood, but probably attests to early subduction of the outermost Baltic margin.

1.3.1 The Trondheim Nappe Complex

The Seve/Blåhø nappes are tectonically overlain by rocks with an oceanic affinity; ophiolites, arc rocks and cover successions mainly assigned to the Köli Nappe Complex and correlatives which

are preserved in a large structural depression (e.g. Gee, 1975; Gee et al., 1985). In the Trondheim region, these rocks are separated into three main units, from east to west: the Meråker, Gula and Støren nappes (Fig. 6,7), collectively known as the Trondheim Nappe Complex (TNC; Gee et al., 1985). Both the Støren and Meråker nappes contain Early Ordovician ophiolite and arc complexes, which are unconformably overlain by Late Ordovician to early Silurian sedimentary successions with subordinate volcanic rocks. The Gula Nappe (Fig. 7) consists of continental and oceanic clastic rocks of unknown depositional age and has variable metamorphic grade (Engvik et al., 2014), though generally higher than to the Meråker and Støren nappes. The relation between these nappes is still unresolved and the structural position of the Gula Nappe relative to the Meråker and Støren nappes is enigmatic; it may represent a klippe above, a thrust sheet between, or a mushroom-shaped antiformal unit below the Støren and Meråker nappes (e.g. Gee et al., 1985).

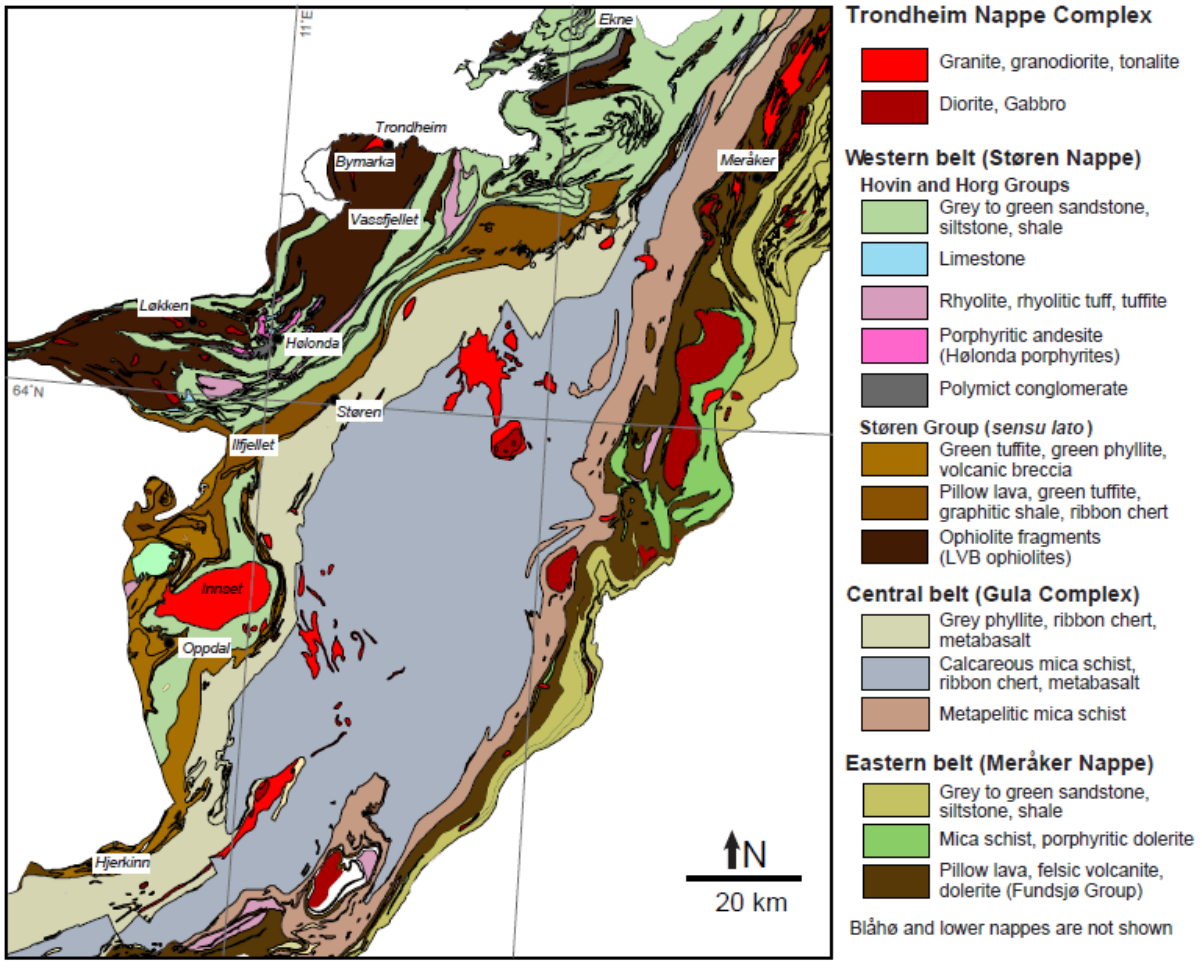

Fig. 7: Map of the Trondheim Nappe Complex, modified from Stokke et al. (2018). For relations to the Blåhø and lower nappes see Fig. 6.

The Meråker Nappe (Fig. 7) consists of basaltic to intermediate volcanic rocks with a geochemical signature transitional between island arc tholeiite (IAT) and Mid-Oceanic Ridge

Basalt (MORB), overlain by sediments and pyroclastic/volcaniclastic rocks (Grenne and Lagerblad, 1985). Gee (1981) proposed a Baltic origin for the Meråker Nappe based on geochemical similarities between Ordovician black shales in the Meråker Nappe and in the autochthonous Baltican cover successions. On the other hand, Grenne and Lagerblad (1985) argue that the geochemical differences between the Meråker and Støren volcanic rocks imply that they are separate units.

The Støren Nappe is traditionally divided into the Løkken – Vassfjellet – Bymarka (LVB) ophiolite fragments, the Støren Group *sensu stricto* basaltic rocks, and the sedimentary rocks traditionally assigned to the overlying Hovin and Horg groups (Fig. 7). There are several internal unconformities within the Støren Nappe, where the contact between the LVB ophiolite and the overlying sediments is the most prominent (the Trondheim disturbance of Vogt, 1945); an unconformity between the Støren basaltic rocks and overlying sediments is also described. The LVB ophiolitic fragments consist of gabbro, sheeted dykes and pillow lavas with a supra-subduction zone (SSZ) signature (Grenne and Roberts, 1980; Heim et al., 1987; Grenne, 1989), and has formation ages ranging from 492 Ma to 478 Ma (Slagstad et al., 2014). At Løkken, the ophiolite evolves from depleted N-MORB tholeiite in the lower and middle members, to immature arc-tholeiites in the upper member (Grenne, 1989). The LVB ophiolite was obducted onto a continental margin or a microcontinent between 478 Ma and 468 Ma as constrained by the last recorded magmatic activity within the ophiolite and the first post-obduction magmatism (e.g. Slagstad et al., 2014). In contrast, the Støren basaltic rocks are characterised by MORB-like geochemical signatures and lack the ophiolite pseudostratigraphy (Grenne and Lagerblad, 1985; Stokke et al., 2018). The age of the Støren Group *senso stricto* basaltic rocks is unknown. Obduction of the LVB ophiolite, and formation of the Støren basaltic rocks, was followed by deposition of the Hovin and Horg groups (Fig. 7); a succession of conglomerates, shales, sandstone, limestone and minor volcanic rocks (e.g. Vogt, 1945; Chaloupsky, 1970; Grenne and Roberts, 1998).

Of special interest for the present study are the Hølonda Porphyrites within the Hovin Group, a shoshonitic volcanic and subvolcanic unit formed in a continental arc setting (Grenne and Roberts, 1998). The absolute age of the Hølonda Porphyrites is unknown, but they are associated with richly fossiliferous sediments of Late Arenig/Early Llanvirn (Middle Ordovician) age that also show an unequivocal Laurentian faunal affinity (Bruton and Bockelie, 1980; Grenne and Roberts, 1998). An origin of the Støren Nappe on the Laurentian side of Iapetus is further supported by geochemical considerations (Slagstad et al., 2014).

1.3.2 Previous work in the Oppdal area

Previous work in the Oppdal area mainly targeted the lower tectonic units or the younger intrusions; pioneering work by Goldschmidt (1916) led to the definition of trondhjemite and opdalite which constitute the Innset Massif, a major intrusion dated to 435 Ma by Nilsen et al. (2003). Rohr-Torp (1972, 1974) described the contact metamorphism around the Innset Massif and interpreted the surrounding rocks to be overturned. Holmsen (1955) described the various volcanic rocks in the area and considered them to be Late Ordovician volcanic-derived conglomerates and lavas. Krill (1980, 1985) described the rocks of the structurally lower nappes and the complex relations between them, and introduced the informal term "Tronget unit" for all units structurally above the Blåhø Nappe, i.e. rocks elsewhere assigned to the Støren and Gula nappes. Finally, the geology of the area was described on the 1:250 000 scale map sheet "Røros og Sveg" by Nilsen and Wolff (1989), where the basaltic rocks in the Oppdal area were interpreted as one single horizon and correlated with the Støren basaltic rocks (Fig. 8). They interpreted the sedimentary succession as unconformably overlying the basaltic rocks and assigned them to the Hovin/Horg groups (Fig. 8), an interpretation in line with Rohr-Torp (1972).

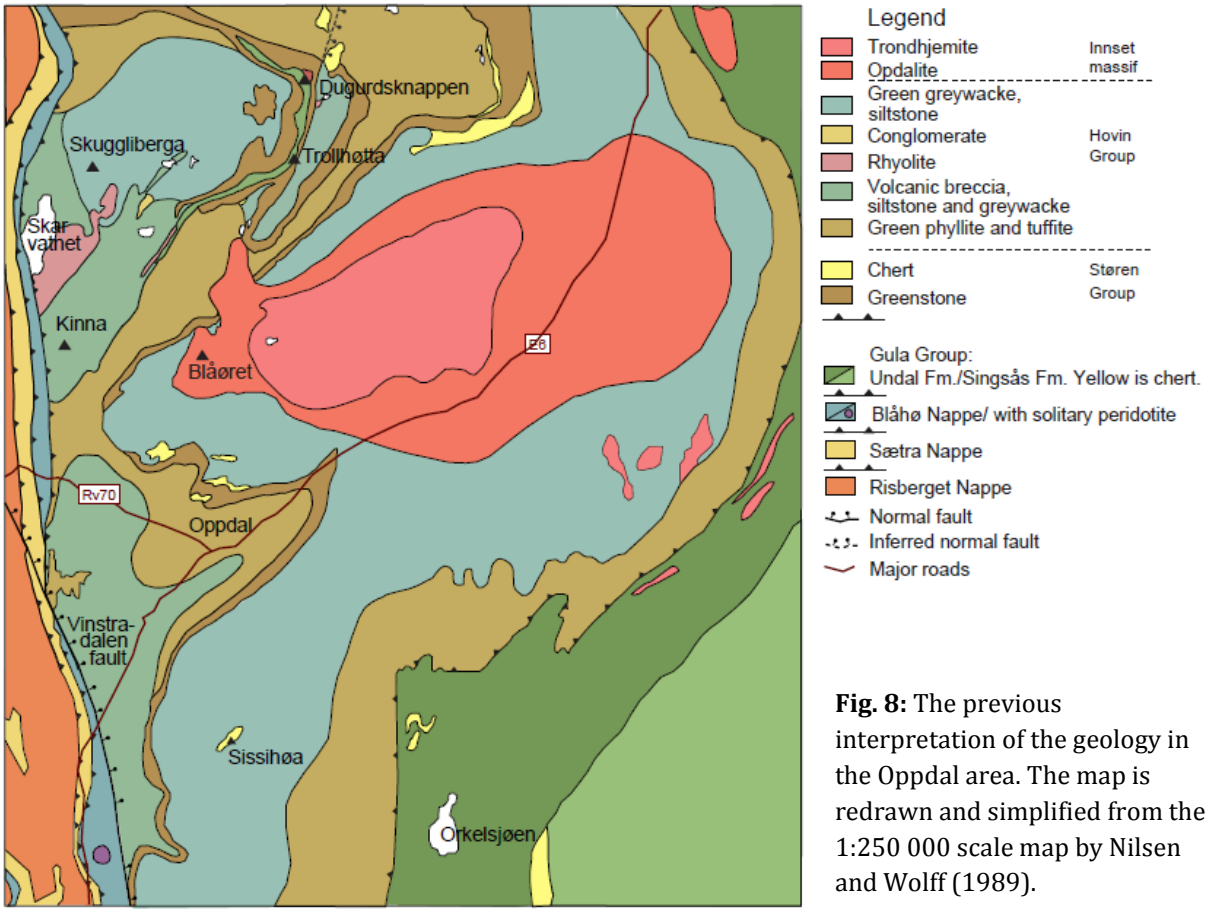

Fig. 8: The previous interpretation of the geology in the Oppdal area. The map is redrawn and simplified from the 1:250 000 scale map by Nilsen and Wolff (1989).

1.3.3 Open questions

Despite being one of the classical areas in Norwegian geology, there are many unanswered questions related to internal correlations and stratigraphy, the paleogeographic origin of the units, and how the Trondheim Nappe Complex has evolved. There are also several unresolved questions regarding the tectonic units structurally below the TNC. Some of the open questions which are relevant for this thesis are:

- Are the mafic units in the western TNC (for instance the LVB ophiolite fragments, the Støren basaltic rocks and the basaltic rocks in the Oppdal area) one large, correlatable unit, or do they represent several independent mafic units with different histories?
- In the relatively well-studied area south of Trondheim where the Hovin and Horg groups were defined, several stratigraphic schemes have been made (Vogt, 1945; Chaloupsky, 1970; Wolff, 1979; Bruton and Bockelie, 1980), but it is unclear how the rocks in the Oppdal area relate to the rocks further north. Can the established stratigraphy in the Støren-Hovin-Hølonda area be extended southwards to include the Oppdal area, following the interpretation of e.g. Nilsen and Wolff (1989)?
- Are the western and eastern nappes (Støren and Meråker, respectively) in the TNC correlatable, or are they two separate units? More geochemical and age data is required to conclude on this issue.

2 Objectives of the project

The work presented herein is part of a project initiated at the Geological Survey of Norway, which aims to improve the knowledge of the geology and geological resources in the county of Trøndelag, central Norway, and contributes data to answer the questions presented in the previous section.

This study focuses on the Oppdal area in the southern part of the western TNC, an area where the geology is poorly described, and the age and geochemistry of the different units and the relationships between them are not well known. The aim of this thesis work is to remap the bedrock geology of the Oppdal area in detail, which is the foundation for reconstructing the geological history and for correlation with rock units elsewhere. This thesis aims at answering the following questions:

- What lithologies are present in the Oppdal area, and how do the lithological units relate to each other?
- What is their age and geochemical signature?

- In what tectonic setting did these rocks form?
- How do these rocks and their evolution compare to similar units elsewhere in the Caledonides and Appalachians?
- Can these rocks help to reconstruct the geometry and evolution of the Iapetus Ocean and processes during its closure?

3 Approach and methods

Despite the relatively well preserved geological features and the fairly good accessibility of the area, detailed descriptions and studies of the geology around Oppdal are scarce. To make correlations and to understand the TNC as a whole, and on a larger scale the evolution of the Scandinavian Caledonides, basic knowledge about the rock types, age, chemistry and internal relations is fundamental. The Oppdal area was chosen as a field area because of the need to gain more knowledge about the geology of this area. Lithological and structural mapping, sampling and lab work has been a major part of this field-based study, in order to provide new data and interpretations of the Oppdal area. More than 2500 localities have been visited, and field observations are stored in a digital database and have been visualised and studied in ArcGIS maps.

For geochemical analyses, representative, fresh, homogeneous samples are preferred, but due to the high content of vesicles in the volcanic rocks of the area, some smaller vesicles or phenocrysts are likely to be present in the analysed material. In fragment-bearing rocks, samples are either from individual fragments or the matrix; mixed samples are avoided but very small fragments might be present in the matrix samples. Whole rock geochemical analyses have been done with standard methods at the Geological Survey of Norway: X-ray fluorescence (XRF) on major and minor elements and inductively coupled plasma mass spectrometry (ICP-MS) analyses for trace elements. The Igpet software has been used for data visualisation.

Geochronological data has been collected by three different methods adapted for different purposes. Isotope dilution-thermal ionisation mass spectrometry (ID-TIMS) is a high-precision method for U-Pb zircon geochronology, but is time consuming and therefore mainly used for dating magmatic zircon where only a few grains are needed (Corfu, 2013). Four samples from felsic volcanic rocks have been dated by this method. Laser ablation inductively coupled plasma mass spectrometry (LA-ICP-MS) is also a common method for U-Pb zircon analyses; this method has lower precision, but is efficient for analysing the large number of zircon grains required for

detrital zircon analyses (Corfu, 2013). Detrital zircon grains from 11 sandstone/gritstone samples have been analysed and are published; one additional sample is unpublished but the data are provided in this thesis. The samples are collected from key localities such as below and above unconformities or lava flows. The detrital zircon grains were imaged using cathodoluminescence (CL) prior to analysis to reveal their internal structures and determine the spot position. Metamorphic biotite from a volcanic unit has been dated with the Ar-Ar method (Schaen et al., 2020), which give an age for the post-metamorphic cooling. The data from these methods complement each other well, and provide constraints on depositional age of sediments, the timing of volcanic activity and the Caledonian metamorphism in the Oppdal area.

4 Summary of results

4.1 Paper I

Dalslåen, B.H., Gasser, D., Grenne, T.,Augland, L.E. and Corfu, F., 2020. **Ordovician shoshonitic to ultrapotassic volcanism in the central Norwegian Caledonides: The result of sediment subduction, mantle metasomatism and mantle partial melting.** Lithos, 356.

This paper present field observations, geochemical data and U-Pb TIMS zircon ages leading to the definition of the Skarvatnet unit, consisting of three different subunits: 1) the Kinna volcanic succession, interpreted as a series of submarine pyroclastic flows extruded at c. 474 ± 1 Ma, 2) the subvolcanic Storgruvpiken rhyolite which intruded the Kinna volcanic succession at c. 470 ± 1 Ma, and 3) the overlying, shallow-marine Skaret succession which was deposited in a tectonically active setting. The Skarvatnet unit represents a lithologically and geochemically distinctive volcano-sedimentary phase hitherto unknown in the Ordovician of the Scandinavian Caledonides.

The Kinna volcanic succession consists of metre-thick layers where fragment-bearing and fragment-free layers alternate. The fragments are vesicular, and have characteristic aggregates of biotite and amphibole which probably replace magmatic amphibole. Based on the lack of sorting within layers, the even thickness of the layers (no erosion channels etc.) and the enclosed marine deposits (e.g. chert), the Kinna volcanic succession is interpreted as a submarine pyroclastic deposit. The Kinna volcanic succession shows geochemical signatures far more enriched in for instance Th, U, Pb and LREE than common arc-related rocks. These elements are indicative of a crustal source, but the rocks also have a high content of Mg, Cr and Ni, which points to a mantle source. Rocks with extreme enrichment combined with a mantle signature similar to the Kinna volcanic succession are exceedingly rare in the Caledonian system,

but the rocks are comparable to high-K to ultrapotassic rocks of the Alpine-Himalayan belt and other orogenic settings. Based on the comparison with these better studied rock suites, the Kinna volcanic succession is interpreted as representing partial melts derived from previously enriched mantle sources. Enrichment of the mantle source is related to subduction of large amounts of continent-derived material, releasing highly enriched partial melts interacting with the overlying mantle. In the case of the Kinna volcanic succession, this mantle enrichment may have occurred during initial subduction of the Laurentian margin or an associated micro-continent below the originally intra-oceanic LVB arc. Partial melting of the enriched mantle was coeval with, or slightly after, arc-continent collision, possibly facilitated by asthenospheric upwelling related to slab retreat or break-off. The Storgruvpiken rhyolite could be the result of remelting of Kinna-type plutonic rocks at depth, caused by the same upwelling.

Based on geochemical similarities with the slightly younger shohonitic Hølonda porphyrites (Grenne and Roberts, 1998), we suggest that the Skarvatnet unit formed proximal to the Laurentian margin. Additionally, we reinterpret the Hølonda porphyrites to be a part of this tectono-magmatic phase, in contrast to earlier interpretations that postulate the Hølonda magmas formed as a result of subduction below Laurentia subsequent to slab polarity reversal. The existence of extremely enriched volcanic rocks of this type long before the final closure of the Iapetus Ocean demonstrates that such rocks may form not only during or after major continent-continent collisions like the Himalayas (e.g. Cheng and Guo, 2017) or the Variscan orogen (e.g. Soder and Romer, 2018), but also during earlier phases in complex subduction–accretion–collision systems (such as in the Mediterranean, e.g. Conticelli et al., 2010).

4.2 Paper II

Dalslåen, B.H., Gasser, D., Grenne, T., Augland, L.E. and Andresen, A., 2020. **Early to Middle Ordovician sedimentation and bimodal volcanism at the margin of Iapetus: The Trollhøtta–Kinna basin of the Central Norwegian Caledonides.** *In*: Murphy, J.B., Strachan, R. & Quesada, C. (eds) *Pannotia to Pangaea: Neoproterozoic and Paleozoic Orogenic Cycles in the Circum-Atlantic Region.* Geological Society, London, Special Publications, 503.

In this paper we present field observations and geochemical and geochronological data which led to the definition of a new lithostratigraphic unit, the Trollhøtta unit. This Early to Middle Ordovician basin is coeval with, and interfingers with the Kinna volcanic succession defined in Paper I. Together they constitute the Trollhøtta–Kinna basin, where alternating siliciclastic and bimodal volcanic rocks are interpreted to have accumulated in a marginal basin that probably developed along the margin of Laurentia or an associated micro-continent. The Trollhøtta unit is

dominated by turbiditic, siliciclastic sediments and MORB-like basalts, and minor felsic volcanic rocks.

The turbiditic sandstones have detrital zircon spectra which indicate deposition after c. 480 Ma, and derivation from a composite Cambro–Ordovician and Proterozoic to Archean landmass. This requires a complex, subaerially exposed source region that included both ancient continental crust and Palaeozoic rocks; the latter inferred to be obducted supra-subduction zone ophiolites and/or island arcs. The Trollhøtta succession also contains a peculiar association of D-, N- and E-MORB basalts along with minor felsic lavas extremely enriched in for instance Th, U and LREE, requiring an extremely heterogeneous mantle source. Rhyolites from the stratigraphically upper part are dated by zircon U-Pb TIMS to 473.3 ± 1.0 and 472.4 ± 0.7 Ma. The enriched felsic rocks are related to the coeval Kinna volcanic succession (discussed in Paper I), and are interpreted to represent fractionation products of mafic melts derived from metasomatised, highly enriched mantle domains. The peculiar bimodal volcanic association is interpreted as an intermittent phase of marginal basin rifting. The tectonic mechanisms responsible for sedimentation and volcanism are not fully resolved, but we envisage two possible explanations: (1) extension and basin subsidence caused by slab retreat and/or break-off following arc–continent collision and ophiolite obduction, or (2) far-field tectonic forces within the shrinking Iapetan realm. Comparison of this basin with other Iapetus-related volcano-sedimentary successions of similar age along the Caledonian–Appalachian orogen indicate that the Trollhøtta–Kinna basin represents a tectonic phase that is apparently not found elsewhere along the Caledonian orogen. Volcanic rocks of similar age in southern Norway, Ireland and Newfoundland do not contain the peculiar association of MORB basalts and extremely enriched mafic to felsic rocks which characterise the Trollhøtta–Kinna basin. The closest analogue is the Lloyds River ophiolite complex of Newfoundland, which is intruded by the shoshonitic Portage Lake monzogabbro (Lissenberg et al., 2005).

4.3 Paper III

Dalslåen, B.H., Gasser, D., Grenne, T., Ganerød, M. and Andresen, A. **The Skuggliberga unit of the Oppdal area, central Scandinavian Caledonides: calc-alkaline andesitic pyroclastic volcanism in a fluvial to shallow marine basin following mid-Ordovician tectonism.** Accepted for publication in Norwegian Journal of Geology.

Previously, an area dominated by greywackes has been mapped in the northwestern part of the study area. The new results presented in this paper indicate that the rocks in the area consist of sandstones and volcanic rocks, and should be considered as a separate regional-scale

lithostratigraphic unit, the Skuggliberga unit. We present new field observations, geochemical data, detrital zircon U-Pb LA-ICPMS ages and an Ar-Ar biotite metamorphic age from this newly-defined volcano-sedimentary unit. The Skuggliberga unit occurs in two separate areas, where it unconformably overlies the c. 480–470 Ma Trollhøtta and Skarvatnet units. The Skuggliberga unit consists of a local basal conglomerate and a cross-stratified to massive, structureless sandstone, overlain by bedded, fragment-bearing volcanic rocks. This is the first description of the volcanic rocks in this area, which are interpreted as pyroclastic rocks erupted in a terrestrial or shallow-marine setting.

The volcanic rocks show calc-alkaline basaltic andesitic and andesitic compositions, with a geochemical signature (including a negative Nb–Ta anomaly) which indicates formation in a continental arc-setting. This is distinctly different from the underlying, MORB-like, Trollhøtta basaltic rocks and the extremely enriched volcanic rocks from the Skarvatnet unit. One sandstone sample from the Skarvatnet unit below the unconformity is dominated by Palaeozoic detrital zircons, with a major peak at c. 490 Ma. Two sandstone samples from the Skuggliberga unit contain Archean, Palaeo- to Neoproterozoic and Palaeozoic detrital zircons. Different methods employed to calculate the maximum depositional age for these samples gave results that vary through a range of about 50 m.y. (from c. 427 to c. 475 Ma). Some estimates are younger than the c. 435 Ma plutonic Innset massif that intrudes the Skuggliberga unit, indicating that the youngest detrital zircons must have experienced concealed lead loss. This lead loss could have occurred during regional metamorphism of the unit; an Ar–Ar plateau age of 416 ± 3 Ma was derived for biotite in one Skuggliberga volcanic sample dating this metamorphism.

Comparison with other Middle Ordovician to early Silurian volcano-sedimentary units within the Scandinavian Caledonides suggests that the Skuggliberga unit has most in common with Late Ordovician to early Silurian (c. 450–435 Ma) units such as the Vikafjord Group of Bømlo, the Solund-Stavfjord ophiolite complex or the Furulund Group of the Sulitjelma area. Our data imply that the unit has no direct correlative within the TNC and represents a hitherto unknown volcano-sedimentary phase within the Central Norwegian Caledonides. However, it has geochemical similarities with several continental arc-related plutonic complexes spanning the same age interval along the coastal area of central Norway, and the Skuggliberga volcanic rocks may be an extrusive part of this magmatic arc system. Deposition of the Skuggliberga units is preceded by an orogenic phase resulting in deformation of the underlying Trollhøtta and Skarvatnet units, probably related to Taconian accretionary events along the Laurentian margin.

4.4 Results not published elsewhere: The transition to the Gula Nappe

An unresolved issue in the Oppdal area is the nature of the contact to the Gula Nappe farther east. The units present in the area on the 250 000 scale map by Nilsen and Wolff (1989) are from west to east: 1) sandstone (assigned to the Hovin Group), 2) "green tuffite and phyllite" assigned to the Elgsjø Formation and correlated with the Støren basaltic rocks, 3) the Gula Nappe with the Undal and Singsås formations. The siliciclastic rocks assigned to the Hovin Group are relatively undeformed, while the green phyllitic rocks of the Elgsjø Formation are pervasively foliated. The Undal Formation is mainly phyllitic, with minor chert, graphitic schist and mica schist, while the Singsås Formation has similar lithologies but at higher metamorphic grade and with higher content of calcareous material. Further work is required to map out and describe the Gula Nappe contact. The reconnaissance mapping also indicates that the rocks east of the main road (E6) and west of the Elgsjø Formation belong to a hitherto undescribed sandstone-dominated unit (Fig. 9) and not to the Trollhøtta unit, although they are lithologically similar.

We infer a faulted contact (roughly parallel to the E6 highway), between the Trollhøtta unit and the unnamed unit to the east (Fig. 9), based on the following: 1) The rocks belonging to the Trollhøtta unit strike approximately in a NNE–SSW direction, while the unnamed unit strikes (N)NW–(S)SE, and turns into a westward orientation of the strike in the northern part of the area. The graded beds in the sandstone-dominated rocks indicate overturning of the rocks in this area (Fig. 10A). The orientation of the bedding is incompatible with the structural interpretation of the Trollhøtta unit, and we suggest that the units east and west of E6 are separated by a faulted boundary and not a depositional contact. 2) There are lithological similarities (e.g. dominance of siliciclastic rocks) between the Trollhøtta unit and this eastern, unnamed unit, but there are also significant differences. Basaltic rocks have been observed at a few localities, but are scarce compared to the Trollhøtta unit. Chert is also present, but is not associated with basalt in contrast to the Trollhøtta unit where chert is commonly found in contact with volcanic rocks.

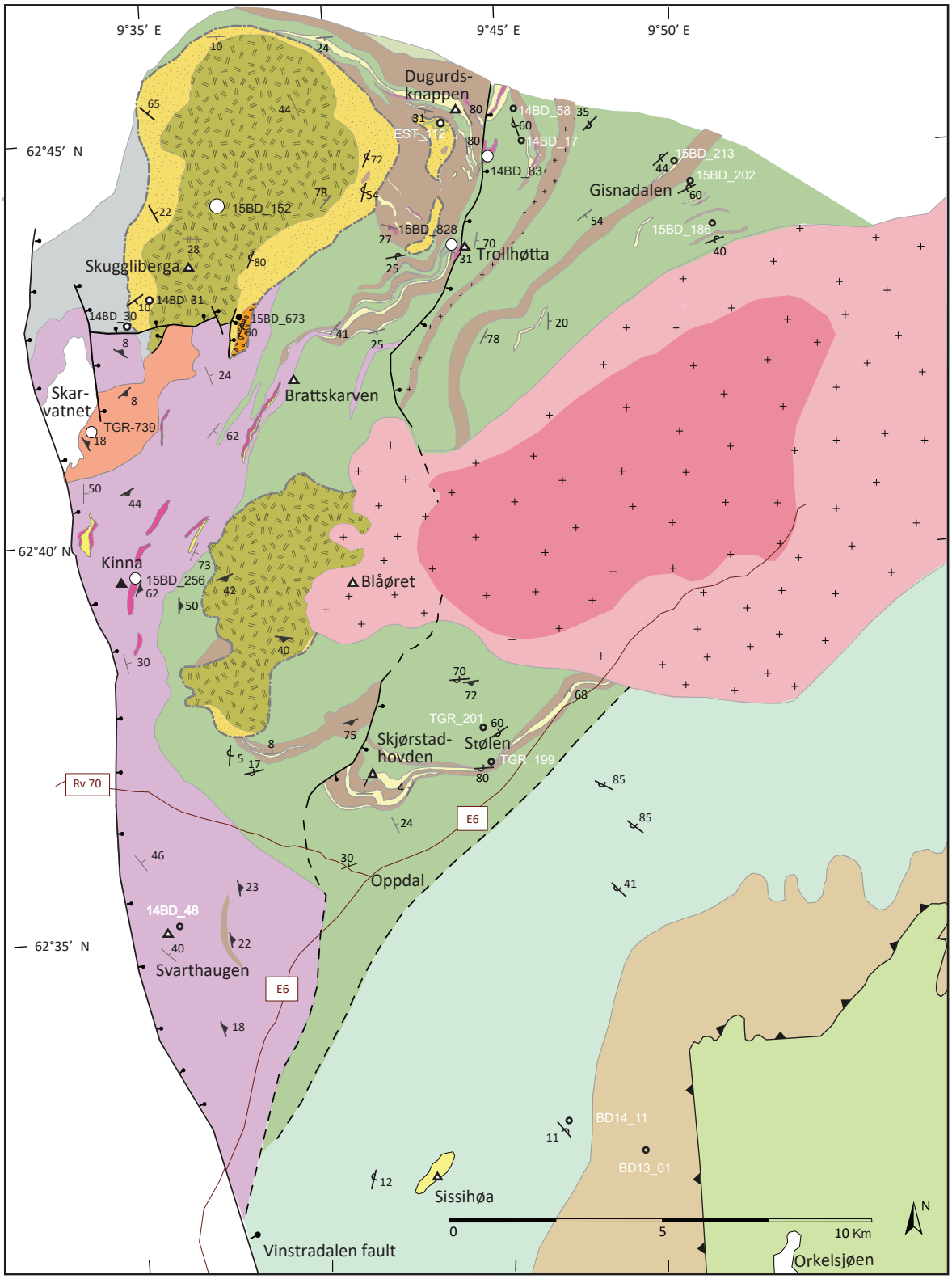
9°35' E
9°45' E
9°50' E
62°45' N
62°40' N
62°35' N
Dugurds-knappen
14BD_58
14BD_17
14BD_83
EST_12
15BD_213
15BD_202
Gisnadalen
15BD_186
15BD_152
15BD_828
Trollhøtta
Skuggliberga
14BD_31
14BD_30
15BD_673
Brattskarven
Skar-vatnet
TGR-739
Kinna
15BD_256
Blåøret
TGR_201
Stølen
TGR_199
Skjørstad-hovden
Rv 70
E6
Oppdal
14BD_48
Svarthaugen
BD14_11
BD13_01
Sissihøa
Vinstradalen fault
Orkelsjøen
0
5
10 Km
N
Innset massif
Granodiorite, opdalite
Trondhjemite
Skuggliberga unit
Andeste, basaltic andesite
Sandstone, commonly cross-stratified
Polymict conglomerate
Unconformity
Skarvatnet unit
Skaret succession
Storgruvpiken rhyolite
Chert
Trachyandesite, trachydacite
Kinna volcanic succession
Trollhøtta unit
Trachyandesite, trachydacite
Siltstone, turbiditic sandstone
Chert and silty chert
Metabasalt
Diabase
Other units
Un-named unit
Elgsjø Formation
Thrusted contact
Gula Nappe
Symbols
Detrital sample location, sample number in white
TIMS or Ar-Ar sample location
Mountain top
Roads and road numbers
Normal fault
Inferred normal fault
Lithological boundary
Strike and dip of bedding; no way up indicators
Strike and dip of foliation
Strike and dip of overturned bedding
Strike and dip of right way up bedding

Fig. 9 (previous page)**:** Map of the Oppdal area, mainly based on the results from this work. The lower nappes and the Gula Nappe Complex is based on Nilsen and Wolff (1989). See also the enlarged version of this map, which is enclosed in the back cover.

There are also differences in the sedimentary structures; turbiditic sandstones are present in both units but fine-grained sandstone with hummocky cross stratification (Fig. 10B) is only present in the eastern unit. This indicates that parts of the eastern, unnamed unit were deposited above the storm wave base; no indication of wave influence is observed in the Trollhøtta unit.

Fig. 10: Rocks from the unnamed eastern unit. **(A)** Graded beds which indicate overturning. **(B)** Graded beds and hummocky cross-stratification, up is to the south.

3) We have analysed detrital zircon from one sample (14BD_11) from this eastern unit; a sandstone close to the contact to the Elgsjø Formation. It has a strong dominance of Cambrian grains, where a large fraction in the age range 540–500 Ma attests to a significant difference from the Trollhøtta detrital zircon spectra. It is also different from sample 13BD_01; a sandstone from the Elgsjø Formation with dominantly Cambro-Ordovician and Palaeozoic populations. The data for these two samples are presented in Fig. 11, and the full analytical dataset in Supplementary material D.

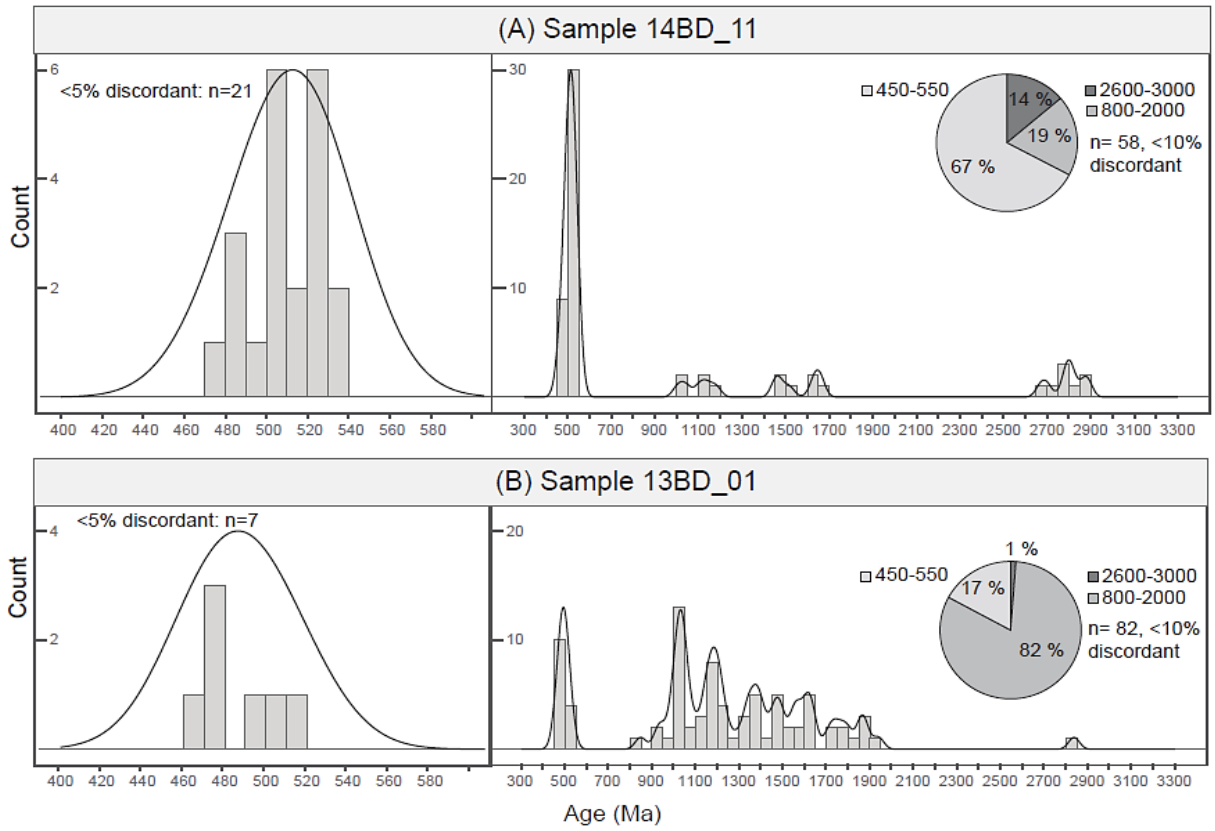

Fig. 11: Detrital zircon spectra. **(A)** Sample 14BD_11: From the unnamed unit, close to the contact to Elgsjø Formation. UTM32V 540458. 6935282. The sample is from a gravel conglomerate bed in sandstone, where graded bedding indicate overturning of the strata. N= 58. 67% of the analysed zircon are Cambrian to Ordovician. **(B)** Sample 13BD_01: From the Elgsjø Formation, southeast of sample 14BD_11. UTM32V 541910 6934404. The sample is from a quartz-rich grey, weakly greenish sandstone. N= 82; one run excluded because of poor analytical quality. The analysed zircon are dominantly Proterozoic.

4) South of the Oppdal area, the Drivdalen valley is a distinct topographic feature which is partly associated with E-dipping normal faults (Krill, 1987). For instance, in the Tverrfjellet mine at the southern end of the Drivdalen valley a N-S striking, E-dipping normal fault is exposed underground, with at least 1100 m displacement of the ore body (Krupp and Krupp, 1985). We infer a continuation of this fault system to the east of Oppdal, separating the Trollhøtta and the eastern, unnamed unit. More mapping in the eastern unit and detrital zircon studies are required to prove the existence of such a fault, and to properly describe the eastern, unnamed unit and its extent.

5 Synthesis

The three papers presented in this thesis together propose a new lithostratigraphy for the area consisting of the Skarvatnet, Trollhøtta and Skuggliberga units, fundamentally revising the understanding of the geological history of the Oppdal area. In Paper I we define the Skarvatnet unit, consisting of the Kinna volcanic succession, the Storgruvpiken rhyolite and the Skaret succession, and we examine volcanic rocks with an exceptional geochemistry. Their chemistry is most likely caused by mantle metasomatism by partially melted subducted continental material, and the age indicates that they formed subsequent to arc-continent collision and obduction of the Løkken – Vassfjellet – Bymarka ophiolite. These potassic to ultrapostasssic rocks are considered to be related to the shoshonitic Hølonda porphyrites farther north (Grenne and Roberts, 1998) and thus provide a link between the rocks in the Oppdal area and the Hølonda area which also indicates that the Skarvatnet unit formed on the Laurentian side of the Iapetus Ocean.

The link to the rocks further north is elaborated in Paper II, where we define the Trollhøtta unit and compare its MORB-like basaltic rocks with the Støren basaltic rocks, and suggest that the Støren – Trollhøtta magmatism was part of the same, extensive marginal basin system. The detrital zircon spectra from the turbiditic sandstones of the Trollhøtta unit suggest proximity to Laurentia. After formation of the Kinna – Trollhøtta system, the rocks were accreted (probably to Laurentia or an associated microcontinent), folded and eroded, before deposition of the Skuggliberga unit which consists of sandstone and andesitic volcanic rocks (Paper III). This event is constrained by the age of the underlying units (475–470 Ma) and of the Innset massif (435 Ma) which intrudes the Skuggliberga unit; detrital zircon data suggest deposition after c. 455 Ma based on the conservative method “youngest graphical peak”. The age and continental arc-signature of these rocks indicate a connection to the extensive arc magmatism which is preserved in the Laurentia-derived nappes along the coastal area of central and northern Norway, associated with long-lasting subduction under Laurentia.

5.1 Key findings

The key findings from this work are listed below, and provide the basis for a new interpretation of the volcano-sedimentary Ordovician–Silurian rocks in the Oppdal area:

- Within the Trollhøtta unit, several horizons of basaltic lavas occur without significant hiatus to the sedimentary rocks, contrary to previous interpretations which assigned all sedimentary rocks to the Hovin Group unconformably overlying the basaltic rocks. The association of basalt, chert and turbiditic sandstone can therefore be considered to have a common history within a marginal basin, which we informally name the Trollhøtta basin.

- The volcanic rocks within the Trollhøtta unit are highly bimodal; basaltic rocks with a MORB-like chemistry dominate, but are interbedded with minor highly enriched felsic rocks. The field relations indicate that the contrasting volcanic rocks are coeval, and the felsic rocks give U–Pb TIMS zircon ages of 472 ± 1 and 473 ± 1 Ma.
- We have defined the extremely enriched, arc-related volcanic rocks of the Skarvatnet unit, and suggest that the Kinna volcanic succession is a submarine pyroclastic deposit while the Storgruvpiken rhyolite is a subvolcanic plug or dome. Their U–Pb TIMS ages are 474 ± 1 and 470 ± 1 Ma, respectively.
- The remarkable chemistry of the Kinna volcanic succession was probably caused by partial melting of metasomatically altered mantle domains. Subducted continental material (sediments or continental crust) that partially melted are a likely metasomatic agent, and probably reacted with the surrounding mantle to form trace element enriched veins dominated by mica and clinopyroxene; this is in accordance with models for similar rocks e.g. in the Alps–Himalaya belt (e.g. Foley, 1992; Spandler and Pirard, 2013; Förster et al., 2017). Partial melting of such veins led to magma exceptionally enriched in incompatible trace elements (e.g. U, Th, LREE), with a high content of Cr, Ni and Mg that attests the mantle origin of these rocks.
- The Kinna volcanic succession interfingers with the upper part of the Trollhøtta unit, and the felsic volcanic rocks in the Trollhøtta unit share several of the geochemical features of the Kinna volcanic rocks. They are also of comparable age. We consider the two units to have formed in the proximity of each other, in the Trollhøtta–Kinna basin.
- We suggest that the Kinna volcanic succession and the broadly contemporaneous, shoshonitic Hølonda Porphyrites farther north are derived from similar mantle sources. This links the Trollhøtta – Kinna basin to the classical Hølonda terrane; rocks deposited unconformably on the obducted LVB ophiolite. The Laurentian fauna found in the Hølonda area are consistent with the detrital zircon signature in the Trollhøtta rocks.
- We have defined the unconformably overlying Skuggliberga unit, which consists of a cross-stratified to planar bedded sandstone and calc-alkaline andesitic rocks with a continental arc signature, previously mapped as a greywacke. These volcanic rocks have not been previously described apart from in Stokke et al. (2018).
- An updated map of the area has been made (Fig. 9; the larger version of the map, with all sample localities, is enclosed in the back cover), incorporating the new findings and interpretations in this work.

5.2 The evolution of the Cambrian – Silurian units preserved in the Oppdal area

The three papers together provide a solid basis for new interpretation of the upper tectonostratigraphic unit of the Oppdal area, where detailed mapping, descriptions and age/chemistry data previously have been sparse. In the earlier interpretations, such as the 1:250 000 scale map by Nilsen and Wolff (1989), the basaltic rocks are interpreted as one horizon, with the sedimentary rocks unconformably overlying the lavas (Fig. 8). We separate the sedimentary rocks into two main units; the turbiditic rocks and greenish siltstones are now assigned to the Trollhøtta unit and are coeval with the basaltic units, whereas the cross-stratified sandstones belong to the Skuggliberga unit which unconformably overlies the Trollhøtta unit (Fig. 9).

From further north in the Trondheim Nappe Complex it is known that the evolution of the western TNC starts with suprasubduction-zone magmatism and obduction of the 487-480 Ma Løkken–Vassfjellet–Bymarka (LVB) ophiolite, an event which took place sometime between 478 Ma and 468 Ma (e.g. Slagstad et al., 2014). The LVB ophiolite probably formed over an east-dipping (present co-ordinates) intra-oceanic subduction zone, and was obducted onto the Laurentian margin or an associated microcontinent. Although there are no ophiolite fragments preserved in the Oppdal area their formation is still relevant for the geological evolution of the area. In Paper I we suggest that continental-derived material was subducted during this event, partially melted and reacted metasomatically with the overlying mantle rocks. Partial melting of such anomalous, metasomatised mantle domains in a "dying" subduction zone are a likely source for the Kinna volcanic succession; its chemistry cannot be explained by processes like crustal contamination and fractional crystallisation. However, the coexistence of Kinna-type, exceptionally enriched and MORB-like basaltic rocks complicates the picture, and requires extremely heterogeneous mantle sources, where metasomatically altered and pristine mantle peridotite domains are tapped in near-contemporaneous but separate melting events. The two different tectonic scenarios we envisage could have caused the amount of rifting required for MORB-like basaltic magmatism and melting of the anomalous mantle domains are:

1) If the presupposed link to the Hølonda–LVB terrane is correct, obduction could have been followed by steepening and possibly break-off of the downgoing oceanic slab. In this setting, influx of hotter asthenospheric mantle could cause melting of the juxtaposed mantle domains, producing magma with contrasting geochemical characteristics. Slab rollback or break-off has been suggested as the trigger for partial melting of similar,

metasomatised mantle in the Alpine-Himalayan system (e.g. Pe-Piper et al., 2009; Cheng and Guo, 2017).

2) Rifting could also result from far-field tectonic forces, either as a short-lived, local extension in response to large-scale changes in the Laurentia–Baltica–Gondwana system, or local stress along the Laurentian margin could have led to extensional or transtensional rifting. More details on the age and palaeotectonic setting of the adjacent units (e.g. Gula and Meråker nappes) and the number of Middle Ordovician Iapetan subduction zones and their polarities, could help to resolve whether the Trollhøtta basin formation was related to the Hølonda–LVB system, or far-field tectonic forces.

Regardless of what caused the melting event, the Skarvatnet–Trollhøtta system likely formed in a marginal basin close to a continental landmass able to provide a substantial volume of siliciclastic sediments to the basin. The onset of basin formation is loosely constrained by the detrital zircon signatures to have started after c. 480 Ma, and continued to at least c. 472 Ma as constrained by the U-Pb TIMS age from a felsic rock in the upper part of the Trollhøtta succession; the magmatic activity continued until 470 Ma with the formation of the Storgruvpiken rhyolite. However, we cannot exclude that the mafic volcanism and sedimentation continued after c. 472 Ma; the shoshonitic Hølonda Porphyrites farther north are enclosed by fossiliferous rocks giving c. 467–463 Ma ages (Neuman and Bruton, 1974). If the Hølonda Porphyrites are related to the shoshonitic to ultrapotassic rocks in the Oppdal area, the K-rich volcanism at least continued until that age. After formation, the Trollhøtta and Skarvatnet units underwent a deformation phase regionally represented by tilting and overturning of the successions towards west. In Paper III we propose that accretion of the Trollhøtta and Skarvatnet units to the Laurentian margin or an associated microcontinent caused the folding and tilting of the rocks. This accretion event could be related to the onset of proper subduction under the Laurentian margin within the mid-Norwegian sector, which is marked by the voluminous arc magmatism that started at c. 460 Ma (e.g. Tucker et al., 2004).

Tilting and folding of the Trollhøtta and Skarvatnet units was followed by an erosional phase and renewed sedimentation and volcanism; the Skuggliberga unit. The Skuggliberga unit consists of a cross-stratified to structureless sandstone with local polymictic basal conglomerate, overlain by a fragment-bearing basaltic andesite to andesitic pyroclastic deposit with a continental arc signature. The age of the Skuggliberga unit is poorly constrained but the volcanic rocks are intruded by the 435 Ma Innset massif. The Skuggliberga unit has no direct correlative within the Trondheim Nappe Complex, but has geochemical similarities with several continental arc-related plutonic complexes spanning the same age

interval along the coastal area of central Norway. We propose that the Skuggliberga volcanic rocks may be an extrusive part of this magmatic arc system, which was active until the Scandian phase of the Caledonaian orogeny. In Paper III we provide a 416 Ma biotite Ar-Ar cooling age for the Scandian metamorphic event in the Oppdal area. Except for the regional greenschist metamorphism, the upper nappe in the Oppdal area is relatively unaffected by the main, Scandian collisional event between Baltica and Laurentia.

The post-collisional evolution of the Oppdal area is not treated in detail in this work, but a few comments should be made. The rocks studied herein are preserved within a (half)graben structure, separated from the Blåhø and lower nappes by an E-dipping normal fault which is nicely exposed at several localities, especially west of lake Skarvatnet. The presence of another E-dipping normal fault (east of Dugurdsknappen) which cuts across the field area has been established in this work, this fault probably connects to a fault system further north. In addition, small-scale, gently E-dipping structures with top-to-the-east kinematics are present, especially in the area interpreted as the lower part of the studied rocks (around Svarthaugen), indicative of foreland-directed transport.

5.3 Relation to similarly aged rocks in the Caledonian-Appalachian system

Based on the geochemical similarities of the Kinna volcanic succession and the near-contemporaneous Hølonda Porphyrites further north, we suggest a palaeogeocraphical connection between the Kinna rocks and the LVB-Hølonda terrane (Paper I). In Paper II we elaborate this connection and also include the Trollhøtta and Støren basalts based on their geochemical and lithological similarities. This is also in line with the work done by Stokke et al. (2018, supplementary material A). The basaltic rocks probably extruded within a marginal basin spanning at least 100-150 km, proximal to a continental landmass. The Trollhøtta and Støren basaltic rocks extruded in basins volumetrically dominated by turbiditic, siliciclastic rocks, i.e. a deep-marine setting, in contrast to the limestone and shale deposited in the Hølonda area, which probably reflect a shallow- to intermediate shelf location (e.g. Grenne and Roberts, 1998).

Within the Scandinavian Caledonides, latest Cambrian to Early Ordovician rocks formed in a marginal basin or arc setting are preserved along large parts of the orogen, from Lyngen in the north to Karmøy in the southwest (Fig. 5B). In several of these areas, e.g. in Karmøy, Siggjo and Stord (Fig. 5B), ophiolite formation was soon followed by renewed marginal basin and arc magmatism, similar to the evolution of the LVB-Hølonda–Støren–Trollhøtta system which we present in Papers I and II. The continental arc-related magmatism in Stord and Siggjo also overlaps in age with the Trollhøtta–Kinna rocks, and ranges from basaltic to intermediate and

felsic magmatism (Pedersen and Dunning, 1997). Although contemporaneous rocks that formed in arc- or marginal basin settings are common, it should be pointed out that rocks of a comparable bimodal character, with MORB-like basaltic and extremely enriched intermediate to felsic rocks, are not described from elsewhere in the Scandinavian Caledonides.

Several ophiolite and arc rocks of latest Cambrian to Early Ordovician age are also preserved in the Appalachians and British/Irish Caledonides where they are constituents of the Taconian and Grampian orogens, respectively (Fig. 5A). The most comparable units overlap in age with the Trollhøtta–Kinna rocks and share some lithological and geochemical features with the latter: The Tyrone Volcanic Group (Northern Ireland) consists of a combination of depleted island-arc tholeiites and relatively LREE-enriched MORB (Hollis et al., 2012), though the enrichment is far below the levels seen in the Kinna volcanic succession.

The Lloyds River ophiolite complex within the Annieopsquotch accretionary tract, Newfoundland, is of similar age to the Trollhøtta – Kinna basin and contains a combination of MORB and rocks enriched in Th and LREE (Lissenberg et al., 2005), although less enriched than the Kinna-type rocks. Interestingly, the Annieopsquotch accretionary tract also hosts the only described Taconian/Grampian rock unit with Th-LREE enrichments comparable to the Kinna volcanic succession; the shoshonitc 464–462 Ma Portage Lake monzogabbro (Lissenberg et al., 2005). It is chemically similar to the least-enriched Kinna rocks and the Hølonda Porphyrites, and is interpreted as representing melting of metasomatised mantle during slab break-off (Lissenberg et al., 2005) similar to our interpretation of the enriched rocks in the Opppdal area. The overlapping age and similar chemistry does not imply that the Lloyds River ophiolite complex and Portage Lake monzogabbro are directly related to the Trollhøtta – Kinna basin, but rather indicate that similar processes of mantle metasomatism and possibly slab break-off induced melting shortly after ophiolite obduction were active at multiple locations along the Laurentian margin.

The Skuggliberga unit represents a renewed phase of sediment deposition and arc-related volcanism, after deformation of the underlying Trollhøtta and Skarvatnet units. The detrital zircon signature of the Skuggliberga unit indicates deposition after c. 455 Ma; the age of the unit is constrained by the underlying units and the 435 Ma intrusive Innset massif. This assumed depositional age is similar to the presumed age of parts of the Ekne Group in the northern part of central Norway (Fig. 7), however, the Ekne Group sedimentation was deep-marine, probably continued until c. 427 Ma and does not contain any volcanic rocks (Roberts et al., 2019), so there is no direct correlation. The Vikafjord Group in southwestern Norway (Bømlo/Siggjo, Fig. 5B) is contemporaneous with the estimated age for Skuggliberga, it is

deposited unconformably on arc-rocks of similar age to the Trollhøtta and Skarvatnet units, and contains calc-alkaline volcanic rocks (Nordås et al., 1985). We consider the Vikafjord Group to be the closest analogy of the Skuggliberga unit.

The Skuggliberga unit was deposited on the folded and eroded Skarvatnet and Trollhøtta units, indicating the presence of a deformation phase between the 480-470 Ma formation of the Skarvatnet and Trollhøtta units and deposition of the Skuggliberga unit. This orogenic phase is represented by deformation phases D_1 and D_2 of Stokke et al. (2018). Constraining the age of this deformation phase is hampered by the uncertain depositional age of the Skuggliberga unit; but assuming a depositional age of c. 450–435 Ma, the deformation phase must have happened between c. 470 and 450 Ma. Arc-related magmatism was extensive along the Laurentian margin from around 480–424 Ma (e.g. Yoshinobu et al., 2002; Barnes et al., 2011), and is preserved along the coastal area of central Norway and in northern Norway. Arc-related, extrusive rocks from around 450–435 Ma are rare in the Scandinavian Caledonides and no direct correlatives can be found, but we suggest that the Skuggliberga volcanic rocks are an extrusive part of the extensive arc-related magmatism that was active during this time interval.

5.4 Extremely enriched magmatism along the Iapetus margin

Formation of the Trollhøtta basin with MORB-like basaltic rocks and the enriched volcanism of Kinna and Storgruvpiken happened around 480-470 Ma, i.e., shortly after obduction of the LVB ophiolite. Such a line of events fits well with the general narrative of repeated events of basin- and arc-formation and accretion, similar to what is described from southwestern Norway, the Appalachians and the Irish/British Caledonides, but adds an interesting aspect to the story. We suggest that the Kinna volcanic succession formed over a “dying” subduction zone by partial melting of metasomatised mantle. In this setting, asthenospheric upwelling after slab retreat (or possibly slab break-off) could cause partial mantle melting, in contrast to the normal subduction-related arc magmatism suggested for rocks of similar age in for instance southwestern Norway.

As discussed in chapter 1.1, mass transfer in subduction zones is a complex process where volatiles and fluid mobile elements are easily mobilised and migrate from the slab to the mantle, while transfer of immobile elements requires a certain degree of slab melting. “Normal” arc rocks are sourced in the mantle wedge where volatiles from the slab cause the mantle to partially melt and the slab component contributes to the “arc signature”. Formation of extremely enriched, potassic mantle-derived rocks commonly takes place in within-plate settings or (micro)continent-continent collision zones. There, partial melting of subducted continental-derived material and metasomatic reaction between this melt and the mantle

rocks lead to anomalous mantle domains capable of producing potassic rocks with an extreme enrichment in incompatible elements. The magma generation is commonly associated with slab roll-back or break-off, initial collapse or lithospheric delamination after subduction (e.g. Pe-Piper et al., 2009; Cheng and Guo, 2017). Although such rocks are relatively rare, they have received considerable attention (especially in the Alpine-Himalayan system) since they provide valuable insight into slab-to-mantle mass transfer processes.

The presence of such potassic, extremely enriched rocks in the Scandinavian Caledonides is interesting for several reasons. The presence of such rocks attests to a hitherto undescribed magmatic phase in the Caledonides, possibly recording slab break-off after obduction of the LVB ophiolite. Also, the co-existence of extremely enriched and MORB-like rocks is highly unusual, and probably implies that the post-obduction extension was stronger compared to similar potassic-rock forming events along e.g. the Mediterranean. It also opens up the possibility that rocks belonging to this suite can be found elsewhere along the Caledonides and Appalachians, which could help in correlating events and units across the orogen.

5.5 A note on the use of detrital zircon ages and maximum depositional age

Detrital zircon studies are widely used for constraining maximum depositional ages (MDA) of sedimentary successions, especially where the biostratigraphic record is poor or dateable volcanic horizons are absent (Dickinson and Gehrels, 2009; Coutts et al., 2019). MDA can be calculated using several methods, such as youngest single grain (YSG), a weighted mean of the youngest grain cluster composed of three or more grains that overlap at 2σ (YGC 2σ), or the youngest graphical peak (YPP), these and other methods are summaried in Coutts et al. (2019). Some authors, e.g. Spencer et al. (2016), recommend that the YGC 2σ method should only be used when the zircon grains formed during one single event of zircon growth, for instance in a volcaniclastic deposit. This is commonly not the case for detrital zircon, and other methods should be used for MDA calculations. According to Coutts et al. (2019) the YSG is the most widely used method for estimating MDA, a method which according to Dickinson and Gehrels (2009) produced MDA younger than the true depositional age in 15% of their 58 Mesozoic samples with depositional age constrained by biostratigraphy. This is well exemplified in Papers II and III, where we present detrital zircon age data which provide unreliably young estimates for MDA, although we have applied a rigorous discordance filter with only grains less than 5% discordant included in the MDA calculations. In the cases reported from Papers II and III, the depositional age is limited by the U-Pb TIMS ages of an overlying volcanic rock or an intrusion, respectively, while the YSG and (for some samples) the YGC 2σ are younger than these magmatic ages. We suggest that these spurious young ages

result from concealed lead loss possibly caused by recrystallisation of zircon domains in the thermal aureole of the 435 Ma Innset massif, or during the c. 416 Ma regional greenschist facies metamorphism. Although there is no doubt that detrital zircon provides useful information about probable depositional age and the composition of the source area, it must be stressed that detrital zircon data should be combined with data from other methods which provide a context for interpretation.

6 Concluding remarks and recommendations for future research

This work has provided a large, new dataset on the geology of the structurally higher nappes in the Oppdal area, which is useful for correlations and improved understanding of the Caledonian orogeny. We have defined three separate lithostratigraphic units, shown the existence of a large volcano-sedimentary basin which probably correlates with similar rocks further north, and constrained the age of this basin to c. 480–470 Ma. We have also reported the first potassic- to ultrapotassic, extremely enriched volcanic rocks in the Caledonides similar to those in the Alpine-Himalayan orogenic belt, which suggests that such rocks also can form subsequent to arc-continent collisional settings. Additionally, we have for the first time described Late Ordovician, extrusive arc-related rocks in the central Scandinavian Caledonides.

The extremely enriched volcanic rocks are the first reported rocks with such peculiar chemistry in the Scandinavian Caledonides, and deserve more attention. It could be interesting to use geochemical modelling in an attempt to constrain the initial melt composition, and Sr–Nd–Pb isotope data to further investigate the mantle source and the continental component we assume to have metasomatically altered the mantle. Also, the presence of such rocks in the Oppdal area opens up the possibility that similar rocks are present elsewhere in the Caledonides and Appalachians, and could in general be more common in accretional and collisional systems than previously known.

In this work it is also pointed out that there might be an unnamed unit present between the Trollhøtta unit and the Gula Nappe. This zone needs further examination; more geochronological, geochemical and structural data is required to confirm its presence and significance. The transition to the Gula Nappe is also not well described or understood, nor is the nature of the Gula Nappe. Perhaps the key to understanding the evolution of the Caledonian orogeny is hidden somewhere within the Gula Nappe?

7 Other contributions

7.1 Co-author papers

Ella W. Stokke, Deta Gasser, Bjørgunn H. Dalslåen and Tor Grenne. «*Tectonic evolution of syn- to late-orogenic sedimentary–volcanic basins in the central Norwegian Caledonides*». Journal of the Geological Society, 175, 605-618, 2018. https://doi.org/10.1144/jgs2017-091 This paper is included in the Supplementary material to this thesis.

Malin Andersson, Ola A. Eggen, Deta Gasser, Clemens Reimann, Fredrik Høgaas and Bjørgunn H. Dalslåen. «*Fifty-one chemical elements in till from the Oppdal region, Mid-Norway: relation to mineralization, Quaternary and bedrock geology*». Geochemistry: Exploration, Environment, Analysis, 18, 229-240, 2018. https://doi.org/10.1144/geochem2017-096

7.2 Conference proceedings

Dalslåen, B. H., Gasser, D., Grenne, T., Augland, L. E., Corfu, F. and Andresen, A. (2018) *Chemistry, age and tectonic evolution of the western Trondheim Nappe Complex in the Oppdal area, Central Norway*. Nordic geologic winter meeting; oral presentation.

Gasser, D., Grenne, T., Dalslåen, B., Corfu, F., Augland, L. E., Bøe, R. and Slagstad, T. (2019). *Contemporaneous MORB-type and extremely enriched volcanic rocks in the central Scandinavian Caledonides: the effect of slab break-off after arc-continent collision and/or subduction initiation after polarity flip?* EGU, oral presentation

Dalslåen, B. H., Gasser, D., Grenne, T., Augland, L. E. and Corfu, F. (2019) *The origin of Th-enriched volcanic rocks in Oppdal, central Norwegian Caledonides – implications for the evolution of Ordovician arc magmatism.* NGF winter meeting, oral presentation.

Dalslåen, B. H., Gasser, D., Grenne, T., Andresen, A., Augland, L. E. And Corfu, F. (2020) *Tectonic evolution of Ordovician-Silurian rocks in the Oppdal area, southern Trondheim Nappe Complex*. Nordic geologic winter meeting; poster presentation.

7.3 Public outreach

Dalslåen, B.H. (2018) *Kinna – Mitt geofunn*. Geo (Norwegian popular scientfic geological magazine)

Gasser, D., Grenne, T. and Dalslåen, B. H. (2019)
https://www.geoforskning.no/nyheter/grunnforskning/2029-i-berget-det-bla (Entry in Aftenposten and geoforskning.no popular science competition)

8 References

Andersen, T. B., Corfu, F., Labrousse, L. and Osmundsen, P.-T., 2012, Evidence for hyperextension along the pre-Caledonian margin of Baltica: Journal of the Geological Society, v. 169, no. 5, p. 601-612.

Andersen, T. B., Jamtveit, B., Dewey, J. F. and Swensson, E., 1991, Subduction and eduction of continental crust: Major mechanisms during continent-continent collision and orogenic extensional collapse, a model based on the south Norwegian Caledonides: Terra Nova, v. 3, no. 3, p. 303-310.

Andréasson, P.-G., Svenningsen, O. M. and Albrecht, L., 1998, Dawn of Phanerozoic orogeny in the North Atlantic tract; evidence from the Seve-Kalak superterrane, Scandinavian Caledonides: Geologiska Föreningen i Stockholm Förhandlingar, v. 120, no. 2, p. 159-172.

Augland, L. E., Andresen, A., Corfu, F., Simonsen, S. L. and Andersen, T., 2012, The Beiarn nappe complex: a record of Laurentian Early Silurian arc magmatism in the Uppermost Allochthon, Scandinavian Caledonides: Lithos, v. 146, p. 233-252.

Augland, L. E., Andresen, A., Gasser, D. and Steltenpohl, M. G., 2014, Early Ordovician to Silurian evolution of exotic terranes in the Scandinavian Caledonides of the Ofoten–Troms area–terrane characterization and correlation based on new U–Pb zircon ages and Lu–Hf isotopic data: Geological Society, London, Special Publications, v. 390, p. SP390. 319.

Barnes, C. G., Frost, C. D., Yoshinobu, A. S., McArthur, K., Barnes, M. A., Allen, C. M., Nordgulen, Ø. and Prestvik, T., 2007, Timing of sedimentation, metamorphism, and plutonism in the Helgeland Nappe Complex, north-central Norwegian Caledonides: Geosphere, v. 3, no. 6, p. 683-703.

Barnes, C. G., Reid, K., Frost, C. D., Barnes, M. A., Allen, C. M. and Yoshinobu, A. S., 2011, Ordovician and Silurian magmatism in the Upper Nappe, Uppermost Allochthon, Helgeland Nappe Complex, north-central Norway: Norwegian Journal of Geology, v. 91, no. 3, p. 121-136.

Be'eri-Shlevin, Y., Gee, D., Claesson, S., Ladenberger, A., Majka, J., Kirkland, C., Robinson, P. and Frei, D., 2011, Provenance of Neoproterozoic sediments in the Särv nappes (Middle Allochthon) of the Scandinavian Caledonides: LA-ICP-MS and SIMS U–Pb dating of detrital zircons: Precambrian Research, v. 187, no. 1-2, p. 181-200.

Bebout, G. E. and Penniston-Dorland, S. C., 2016, Fluid and mass transfer at subduction interfaces—The field metamorphic record: Lithos, v. 240, p. 228-258.

Bingen, B. and Demaiffe, D., 1999, Geochemical signature of the Egersund basaltic dyke swarm, SW Norway, in the context of late-Neoproterozoic opening of the Iapetus Ocean: Norsk geologisk tidsskrift, v. 79, no. 2, p. 69-86.

Bruton, D. L. and Bockelie, J. F., 1980, Geology and paleontology of the Hølonda area, western Norway—A fragment of North America: The Caledonides in the USA. Virginia Polytechnic Institute and State University, Department of Geological Sciences Memoir, v. 2, p. 41-47.

Chaloupsky, J., 1970, Geology of the Hoelonda-Hulsjoeen area, Trondheim region: Norges geologiske undersøkelse Bulletin, v. 266, p. 277-304.

Cheng, Z. and Guo, Z., 2017, Post-collisional ultrapotassic rocks and mantle xenoliths in the Sailipu volcanic field of Lhasa terrane, south Tibet: Petrological and geochemical constraints on mantle source and geodynamic setting: Gondwana Research, v. 46, p. 17-42.

Clift, P. D., Schouten, H. and Vannucchi, P., 2009, Arc-continent collisions, sediment recycling and the maintenance of the continental crust, *in* Cawood, P., and Kröner, A., eds., Earth Accretionary Systems in Space and Time, Volume 318, Geological Society, London, Special Publications, p. 75-103.

Conticelli, S., Guarnieri, L., Farinelli, A., Mattei, M., Avanzinelli, R., Bianchini, G., Boari, E., Tommasini, S., Tiepolo, M. and Prelević, D., 2009, Trace elements and Sr–Nd–Pb isotopes

of K-rich, shoshonitic, and calc-alkaline magmatism of the Western Mediterranean Region: genesis of ultrapotassic to calc-alkaline magmatic associations in a post-collisional geodynamic setting: Lithos, v. 107, no. 1-2, p. 68-92.

Conticelli, S. and Peccerillo, A., 1992, Petrology and geochemistry of potassic and ultrapotassic volcanism in central Italy: petrogenesis and inferences on the evolution of the mantle sources: Lithos, v. 28, no. 3-6, p. 221-240.

Corfu, F., 2013, A century of U-Pb geochronology: The long quest towards concordance: Geological Society of America Bulletin, v. 125, no. 1-2, p. 33-47.

Corfu, F., Andersen, T. and Gasser, D., 2014, The Scandinavian Caledonides: main features, conceptual advances and critical questions: Geological Society, London, Special Publications, v. 390, no. 1, p. 9-43.

Coutts, D. S., Matthews, W. A. and Hubbard, S. M., 2019, Assessment of widely used methods to derive depositional ages from detrital zircon populations: Geoscience Frontiers, v. 10, no. 4, p. 1421-1435.

Defant, M. J. and Drummond, M., 1990, Derivation of some modern arc magmas by melting of young subducted lithosphere: Nature, v. 347, no. 6294, p. 662-665.

Dickinson, W. R., 1970, Global tectonics: Science, p. 1250-1259.

Dickinson, W. R. and Gehrels, G. E., 2009, Use of U–Pb ages of detrital zircons to infer maximum depositional ages of strata: a test against a Colorado Plateau Mesozoic database: Earth and Planetary Science Letters, v. 288, no. 1-2, p. 115-125.

Dilek, Y. and Furnes, H., 2011, Ophiolite genesis and global tectonics: Geochemical and tectonic fingerprinting of ancient oceanic lithosphere: Geological Society of America Bulletin, v. 123, no. 3-4, p. 387-411.

Domeier, M., 2016, A plate tectonic scenario for the Iapetus and Rheic oceans: Gondwana Research, v. 36, p. 275-295.

Draut, A. E., Clift, P. D., Amato, J. M., Blusztajn, J. and Schouten, H., 2009, Arc–continent collision and the formation of continental crust: a new geochemical and isotopic record from the Ordovician Tyrone Igneous Complex, Ireland: Journal of the Geological Society, v. 166, no. 3, p. 485-500.

Dunning, G. and Pedersen, R., 1988, U/Pb ages of ophiolites and arc-related plutons of the Norwegian Caledonides: implications for the development of Iapetus: Contributions to Mineralogy and Petrology, v. 98, no. 1, p. 13-23.

Engvik, A. K., Grenne, T., Lutro, O. J. and Meyer, G. B., 2014, Metamorphic constraints on the Caledonian Upper Allochthon of Central Norway: the Gula Complex staurolite–garnet–kyanite mica schist: Geological Society, London, Special Publications, v. 390, no. 1, p. 563-581.

Faure, G. and Mensing, T.M. 2005: *Principles and applications*. John Wiley & Sons, Inc, Hoboken, New Jersey

Foley, S., 1992, Vein-plus-wall-rock melting mechanisms in the lithosphere and the origin of potassic alkaline magmas: Lithos, v. 28, no. 3-6, p. 435-453.

Furnes, H., Dilek, Y. and Pedersen, R. B., 2012, Structure, geochemistry, and tectonic evolution of trench-distal backarc oceanic crust in the western Norwegian Caledonides, Solund-Stavfjord ophiolite (Norway): Geological Society of America Bulletin, v. 124, no. 7-8, p. 1027-1047.

Förster, M. W., Prelević, D., Schmück, H. R., Buhre, S., Veter, M., Mertz-Kraus, R., Foley, S. F. and Jacob, D. E., 2017, Melting and dynamic metasomatism of mixed harzburgite+ glimmerite mantle source: Implications for the genesis of orogenic potassic magmas: Chemical Geology, v. 455, p. 182-191.

Gale, A., Dalton, C. A., Langmuir, C. H., Su, Y. and Schilling, J. G., 2013, The mean composition of ocean ridge basalts: Geochemistry, Geophysics, Geosystems, v. 14, no. 3, p. 489-518.

Gao, Y., Hou, Z., Kamber, B. S., Wei, R., Meng, X. and Zhao, R., 2007, Lamproitic rocks from a continental collision zone: evidence for recycling of subducted Tethyan oceanic sediments in the mantle beneath southern Tibet: Journal of Petrology, v. 48, no. 4, p. 729-752.

Gee, D., Guezou, J., Roberts, D. and Wolff, F., 1985, The central-southern part of the Scandinavian Caledonides: The Caledonide orogen-Scandinavia and related areas, v. 1, p. 109-133.

Gee, D. G., 1975, A tectonic model for the central part of the Scandinavian Caledonides: American Journal of Science, v. 275, no. A, p. 468-515.

Gee, D. G., 1981, The Dictyonema-bearing phyllites at Nordaunevoll, eastern Trøndelag, Norway: Norsk Geologisk Tidsskrift, v. 61, no. 1, p. 93-95.

Goldschmidt, V. M., 1916, Geologisch-Petrographische Studien im Hochgebirge des Südlischen Norwegens. IV Überschit der Eruptivgesteine im Kaledonishen Gebirge Zwischen Stavanger und Trondhjem: Skr. Vidensk.-Selsk. Christiania I. Mat-naturv. Kl.no. 2, v. 2, p. 140.

Green, T. H. and Ringwood, A., 1968, Genesis of the calc-alkaline igneous rock suite: Contributions to Mineralogy and Petrology, v. 18, no. 2, p. 105-162.

Grenne, T., 1989, Magmatic evolution of the Løkken SSZ Ophiolite, Norwegian Caledonides: Relationships between anomalous lavas and high-level intrusions: Geological Journal, v. 24, no. 4, p. 251-274.

Grenne, T., Ihlen, P. and Vokes, F., 1999, Scandinavian Caledonide metallogeny in a plate tectonic perspective: Mineralium Deposita, v. 34, no. 5-6, p. 422-471.

Grenne, T. and Lagerblad, B., 1985, The Fundsjø Group, central Norway—a Lower Paleozoic island arc sequence: geochemistry and regional implications: The Caledonide orogen-Scandinavia and related areas, p. 745-760.

Grenne, T. and Roberts, D., 1980, Geochemistry and volcanic setting of the Ordovician Forbordfjell and Jonsvatn greenstones, Trondheim region, central Norwegian Caledonides: Contributions to Mineralogy and Petrology, v. 74, no. 4, p. 375-386.

Grenne, T. and Roberts, D., 1998, The Hølonda Porphyrites, Norwegian Caledonides: geochemistry and tectonic setting of Early–Mid-Ordovician shoshonitic volcanism: Journal of the Geological Society, v. 155, no. 1, p. 131-142.

Hacker, B. R., Andersen, T. B., Johnston, S., Kylander-Clark, A. R., Peterman, E. M., Walsh, E. O. and Young, D., 2010, High-temperature deformation during continental-margin subduction & exhumation: The ultrahigh-pressure Western Gneiss Region of Norway: Tectonophysics, v. 480, no. 1-4, p. 149-171.

Handke, M., Tucker, R. and Robinson, P., 1995, Contrasting U–Pb ages for the Risberget Augen Gneiss in the Norwegian Caledonides: getting to the root of the problem, *in* Proceedings Geological Society of America Abstracts with Programs, Volume 27.

Hawkesworth, C., Gallagher, K., Hergt, J. and McDermott, F., 1993, Mantle and slab contributions in arc magmas: Annual Review of Earth and Planetary Sciences, v. 21, no. 1, p. 175-204.

Heim, M., Grenne, T. and Prestvik, T., 1987, The Resfjell ophiolite fragment, southwest Trondheim region, central Norwegian Caledonides: Norges geologiske undersøkelse Bulletin, v. 409, p. 49-71.

Hermann, J. and Rubatto, D., 2009, Accessory phase control on the trace element signature of sediment melts in subduction zones: Chemical Geology, v. 265, no. 3-4, p. 512-526.

Hollis, S. P., Roberts, S., Cooper, M. R., Earls, G., Herrington, R., Condon, D. J., Cooper, M. J., Archibald, S. M. and Piercey, S. J., 2012, Episodic arc-ophiolite emplacement and the growth of continental margins: Late accretion in the Northern Irish sector of the Grampian-Taconic orogeny: Bulletin, v. 124, no. 11-12, p. 1702-1723.

Hollocher, K., Robinson, P., Seaman, K. and Walsh, E., 2016, Ordovician–early Silurian intrusive rocks in the northwest part of the Upper Allochthon, mid-Norway: Plutons of an Iapetan volcanic arc complex: American Journal of Science, v. 316, no. 10, p. 925-980.

Holmsen, P., 1955, Trekk av Opdalsfeltets geologi: Norsk Geologisk Tidsskrift, v. 35, p. 135-150.

Jakob, J., Andersen, T. B. and Kjøll, H. J., 2019, A review and reinterpretation of the architecture of the South and South-Central Scandinavian Caledonides—A magma-poor to magma-rich

transition and the significance of the reactivation of rift inherited structures: Earth-science reviews, v. 192, p. 513-528.
Kessel, R., Schmidt, M. W., Ulmer, P. and Pettke, T., 2005, Trace element signature of subduction-zone fluids, melts and supercritical liquids at 120–180 km depth: Nature, v. 437, no. 7059, p. 724-727.
Kjøll, H. J., Andersen, T. B., Corfu, F., Labrousse, L., Tegner, C., Abdelmalak, M. M. and Planke, S., 2019, Timing of Breakup and Thermal Evolution of a Pre-Caledonian Neoproterozoic Exhumed Magma-Rich Rifted Margin: Tectonics, v. 38, no. 6, p. 1843-1862.
Klonowska, I., Majka, J., Janák, M., Gee, D. G. and Ladenberger, A., 2014, Pressure–temperature evolution of a kyanite–garnet pelitic gneiss from Åreskutan: evidence of ultra-high-pressure metamorphism of the Seve Nappe Complex, west-central Jämtland, Swedish Caledonides: Geological Society, London, Special Publications, v. 390, no. 1, p. 321-336.
Krill, A. G., 1980, Tectonics of the Oppdal area, central Norway: Geologiska Föreningen i Stockholm Förhandlingar, v. 102, no. 4, p. 523-530.
Krill, A. G., 1985, Relationships between the Western Gneiss Region and the Trondheim Region : Stockwerk-tectonics reconsiderd, *in* Gee, D., and Sturt, B., eds., The Caledonide Orogen - Scandinavia and Related Areas, John Wiley & Sons Ltd, p. 475-483.
Krill, A. G., 1987, Berggrunnskart Snøhetta 15194, scale 1:50 000.
Krupp, R. and Krupp, G., 1985, Geological setting of the Tverrfjell copper/zinc deposit, Central Norway: Geologische Rundschau, v. 74, no. 3, p. 467-482.
Kushiro, I., 1973, Origin of some magmas in oceanic and circum-oceanic regions: Tectonophysics, v. 17, no. 3, p. 211-222.
Labrousse, L., Hetényi, G., Raimbourg, H., Jolivet, L. and Andersen, T. B., 2010, Initiation of crustal-scale thrusts triggered by metamorphic reactions at depth: Insights from a comparison between the Himalayas and Scandinavian Caledonides: Tectonics, v. 29, no. 5.
Li, Z.-X., Bogdanova, S., Collins, A., Davidson, A., De Waele, B., Ernst, R., Fitzsimons, I., Fuck, R., Gladkochub, D. and Jacobs, J., 2008, Assembly, configuration, and break-up history of Rodinia: a synthesis: Precambrian research, v. 160, no. 1-2, p. 179-210.
Lissenberg, C. J., Zagorevski, A., McNicoll, V. J., van Staal, C. R. and Whalen, J. B., 2005, Assembly of the Annieopsquotch accretionary tract, Newfoundland Appalachians: Age and geodynamic constraints from syn-kinematic intrusions: The Journal of Geology, v. 113, no. 5, p. 553-570.
Manning, C. E., 2004, The chemistry of subduction-zone fluids: Earth Planetary Science Letters, v. 223, no. 1-2, p. 1-16.
Marschall, H. R. and Schumacher, J. C., 2012, Arc magmas sourced from mélange diapirs in subduction zones: Nature Geoscience, v. 5, no. 12, p. 862.
Neuman, R. B. and Bruton, D. L., 1974, Early middle Ordovician fossils from the Hølonda area, Trondheim region, Norway.: Norsk geologisk tidsskrift, v. 54, no. 1, p. 69-115.
Nilsen, O., Sundvoll, B., Roberts, D. and Corfu, F., 2003, U-Pb geochronology and geochemistry of trondhjemites and a norite pluton from the SW Trondheim Region, Central Norwegian Caledonides: NORGES GEOLOGISKE UNDERSOKELSE, v. 441, p. 5-16.
Nilsen, O. and Wolff, F. C., 1989, Røros og Sveg. Berggrunnskart Røros og Sveg M 1:250000: Norges Geologiske Undersøkelse.
Nordås, J., Amaliksen, K., Brekke, H., Suthern, R., Furnes, H., Sturt, B., Robins, B. and Gee, D., 1985, Lithostratigraphy and petrochemistry of Caledonian rocks on Bømlo, SW Norway, The Caledonide Orogen—Scandinavia and Related Areas: New York, John Wiley & Sons Ltd, p. 679-692.
Nystuen, J. P., Andresen, A., Kumpulainen, R. A. and Siedlecka, A., 2008, Neoproterozoic basin evolution in Fennoscandia, East Greenland and Svalbard: Episodes, v. 31, no. 1, p. 35-43.
Pe-Piper, G., Piper, D. J., Koukouvelas, I., Dolansky, L. M. and Kokkalas, S., 2009, Postorogenic shoshonitic rocks and their origin by melting underplated basalts: The Miocene of Limnos, Greece: Geological Society of America Bulletin, v. 121, no. 1-2, p. 39-54.

Peacock, S. M., 1996, Thermal and petrologic structure of subduction zones, *in* Bebout, G. E., Scholl, D. H., Kirby, S. P. and Platt, J., eds., Subduction: Top to Bottom. Geophysical Monographs Volume 96: Washington, D.C., American Geophysical Union, p. 119-133.

Pearce, J. A. and Stern, R. J., 2006, Origin of back-arc basin magmas: trace element and isotope perspectives: Geophysical Monograph-American Geophysical Union, v. 166, p. 63.

Peccerillo, A., 1999, Multiple mantle metasomatism in central-southern Italy: geochemical effects, timing and geodynamic implications: Geology, v. 27, no. 4, p. 315-318.

Pedersen, R.-B., Furnes, H. and Dunning, G., 1991, A U/Pb age for the Sulitjelma Gabbro, North Norway: further evidence for the development of a Caledonian: Geological Magazine, v. 128, no. 2, p. 141-153.

Pedersen, R. and Furnes, H., 1991, Geology, magmatic affinity and geotectonic environment of some Caledonian ophiolites in Norway: Journal of Geodynamics, v. 13, no. 2-4, p. 183-203.

Pedersen, R. B, and Dunning, G. R., 1997, Evolution of arc crust and relations between contrasting sources: U-Pb (age), Nd and Sr isotope systematics of the ophiolitic terrain of SW Norway: Contributions to Mineralogy and Petrology, v. 128, no. 1, p. 1-15.

Plank, T. and Langmuir, C. H., 1998, The chemical composition of subducting sediment and its consequences for the crust and mantle: Chemical geology, v. 145, no. 3, p. 325-394.

Prelević, D., Jacob, D. E. and Foley, S. F., 2013, Recycling plus: a new recipe for the formation of Alpine–Himalayan orogenic mantle lithosphere: Earth and Planetary Science Letters, v. 362, p. 187-197.

Reymer, A. and Schubert, G., 1984, Phanerozoic addition rates to the continental crust and crustal growth: Tectonics, v. 3, no. 1, p. 63-77.

Roberts, D. and Gee, D., 1985, An introduction to the structure of the Scandinavian Caledonides: The Caledonide orogen–Scandinavia and related areas, v. 1, p. 55-68.

Roberts, D., Morton, A. and Frei, D., 2019, A Silurian age for the metasedimentary rocks of the Ekne Group, Trøndelag, Mid-Norwegian Caledonides: and inferences for a peri-Laurentian provenance: Norsk Geologisk Tidsskrift, v. 99, no. 4.

Rohr-Torp, E., 1972, A major inversion of the western part of the Trondheim nappe: Norsk Geologisk Tidsskrift, v. 52, p. 453-458.

Rohr-Torp, E., 1974, Contact metamorphism around the Innset massif: Norsk Geologisk Tidsskrift, v. 54, p. 13-33.

Root, D. and Corfu, F., 2012, U–Pb geochronology of two discrete Ordovician high-pressure metamorphic events in the Seve Nappe Complex, Scandinavian Caledonides: Contributions to Mineralogy and Petrology, v. 163, no. 5, p. 769-788.

Schaen, A. J., Jicha, B. R., Hodges, K. V., Vermeesch, P., Stelten, M. E., Mercer, C. M., Phillips, D., Rivera, T. A., Jourdan, F. and Matchan, E. L., 2020, Interpreting and reporting 40Ar/39Ar geochronologic data: Geological Society of America Bulletin.

Slagstad, T., Anderson, M., Saalmann, K. and Hagen-Peter, G., 2020, The >494 Ma Lillevik ophiolite fragment (Gratangseidet Igneous Complex) near Narvik, Scandinavian Caledonides.: Norwegian Journal of Geology, v. 100, no. 202022.

Slagstad, T. and Kirkland, C. L., 2018, Timing of collision initiation and location of the Scandian orogenic suture in the Scandinavian Caledonides: Terra Nova, v. 30, no. 3, p. 179-188.

Slagstad, T., Pin, C., Roberts, D., Kirkland, C. L., Grenne, T., Dunning, G., Sauer, S. and Andersen, T., 2014, Tectonomagmatic evolution of the Early Ordovician suprasubduction-zone ophiolites of the Trondheim Region, Mid-Norwegian Caledonides: Geological Society, London, Special Publications, v. 390.

Soder, C. G. and Romer, R. L., 2018, Post-collisional potassic–ultrapotassic magmatism of the Variscan Orogen: implications for mantle metasomatism during continental subduction: Journal of Petrology, v. 59, no. 6, p. 1007-1034.

Spandler, C. and Pirard, C., 2013, Element recycling from subducting slabs to arc crust: A review: Lithos, v. 170, p. 208-223.

Spencer, C. J., Kirkland, C. L. and Taylor, R. J., 2016, Strategies towards statistically robust interpretations of in situ U–Pb zircon geochronology: Geoscience Frontiers, v. 7, no. 4, p. 581-589.

Stephens, M. B., 2020, Upper and uppermost thrust sheets in the Caledonide orogen, Sweden: outboard oceanic and exotic continental terranes, *in* Stephens, M. and Bergman Weihed, J., eds., Sweden: Lithotectonic Framework, Tectonic Evolution and Mineral Resources, Volume 50: London, Geological Society, Memoirs, p. 549-575.

Stern, R. J., 2002, Subduction zones: Reviews of geophysics, v. 40, no. 4, p. 3-1-3-38.

Stern, R. J. and Gerya, T., 2018, Subduction initiation in nature and models: A review: Tectonophysics, v. 746, p. 173-198.

Stokke, E. W., Gasser, D., Dalslåen, B. H. and Grenne, T., 2018, Tectonic evolution of syn-to late-orogenic sedimentary–volcanic basins in the central Norwegian Caledonides: Journal of the Geological Society, v. 175, no. 4, p. 605-618.

Sun, S.-S. and McDonough, W.-s., 1989, Chemical and isotopic systematics of oceanic basalts: implications for mantle composition and processes: Geological Society, London, Special Publications, v. 42, no. 1, p. 313-345.

Syracuse, E. M., van Keken, P. E. and Abers, G. A., 2010, The global range of subduction zone thermal models: Physics of the Earth Planetary Interiors, v. 183, no. 1-2, p. 73-90.

Tatsumi, Y., 1989, Migration of fluid phases and genesis of basalt magmas in subduction zones: Journal of Geophysical Research: Solid Earth, v. 94, no. B4, p. 4697-4707.

Tera, F., Brown, L., Morris, J., Sacks, I. S., Klein, J. and Middleton, R., 1986, Sediment incorporation in island-arc magmas: Inferences from 10Be: Geochimica et Cosmochimica Acta, v. 50, no. 4, p. 535-550.

Tucker, R. D., Robinson, P., Solli, A., Gee, D. G., Thorsnes, T., Krogh, T. E., Nordgulen, Ø. and Bickford, M., 2004, Thrusting and extension in the Scandian hinterland, Norway: New U-Pb ages and tectonostratigraphic evidence: American Journal of Science, v. 304, no. 6, p. 477-532.

van Staal, C. R., Whalen, J. B., Valverde-Vaquero, P., Zagorevski, A. and Rogers, N., 2009, Pre-Carboniferous, episodic accretion-related, orogenesis along the Laurentian margin of the northern Appalachians: Geological Society, London, Special Publications, v. 327, no. 1, p. 271-316.

Vogt, T., 1945, The geology of part of the Hølonda-Horg district, a type area in the Trondheim region: Norsk Geologisk Tidsskrift, v. 25, p. 449-528.

Wilson, J. T., 1966, Did the Atlantic close and then re-open?: Nature, v. 211, no. 5050, p. 676-681.

Wolff, F., 1979, Beskrivelse til de berggrunnsgeologiske kart Trondheim og Østersund 1:250 000: NGU Skrifter, v. 353, p. 1-76.

Wyllie, P. J. and Sekine, T., 1982, The formation of mantle phlogopite in subduction zone hybridization: Contributions to Mineralogy and Petrology, v. 79, no. 4, p. 375-380.

Yoshinobu, A. S., Barnes, C. G., Nordgulen, Ø., Prestvik, T., Fanning, M. and Pedersen, R., 2002, Ordovician magmatism, deformation, and exhumation in the Caledonides of central Norway: An orphan of the Taconic orogeny?: Geology, v. 30, no. 10, p. 883-886.

Paper I

I

Lithos 356–357 (2020) 105372

Contents lists available at ScienceDirect

Lithos

journal homepage: www.elsevier.com/locate/lithos

Research Article

Ordovician shoshonitic to ultrapotassic volcanism in the central Norwegian Caledonides: The result of sediment subduction, mantle metasomatism and mantle partial melting

B.H. Dalslåen [a,*], D. Gasser [b,c], T. Grenne [c], L.E. Augland [d], F. Corfu [a]

[a] Department of Geosciences, University of Oslo, Oslo, Norway
[b] Department of Environmental Sciences, Western Norway University of Applied Sciences, Sogndal, Norway
[c] Geological Survey of Norway, Trondheim, Norway
[d] CEED, University of Oslo, Norway

ARTICLE INFO

Article history:
Received 23 August 2019
Received in revised form 7 January 2020
Accepted 9 January 2020
Available online 13 January 2020

Keywords:
Scandinavian Caledonides
Shoshonitic
Ultrapotassic
LREE enrichment
Beryllium
Thorium

ABSTRACT

Shoshonitic to ultrapotassic, mantle-derived volcanic rocks found within certain accretionary and collisional settings have trace element patterns comparable to those of common arc-related rocks, but with extreme enrichments in highly incompatible elements. Such rocks, previously unknown in the Scandinavian Caledonides, have been discovered in the Oppdal area in the Trondheim Nappe Complex, central Norway. The volcanic rocks are part of the Skarvatnet unit, which consists of (1) the Kinna volcanic succession, (2) the Storgruvpiken rhyolite, and (3) the Skaret conglomeratic succession. The Kinna volcanic succession is interpreted as consisting mainly of submarine pyroclastic flows. A trachytic bed from within this succession is dated to 474 ± 1 Ma. The Storgruvpiken rhyolite is interpreted as a shallow, subvolcanic intrusion or volcanic dome, and is dated to 470 ± 1 Ma. The Skaret conglomerates were deposited in a shallow-marine, tectonically active setting post-dating the Storgruvpiken rhyolite. The Kinna volcanic succession is highly enriched in Th, U, Pb and LREE, with trace element signatures remarkably similar to high-K to ultrapotassic rocks of the Alpine-Himalayan and other orogenic belts. By analogy with these recent examples, the Kinna volcanic succession is interpreted as the result of a two-stage process: (1) subduction and partial melting of continent-derived material caused extensive metasomatism of the overlying mantle wedge, (2) partial melting of this heterogeneous mantle source produced the highly enriched mantle melts. The Storgruvpiken rhyolite, particularly enriched in beryllium, is interpreted as the result of partial melting of Kinna-type rocks at depth. The Skarvatnet unit is interpreted as the result of a complex tectonic evolution at the margin of the Iapetus Ocean, involving the following stages: (1) intra-oceanic subduction, producing the Løkken-Vassfjellet-Bymarka ophiolite at 487–480 Ma, followed by (2) the arrival of the Laurentian margin or an associated micro-continent at ca. 480 Ma, leading to the subduction of large amounts of continent-derived material and subsequent metasomatism of the overlying mantle wedge, (3) arc-continent-collision and slab retreat/slab break-off, causing an intermittent phase of mantle-derived, highly enriched magmatism preserved as the Kinna volcanic succession and the Storgruvpiken rhyolite at 475–470 Ma.

1. Introduction

Magmatism above subduction zones is important for the growth of the continental crust and for refining its chemistry. This complex geological environment produces abundant highly evolved plutonic and volcanic rocks. Magmatic rocks with intermediate SiO_2 contents, primarily andesitic rocks, are considered to be the hallmark of subduction zone magmatism, while they are relatively rare in other geological settings. Typically, arc-related andesites are relatively enriched in large ion lithophile elements (LILE, e.g. K, Rb, Ba), light rare earth elements (LREE) and certain high field strength elements (HFSE) such as Th and U, with abundances commonly on the order of 10–100 x primitive mantle. These enrichments are generally accompanied by negative anomalies in Nb, Ta and Ti, with abundances of <10 x primitive mantle (e.g. Marschall and Schumacher, 2012; Pearce and Peate, 1995).

Some basaltic to intermediate volcanic rocks can be far more enriched in these incompatible elements (on the order of 100–1000 x primitive mantle), indicating a similar, but more extreme process of formation compared to the more common arc-related rocks. They are the product of potassic to ultrapotassic mantle-derived magmatism found in accretionary, collisional and post-collisional magmatic settings (e.g. Conticelli et al., 2009; Ersoy and Palmer, 2013; Peccerillo, 1999; Peccerillo and Martinotti, 2006).

* Corresponding author.
E-mail address: b.h.dalslaen@geo.uio.no (B.H. Dalslåen).

https://doi.org/10.1016/j.lithos.2020.105372

The enrichment of various elements in arc-related magmatic rocks is generally attributed to the transfer of these elements from subducted crustal material in the down-going slab into the overlying mantle, which then melts to produce arc magmas (e.g. Hermann and Rubatto, 2009; Plank and Langmuir, 1998; Spandler and Pirard, 2013; Tommasini et al., 2011). The details of such complex element transfers are still not fully understood and the budget for each of the enriched elements is probably controlled by several factors, including, e.g., the original composition of subducted sediments or continental crust, the type of reactions releasing fluids and partial melts from the subducting slab, the composition and mineralogy of the mantle and its reaction with the released fluids and melts, the mechanisms and degrees of partial melting of the mantle source and, ultimately, fractional crystallisation and assimilation processes during magma ascent.

In the case of extremely enriched, potassic to ultrapotassic mantle-derived rocks, a complex polyphase petrogenetic model is generally envisaged, with several stages of mantle metasomatism and enrichment prior to partial melting and magma formation (e.g. Conticelli et al., 2009; Peccerillo, 1999). This model involves K-rich melts or fluids derived from the subducted crustal material that react with the surrounding mantle to form plogophite-rich veins prior to partial melting. Mixing different proportions of magmas derived from the phlogopite-rich veins and the surrounding mantle might explain the range of observed rock types from ultrapotassic to shoshonitic and calk-alkaline (e.g. Foley, 1992a, 1992b; Förster et al., 2017). The mantle metasomatism is attributed to subduction processes, whereas the final partial melting of the enriched mantle is related to other tectonic processes such as slab roll-back and break-off, strike-slip faulting, or orogenic collapse and lithosphere delamination (e.g. Cheng and Guo, 2017; Ersoy and Palmer, 2013; Guo et al., 2014; Pe-Piper et al., 2009; Pérez-Valera et al., 2013; Prelević et al., 2008).

In this contribution we present field observations, geochemical and geochronological data from a hitherto unknown suite of Ordovician (c. 475–470 Ma) mafic, intermediate and felsic volcanic rocks from the Oppdal area in the central Scandinavian Caledonides (Fig. 1). These rocks have a geochemical signature that in many respects resembles that of typical arc settings, but with far stronger enrichments of elements like Th, U, Be and LREE, similar to potassic to ultrapotassic rocks of the Mediterranean area (e.g. Peccerillo, 1999). No similarly enriched, mafic to felsic volcanic rocks have been documented in the Scandinavian Caledonides so far. Younger, *syn*- to post-collisional (c. 430–400 Ma) shoshonitic and ultrapotassic rocks are documented by e.g. Thompson and Fowler (1986) from the Scottish Caledonides, and a c. 418 Ma ultrapotassic syenite is reported from the Appalachians (West et al., 2007). Similarly enriched rocks from the early, pre-collisional phase of Iapetus closure are extremely rare in the Caledonian orogen, with a c. 464–462 Ma shoshonitic monzogabbro in the Appalachians (Lissenberg et al., 2005) being the only described occurrence. Based on our new results we discuss potential petrogenetic models and tectonic implications for the subduction history of the Iapetus Ocean.

2. Geological setting

2.1. Subduction-related rocks within the central Scandinavian Caledonides

The Caledonian orogen represents a major continent-continent collision zone resulting from the closure of the Cambrian–Ordovician Iapetus Ocean and collision of the continents Laurentia and Baltica in Silurian times (e.g. Corfu et al., 2014; Roberts and Gee, 1985). Several subduction zones were probably active in the Iapetus Ocean, and volcanic rocks related to these subduction zones are preserved all along the orogenic belt (Fig. 1). The most prominent remnants of intra-oceanic Iapetus crust are Late Cambrian to Early Ordovician island-arc fragments and supra-subduction zone (SSZ) ophiolites (e. g. Grenne et al., 1999; Pedersen et al., 1992; Slagstad et al., 2014) (Fig. 1).

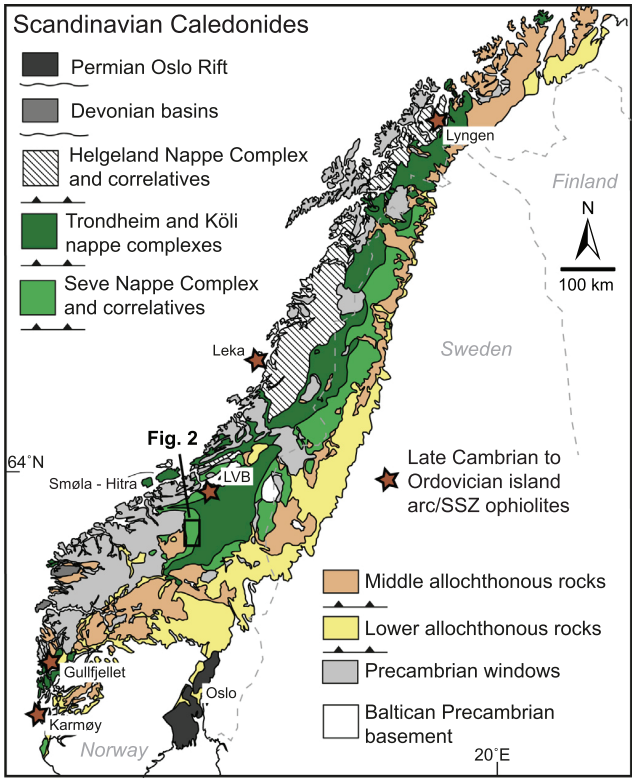

Fig. 1. Overview map of the Scandinavian Caledonides, with localities mentioned in the text.

The Trondheim Nappe Complex (TNC) of central Norway (Fig. 1) contains some of the best-preserved Iapetus-derived terranes within the Scandinavian Caledonides (Grenne et al., 1999; Slagstad et al., 2014). Within the western TNC, oceanic crust is represented by the 487 to 480 Ma Løkken–Vassfjellet–Bymarka (LVB) ophiolite fragments (Fig. 1), comprising gabbros, sheeted dykes and pillow lavas (Grenne et al., 1999; Slagstad et al., 2014). The LVB ophiolite is interpreted to have formed over an intra-oceanic subduction zone, and was obducted onto a continental margin between 478 Ma and 468 Ma as constrained by the last recorded magmatic activity within the ophiolite and the first post-obduction magmatism (e.g. Slagstad et al., 2014). Obduction and erosion were followed by deposition of the sedimentary and volcanic rocks of the Hovin and Horg Groups (Vogt, 1945). The Hovin Group contains the Hølonda Porphyrites, a shoshonitic volcanic and subvolcanic suite with geochemical signatures that were interpreted by Grenne and Roberts (1998) as indicating formation in a continental arc setting. The absolute age of the Hølonda Porphyrites is unknown, but they are associated with richly fossiliferous sediments of Late Arenig/Early Llanvirn (Middle Ordovician, ca. 468–465 Ma) age that show an unequivocal Laurentian faunal affinity (e.g., Bruton and Bockelie, 1980). The Early to Middle Ordovician arc volcanism represented by the SSZ ophiolites and the Hølonda Porphyrites was succeeded by arc type magmatism in the Late Ordovician to Silurian, represented in the central Scandinavian Caledonides by e.g. the Smøla-Hitra batholith (ca. 445–440 Ma; Tucker et al., 2004). This magmatism was followed in the Silurian by widespread mafic intrusives, including the Innset massif of the Oppdal area (Fig. 2; Nilsen et al., 2003), reflecting short-lived extension prior to the main Caledonian continental collision (Slagstad and Kirkland, 2018).

2.2. Geology of the Oppdal area

The area investigated in this study is located in a late/post-Caledonian half-graben structure in the south-western part of the TNC

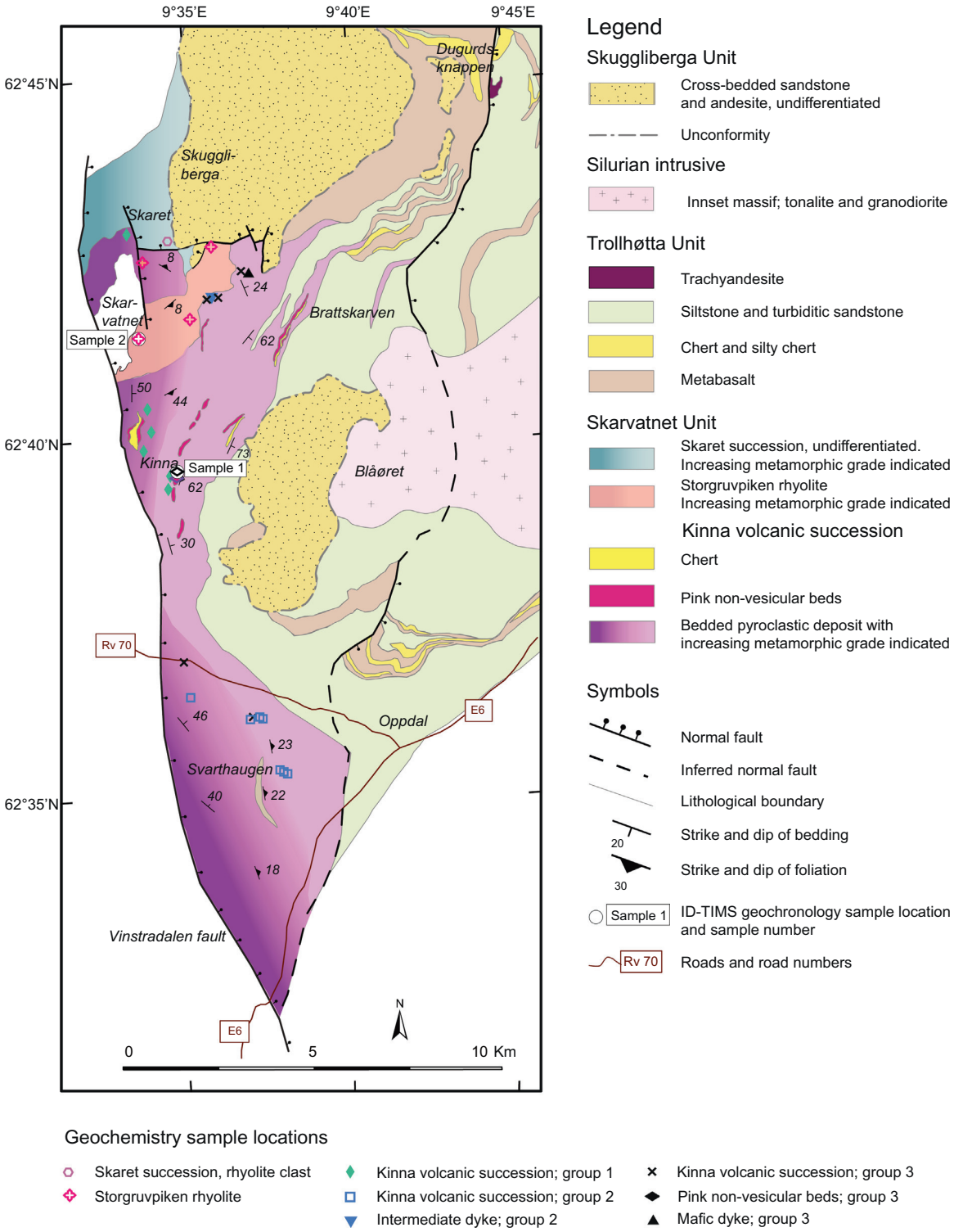

Fig. 2. Geological map of the study area with sample localities; the symbols correspond to those of Figs. 7–10.

(Figs. 1, 2), separated from the underlying, higher-grade nappes by the Vinstradalen fault (Fig. 2). The rocks of the area are generally moderately deformed with an *E*-dipping regional foliation and are metamorphosed to greenschist facies. Towards the Vinstradalen fault, they grade into amphibolite facies, strongly foliated rocks (Fig. 2). On the 1:250000 scale bedrock map of Nilsen and Wolff (1989), the rocks investigated in the present study were mapped as volcanic breccias, siltstones and greywackes interlayered with rhyolite. In some literature these relatively low-grade rocks have been referred to as the Tronget unit (e.g., Gee et al., 1985), a loose term originally introduced by Krill (1980) for rocks farther south. Recent, detailed work by Stokke et al. (2018) around Dugurdsknappen (Fig. 2) defined a sequence of E-MORB basalts, chert, cherty siltstone and turbiditic sandstone, referred to in the following as the Trollhøtta unit, which was isoclinally folded

and unconformably overlain by Silurian sandstones and calc-alkaline volcanic rocks of the Skuggliberga unit (Fig. 2).

3. Results

3.1. Field relations

We remapped the volcanic breccia/siltstone/greywacke and rhyolite units of Nilsen and Wolff (1989), which stretch from south of Oppdal northwards to Skaret, covering an area of approximately 60 km^2 (Fig. 2). These rocks, here collectively referred to as the Skarvatnet unit, were subdivided into three different rock associations. These are (1) the Kinna volcanic succession, including associated dykes and minor intercalated chert, (2) the Storgruvpiken rhyolite, and (3) the sedimentary Skaret succession (Fig. 2). Primary macrostructures are generally well preserved, particularly within the pressure shadow of the Storgruvpiken rhyolite. However, metamorphism and regional-scale deformation have partly erased small-scale primary textures. All three associations have undergone regional metamorphism, but the prefix 'meta' is omitted in the following descriptions and discussions for simplicity.

3.1.1. The Kinna volcanic succession

The c. 2.5 km thick Kinna volcanic succession is the most voluminous of the three units, covering an area of approximately 40 km^2 (Fig. 2). It is mostly bedded, with up to 5 m thick, light- to medium-grey fragment-bearing beds alternating with finer grained, fragment-free beds of similar composition (Fig. 3a). The boundaries between the beds are sharp, and grading or other way-up criteria have not been observed. In some areas the rocks have experienced bedding-parallel tectonic flattening (Fig. 3a) whereas others are virtually undeformed (Fig. 3b). The fragment-bearing beds consist of either scattered fragments (Fig. 3b) or densely packed fragments (Fig. 3c, d) in a fine-grained matrix. The fragments are angular to rounded and fragment size is highly variable; 10–50 cm is most common but fragments up to 1.5 m have been observed. There is no systematic variation in grain or fragment size within individual beds. Crusted fragments are observed (Fig. 3e). Towards the Vinstradalen fault (Fig. 2) the Kinna succession occurs as alternating beds of biotite–amphibole–quartz schists and more gneissic-looking, strongly deformed fragment-bearing beds (Fig. 3d). Towards the northeast, the Kinna volcanic beds are intercalated with metabasalts, cherts and siltstones of the Trollhøtta unit; minor chert layers also occur within the western part of the Kinna succession (Fig. 2).

The fragments within the bedded Kinna succession are dominated by feldspar, fine-grained dark mica (partly replaced by chlorite), epidote and carbonate minerals. Porphyritic fragments are abundant, with dark green to black, 2–10 mm phenocrysts of euhedral amphibole commonly replaced by a fine-grained aggregate of dark mica, chlorite and epidote (Fig. 3f-h). Some dark mica that forms euhedral hexagonal crystals 2–4 mm across is also considered a primary magmatic phase. Most fragments are vesicular with the vesicles ranging from 0.5 mm to 3 mm and constituting up to 50% by volume. Vesicle shape vary from spherical to elongate; vesicles are filled with carbonate, quartz or feldspar (Fig. 3i), the latter two locally forming a thin outer rim of the vesicles (Fig. 3j). Some elongated and densely packed fragments still have spherical vesicles, demonstrating that fragment flattening is a primary feature at least locally. Unequivocal evidence of welding is not observed but cannot be ruled out. The fine-grained beds and the matrix between fragments consist of a homogenous, fine-grained assemblage of epidote, chlorite, biotite, feldspar, calcite, magnesite and minor quartz.

The central part of the Kinna volcanic succession locally contains fine-grained, non-vesicular, volcanic rocks characterized by a light pinkish colour (pink non-vesicular beds, Kinna group 3 in Fig. 2; Fig. 3k). These volcanic rocks are up to 60 m thick. Individual outcrops are up to 300 m along strike and their linear arrangement indicates that they occur mainly at two stratigraphic levels (Fig. 2). These rocks contain abundant fine-grained K-feldspar and consist of fine-grained, non-vesicular, densely packed subangular to angular fragments of a few millimetres to 3 cm in size (Fig. 3l). The fragment size is substantially smaller than in the bedded Kinna volcanic succession.

Close to the Storgruvpiken rhyolite, the Kinna volcanic succession is cut by several parallel, up to 2 m thick, fine- to medium-grained intermediate dykes with chilled margins (intermediate dyke, Kinna group 2 in Fig. 2; Fig. 4a). The centres of the dykes have a porphyritic texture, where K-feldspar laths up to 3 cm are partly aligned with the margins of the dykes (Fig. 4b); the groundmass has a trachytic texture dominated by fine-grained alkali feldspar (Fig. 4c). Farther north, a mafic dyke with scattered, 2–3 mm amphibole phenocrysts in a fine- to medium-grained biotite-rich matrix cuts the Kinna volcanic succession (Mafic dyke, Kinna group 3 in Fig. 2). The relationship between the dykes and the Storgruvpiken rhyolite is uncertain due to lack of exposure.

3.1.2. The Storgruvpiken rhyolite

The bedding of the Kinna volcanic succession is cut to the northwest by the Storgruvpiken rhyolite, an elongate body oriented approximately NNE–SSW that covers approximately 2.5 km^2 (Fig. 2). The rhyolite body contains large (up to 10 m) xenoliths of Kinna rocks (Fig. 5a). The Storgruvpiken rhyolite is a very fine-grained, grey to light pinkish rock almost devoid of mafic minerals; only few, small biotite grains and opaques are present. Euhedral phenocrysts of millimetre-size alkali feldspar are observed in thin section at several localities (Fig. 5b). Some parts of the rhyolite are massive with no internal structure. Other parts show millimetre-thick planar features interpreted as primary igneous flow-banding with an orientation different from the regional foliation and the bedding of the Kinna volcanic rocks (Fig. 5c). Millimetre- to centimetre-size angular fragments in a darker, finer grained matrix occur locally (Fig. 5d).

3.1.3. The Skaret succession

The area to the north of the Kinna volcanic succession is dominated by different conglomerates and clastic sedimentary rocks, here referred to as the Skaret succession (Fig. 2). Conglomerates constitute approximately 60% of the rocks in the area. Three main types of conglomerates were observed.

(1) The most abundant type is a polymict conglomerate with a calcareous, biotite-rich greywacke matrix. The clast material is highly diverse; felsic/intermediate and mafic volcanic rocks, siltstone, sandstone, jasper, chert, fine-grained marble and clasts of Kinna-type volcanic rocks have been observed. The clasts are angular to subrounded, ranging in size from pebble to meter-sized boulders; the largest blocks consist of immature sandstone and fine-grained marble and are up to 1.5 m across (Fig. 6a). This conglomerate is associated with thick-bedded to laminated calcareous greywacke (Fig. 6b), marble beds and monomict marble conglomerate.
(2) A different conglomerate is characterized by abundant fine-grained, pink felsic or intermediate volcanic clasts mostly <30 cm; clasts up to 1 m are also found. The shape of the clasts is highly diverse; sub-angular clasts are most common. Local medium-grained mafic clasts are up to 70 cm and are more rounded than the felsic/intermediate ones. The conglomerate is clast-supported, and the clasts are embedded in a very fine-grained, biotite- and chlorite-rich matrix.
(3) The third type of conglomerate consists almost exclusively of angular metabasaltic fragments (1–5 cm), with subordinate pink, fine-grained felsic/intermediate volcanic clasts and small grains of jasper set in an epidote-rich matrix (Fig. 6c).

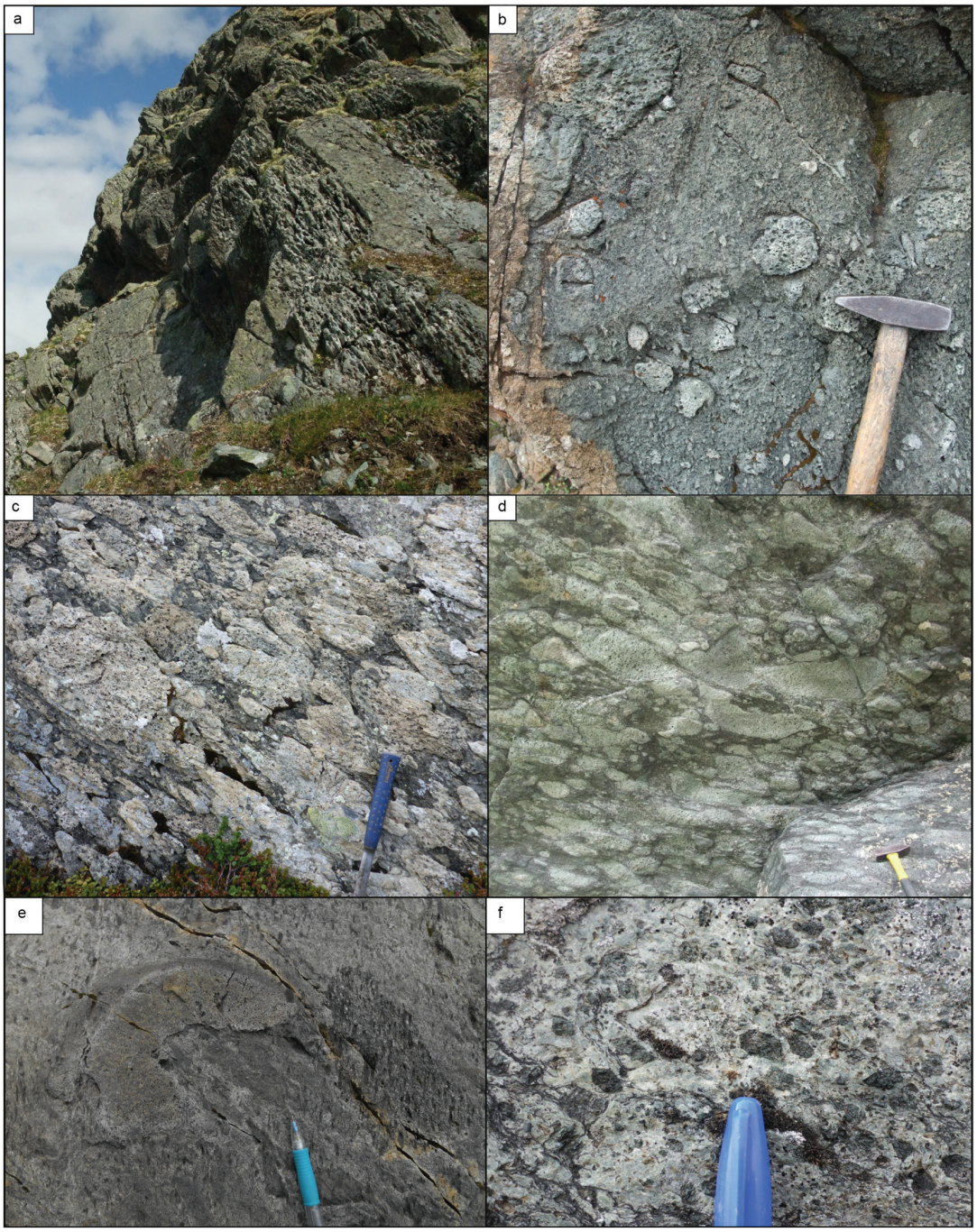

Fig. 3. Field and thin section photographs of the Kinna volcanic succession. a Alternating fragment-bearing and fragment-free beds. b Scattered, vesicular volcanic fragments in fine-grained matrix of similar composition; black spots are aggregates of biotite and chlorite that replace amphibole phenocrysts. c Densely packed, angular volcanic fragments. d Densely packed fragments within a biotite-rich matrix (amphibolite facies, close to the Vinstradalen fault). Kinna volcanic succession continued. e Broken fragment of a rounded, partly crusted fragment in a grey matrix with biotite-chlorite aggregates probably replacing amphibole; the crust and rounded shape suggest this is a fragment of a volcanic bomb. f Euhedral phenocrysts of amphibole replaced by aggregates of dark mica and chlorite. g Thin section photo from a basaltic fragment (Kinna group 1), with an amphibole phenocryst partly replaced by dark mica and chlorite. Plane polarized light. h Thin section photo of dark mica – chlorite aggregate completely replacing euhedral, rhomb-shaped mineral, probably amphibole. Plane polarized light. i Fragment with spherical vesicles partly filled with quartz, carbonate and/or feldspar. j Thin section photo from a fine-grained trachyandesitic rock (Kinna group 3) with a vesicle filled with a quartz – feldspar rim and carbonate core. Crossed polars. k Non-vesicular pink volcanic rock that locally occurs interbedded within the fragment-bearing Kinna volcanic succession. Phenocrysts are mainly K-feldspar; mafic minerals are only a minor constituent (the dark spots are lichen). l Thin section photo of the non-vesicular pink volcanic rock, with fine-grained partly flattened fragments and minor dark mica. Plane polarized light.

All three conglomerate types are interbedded with greenish, biotite-rich bedded immature sandstones with no internal grading, grey calcareous greywackes, and minor chert and marble. Slump folds and other soft-sediment deformation structures are common (Fig. 6d), and lithological boundaries within the succession are commonly distorted and/or truncated by other lithologies.

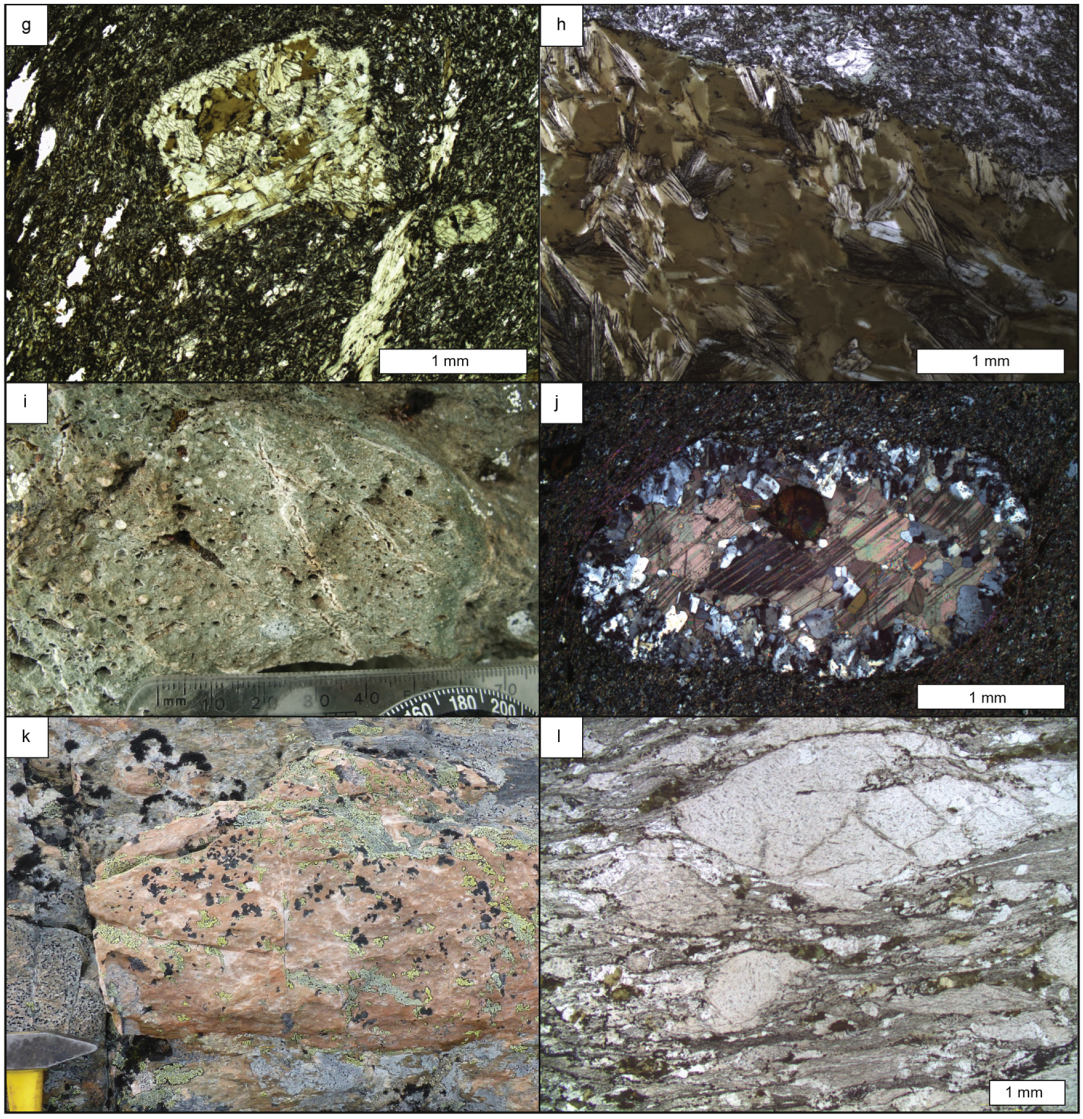

Fig. 3 (*continued*).

3.2. Geochemistry

3.2.1. Sampling and analytical procedure

We analysed 27 samples from the Skarvatnet Unit for major and trace elements. Sample localities are shown in Fig. 2. Samples with very high contents of phenocrysts and >5% vesicles were avoided. All samples were analysed at the Geological Survey of Norway, Trondheim. Major elements were analysed by X-ray fluorescence (XRF) spectrometry on glass beads fused with lithium tetraborate, and trace elements were analysed by XRF spectrometry on pressed powder. Rare Earth Elements (REE) were analysed by inductively coupled plasma – mass spectrometry (ICP-MS) on the same glass bead used for XRF major element analysis. Common international standards were followed for all methods; details on standards and methods can be provided on request. The results are reported in Table 1 and in Figs. 7–10.

Eighteen of the samples are from the typical bedded Kinna volcanic succession. Eleven of these are fragments, five are from fine-grained fragment-free beds, and two are from the matrix of fragment-bearing beds. Two samples are from the pinkish, non-vesicular volcanic rocks in the Kinna volcanic succession. One sample is from an intermediate dyke and one from the mafic dyke in the Kinna volcanic succession. Four samples are from the Storgruvpiken rhyolite, and one is a rhyolite clast from the type 2 conglomerate of the Skaret succession (Fig. 2; Table 1).

3.2.2. The Kinna volcanic succession

The samples from the Kinna volcanic succession represent a spectrum of geochemical compositions which we have separated into three different groups based on specific geochemical features (Figs. 7–10). These three groups are not distinguishable in the field. Their random geographic distribution (Fig. 2) does not reveal any systematic age relationship, and we interpret them to be broadly coeval. Due to mobility of alkalies in the standard TAS diagram, we apply the Zr/Ti vs. Nb/Y diagram of Pearce (1996) for a general classification or our rocks (Fig. 7a). Kinna group 1 samples are subalkaline basaltic andesites and andesites, whereas Kinna group 2 and 3 samples are alkaline rocks ranging from trachyandesite to alkali rhyolite (Fig. 7a). All three groups are strongly enriched in most incompatible high field strength elements (HFSE), including the light rare earth elements (LREE), relative to continental crust and common oceanic or continental arc-related rocks (Table 1; Fig. 7b) (Pearce, 2008; Pearce and Peate, 1995; Rudnick and Gao, 2003). All three groups have relatively high contents

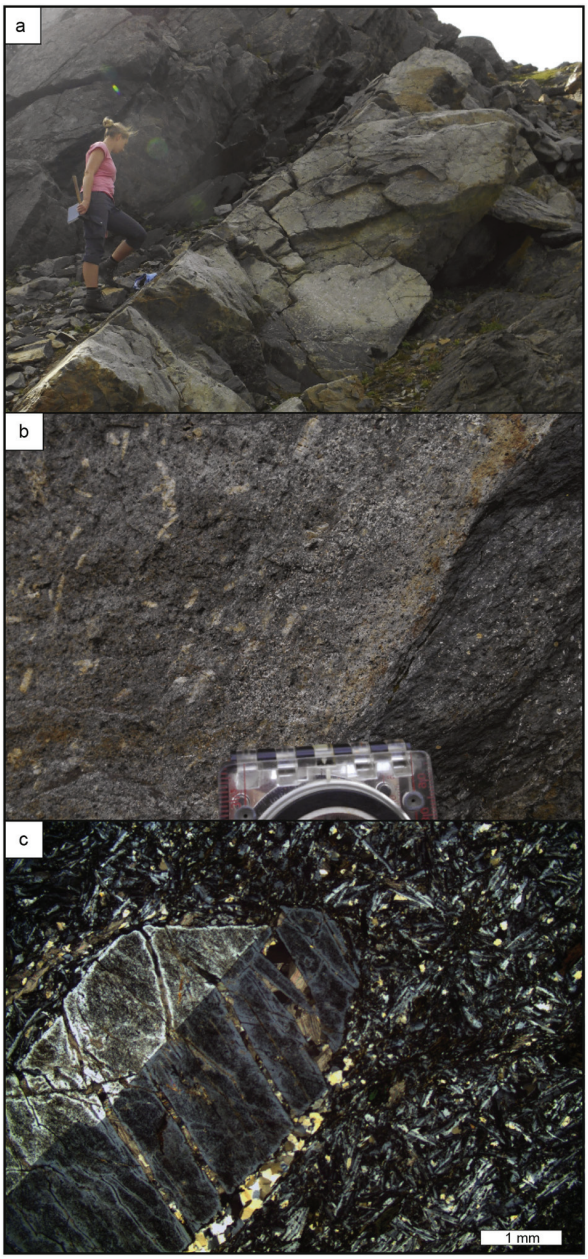

Fig. 4. a Trachytic dyke cutting the Kinna volcanic succession. b Contact between dyke and Kinna volcanic succession, with increasing grain size away from the chilled margin. Alkali feldspar phenocrysts are partly aligned with the dyke margin. c Thin section photo of simple twinned alkali feldspar phenocryst in a fine-grained alkali feldspar-dominated matrix. Crossed polars.

of MgO (up to 11 wt%; 5 samples have Mg# >70), Cr (up to 792 ppm) and Ni (up to 300 ppm), and even intermediate volcanic rocks can have concentrations of Cr up to 378 ppm at 57.1% SiO_2 (Table 1).

The SiO_2 vs. K_2O plot (Fig. 7c) must be considered with care in view of the potential mobility of potassium during sea-floor alteration and regional metamorphism; however, it is noteworthy that many Kinna samples have elevated K_2O values comparable to High-K calc-alkaline, shoshonitic and even ultrapotassic rocks. Although potassium values are obviously not reliable at individual sample level and some Kinna rocks may have experienced gross K_2O loss, several samples classify as ultrapotassic also based on the commonly used criteria of Foley et al. (1987): K_2O > 3 wt%, MgO > 3 wt%, K_2O/Na_2O > 2 (Table 1).

The basaltic-andesitic to andesitic Kinna group 1 samples have SiO_2 vs. K_2O contents comparable to high-K calc-alkaline to shoshonitic rocks (Fig. 7c). They are relatively rich in Th (9.5–48.1 ppm; the group 1 samples have an average Th content of 101 x N-MORB – this and all following values are averages compared with the mean N-MORB composition given in Gale et al., 2013), U (3.3–9.9 ppm; on average 70 x N-MORB,), Pb (11.9–36.5 ppm; on average 38 x N-MORB), and LREE (La on average 15 x N-MORB, Ce on average 11 x N-MORB). They have large negative Nb—Ta and Ti anomalies and exhibit a minor trough at Zr—Hf in the N-MORB-normalised multielement plot (Table 1 and Fig. 8a). Chondrite-normalised REE patterns (Fig. 8b) are steep (La_N/Lu_N = 16.8–34.9), showing an even slope towards the heavy REE (HREE) and minor negative Eu anomalies (0.71–0.85). Kinna group 1 samples contain up to 417 ppm Cr and 117 ppm Ni (Table 1), with a steep negative correlation between Zr and Cr (Fig. 9). Sm/La values are mostly <0.2, and the samples plot close to the estimated average upper crust (UC, Rudnick and Gao, 2003) and the estimates for Global Subducting Sediment (GLOSS, Plank and Langmuir, 1998) in a Sm/La vs. Th/La plot (Fig. 10).

The trachytic to alkali-rhyolitic Kinna group 2 samples, including the intermediate dyke, are even more enriched in Th (43.9–117 ppm; on average 284 x N-MORB), U (11.8–26.6 ppm; on average 227 x N-MORB), Pb (30.2–80.3 ppm; on average 91 x N-MORB), LREE (La on average 28.45 x N-MORB, Ce on average 20 x N-MORB), Be (1.4–44.9 ppm; on average 20 x N-MORB), and Zr (594–1060 ppm; on average 8 x N-MORB) (Table 1 and Fig. 8c). Compared to Kinna group 1 rocks they also have significantly higher Ta/La and Th/La ratios and lack the minor Zr—Hf trough (Fig. 8c). Chondrite-normalised REE patterns (Fig. 8d) have a very steep slope (La_N/Lu_N = 32.4–53.0), especially among the MREE, and have a slightly flatter trend among the HREE. Increasing SiO_2 with Zr is accompanied by decreasing MgO, P_2O_5 and Cr (Fig. 9a–c), suggesting that much of the group-internal variation can be attributed to fractional crystallisation of mafic phases and apatite. Similarly, a fairly wide range of negative Ti anomalies (Fig. 8c) and the Eu anomalies of 0.54–0.67 (Fig. 8d) likely reflect fractionation of titaniferous oxides and feldspar, respectively. Kinna group 2 samples have Sm/La ratios similar to those of Kinna 1, close to UC and GLOSS in the Sm/La vs Th/La plot (Fig. 10). They generally resemble shoshonitic to ultrapotassic rocks in the K_2O vs. SiO_2 diagram (Fig. 7c); the very low K_2O of three samples is considered to result from seafloor weathering, hydrothermal alteration and/or regional metamorphic processes in view of (1) their stable trace element patterns that are identical to other Kinna 2 samples and (2) the typical enrichment of K_2O along with Th and other highly incompatible elements in magma-forming processes in general (Hastie et al., 2007; Pearce and Peate, 1995).

The trachyandesitic Kinna group 3 samples, including the mafic dyke and the pink non-vesicular volcanic rocks, plot as shoshonitic to ultrapotassic (Fig. 7c). Their trace element patterns (Fig. 8e) generally follow those of Kinna group 2, although with even higher values of Th (53–192 ppm, on average 114 x N-MORB), U (12.9–30.2 ppm, on average 22 x N-MORB), Pb (50–299 ppm, on average 118 x N-MORB), Be (7.1–60.1 ppm, on average 21 x N-MORB) and Zr (410–1130 ppm, on average 703 x N-MORB). A moderately negative Eu anomaly of 0.52–0.74 is comparable to that of Kinna 2 (Fig. 8f). A notable difference, however, is a peculiar, convex upward pattern at the La—Sm part of the chondrite-normalised REE diagram (Fig. 8f). Accordingly, Kinna group 3 samples have significantly higher Sm/La ratios (>0.2) than those of the other Kinna samples, plotting towards the Samarium – Lanthanum – Thorium (SALATHO) end-member of Tommasini et al. (2011) on the Sm/La vs. Th/La diagram (Fig. 10).

3.2.3. The Storgruvpiken rhyolite

The Storgruvpiken samples, including the clast from the Skaret conglomerate, are highly evolved, peraluminous and A-type alkaline rhyolites (Fig. 7a). They share many of the geochemical characteristics with the Kinna group 2 and 3 samples, but are even more enriched in Th

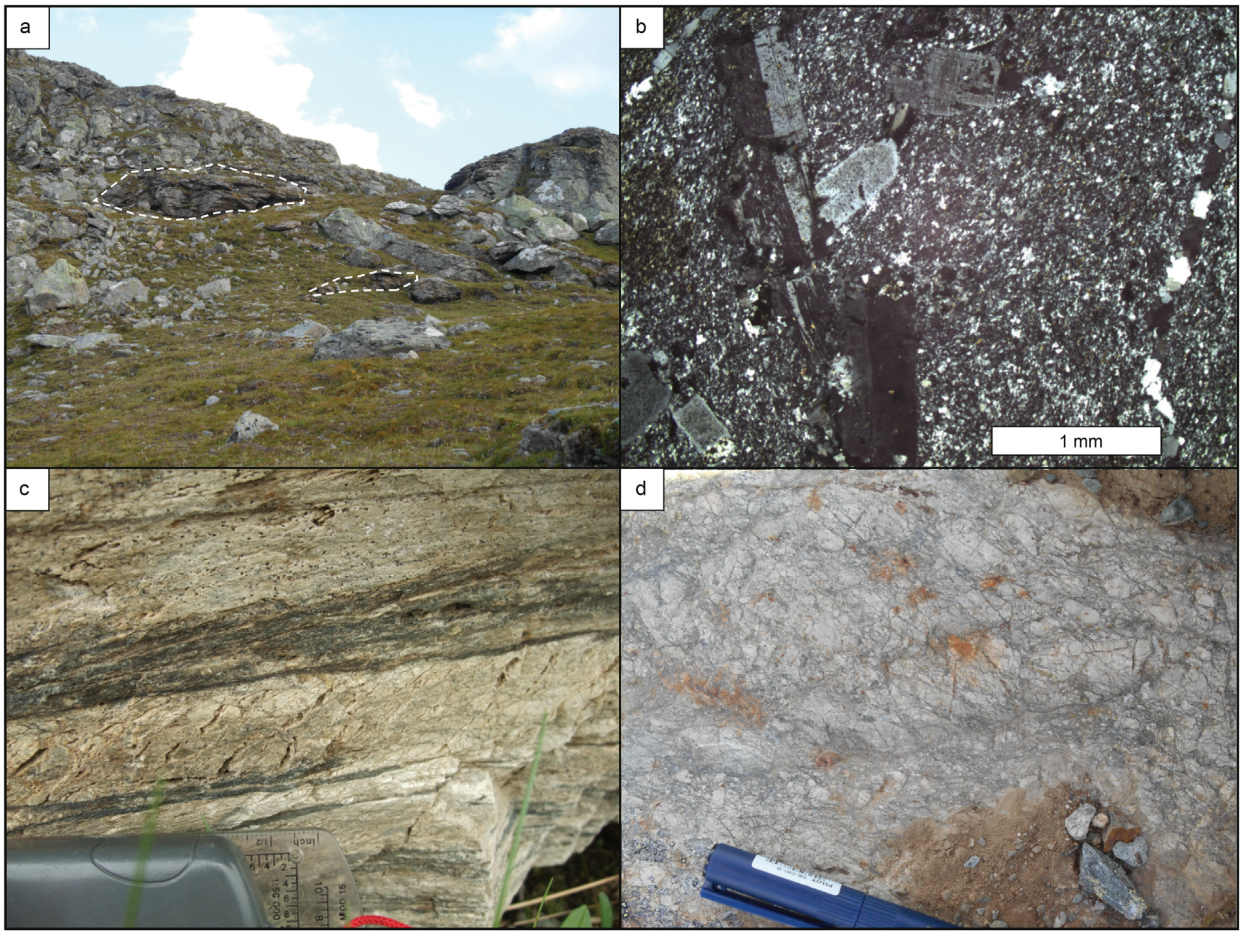

Fig. 5. Storgruvpiken rhyolite. a Massive rhyolite with large rafts of darker Kinna volcanic rocks (white outline). b Thin section photo from the Storgruvpiken rhyolite; subhedral phenocrysts of alkali feldspars with no, simple and gridiron twinning set in a fine-grained matrix. Crossed polars. c Rhyolite flowbanding. d Rhyolite with small, angular fragments embedded in a fine-grained light-grey matrix.

(113–278 ppm, on average 175 x N-MORB) and U (23.0–61.8 ppm, on average 42 x N-MORB) and have somewhat lower contents of LREE (La on average 15 x N-MORB; Ce on average 13 x N-MORB), Zr (329–530 ppm, on average 425 x N-MORB) and Hf (11.4–24.7 ppm, on average 7 x N-MORB) (Table 1, Fig. 8g). Notably, Be is extremely enriched in some samples (6.7–66.5 ppm; on average 38 x N-MORB, Table 1). Th/Ta ratios are similar to those of Kinna 2 and 3, but the generally lower concentrations of LREE produce a less pronounced trough at Ta—Nb (Fig. 8g). REE-patterns (Fig. 8h) have a significantly gentler slope than the Kinna 2 and 3 rocks (La_N/Yb_N 9.4–17.0), partly overlapping with Kinna 1 patterns (La_N/Lu_N 16.8–34.9). Compared to the Kinna volcanic succession, the more evolved Storgruvpiken rhyolite has much larger negative Ti and Eu (0.02–0.17) anomalies (Fig. 8g–h).

3.3. Geochronology

3.3.1. U—Pb TIMS method

Two samples were crushed, and heavy minerals were separated by standard magnetic and heavy liquid techniques at the University of Oslo. Selected zircons from sample 1 were annealed for ca. 72 h at 900 °C and chemically abraded with HF (+HNO_3) at 195 °C for 14 h (Mattinson, 2005). The high-U zircons from sample 2 were air abraded (Krogh, 1982) because of advanced metamictization. After optical inspection, euhedral high aspect ratio (>1:4) zircon grains were chosen for analysis, spiked with a mixed ^{202}Pb–^{205}Pb–^{235}U tracer that has recently been calibrated to the EARTHTIME (ET) 100 Ma solution (Svensen et al., 2015), and dissolved in HF (+HNO_3) at ca. 210 °C for >48 h in Teflon micro capsules and a Parr type bomb. All dissolved grains subsequently went through column chemistry in order to separate U and Pb from potentially interfering and ionization inhibiting elements (Krogh, 1973). Details of the general mass spectrometric techniques and parameters used are presented in Augland et al. (2010) with upgraded laboratory parameters: Pb blank generally <1 pg with a composition of $^{206}Pb/^{204}Pb = 18.04 \pm 0.40$; $^{207}Pb/^{204}Pb = 15.22 \pm 0.30$; $^{208}Pb/^{204}Pb = 36.67 \pm 0.50$; improved precision of fractionation on U and Pb fractionation parameters of 0.02% and down to 0.003% 1σ for U and Pb, respectively. Reduction of raw data was conducted using Tripoli (Bowring et al., 2011) and analytical errors and corrections (including common Pb, fractionation corrections and Th corrections, assuming Th/U in the magma of 3) were incorporated and propagated in the Excel macro based on the algorithms published in Schmitz and Schoene (2007). Ages were calculated by the use of the ISOPLOT Excel macro of Ludwig (2003) using the decay constants of Jaffey et al. (1971) and are presented in Fig. 11 and Table 2.

3.3.2. Results U—Pb TIMS dating

3.3.2.1. Sample 1 (15BD_256; UTM (32) 529655/6947568). Sample 1 is from a pink non-vesicular volcanic bed within the Kinna succession (Fig. 2), which shows a trachytic composition belonging to Kinna group 3 (Figs. 7-10). Four clear, colourless to slightly yellow zircon fragments were analysed. All analyses are concordant and overlapping, giving a weighted mean $^{206}Pb/^{238}U$ age of 474 ± 1 Ma (2σ; MSWD = 1.8) (Fig. 11a; Table 2).

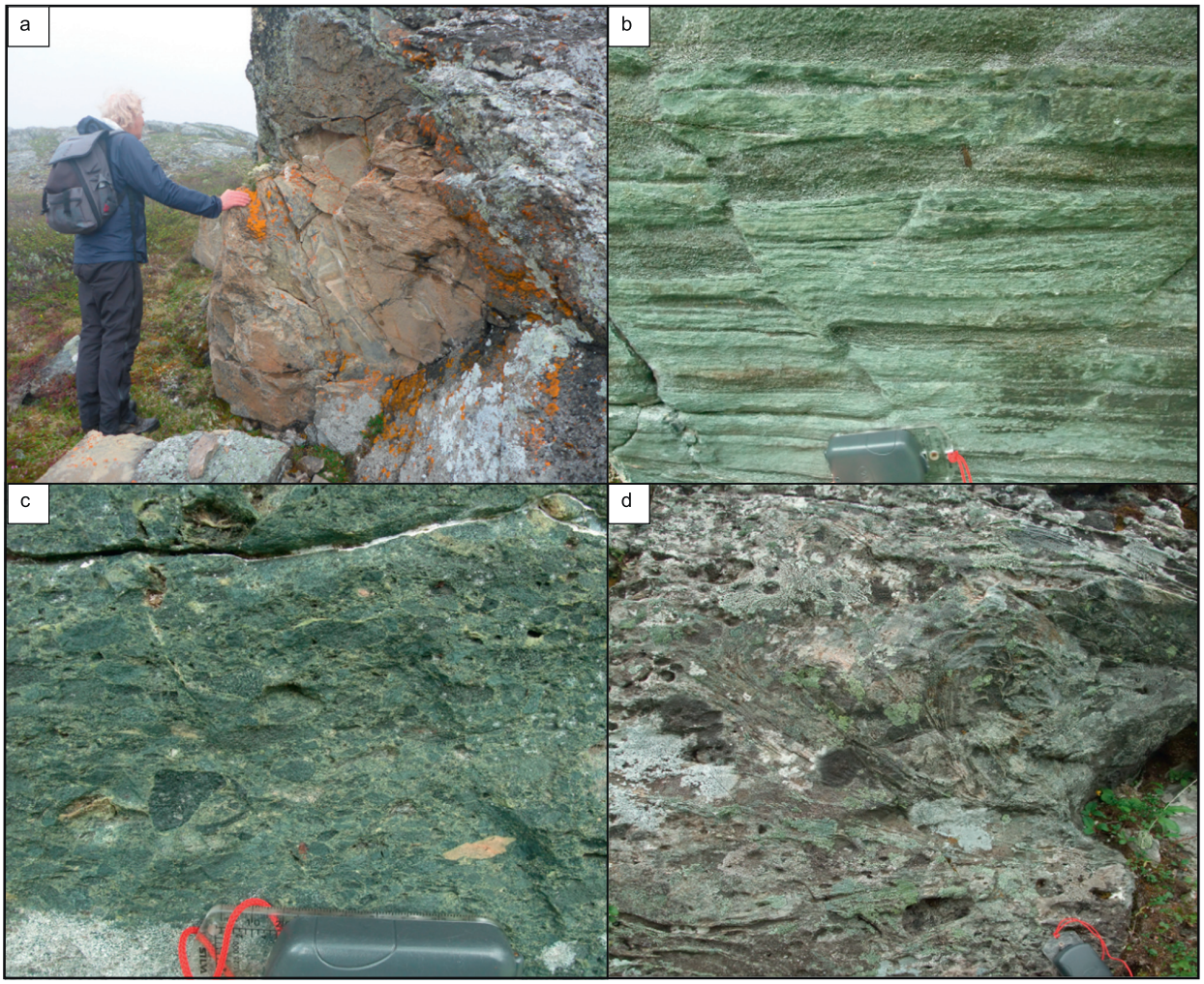

Fig. 6. The Skaret succession. a Large, angular block of fine-grained marble in a greywacke matrix. b Green, bedded sandstone with biotite-rich layers. Carbonate clasts are weathered out. c Angular basaltic and felsic volcanic fragments in an epidote-rich matrix. d Polymict conglomerate with calcareous, biotite-rich greywacke matrix, disturbed by slump folding.

3.3.2.2. Sample 2 (TGR12–739; UTM (32) 528662.6951317). Sample 2 is from the Storgruvpiken rhyolite (Fig. 2). In this area the rhyolite has a fragmental texture with planar features interpreted to be related to movement of viscous magma. Zircon occurs as euhedral, mostly brown and opaque, equant crystals dominated by {100} and {101} crystal faces. Inferred cores are seen in some grains, but they are rare and such grains were avoided during selection. Three zircons, one pink and two brown grains were analysed and are all concordant. The weighted mean $^{206}Pb/^{238}U$ age is 470 ± 1 Ma (2σ; MSWD = 1.3) (Fig. 11b; Table 2).

4. Discussion

4.1. Depositional setting of the Skarvatnet unit

4.1.1. The Kinna volcanic succession

The fairly uniform mineralogical and geochemical composition of the Kinna volcanic succession indicates that these deposits had little input from non-volcanic sources. In addition, the lack of graded beds, erosional channels or other sedimentary features typical of clastic sedimentation in water rules out re-deposition of volcanic rocks as clastic debris flows. Hence, we consider it most likely that the Kinna succession represents primary volcanic deposits. The alternation of beds with and without fragments shows that similar processes occurred repeatedly, probably with similar intensities in each cycle since the beds typically have a restricted thickness ranging from 50 to 100 cm. Several eruptive pulses capable of producing the variation in fragment amount are considered more likely than repeated erosional and clastic depositional processes, which would probably lead to more variation in bed thickness and content. Possible volcanic deposit types discussed in the following include lava flows, lahars, pyroclastic flows and ash fallouts.

An origin as individual lava flows where fragment-free portions are central parts and fragment-bearing portions represent auto-brecciated upper parts of flow units is considered unlikely as the fragments within one bed have a large variation in content of phenocrysts. Subrounded fragments are also not typical for auto-brecciation. The pink non-vesicular beds in contrast, with their internal small-scale fragmentation, might possibly represent felsic lava flows with limited extent, although other origins cannot be ruled out.

The unsorted nature of the fragment-bearing beds of the Kinna volcanic succession could result from several types of debris flow; lahars and pyroclastic flows (subaerial or submarine) being the most relevant. There are no single features that can distinguish between unwelded pyroclastic deposits and lahars (Fisher and Schmincke, 1984), but since pumice and highly vesicular material is more common in pyroclastic flows than in lahars, it is considered more likely that the Kinna succession represents pyroclastic flow deposits.

Table 1
Major and trace element analyses. Elements in italics are analysed on ICP-MS, other elements are analysed on XRF. * = W analysed on XRF. Mg# = 100xMg/(Mg + Fe). RG-2003 are estimates for average continental crust composition from Rudnick and Gao (2003).

Group	Kinna volcanic succession group 1						Kinna volcanic succession group 2							
Sample	15BD_1471	15BD_249	15BD_259	15BD_306	17BD_43	BD15_538	15BD_1061	17BD_39	17BD_41A	17BD_41B	17BD_42C	BD15_272	BD15_273	17BD_67
SiO_2%	46.4	54.2	57.5	48.3	48.4	54.9	58.3	57.1	51.6	49.7	48.5	63.3	67.7	59.5
Al_2O_3	13.2	16.8	14.2	13.3	15.6	14.6	16.0	19.0	15.1	14.6	13.5	16.7	15.6	16.6
Fe_2O_3	6.88	10.1	5.20	10.8	10.1	6.85	3.82	4.55	6.92	6.53	6.89	4.05	1.07	3.61
TiO_2	0.739	0.686	0.748	0.604	0.693	0.591	0.372	0.973	0.781	0.986	0.942	0.338	0.253	0.657
MgO	8.98	1.84	3.07	9.98	8.46	7.04	3.40	2.49	7.09	9.08	9.83	1.07	0.209	2.28
CaO	12.4	3.52	7.40	7.15	8.75	7.56	6.10	2.23	5.30	7.41	8.00	5.29	3.35	1.86
Na_2O	1.76	6.54	4.24	1.31	2.94	4.28	7.43	3.35	4.28	1.29	1.13	6.78	8.45	1.46
K_2O	2.57	2.68	1.76	3.68	1.76	1.82	0.79	5.89	3.74	5.21	5.00	0.60	0.37	11.0
MnO	0.164	0.108	0.070	0.142	0.152	0.116	0.066	0.048	0.076	0.100	0.116	0.045	0.083	0.045
P_2O_5	0.433	0.601	0.562	0.331	0.366	0.417	0.152	0.328	0.469	0.608	0.535	0.184	0.197	0.317
LOI	4.93	2.04	4.33	3.14	2.12	1.30	2.51	2.38	2.92	3.23	4.04	1.15	1.84	1.76
Ba ppm	2880	680	712	1080	630	476	308	1470	902	3080	2420	82	59	1430
Co	31.1	21.5	29.4	45.9	39.1	25.8	10.2	13.4	27.2	32.2	38.3	9.9	<4	11.1
Cr	170	18.0	205	399	228	290	50.1	378	443	268	658	18.9	51.4	88.3
Cu	99.8	50.4	36.4	236	91.2	11.8	147	29.4	44.9	128	124	6.5	14.3	7.0
Ga	11.5	11.9	10.9	13.5	15.5	11.2	8.40	23.2	19.5	19.9	16.8	12.2	5.10	23.9
Ni	106	45.3	74.2	108	79.5	115	34.3	47.5	163	201	244	43.0	<5	34.2
Pb	16.1	36.5	18.3	15.5	18.1	11.9	80.3	30.2	37.3	51.7	22.1	48.8	39.6	62.5
Rb	81.0	77.9	78.8	148	74.5	67.4	30.8	219	223	213	215	24.9	7.0	455
Sc	24.7	8.0	27.1	28.0	34.4	27.7	8.6	21.8	21.8	22.5	34.1	<5	<5	14.7
Sn	<5	<5	<5	<5	<5	<5	6.00	8.70	13.1	12.6	10.4	12.7	9.30	27.6
Sr	439	323	283	503	314	220	591	237	430	301	259	519	251	278
V	268	145	224	336	241	184	76.2	222	129	189	196	53.2	23.6	47.2
Y	20.6	30.8	22.1	20.1	26.6	20.9	22.8	31.1	21.3	23.5	21.2	22.7	23.5	18.4
Zn	49.1	96.9	38.4	79.5	85.2	46.3	22.7	55.6	70.2	53.0	49.8	14.5	5.2	40.6
Zr	203	287	171	131	161	154	854	862	628	594	481	1060	964	1020
Cs	<0.4	<0.4	<0.4	19.0	2.83	12.0	<0.4	8.28	15.6	9.34	10.3	12.0	<0.4	13.7
Ge	N.A	N.A	N.A	N.A	N.A	2.1	N.A	N.A	N.A	N.A	N.A	2.3	<2	N.A
Be	4.2	1.8	2.8	2.8	2.5	3.6	5.7	8.1	6.0	16.3	11.4	6.1	1.4	44.9
Nb	15.6	17.3	10.2	3.85	8.03	10.6	24.5	44.0	26.3	38.1	29.8	32.9	28.7	53.0
La	81.0	105	56.4	30.4	55.9	54.7	151	161	101	102	83.3	139	96.4	120
Ce	151	221	121	68.1	116	106	288	349	218	207	173	280	217	267
Pr	19.3	25.7	13.9	8.04	13.0	12.2	34.6	38.4	24.4	24.3	20.6	32.1	24.1	29.1
Nd	74.7	98.1	56.3	30.6	49.5	45.4	127	132	93.3	94.7	80.3	103	79.9	104
Sm	14.4	16.4	9.38	6.27	9.22	8.88	19.2	18.1	15.0	15.2	13.7	16.3	12.0	15.9
Eu	2.88	3.30	2.11	1.57	1.99	1.95	2.75	2.65	2.36	2.66	2.20	2.63	2.12	2.52
Gd	9.39	9.93	5.77	4.63	6.58	6.23	10.1	9.16	7.39	8.65	7.63	8.03	6.35	7.21
Tb	1.20	1.30	0.715	0.624	0.909	0.888	1.28	1.11	0.838	1.03	0.983	0.993	0.735	0.851
Dy	5.78	6.33	3.65	3.38	4.83	4.79	6.27	5.03	3.67	4.99	4.53	4.99	3.94	3.75
Ho	1.05	1.13	0.618	0.612	0.913	0.890	1.11	0.945	0.668	0.894	0.807	0.929	0.728	0.674
Er	2.51	2.70	1.49	1.51	2.32	2.11	2.93	2.59	1.74	2.37	2.16	2.19	1.86	1.83
Tm	0.360	0.374	0.206	0.203	0.319	0.292	0.431	0.362	0.248	0.309	0.275	0.325	0.290	0.242
Yb	2.15	2.32	1.19	1.24	2.05	1.84	2.71	2.18	1.45	1.75	1.80	2.02	1.95	1.49
Lu	0.334	0.311	0.173	0.187	0.309	0.258	0.452	0.324	0.235	0.290	0.266	0.276	0.268	0.234
Hf	6.70	6.92	3.23	2.32	3.90	3.95	29.0	20.7	15.2	17.1	13.6	22.7	17.1	28.4
Ta	0.691	0.911	0.445	0.183	0.388	0.561	2.83	2.70	2.29	3.16	2.28	3.31	2.30	4.92
W	1.74	1.53	0.82	0.25	0.54	0.39	0.57	4.85	0.86	4.22	3.43	0.32	0.31	3.08
Bi	<0.5	<0.5	<0.5	<0.5	<0.5	<0.5	0.83	<0.2	<0.2	0.52	<0.2	0.54	0.51	0.52
Th	35.7	48.1	24.9	9.45	18.0	17.5	117	68.8	56.4	56.8	43.9	78.1	57.7	94.6
U	5.59	9.93	6.70	3.29	5.09	4.18	17.2	21.8	18.2	15.7	11.8	20.7	19.6	26.2
La_N/Lu_N	25.07	34.90	33.70	16.81	18.70	21.92	34.54	51.37	44.43	36.36	32.37	52.06	37.18	53.01
Sm/La	0.178	0.156	0.166	0.206	0.165	0.162	0.127	0.112	0.149	0.149	0.105	0.117	0.125	0.133
Th/La	0.41	0.458	0.441	0.311	0.322	0.319	0.775	0.427	0.558	0.557	0.527	0.562	0.599	0.788
Mg#	72	27	54	65	62	67	64	52	67	73	74	34	27	56

Group	Kinna volcanic succession group 3								Clast	Storgruvpiken rhyolite				RG-2003
Sample	15BD −1329	15BD −592	BD14 −24	BD14 −80	BD14 −84	17BD −42B	15BD −256B	BD15 −256A	BD15 −163	15BD −178	BD14_20	TG12 −739	TGR_ 445	Cont. crust
SiO_2%	50.6	48.4	48.3	48.4	54.7	47.3	58.5	60.1	68.9	69.0	69.8	69.8	68.8	60.6
Al_2O_3	11.7	13.7	17.2	12.7	16.8	17.4	17.8	17.8	15.7	15.6	15.3	15.8	15.4	15.9
Fe_2O_3	6.08	7.75	4.95	8.20	4.76	5.71	2.01	2.38	2.54	1.95	2.31	2.23	2.60	6.71
TiO_2	0.863	1.10	1.03	1.21	1.07	1.45	0.631	0.616	0.114	0.069	0.092	0.049	0.082	0.72
MgO	9.26	10.9	4.29	8.49	3.21	5.12	0.994	1.13	1.05	0.064	0.725	0.649	0.686	4.66
CaO	10.7	6.07	6.54	6.41	3.84	7.82	3.61	2.95	0.718	0.771	0.091	0.145	0.334	6.41
Na_2O	1.55	1.46	1.88	1.53	3.57	1.67	3.52	4.49	6.68	6.18	6.18	4.36	4.30	3.07
K_2O	2.99	5.75	7.93	5.79	7.07	5.94	8.16	6.24	2.91	4.03	3.69	5.05	5.36	1.81
MnO	0.115	0.110	0.092	0.172	0.086	0.083	0.033	0.034	0.028	0.097	0.024	0.024	0.03	0.10
P_2O_5	0.436	0.858	0.723	1.15	0.720	0.606	0.374	0.382	0.076	0.029	0.020	0.020	0.010	0.13
LOI	3.58	1.76	4.22	4.38	1.76	5.09	2.64	2.41	1.02	1.26	0.42	0.96	0.75	
Ba ppm	2650	1700	3070	473	2250	3970	2160	1360	671	179	240	157	374	456
Co	29.0	37.9	22.9	38.0	15.9	27.8	5.3	5.4	<4	<4	<4	<4	<4	26.6
Cr	627	761	51.7	610	36.9	43.3	87.0	70.3	99.5	40.6	32.1	<5	9.6	135
Cu	93.3	<5	543	<5	218	371	8.0	5.7	10.9	<5	<5	21.2	31.2	27
Ga	16.6	15.4	17.6	15.5	13.7	22.7	12.8	13.6	14.4	20.7	20.9	26.5	32.4	16
Ni	250	294	49.7	221	32.6	40.8	13.8	16.9	17.5	<5	<5	4.5	7.2	59
Pb	49.7	55.1	130	56.4	77.7	299	165	111	88.8	30.4	58.4	64.0	79.6	11
Rb	114	386	366	574	352	205	187	172	122	192	242	280	190	49
Sc	22.7	23.2	15.6	24.7	11.2	24.4	13.9	15.1	<5	<5	<5	<5	<5	21.9
Sn	16.7	19.3	21.1	12.4	11.3	18.4	25.5	23.1	13.9	21.7	10.8	18.0	31.6	1.7
Sr	455	207	854	314	592	376	532	403	108	62.3	127	41.2	87.6	320
V	206	165	198	196	127	220	50.5	62.3	36.0	<5	<5	<5	<5	138
Y	21.0	35.7	20.8	17.0	22.6	35.5	27.6	29.4	24.7	63.5	41.4	28.3	67.0	19
Zn	42.7	62.8	31.9	86.7	42.2	33.1	35.9	42.2	13.5	22.3	73.9	62.0	96.0	72
Zr	410	615	659	559	518	778	1130	956	482	530	393	329	525	132
Cs	<0.4	31.0	16.0	54.0	27.0	6.56	<0.4	<0.4	<0.4	<0.4	13.0	<0.4	<0.4	2
Ge	N.A	N.A	17.6	18.1	13.3	N.A	<0.2	2.2	<0.2	<0.2	<0.2	1.1	<0.2	1.3
Be	19.0	15.0	14.8	27.2	60.1	12.7	7.1	8.8	9.0	29.6	6.7	66.5	10.3	1.9
Nb	24.4	41.1	52.9	40.2	40.3	59.0	58.5	48.9	19.6	158	94.8	81.4	176	8
La	78.9	121	110	79.1	84.4	113	110	76.4	58.1	126	39.8	29.6	66.8	20
Ce	179	224	221	188	171	245	228	175	108	273	126	85.8	185	43
Pr	23.0	34.6	27.9	27.7	22.2	30.6	30.4	21.7	14.5	34.1	15.1	9.36	20.0	4.9
Nd	92.7	153	122	141	104	128	129	85.4	58.5	120	62.2	35.5	80.8	20
Sm	16.8	28.5	23.2	29.5	19.0	23.3	22.3	16.2	11.8	25.4	13.5	7.36	18.3	3.9
Eu	3.28	4.40	4.00	3.89	2.95	3.68	3.76	2.67	0.552	0.342	0.179	0.135	0.109	1.1
Gd	8.67	14.8	13.5	13.8	9.98	12.1	11.4	7.89	6.49	14.6	8.84	4.63	11.2	3.7
Tb	1.08	1.65	1.72	1.60	1.34	1.47	1.47	0.988	0.893	2.16	1.30	0.731	2.04	0.6
Dy	5.32	7.43	8.60	7.25	6.81	6.64	6.79	4.89	4.75	12.2	6.45	3.74	10.8	3.6
Ho	0.946	1.25	1.47	1.19	1.21	1.14	1.14	0.865	0.921	2.35	1.17	0.689	2.08	0.77
Er	2.31	2.91	3.95	2.87	2.87	2.94	2.76	2.11	2.37	6.33	2.96	1.98	5.04	2.1
Tm	0.325	0.407	0.538	0.394	0.400	0.391	0.403	0.321	0.385	0.970	0.476	0.299	0.747	0.28
Yb	1.89	2.39	3.24	2.30	2.63	2.37	2.69	1.88	2.54	5.86	3.10	1.99	4.25	1.9
Lu	0.259	0.358	0.464	0.319	0.398	0.358	0.413	0.25	0.380	0.769	0.440	0.274	0.637	0.30
Hf	12.1	19.2	23.9	16.6	14.5	21.3	34.7	20.4	22.9	24.7	14.3	11.4	18.1	3.7
Ta	1.79	2.90	3.83	2.21	2.31	3.44	4.83	3.50	3.13	12.7	8.71	6.95	9.59	0.7
W	3.16	2.10	10.5*	13.0*	10.6*	5.08	1.79	1.83	1.07	3.80	1.21	10.1*	23.3*	1.0
Bi	0.78	0.64	2.12	0.68	0.68	3.71	<0.2	<0.2	3.08	<0.2	1.99	1.34	0.586	0.18
Th	53.5	97.8	136	114	87.4	104	192	131	211	278	120	113	152	5.6
U	18.7	19.2	30.2	24.7	21.5	27.9	12.9	16.5	29.4	36.3	23.0	61.8	58.9	1.3
La_N/Lu_N	31.49	34.94	24.51	25.63	21.92	32.63	27.53	31.59	15.80	16.94	9.35	11.17	10.84	6.89
Sm/La	0.213	0.236	0.211	0.373	0.225	0.206	0.203	0.212	0.203	0.202	0.339	0.249	0.274	0.195
Th/La	0.320	0.808	1.236	1.441	1.036	0.920	1.745	1.725	3.632	2.206	3.015	3.818	2.275	0.28
Mg#	75	74	63	67	57	64	50	49	45	7	38	37	34	

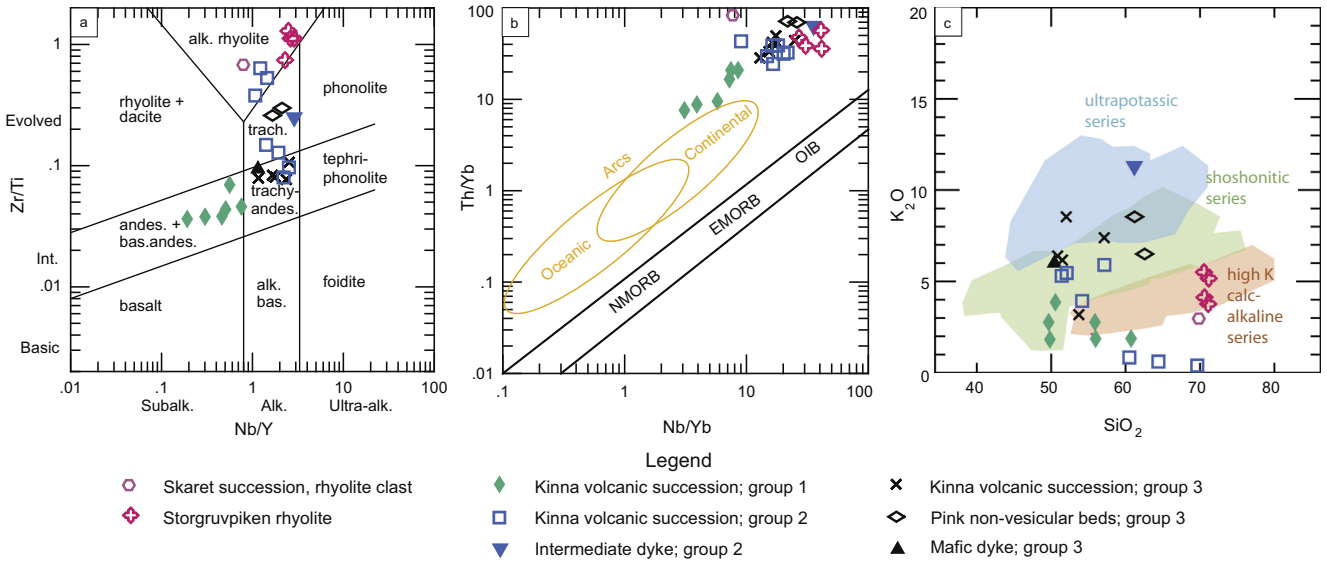

Fig. 7. a. Classification of Skarvatnet unit samples based on the stable elements Zr, Ti, Nb and Y (Pearce, 1996). b Th/Yb vs. Nb/Yb plot (Pearce, 2008) with fields of volcanic rocks from oceanic and continental arcs. All samples from the Skarvatnet unit are highly enriched compared to normal arc rocks. c K_2O vs. SiO_2 plot with fields for high-K calc-alkaline (orange), shoshonitic (green) and ultrapotassic (blue) Italian rocks summarized by Conticelli et al. (2010) for comparison.

According to White (2000), one of the main diagnostic features of submarine pyroclastic flows are enclosing submarine deposits. The Kinna succession interfingers with cherts, siltstones and pillow lavas (Fig. 2), and the associated Skaret succession is clearly shallow-marine. Therefore, we envisage a submarine deposition of the Kinna succession as most likely. However, there is no evidence that the deposits have been sorted by water; the fragments are for instance randomly distributed with respect to fragment size and vesicularity. The regular nature of the beds and the lack of erosional channels or valley fills point to either deposition below wave base or ash fall-outs (Fisher and Schmincke, 1984). However, the lack of sorting within beds is atypical for both subaerial and submarine fallout deposits; poorly sorted, massive but stratified deposits are rather associated with deposition from density currents formed during collapse of subaqueous plumes (Kano, 2003; White, 2000).

Available evidence thus suggests an origin as submarine pyroclastic flows from submarine volcanic eruptions. We envisage a depositional environment around predominantly intermediate to felsic submarine volcanic centres comparable to the recent Myojin Knoll caldera in the Izu-Bonin arc (Fiske et al., 2001), where thick pumice deposits similar to the Kinna fragment-bearing beds are observed. The Kinna volcanic succession also has similarities with the VMS-hosting Bald Mountain, Maine, USA; this deposit consists of beds with pumice and medium- to coarse-grained ash separated by fine-grained tuff beds (Busby, 2005). The pumiceous beds of the Bald Mountain are considered to have formed from an eruption column with limited mixing with ambient water, while the tuff beds represent erupting phases with more admixed water (Busby, 2005; Kessel et al., 2003). Submarine pyroclastic deposits have varying degrees of sorting, depending on size and vesicularity of the fragments, their temperature during eruption and water depth. Products of deep-water eruptions are generally considered to be depleted in fine ash, as a result of either removal of fine ash because of mixing with water (Kano, 2003), or limited fragmentation due to high hydrostatic pressure (Busby, 2005). Unfortunately, the original grain size of the finer material in the Kinna volcanic succession cannot be identified due to metamorphic recrystallization, and can therefore not be used to constrain the depth of water during eruption. However, the Bald Mountain erupted at >1.45 km below sea level (Kessel et al., 2003) and a comparable deep marine setting is possible also for the Kinna volcanic succession.

4.1.2. The Storgruvpiken rhyolite

The Storgruvpiken rhyolite cuts obliquely through the Kinna volcanic succession and has large inclusions of country rock in parts of the body (Fig. 5a), suggesting that it had at least partly an intrusive rather than volcanic origin. The very fine-grained nature is most consistent with a shallow emplacement, and a composite volcanic plug and dome structure is also conceivable. The rhyolite is non-vesicular and almost devoid of hydrous minerals, indicating a volatile-poor magma compared to the Kinna volcanic succession. The high viscosity of such a SiO_2-rich, dry magma would promote the formation of flow-banding, as observed at Storgruvpiken, whether it was in a volcanic dome or in a subvolcanic plug. Phenocrysts of K-feldspar are euhedral, and fragmented phenocrysts are not observed. This indicates that explosive fragmentation was very limited or absent, as phenocrysts are commonly shattered during fragmentation of a magma (e. g. Fisher and Schmincke, 1984).

4.1.3. The Skaret succession

The abundant conglomerates of the Skaret succession, with large blocks and soft-sediment deformation structures in associated sandstones, indicate an origin largely as coarse debris flow deposits. The high diversity of the clast material (basaltic and rhyolitic rocks (Skaret clast; Figs. 7-9), jasper, chert, Kinna-type volcanic clasts, marble, siltstone and sandstone) shows that the source area was complex, but all the material observed could have been derived from local sources within the low-grade metamorphic part of the TNC. The carbonate content of the greywacke, the carbonate clasts and blocks, and presence of carbonate beds show that the sediment was derived from a shallow marine source, and the metre-sized blocks suggest that the source is proximal. The soft-sediment deformation structures, chaotic deposits and large blocks attest to a tectonically active environment and strong relief. There are no direct constraints on the age of the Skaret succession, but conglomerate clasts similar to the Kinna volcanic succession and rhyolite clasts comparable to the Storgruvpiken rhyolite (Skaret clast; Figs. 7-9) indicate that the Skaret succession was deposited after emplacement of the Storgruvpiken rhyolite.

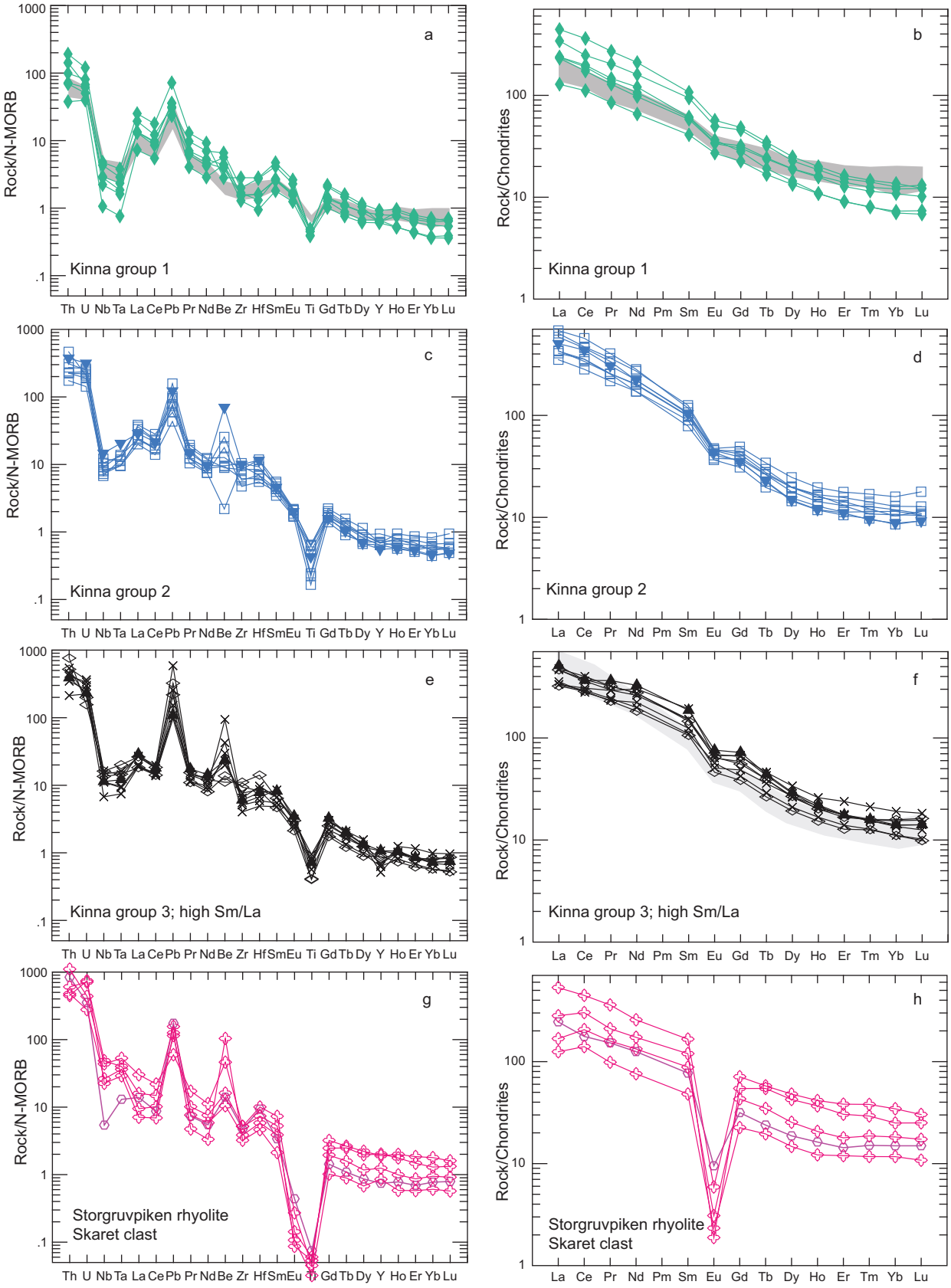

Fig. 8. Left column: Sample versus N-MORB, normalization values from Gale et al. (2013). The position of beryllium is chosen on the basis of its geochemical similarity to Nd and Zr (Ryan, 2002). Right column: Sample versus chondrite, normalization values from Sun and McDonough (1989). The dark grey shaded fields in Fig. 8a and Fig. 8b correspond to the Hølonda porphyrites (Grenne and Roberts, 1998). The light grey shaded field in Fig. 8f corresponds to the REE-patterns of Kinna group 2.

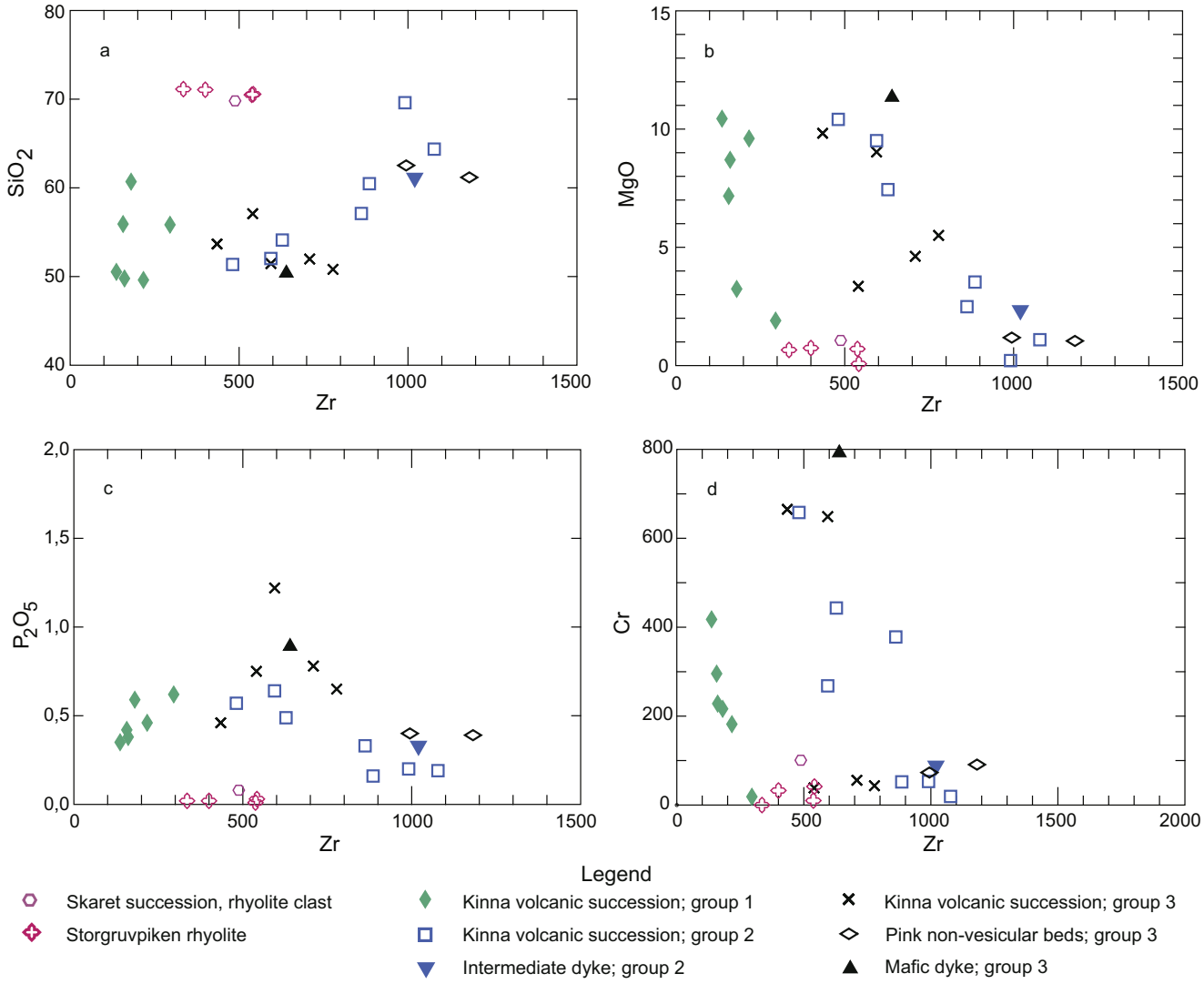

Fig. 9. Zirconium versus SiO_2, MgO, P_2O_5 and Cr. Kinna group 1 and the Storgruvpiken rhyolite plot in separate groups, while there is more overlap between Kinna groups 2 and 3. See text for discussion.

4.2. Petrogenesis

4.2.1. The Kinna volcanic succession

The overall geochemical characteristics of the Kinna volcanic succession, such as Nb, Ta and Ti depletion and Pb enrichment (Fig. 8), show a clear affinity to subduction-related, arc-type rocks. However, compared to more common arc-type rocks, the Kinna rocks are extremely enriched in elements like Th, U, LREE, Be and Zr, they have relatively high K_2O (up to 11 wt%), but also relatively high MgO and Mg#, Cr and Ni (Table 1; Figs. 7–10).

Similar potassic to ultrapotassic, highly enriched volcanic rocks with mantle affinities are rare in modern settings, but the ones that exist have received considerable attention (e.g. Bergman, 1987; Foley, 1992a; Foley et al., 1987; Förster et al., 2017; Prelević et al., 2008; Tommasini et al., 2011). They occur both within plate (anorogenic settings) and along plate boundaries (orogenic or subduction-related settings; e.g. Bergman, 1987; Prelević et al., 2008). Orogenic-type potassic rocks are most common in the Mediterranean and along the Alpine-Himalayan belt, for instance in Spain (e.g. Pérez-Valera et al., 2013), Italy (e.g. Conticelli et al., 2009; Peccerillo, 1999), the Balkan Peninsula (e.g. Prelević et al., 2005), the Aegean (e.g. Ersoy and Palmer, 2013; Pe-Piper et al., 2009), Turkey (Dilek and Altunkaynak, 2009), Iran (e.g. Shafaii Moghadam et al., 2018) and Tibet (e.g. Cheng and Guo, 2017). Plutonic and volcanic rocks with similar geochemical characteristics have also been reported from the older Variscan (e.g. Soder and Romer, 2018) and Caledonian (e.g. Thompson and Fowler, 1986; West et al., 2007) orogenic belts. The striking geochemical similarities noted above lead us to consider these orogenic potassic volcanic rocks the closest analogue for the interpretation of petrogenesis and tectonic setting of the Kinna volcanic succession.

There seems to be a consensus in the literature that the extreme enrichment of various elements in orogenic potassic rocks with obvious mantle signatures (Mg# >70, high MgO, Ni and Cr values) cannot be the result of crustal contamination, assimilation and fractionation of a mantle-derived magma on its way up through the continental crust, but has to be a primary feature of melts derived from anomalously enriched subcontinental lithospheric mantle domains (e.g. Bergman, 1987; Conticelli et al., 2009; Foley et al., 1987; Förster et al., 2017; Prelević et al., 2008; Prelević et al., 2013). Where phenocrysts of olivine, spinel or pyroxene are present, the mineral chemistry (very high Mg#, high Cr and Ni contents) indicate a depleted mantle source for the ultrapotassic rocks (e.g. Förster et al., 2017; Prelević et al., 2013). The

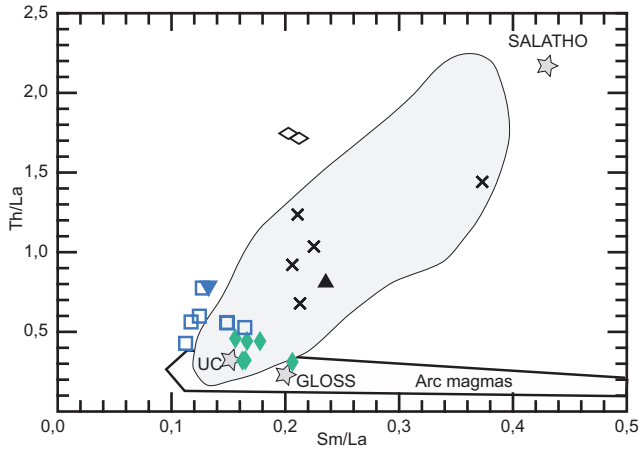

Fig. 10. Th/La versus Sm/La plot for the Kinna volcanic succession. The Storgruvpiken rhyolite samples have extreme Th/La ratios and plot outside the diagram. GLOSS (Global Subducting Sediment; Plank and Langmuir, 1998) and UC (Upper Crust; Rudnick and Gao, 2003) represent average composition of recycled crustal material. The arc magma field is from Plank (2005) and represents 'normal' arc magmas. The grey field represents analyses from Tethyan lamproites and related rocks from Tommasini et al. (2011). SALATHO is the high Sm/La and Th/La component of Tommasini et al. (2011).

whole rock chemistry of several Kinna rocks is comparable to mantle-derived ultrapotassic rocks studied by e.g. Prelević et al. (2013), but the lack of preserved phenocrysts of olivine or pyroxene in the metamorphosed Kinna rocks hampers more detailed interpretations of the mantle source composition for the latter. The crustal-like enrichment signatures of orogenic potassic rocks are generally assigned to a metasomatic agent derived from subducting continental material (e.g. Conticelli et al., 2009; Plank and Langmuir, 1998; Prelević et al., 2013). Transport of incompatible elements from the subducting slab into the overlying mantle wedge is more efficient by partial melts (including supercritical fluids) of slab components, than by aqueous fluids released during dehydration (e.g. Conticelli et al., 2010; Hermann and Rubatto, 2009; Spandler and Pirard, 2013). High-pressure melts of crustal rocks have K/Na molar ratios of 1.4–2 (Schmidt et al., 2004), and the high K_2O of ultrapotassic rocks indicate addition of such crustal components to the mantle (Soder and Romer, 2018).

Partial melting of slab components at sub-arc depths seems to be a common feature in many subduction zones, with the fluids needed for melting derived from dehydration of serpentinites from either the oceanic lithospheric mantle or from within the mélange zone at the top of the down-going slab (e.g. Spandler and Pirard, 2013), or derived from high pressure dehydration of phengite in subducted continental crust or sediments (Hermann and Rubatto, 2009; Schmidt et al., 2004). The trace element budget of these melts is controlled by the stability of accessory phases such as monazite/allanite (LREE, Th, U), phengite (LILE), titanite (REE, Nb, Ta), rutile (Nb, Ta), zircon (Zr, Hf), garnet (HREE), zoisite/epidote (REE, Sr, Th, U, Pb) and lawsonite (REE, Pb, Sr) (Hermann and Rubatto, 2009; Spandler et al., 2003). Breakdown of for example monazite/allanite together with residual garnet and rutile generally explains the enrichment of LREE over HREE as well as the negative Nb—Ta anomalies of typical arc rocks (e.g.; Hermann and Rubatto, 2009).

The trace element patterns and ratios of Kinna rocks (Figs. 8-10) correspond well with an origin from a mantle metasomatized by partial melts of common subducting slab components (i.e. pelitic sediments, continental crust) with the Th and REE element budget controlled by common accessory phases such as monazite/allanite, rutile and garnet (e.g. Figs. 8-10; Spandler and Pirard, 2013). However, the Sm/La vs. Th/La ratios of the Kinna group 3 samples are distinctly different from those of Kinna 1 and 2 and are also different from common arc magmas, falling along a positive trend towards the SALATHO component of Tommasini et al. (2011; Fig. 11). Such a positive trend is present in many lamproites from the Alpine-Himalayan chain (e.g. Tommasini et al., 2011) as well as in Variscan lamprophyres (Soder and Romer, 2018). This relation requires a component that simultaneously fractionates Th—La and Sm—La, and Tommasini et al. (2011) consider blueschist-facies mélanges rich in lawsonite and zoisite-epidote the source for this unusual composition. Such lithologically complex mélange zones, consisting of a mixture of oceanic crust, sediments and mantle wedge/forarc lithologies enable a variety of fluids and melts to be produced during progressive subduction (Bebout and Penniston-Dorland, 2016; Marschall and Schumacher, 2012) and may add considerable compositional complexity to the mantle wedge (e.g. Guo et al., 2014; Prelević et al., 2013; Spandler and Pirard, 2013).

The Kinna 3 melts could therefore have been derived from a mantle domain strongly metasomatized by a mélange-derived agent, in contrast to the Kinna 1 and 2 melts. Alternatively, Soder and Romer (2018) ascribe high Sm/La vs. Th/La ratios of the Variscan lamprophyres

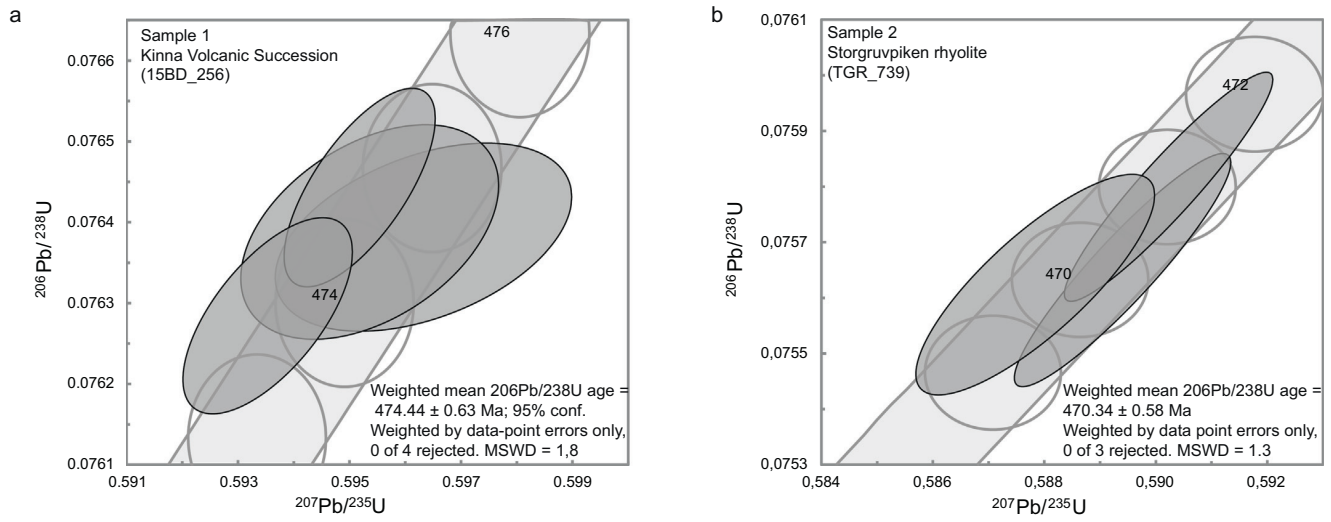

Fig. 11. Concordia plots for the zircon U—Pb TIMS data. Data point ellipses are 2σ; plots are made with ISOPLOT (Ludwig, 2003). a Sample 1: Pink non-vesicular bed from the Kinna volcanic succession, with a mean age of 474 ± 1 Ma (2σ; MSWD = 1.8). b Sample 2: Storgruvpiken rhyolite, with a mean age of 470 ± 1 Ma (2σ; MSWD = 1.3).

Table 2
U—Pb analytical data. a ZR = zircon; lrg = large, fr = fragment, eu = euhedral, eq = equant, br = brown, pnk = pink, AA = air abraded, CA = chemically abraded. b Th/U model ratio inferred from $^{208}Pb/^{206}Pb$ ratio and age of sample. c Pbc = total common Pb (initial + blank). d raw data, corrected for fractionation and spike. e ratio of radiogenic Pb over common Pb (including blank). f corrected for fractionation, spike, blank and initial common Pb (based on Stacey and Kramers, 1975); error calculated by propagating the main sources of uncertainty; The U—Pb ratio of the spike used for this work is adapted to $^{206}Pb/^{238}U = 0.015660$ for the ET100 solution as obtained with the ET2535 spike at NIGL.

						Isotopic ratios							AGE [Ma]					
Sample (a)	U [ppm]	Th/U (b)	Pb_c (pg) (c)	$^{206}Pb/^{204}Pb$ (d)	Pb^*/Pb_c (e)	$^{207}Pb/^{235}U$ (f)	2 sigma % (f)	$^{206}Pb/^{238}U$ (f)	2 sigma % (f)	corr. coef.	$^{207}Pb/^{206}Pb$ (f)	2 sigma % (f)	$^{206}Pb/^{238}U$ (f)	± 2 sigma (f)	$^{207}Pb/^{235}U$ (f)	± 2 sigma (f)	$^{207}Pb/^{206}Pb$ (f)	± 2 sigma (f)
Sample 1, Kinna volcanic succession (15-BD-256A)																		
1 LRG ZR FR CLEAR CA	1670	0.78	1.3	6085	111	0.59518	0.19	0.07644	0.13	0.70	0.05647	0.13	474.9	0.6	472.4	0.7	470.9	3.0
1 ZR FR CLEAR CA	317	0.73	1.2	1249	22	0.59633	0.36	0.07638	0.12	0.43	0.05662	0.33	474.5	0.6	474.9	1.4	476.9	7.3
1 ZR FR CLEAR CA	787	0.71	1.5	2447	44	0.59536	0.32	0.07639	0.14	0.43	0.05653	0.29	474.5	0.6	474.3	1.2	473.1	6.3
1 ZR FR CLEAR CA	1439	0.62	2.5	2738	47	0.59353	0.21	0.07628	0.13	0.65	0.05643	0.16	473.9	0.6	473.1	0.8	469.3	3.5
Sample 2, Storgruvpiken rhyolite (TGR12_739)																		
1 Z EU-EQ. BR AA	5108	0.43	4.2	5755	189	0.58940	0.27	0.07565	0.23	0.92	0.05651	0.11	470.1	1.0	470.5	1.0	472.4	2.3
1 Z EQ-EU BR AA	3576	0.41	1.1	15,947	353	0.59023	0.26	0.07580	0.22	0.94	0.05647	0.09	471.0	1.0	471.0	1.0	471.1	2.0
1 Z EU-EQ PNK AA	2047	0.45	2.7	3579	229	0.58784	0.30	0.07562	0.21	0.81	0.05638	0.18	469.9	1.0	469.5	1.1	467.2	3.9

to the presence of residual allanite in partial melts derived from crustal material under high pressure conditions. A similar origin for the Kinna volcanic succession can be envisaged: Kinna 1 and 2 could be derived from mantle domains that were metasomatized by an agent where allanite was dissolved into the melt, whereas Kinna 3 could be derived from mantle domains metasomatized by an agent where allanite was a residual phase during formation of the agent by partial melting of continental material. Soder and Romer's (2018) explanation of high Sm/La vs. Th/La ratios is more straightforward than the model of Tommasini et al. (2011) and does not require a totally different origin of the metasomatic melts (continental material versus blueschist melange), but only requires variable allanite dissolution into a metasomatic agent derived from subducted continental material. The steep slope of the Kinna REE patterns, with strong LREE enrichment (Fig. 8) might indicate the presence of garnet in the source, either in the subducted continent-derived material or in the metasomatically altered mantle, since garnet easily accommodates HREE but not LREE (e.g. Hermann and Rubatto, 2009).

Mantle metasomatism is generally assumed to occur within localized networks of veins and fractures, leading to mantle domains with phlogopite-, amphibole- and/or pyroxene-rich veins and dykes within peridotitic wall-rocks (e.g. Foley, 1992a; Foley, 1992b; Förster et al., 2017; Marocchi et al., 2010; Spandler and Pirard, 2013). Transitions from high-K through shoshonitic to ultrapotassic rocks are generally explained by processes where partial melts received variable contributions from either vein or wall-rock domains (e.g. Conticelli et al., 2010; Förster et al., 2017; Marocchi et al., 2010). We therefore envisage that the variation from high-K to ultrapotassic rocks observed within the Kinna volcanic succession (Fig. 7c), at least partly could be the result of variable vein/wall-rock contribution during mantle partial melting.

4.2.2. The Storgruvpiken rhyolite

The Storgruvpiken rhyolite is apparently unique in the Scandinavian Caledonides; to our knowledge no other rhyolite in this part of the orogen is similarly enriched in e.g. Be and Th. On the other hand it shares several geochemical features with the older Kinna volcanic succession, including high Th, Zr and Be concentrations and LREE enrichment, potentially indicating that they might have a related origin by, for example, differentiation and fractional crystallisation processes. However, the ca. 4 m.y. difference in age and key geochemical characteristics listed in the following suggest that this is not the case.

Compared to the Kinna 1 samples, the rhyolites have higher Zr (Fig. 9) that could be interpreted in terms of fractional crystallisation, but such a relationship conflicts with their significantly different ratios of highly incompatible trace elements, e.g., Th/La and Ta/La ratios (Fig. 8). Compared to the Kinna 2 samples, the Storgruvpiken rocks have low Zr concentrations that possibly could be interpreted in terms of crystallisation and removal of zircon from strongly fractionated melts; however, again this conflicts with the significantly different trace elements patterns (Fig. 8). Moreover, the lack of a compositional continuum from Kinna rocks to the voluminous Storgruvpiken rhyolite (Fig. 9) is noteworthy and argues against a fractional crystallisation connection. Furthermore, the rhyolites have peraluminous and A-type characteristics, which are commonly associated with partial melting of crustal rocks (Barbarin, 1999) rather than mantle derivation, different from those of Kinna. Therefore, an origin of the Storgruvpiken rhyolite as a differentiation product of one of the Kinna types is ruled out.

Alternatively, The Storgruvpiken rhyolite could have a similar veined mantle source as the Kinna rocks, with a different vein/wall-rock contribution during partial melting. However, the Storgruvpiken rhyolite has a highly evolved chemical composition that requires extensive fractionation from a larger volume of mantle melt. The large volume of the Storgruvpiken rhyolite and the lack of a mafic or intermediate counterpart argue against this explanation.

Another model for the Storgruvpiken rhyolite might involve partial melts of subducted material that rose diapirically directly through the mantle instead of reacting metasomatically with it. Such diapiric rise of subducted mélange material has been suggested by Marschall and Schumacher (2012). Their model suggests that heating from the surrounding mantle and consequent dehydration of such diapirs initially leads to hydrous mantle melting, which produces melts enriched in fluid-mobile elements. Further heating of the rising diapir produces dry magmas with higher contents of immobile elements like Th and Be. In this line of reasoning, Kinna 1 could result from melting of a hydrated mantle and the Storgruvpiken rhyolite could represent late stage dry melting of such a diapir; however, this model does not explain the strong enrichment of immobile elements in the clearly mantle-derived Kinna rocks.

It is also possible that the Storgruvpiken rhyolite genesis involved magmas similar to the Kinna volcanic succession, derived by partial melting of metasomatized mantle and with high Th, LREE, HFSE etc., that crystallized at depth in the crust or at the crust-mantle interface. Subsequent partial melting of such enriched rocks under lower crustal conditions may produce felsic magma and is likely to leave plagioclase and amphibole as residual phases (Qian and Hermann, 2013). With the mineral/melt partition coefficients given by Qian and Hermann (2013), residual plagioclase is consistent with the negative Eu anomaly as well as the higher Th/La and Nb/La of the Storgruvpiken rhyolite compared to the Kinna volcanic succession. Partial melting in the lower crust also allows for melting of some metasedimentary rocks and reaction between melts, possibly accounting for the peraluminous character of the Storgruvpiken rhyolite. In view of the absence of other than strongly

enriched rocks in the area, this scenario requires that remelting of Kinna-type intrusions was more significant than melting of surrounding 'normal' lower crust at least on a local scale. Given the relatively short time span between the dated part of the Kinna volcanic succession and the Storgruvpiken rhyolite (<4 Ma), it is reasonable to assume that the Kinna-type intrusions remained hotter than the surrounding lower crust. Together with a higher content of hydrous minerals (biotite, amphibole), which are common constituents of the Kinna volcanic succession, this would have made the intrusions more susceptible to melting compared to normal lower crust (Annen and Sparks, 2002).

4.2.3. Beryllium enrichments

A peculiar feature of the Storgruvpiken rhyolite, partly also of the Kinna volcanic rocks, is the very strong enrichment in beryllium (up to 66.5 ppm Be; Table 1). For comparison, the Miocene Spor Mountain rhyolites in western Utah, USA, which host the world's largest beryllium deposit, contain up to 75 ppm Be in matrix glass (Dailey et al., 2018). Economic concentrations of bertrandite in adjacent tuffs at Spor Mountain (up to 0.3 wt% Be), may have been facilitated by fluids released from the rhyolite lava during crystallisation or devitrification (Christiansen et al., 1986). Although the Kinna pyroclastic volcanic rocks potentially could have served as a comparable host for Be enrichment from Storgruvpiken-derived fluids, economic-grade Be concentrations remain to be found; the highest value detected in the present study within the Kinna succession is 60.1 ppm Be (Table 1).

Arc magmas generally have higher concentrations of Be compared to MORB; reflecting the mobility of Be from the sedimentary cover of subducted crust to the mantle at high P and T (Marschall et al., 2007). Beryllium is generally thought to be immobile during dehydration; however, only a small amount of Be added to the mantle wedge can be sufficient to produce the enrichment observed in arc rocks (Marschall et al., 2007). Ryan (2002) found that more Be is transferred from the subducted slab to the overlying mantle with increasing pressure and temperature and that Be contents are generally higher in alkaline rocks. Partition coefficient data for Be are scarce, but Be is known to be accommodated in biotite, plagioclase and K-feldspar in peraluminous silica-rich systems (Bea et al., 1994). Hence Be enrichments may be explained by small amounts of partial melting of crustal rocks, leading to break-down of biotite in the source rock, as inferred for the Be—Th rich A-type rhyolites at Spor Mountain (Christiansen et al., 1988) which show several geochemical similarities with the Storgruvpiken rhyolite. The Be-enrichment of the Storgruvpiken rhyolite is therefore interpreted as a result of partial melting of biotite-bearing Kinna-type rocks at crustal depth.

4.3. Tectonic model and regional geological implications

Our new data indicate that high-K to ultrapotassic mantle-derived volcanism occurred at 475–470 Ma in terranes now represented in the TNC, post-dating formation of the supra-subduction zone LVB ophiolites of the northwestern TNC. The timing of this volcanism corresponds with obduction of the LVB ophiolites onto a continental margin, supposedly on the Laurentian side of Iapetus, and we infer a link between the obduction and the onset of the potassic mantle-derived volcanism. Based on these temporal relationships we propose the following three-stage model for the tectonic evolution of the Kinna volcanic succession and associated rocks:

(1) A southeast-dipping intra-oceanic subduction zone produced an oceanic island arc with associated back-arc basin (the LVB ophiolites) at 487 to 480 Ma (Fig. 12a) (e.g. Slagstad et al., 2014).
(2) At ca. 480 Ma, the Laurentian margin or a related microcontinent arrived at this subduction zone, leading to an increased input of terrigenous sediments and possibly crustal slivers into the subduction zone (Fig. 12b). Partial melts derived from these crustal rocks affected the overlying mantle wedge, producing a network of metasomatic veins surrounded by unaltered mantle wall rock. In order to produce Kinna 1 and 2 metasomatic agents, extensive breakdown of allanite must have occurred during melting of the crustal rocks, whereas the Kinna 3 metamorphic agent with high Sm/La and Th/La ratios might be derived from melts where allanite remained as a residual phase (e.g. Soder and Romer, 2018).
(3) Ongoing convergence led to obduction of parts of the LVB island arc, as well as formation of a thrust stack in the underlying continental margin, which resisted subduction due to buoyancy. This may have resulted in slab retreat and finally break-off of the downgoing oceanic slab, where asthenospheric upwelling might have provided the heat for partial melting of previously metasomatized mantle lithologies (Fig. 12c). Some of these partial melts rose directly to the surface, producing the hydrous melts and explosive volcanism of Kinna 1, 2 and 3 type at ca. 474 Ma. Other melt batches may have crystallized as Kinna-type plutons at depth in the crust and were later possibly partially remelted to produce the dry melts of the Storgruvpiken rhyolite at ca. 470 Ma.

This interpretation infers that the Kinna and Storgruvpiken volcanic rocks were not simply related to normal subduction-related arc

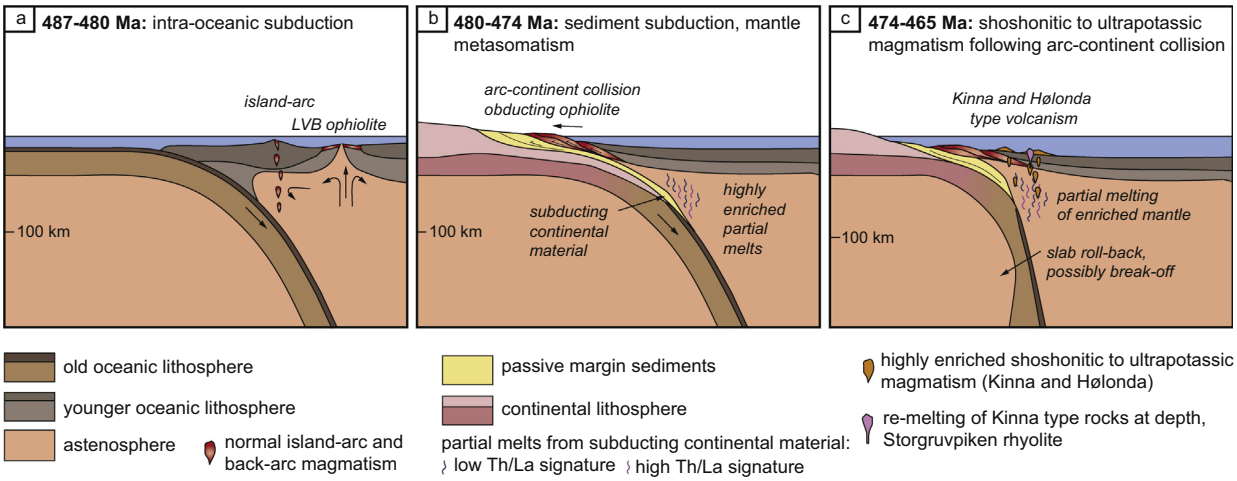

Fig. 12. Tectonic model for the formation of the Skarvatnet unit. See text for discussion.

magmatism, but instead represent the remnants of a distinct tectonic phase along the Laurentian margin of Iapetus, subsequent to the intra-oceanic subduction that dominated the early stages of Iapetus closure. The intra-oceanic subduction terminated when it encountered the Laurentian margin, and slab break-off or other processes led to an intermittent phase producing the highly enriched high-K to ultrapotassic magmatism in the Skarvatnet unit. Such an intermittent tectonic phase has not yet been recognized along the Iapetus margin elsewhere, but the similarly aged Taconian orogen in the Appalachians might have experienced a comparable evolution. There, the Laurentian margin was thrusted under the Notre Dame Arc and equivalents in the Early Ordovician, leading to slab break-off followed by subduction polarity flip and accretion of several ophiolites and arc fragments (e. g. Lissenberg et al., 2005). Although shoshonitic and related potassic rocks are rare in the Appalachians, a 464–462 Ma monzogabbro within the Annieopsquotch Accretionary Tract has shoshonitic geochemical characteristics (Lissenberg et al., 2005) and could be the result of a process similar to that of the Kinna volcanic succession. Slab roll-back (e.g. Cheng and Guo, 2017; Conticelli et al., 2009; Guo et al., 2014) and slab break-off (e.g. Pe-Piper et al., 2009) are also considered as triggering factors for partial melting of metasomatized mantle domains for parts of the Alpine-Himalayan ultrapotassic rocks.

As a consequence of this interpretation, also the tectonic significance of the Hølonda porphyrites has to be reconsidered. These rocks, like the Kinna 1 volcanic rocks, are shoshonitic and are significantly enriched in LREEs and Th (Grenne and Roberts, 1998) although with less extreme compositions (Fig. 8a, b). Many of the Mediterranean potassic to ultrapotassic mantle-derived rocks are associated with less-enriched calc-alkaline to shoshonitic rocks, interpreted to represent partial melts of less-metasomatized mantle domains or larger amounts of wall-rock versus vein-derived mantle melts (e.g. Conticelli et al., 2009; Conticelli et al., 2010; Peccerillo and Martinotti, 2006). Based on the interpretation of these Mediterranean examples of calc-alkaline to ultrapotassic rock suites, we propose that also the Kinna and Hølonda volcanic rocks are related, and that they resulted from the same process of partial melting of variably enriched mantle after arc-continent collision (Fig. 12c). This is at variance with the existing model where the Hølonda porphyrites reflect the first proper subduction below the Laurentian margin, a model that would require very quick polarity flip after obduction of the LVB ophiolite (Grenne and Roberts, 1998). Such a quick subduction polarity flip is not required in our present model, which opens for the possibility that, in this part of the orogen, subduction below the Laurentian margin did not start until ca. 460 Ma, as represented for example by much less enriched arc-type plutons e.g. in the Smøla-Hitra region (Tucker et al., 2004).

5. Conclusions

The Skarvatnet unit, consisting of the Kinna volcanic succession, the Storgruvpiken rhyolite and the Skaret sedimentary succession, represents a lithologically and geochemically distinctive volcano-sedimentary phase hitherto unknown in the Ordovician of the Scandinavian Caledonides. The Kinna volcanic succession is interpreted as a series of submarine pyroclastic flows extruding at ca. 474 Ma, which were intruded by the subvolcanic Storgruvpiken rhyolite at ca. 470 Ma and were subsequently overlain by the shallow-marine Skaret succession in a tectonically active setting. The Kinna volcanic succession shows geochemical signatures far more enriched in for instance Th, U, Pb and LREE than common arc-related rocks, similar to high-K to ultrapotassic rocks of the Alpine-Himalayan belt and other orogenic settings. Based on the comparison with these better studied rock suites, the Kinna volcanic succession is interpreted as representing partial melts derived from previously enriched mantle sources. Enrichment of the mantle source is related to subduction of large amounts of continent-derived material, releasing highly enriched partial melts interacting with the overlying mantle. In the case of the Kinna volcanic succession, this mantle enrichment might have occurred during initial subduction of the Laurentian margin or an associated micro-continent below the originally intra-oceanic LVB arc. Partial melting of the enriched mantle occurred coeval with or slightly after arc-continent collision, possibly facilitated by astenospheric upwelling related to slab retreat or break-off. The Storgruvpiken rhyolite is possibly the result of remelting of Kinna-type plutonic rocks at depth, caused by the same upwelling at ca. 470 Ma.

The slightly younger shoshonitic Hølonda porphyrites are interpreted to be a part of this tectono-magmatic phase, in contrast to earlier interpretations that postulate the Hølonda magmas as a result of subduction below Laurentia subsequent to slab polarity reversal. The existence of extremely enriched volcanic rocks of this type long before the final closure of the Iapetus Ocean demonstrates that such rocks may form not only during or after major continent-continent collisions, but also during earlier phases in complex subduction–accretion–collision systems.

Acknowledgements

E. W. Stokke assisted in the field and lab, G. Fjeld Bye and the technical staff at NGU has prepared and/or analysed samples. Discussions with A. Andresen, J. P. Nystuen and T. Andersen are highly appreciated. Editorial handling by Michael Roden and constructive feedback from reviewers Christian Soder and Dejan Prelević helped to improve the manuscript.

Funding

This work is a part of the first authors PhD thesis, funded by the University of Oslo. The Geological Survey of Norway has funded fieldwork and geochemical analyses under project number 353000.

Declaration of Competing Interests

The authors declare that they have no known competing financial interests or personal relationships that could have appeared to influence the work reported in this paper.

References

Annen, C., Sparks, R., 2002. Effects of repetitive emplacement of basaltic intrusions on thermal evolution and melt generation in the crust. Earth Planet. Sci. Lett. 203, 937–955.
Augland, L.E., Andresen, A., Corfu, F., 2010. Age, structural setting, and exhumation of the Liverpool Land eclogite terrane, East Greenland Caledonides. Lithosphere 2, 267–286.
Barbarin, B., 1999. A review of the relationships between granitoid types, their origins and their geodynamic environments. Lithos 46, 605–626.
Bea, F., Pereira, M., Stroh, A., 1994. Mineral/leucosome trace-element partitioning in a peraluminous migmatite (a laser ablation-ICP-MS study). Chem. Geol. 117, 291–312.
Bebout, G.E., Penniston-Dorland, S.C., 2016. Fluid and mass transfer at subduction interfaces—the field metamorphic record. Lithos 240, 228–258.
Bergman, S.C., 1987. Lamproites and other potassium-rich igneous rocks: a review of their occurrence, mineralogy and geochemistry. Geol. Soc. Lond. Spec. Publ. 30, 103–190.
Bowring, J.F., McLean, N.M., Bowring, S., 2011. Engineering cyber infrastructure for U-Pb geochronology: Tripoli and U-Pb_Redux. Geochem. Geophys. Geosyst. 12 (no. 6).
Bruton, D.L., Bockelie, J.F., 1980. Geology and paleontology of the Hølonda area, western Norway—a fragment of North America. The Caledonides in the USA. Virginia Polytechnic Institute and State University, Department of Geological Sciences. Memoir 2, 41–47.
Busby, C., 2005. Possible distinguishing characteristics of very deepwater explosive and effusive silicic volcanism. Geology 33, 845–848.
Cheng, Z., Guo, Z., 2017. Post-collisional ultrapotassic rocks and mantle xenoliths in the Sailipu volcanic field of Lhasa terrane, South Tibet: Petrological and geochemical constraints on mantle source and geodynamic setting. Gondwana Res. 46, 17–42.
Christiansen, E.H., Burt, D.M., Sheridan, M.F., 1986. The geology and geochemistry of Cenozoic topaz rhyolites from the western United States. Geol. Soc. Am. Spec. Pap. 205.
Christiansen, E.H., Stuckless, J.S., Funkhouser, M., Howell, K., 1988. Petrogenesis of rare-metal granites from depleted crustal sources: an example from the Cenozoic of western Utah, USA. Recent advances in the Geology of Granite-Related Mineral Deposits. Canadian Institute of. Min. Metall. 39, 307–321.
Conticelli, S., Guarnieri, L., Farinelli, A., Mattei, M., Avanzinelli, R., Bianchini, G., Boari, E., Tommasini, S., Tiepolo, M., Prelević, D., 2009. Trace elements and Sr–Nd–Pb isotopes of K-rich, shoshonitic, and calc-alkaline magmatism of the Western Mediterranean Region: genesis of ultrapotassic to calc-alkaline magmatic associations in a post-collisional geodynamic setting. Lithos 107, 68–92.
Conticelli, S., Laurenzi, M.A., Giordano, G., Mattei, M., Avanzinelli, R., Melluso, L., Tommasini, S., Boari, E., Cifelli, F., Perini, G., 2010. Leucite-bearing (kamafugitic/leucititic) and-free (lamproitic) ultrapotassic rocks and associated shoshonites from Italy: constraints on petrogenesis and geodynamics. J. Virtual Explor. 36 (20).

Corfu, F., Andersen, T., Gasser, D., 2014. The Scandinavian Caledonides: main features, conceptual advances and critical questions. Geol. Soc. Lond. Spec. Publ. 390, 9–43.
Dailey, S.R., Christiansen, E.H., Dorais, M.J., Kowallis, B.J., Fernandez, D.P., Johnson, D.M., 2018. Origin of the fluorine-and beryllium-rich rhyolites of the Spor Mountain Formation, Western Utah. Am. Mineralogist: J. Earth and Planetary Mater. 103, 1228–1252.
Dilek, Y., Altunkaynak, Ş., 2009. Geochemical and temporal evolution of Cenozoic magmatism in western Turkey: mantle response to collision, slab break-off, and lithospheric tearing in an orogenic belt. Geol. Soc. Lond. Spec. Publ. 311, 213–233.
Ersoy, E.Y., Palmer, M.R., 2013. Eocene-Quaternary magmatic activity in the Aegean: implications for mantle metasomatism and magma genesis in an evolving orogeny. Lithos 180, 5–24.
Fisher, R.V., Schmincke, H.-U., 1984. Pyroclastic Rocks (Springer Science & Business Media).
Fiske, R.S., Naka, J., Iizasa, K., Yuasa, M., Klaus, A., 2001. Submarine silicic caldera at the front of the Izu-Bonin arc, Japan: Voluminous seafloor eruptions of rhyolite pumice. Geol. Soc. Am. Bull. 113, 813–824.
Foley, S., 1992a. Petrological characterization of the source components of potassic magmas: geochemical and experimental constraints. Lithos 28, 187–204.
Foley, S., 1992b. Vein-plus-wall-rock melting mechanisms in the lithosphere and the origin of potassic alkaline magmas. Lithos 28, 435–453.
Foley, S., Venturelli, G., Green, D., Toscani, L., 1987. The ultrapotassic rocks: characteristics, classification, and constraints for petrogenetic models. Earth Sci. Rev. 24, 81–134.
Förster, M.W., Prelević, D., Schmück, H.R., Buhre, S., Veter, M., Mertz-Kraus, R., Foley, S.F., Jacob, D.E., 2017. Melting and dynamic metasomatism of mixed harzburgite+glimmerite mantle source: Implications for the genesis of orogenic potassic magmas. Chem. Geol. 455, 182–191.
Gale, A., Dalton, C.A., Langmuir, C.H., Su, Y., Schilling, J.G., 2013. The mean composition of ocean ridge basalts. Geochem. Geophys. Geosyst. 14, 489–518.
Gee, D., Guezou, J., Roberts, D., Wolff, F., 1985. The central-southern part of the Scandinavian Caledonides. The Caledonide orogen-Scandinavia and related areas 1, 109–133.
Grenne, T., Roberts, D., 1998. The Hølonda Porphyrites, Norwegian Caledonides: geochemistry and tectonic setting of Early–Mid-Ordovician shoshonitic volcanism. J. Geol. Soc. Lond. 155, 131–142.
Grenne, T., Ihlen, P., Vokes, F., 1999. Scandinavian Caledonide metallogeny in a plate tectonic perspective. Mineral. Deposita 34 (5–6), 422–471.
Guo, Z., Wilson, M., Zhang, L., Zhang, M., Cheng, Z., Liu, J., 2014. The role of subduction channel mélanges and convergent subduction systems in the petrogenesis of post-collisional K-rich mafic magmatism in NW Tibet. Lithos 198, 184–201.
Hastie, A.R., Kerr, A.C., Pearce, J.A., Mitchell, S., 2007. Classification of altered volcanic island arc rocks using immobile trace elements: development of the Th–Co discrimination diagram. J. Petrol. 48, 2341–2357.
Hermann, J., Rubatto, D., 2009. Accessory phase control on the trace element signature of sediment melts in subduction zones. Chem. Geol. 265, 512–526.
Jaffey, A., Flynn, K., Glendenin, L., Bentley, W.t., Essling, A., 1971. Precision measurement of half-lives and specific activities of U 235 and U 238. Phys. Rev. C 4, 1889–1906.
Kano, K., 2003. Subaqueous pumice eruptions and their products: a review. Washington DC American Geophysical Union Geophysical Monograph Series 140, 213–229.
Kessel, L.G., Busby, C.J., White, J., Smellie, J., Clague, D., 2003. Analysis of VHMS-hosting ignimbrites erupted at bathyal water depths (Ordovican Bald Mountain sequence, northern Maine). Geophys. Monograph Am. Geophys. Union 140, 361–379.
Krill, A.G., 1980. Tectonics of the Oppdal area, Central Norway. Geologiska Föreningen i Stockholm Förhandlingar 102, 523–530.
Krogh, T., 1973. A low-contamination method for hydrothermal decomposition of zircon and extraction of U and Pb for isotopic age determinations. Geochim. Cosmochim. Acta 37, 485–494.
Krogh, T., 1982. Improved accuracy of U-Pb zircon ages by the creation of more concordant systems using an air abrasion technique. Geochim. Cosmochim. Acta 46, 637–649.
Lissenberg, C.J., Zagorevski, A., McNicoll, V.J., van Staal, C.R., Whalen, J.B., 2005. Assembly of the Annieopsquotch accretionary tract, Newfoundland Appalachians: Age and geodynamic constraints from syn-kinematic intrusions. J. Geol. 113, 553–570.
Ludwig, K.R., 2003. User's manual for isoplot 3.00, a geochronlogical toolkit for microsoft excel. Berkeley Geochronl. Cent. Spec. Publ. 4, 25–32.
Marocchi, M., Hermann, J., Tropper, P., Bargossi, G.M., Mair, V., 2010. Amphibole and phlogopite in "hybrid" metasomatic bands monitor trace element transfer at the interface between felsic and ultramafic rocks (Eastern Alps, Italy). Lithos 117, 135–148.
Marschall, H.R., Schumacher, J.C., 2012. Arc magmas sourced from mélange diapirs in subduction zones. Nat. Geosci. 5, 862–867.
Marschall, H.R., Altherr, R., Rüpke, L., 2007. Squeezing out the slab—modelling the release of Li, be and B during progressive high-pressure metamorphism. Chem. Geol. 239, 323–335.
Mattinson, J.M., 2005. Zircon U–Pb chemical abrasion ("CA-TIMS") method: combined annealing and multi-step partial dissolution analysis for improved precision and accuracy of zircon ages. Chem. Geol. 220, 47–66.
Nilsen, O., Wolff, F.C., 1989. Røros og Sveg. Berggrunnskart Røros og Sveg M 1:250000. Undersøkelse, Norges Geologiske.
Nilsen, O., Sundvoll, B., Roberts, D., Corfu, F., 2003. U-Pb geochronology and geochemistry of trondhjemites and a norite pluton from the SW Trondheim Region. Central Norwegian Caledonides: Norges Geologiske Undersøkelse Bull. 441, 5–16.
Pearce, J.A., 1996. A user's guide to basalt discrimination diagrams: Trace element geochemistry of volcanic rocks: applications for massive sulphide exploration. Geological Association of Canada, Short Course Notes. 12, pp. 79–113.
Pearce, J.A., 2008. Geochemical fingerprinting of oceanic basalts with applications to ophiolite classification and the search for Archean oceanic crust. Lithos 100, 14–48.
Pearce, J.A., Peate, D.W., 1995. Tectonic implications of the composition of volcanic arc magmas. Annu. Rev. Earth Planet. Sci. 23, 251–285.
Peccerillo, A., 1999. Multiple mantle metasomatism in Central-Southern Italy: geochemical effects, timing and geodynamic implications. Geology 27, 315–318.
Peccerillo, A., Martinotti, G., 2006. The Western Mediterranean lamproitic magmatism: origin and geodynamic significance. Terra Nova 18, 109–117.
Pedersen, R., Bruton, D., Furnes, H., 1992. Ordovician faunas, island arcs and ophiolites in the Scandinavian Caledonides. Terra Nova 4, 217–222.
Pe-Piper, G., Piper, D.J., Koukouvelas, I., Dolansky, L.M., Kokkalas, S., 2009. Postorogenic shoshonitic rocks and their origin by melting underplated basalts: the Miocene of Limnos. Greece. Geol. Soc. Am. Bull. 121, 39–54.
Pérez-Valera, L.A., Rosenbaum, G., Sánchez-Gómez, M., Azor, A., Fernández-Soler, J.M., Pérez-Valera, F., Vasconcelos, P.M., 2013. Age distribution of lamproites along the Socovos Fault (southern Spain) and lithospheric scale tearing. Lithos 180, 252–263.
Plank, T., 2005. Constraints from thorium/lanthanum on sediment recycling at subduction zones and the evolution of the continents. J. Petrol. 46, 921–944.
Plank, T., Langmuir, C.H., 1998. The chemical composition of subducting sediment and its consequences for the crust and mantle. Chem. Geol. 145, 325–394.
Prelević, D., Foley, S., Romer, R., Cvetković, V., Downes, H., 2005. Tertiary ultrapotassic volcanism in Serbia: constraints on petrogenesis and mantle source characteristics. J. Petrol. 46, 1443–1487.
Prelević, D., Foley, S., Romer, R., Conticelli, S., 2008. Mediterranean Tertiary lamproites derived from multiple source components in postcollisional geodynamics. Geochim. Cosmochim. Acta 72, 2125–2156.
Prelević, D., Jacob, D.E., Foley, S.F., 2013. Recycling plus: a new recipe for the formation of Alpine–Himalayan orogenic mantle lithosphere. Earth Planet. Sci. Lett. 362, 187–197.
Qian, Q., Hermann, J., 2013. Partial melting of lower crust at 10–15 kbar: constraints on adakite and TTG formation. Contrib. Mineral. Petrol. 165, 1195–1224.
Roberts, D., Gee, D., 1985. An introduction to the structure of the Scandinavian Caledonides. The Caledonide orogen–Scandinavia and related areas 1, 55–68.
Rudnick, R.L., Gao, S., 2003. Composition of the continental crust. Treatise on geochemistry 3, 659.
Ryan, J.G., 2002. Trace-element systematics of beryllium in terrestrial materials. Rev. Mineral. Geochem. 50, 121–145.
Schmidt, M.W., Vielzeuf, D., Auzanneau, E., 2004. Melting and dissolution of subducting crust at high pressures: the key role of white mica. Earth Planet. Sci. Lett. 228, 65–84.
Schmitz, M.D., Schoene, B., 2007. Derivation of isotope ratios, errors, and error correlations for U-Pb geochronology using 205Pb-235U-(233U)-spiked isotope dilution thermal ionization mass spectrometric data. Geochem. Geophys. Geosyst. 8, 8.
Shafaii Moghadam, H., Griffin, W.L., Kirchenbaur, M., Garbe-Schönberg, D., Zakie Khedr, M., Kimura, J.-I., Stern, R.J., Ghorbani, G., Murphy, R., O'Reilly, S.Y., 2018. Roll-back, extension and mantle upwelling triggered eocene potassic magmatism in NW Iran. J. Petrol. 59, 1417–1465.
Slagstad, T., Kirkland, C.L., 2018. Timing of collision initiation and location of the Scandian orogenic suture in the Scandinavian Caledonides. Terra Nova 30, 179–188.
Slagstad, T., Pin, C., Roberts, D., Kirkland, C.L., Grenne, T., Dunning, G., Sauer, S., Andersen, T., 2014. Tectonomagmatic evolution of the early Ordovician suprasubduction-zone ophiolites of the Trondheim Region, Mid-Norwegian Caledonides. Geol. Soc. Lond. Spec. Publ. 390, 541–561.
Soder, C.G., Romer, R.L., 2018. Post-collisional potassic–ultrapotassic magmatism of the Variscan Orogen: implications for mantle metasomatism during continental subduction. J. Petrol. 59, 1007–1034.
Spandler, C., Pirard, C., 2013. Element recycling from subducting slabs to arc crust: a review. Lithos 170, 208–223.
Spandler, C., Hermann, J., Arculus, R., Mavrogenes, J., 2003. Redistribution of trace elements during prograde metamorphism from lawsonite blueschist to eclogite facies; implications for deep subduction-zone processes. Contrib. Mineral. Petrol. 146, 205–222.
Stacey, J.T., Kramers, J., 1975. Approximation of terrestrial lead isotope evolution by a two-stage model. Earth Planet. Sci. Lett. 26, 207–221.
Stokke, E.W., Gasser, D., Dalslåen, B.H., Grenne, T., 2018. Tectonic evolution of syn-to late-orogenic sedimentary–volcanic basins in the central Norwegian Caledonides. J. Geol. Soc. Lond. 175, 605–618.
Sun, S.-S., McDonough, W.-s., 1989. Chemical and isotopic systematics of oceanic basalts: implications for mantle composition and processes. Geol. Soc. Lond. Spec. Publ. 42, 313–345.
Svensen, H.H., Hammer, Ø., Corfu, F., 2015. Astronomically forced cyclicity in the Upper Ordovician and U–Pb ages of interlayered tephra, Oslo Region, Norway. Palaeogeogr. Palaeoclimatol. Palaeoecol. 418, 150–159.
Thompson, R., Fowler, M., 1986. Subduction-related shoshonitic and ultrapotassic magmatism: a study of Siluro-Ordovician syenites from the Scottish Caledonides. Contrib. Mineral. Petrol. 94, 507–522.
Tommasini, S., Avanzinelli, R., Conticelli, S., 2011. The Th/La and Sm/La conundrum of the Tethyan realm lamproites. Earth Planet. Sci. Lett. 301, 469–478.
Tucker, R.D., Robinson, P., Solli, A., Gee, D.G., Thorsnes, T., Krogh, T.E., Nordgulen, Ø., Bickford, M., 2004. Thrusting and extension in the Scandian hinterland, Norway: New U-Pb ages and tectonostratigraphic evidence. Am. J. Sci. 304, 477–532.
Vogt, T., 1945. The geology of part of the Hølonda-Horg district, a type area in the Trondheim region. Nor. Geol. Tidsskr. 25, 449–528.
West, D.P., Tomascak, P.B., Coish, R.A., Yates, M.G., Reilly, M.J., 2007. Petrogenesis of the ultrapotassic Lincoln Syenite, Maine: late Silurian-early Devonian melting of a source region modified by subduction driven metasomatism. Am. J. Sci. 307, 265–310.
White, J.D., 2000. Subaqueous eruption-fed density currents and their deposits. Precambrian Res. 101, 87–109.

Paper III

III

NORWEGIAN JOURNAL OF GEOLOGY
https://dx.doi.org/10.1785/njg101-2-2

GEOLOGICAL SOCIETY OF NORWAY

The Skuggliberga unit of the Oppdal area, central Scandinavian Caledonides: calc-alkaline pyroclastic volcanism in a fluvial to shallow-marine basin following a mid-Ordovician orogenic event

Bjørgunn H. Dalslåen[1], Deta Gasser[2, 3], Tor Grenne[3], Morgan Ganerød[3] & Arild Andresen[1]

[1]*Department of Geosciences, University of Oslo, PO Box 1047, Blindern, 0316 Oslo, Norway*
[2]*Department of Environmental Sciences, Western Norway University of Applied Sciences, Røyrgata 6, 6856 Sogndal, Norway*
[3]*The Geological Survey of Norway, Leiv Eirikssons vei 39, 7040 Trondheim, Norway*

E-mail corresponding author (b.h.dalslaen@geo.uio.no): b.h.dalslaen@geo.uio.no

Keywords:
- *Scandinavian Caledonides*
- *Arc volcanism*
- *Detrital zircon*
- *Volcanic deposits*
- *Late Ordovician*

Electronic supplement 1: U–Pb detrital zircon data

Electronic supplement 2: Ar–Ar data

Received:
23. November 2020

Accepted:
24. February 20201

Published online:
5. August 2021

We present field observations, geochemical data and detrital zircon U–Pb ages from the newly defined Skuggliberga unit of the Oppdal area, central Norwegian Caledonides. The unit occurs in two separate areas, where it unconformably overlies the c. 475–470 Ma Trollhøtta and Skarvatnet units. The Skuggliberga unit consists of a local basal conglomerate and a cross-stratified to massive sandstone, overlain by bedded, fragment-bearing volcanic rocks, probably representing pyroclastic units erupted in a terrestrial or shallow-marine setting. Geochemical data from nine samples of volcanic rocks show calc-alkaline basaltic andesitic and andesitic compositions, with negative Nb–Ta anomalies indicating a continental arc-related signature, which is distinctly different from the underlying Trollhøtta and Kinna volcanic rocks. One sandstone sample from the Skaret succession, below the unconformity, is dominated by Palaeozoic detrital zircons, with a major peak at c. 490 Ma. Two sandstone samples from the Skuggliberga unit contain Archaean, Palaeo- to Neoproterozoic and Palaeozoic detrital zircons. Different methods to calculate the maximum depositional age for these samples vary by up to 50 Myr (from c. 427 to c. 475 Ma), some estimates being younger than the c. 435 Ma plutonic Innset massif that intrudes the Skuggliberga unit, indicating that the youngest detrital zircons must have experienced concealed lead loss. This lead loss could have occurred during regional metamorphism of the unit; an Ar–Ar plateau age of 416 ± 3 Ma was derived for biotite in one Skuggliberga volcanic sample representing cooling after regional greenschist-facies metahism. The Skuggliberga unit has no known direct correlative in the Trondheim Nappe Complex but overlaps in age and geochemical characteristics

Dalslåen, B.H., Gasser, D., Grenne, T., Ganerød, M. & Andresen, A. 2021: The Skuggliberga unit of the Oppdal area, central Scandinavian Caledonides: calc-alkaline pyroclastic volcanism in a fluvial to shallow-marine basin following a mid-Ordovician orogenic event. *Norwegian Journal of Geology 101*, 202107. https://dx.doi.org/10.17850/njg101-2-2.

with arc-related plutonic rocks along the central Norwegian coast, indicating that it represents the surface expression of the latter. The orogenic phase predating Skuggliberga deposition is probably related to Taconian accretionary events along the Laurentian margin.

Introduction

The Scandinavian Caledonides preserve remnants of the ancient Iapetus Ocean, which opened in the Late Neoproterozoic and closed during the convergence and final collision of Laurentia, Baltica and Avalonia in the Palaeozoic (e.g., Wilson, 1966; Gee et al., 2008; Corfu et al., 2014; Domeier, 2016). Remnants of this ocean can be found all along the Scandinavian Caledonides and are particularly abundant in the Trondheim and Köli nappe complexes (Fig. 1A). These Iapetus-derived rock units mainly comprise Cambrian to Early Ordovician supra-subduction zone (SSZ) ophiolites and their volcano-sedimentary cover successions, as well as arc-related plutonic rocks. Whereas most of the c. 500–480 Ma SSZ ophiolite fragments, including Lyngen, Leka, Løkken–Vassfjellet–Bymarka (LVB), Gullfjellet and Karmøy (Fig. 1A; e.g., Pedersen et al., 1992; Pedersen & Dunning, 1997; Slagstad et al., 2014) have been investigated in detail, many aspects of the stratigraphy, depositional environment, tectonic setting and absolute ages of the overlying Ordovician to Silurian cover successions remain unresolved.

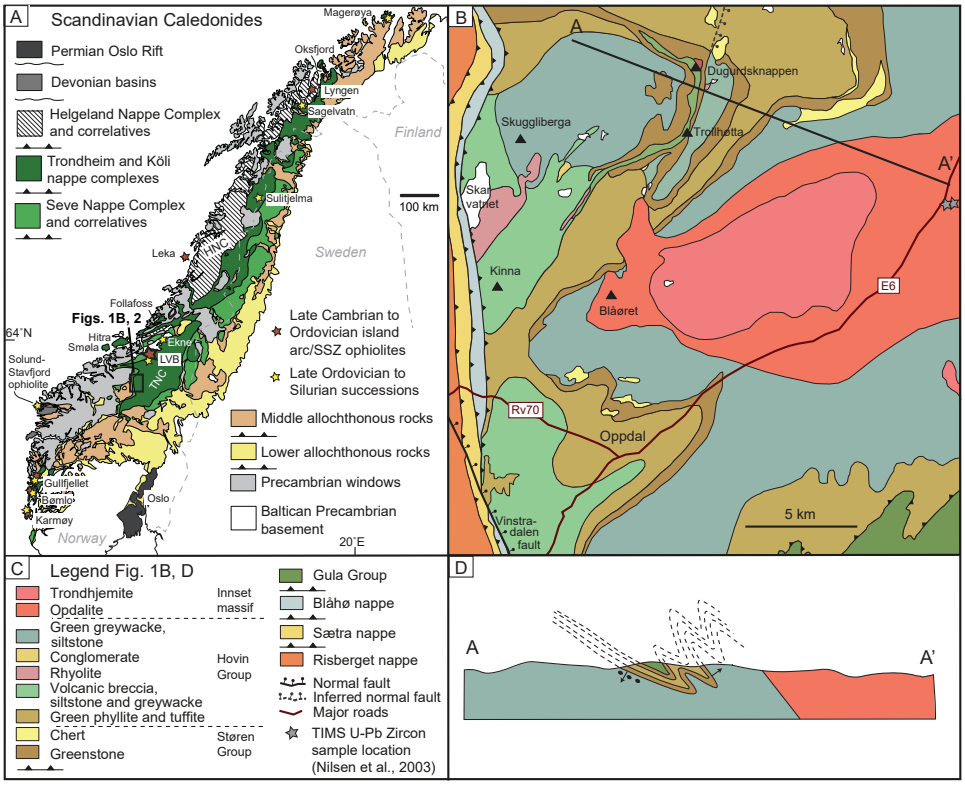

Figure 1. (A) Regional map of the Scandinavian Caledonides. Abbreviations: TNC – Trondheim Nappe Complex; LVB – Løkken–Vassfjellet–Bymarka ophiolite; HNC – Helgeland Nappe Complex. (B) Geological map of the Oppdal area according to Nilsen & Wolff (1989), showing the extent of the Støren and Hovin groups. (C) Legend to Fig. 1B; applies also to Fig. 1D. (D)Interpretative cross-section of the Oppdal area by Rohr-Torp (1972) (slightly modified). Parts of the Trollhøtta succession were correlated with the Gula Group (dark green) and interpreted to lie in the core of a synformal anticline in the overturned and folded succession, whereas the Skuggliberga unit was not recognised as a separate unit but interpreted to be part of the overturned Hovin succession. See Fig. 2B for comparison.

The Trondheim Nappe Complex (TNC) is one of the larger areas within the Scandinavian Caledonides where Iapetus-derived SSZ ophiolites, marginal basins and their cover successions are preserved (Fig. 1A). The Oppdal area within the southern TNC has recently received considerable attention due to the discovery of a peculiar volcano-sedimentary succession consisting of highly enriched, largely pyroclastic, mafic to felsic volcanic rocks and MORB-like pillow basalts intercalated with turbiditic sedimentary rocks, indicating a hitherto little-known spreading environment within a marginal basin of Iapetus at c. 475–470 Ma (Stokke et al., 2018; Dalslåen et al., 2020a; Dalslåen et al., 2020b). This succession was shown by Stokke et al. (2018) to have been deformed and eroded prior to the deposition of cross-stratified sandstones and andesitic volcanic rocks, highlighting the existence of a major angular unconformity in the area. Based on five overlapping near-concordant detrital zircon grains within one sandstone sample, Stokke et al. (2018) concluded with a post-427 Ma age for the sandstones and andesitic rocks, postulating a hitherto unknown Late-Silurian or younger volcano-sedimentary phase within the area.

In this contribution, we review the geology of the TNC in the Oppdal area, and add new field observations, geochemical data, U–Pb detrital zircon and Ar–Ar data from the sandstones and volcanic rocks above the regional unconformity. We compare our results with the earlier map compilation of Nilsen & Wolff (1989) and the interpretations of Stokke et al. (2018), and discuss our findings within the framework of other Iapetus-related cover successions within the Scandinavian Caledonides.

Geology of the TNC in the Oppdal area

The geology of the Oppdal area is well known for the occurrence of quartzite schist (‘Oppdalsskifer’) mined in numerous quarries south of the Oppdal town centre, within the Sætra nappe. The tectono-stratigraphically lower nappes in the Oppdal region (Åmotsdal, Risberget, Sætra and Blåhø; Fig. 1B, C) are amphibolite to granulite facies (e.g., Krill, 1985). The lower-grade metamorphic rocks of the overlying Trondheim Nappe Complex are less well known, and have been loosely referred to as the Tronget unit (e.g., Krill, 1980; Gee et al., 1985). Holmsen (1955) described a variety of sedimentary and volcanic rocks from this area, which Nilsen & Wolff (1989) on their regional geological map assigned to the following two main groups: (1) metabasalts and green layered tuffite and phyllite with minor rhyolite, volcanic breccia, siltstone and greywacke of the Støren Group, and (2) green greywacke and shale as well as grey siltstone and shale of the younger Hovin Group (Fig. 1B, C). Farther north in the Trondheim area, where the Støren and Hovin groups were originally defined, the two are separated by an unconformity which marks a tectonic event traditionally referred to as “the Trondheim disturbance” (e.g., Vogt, 1945). The contact between the Støren and Hovin groups is not easily recognised as an unconformity on the map of Nilsen & Wolff (1989; Fig. 1B), but Rohr-Torp (1972) described several deposits of polymictic conglomerates which he interpreted as being positioned at the base of the Hovin Group (Fig. 1D). Moreover, Rohr-Torp (1972) interpreted grey siltstones and shales running through the Trollhøtta mountain (Fig. 1B, C) as western correlatives of the Gula Group, which has its principal location farther east in the TNC. Based on this correlation, Rohr-Torp (1972) postulated a general inversion of the tectonostratigraphy, with the presumably oldest Gula Group being located structurally above the younger Støren and Hovin groups (Fig. 1D). The supracrustal rocks of the Oppdal area were intruded by a major pluton (Fig. 1B, C) termed the Innset massif (Goldschmidt, 1916; Rohr-Torp, 1974), which ranges from norite through orthopyroxene-bearing granodiorite (‘opdalite’) to trondhjemite (Fig. 1B; Nilsen et al., 2003). Zircons from a biotite norite and a trondhjemite from this body have been dated by U–Pb TIMS at 435.8 ± 0.9 Ma and 434.8 ± 0.5 Ma, respectively (Nilsen et al., 2003; Fig. 1B).

Stokke et al. (2018) demonstrated the existence of metabasaltic rocks with a clear MORB-type geochemical composition within the Støren Group rocks at Dugurdsknappen (Fig. 2A). This geochemical composition is different from that of the SSZ-type LVB ophiolites with which the Støren Group traditionally has been correlated. These MORB-type metabasalts, together with intercalated turbiditic silt- and sandstones and minor rhyolites dated at 473 ± 1 and 472 ± 1 Ma, were referred to as the Trollhøtta unit by Dalslåen et al. (2020b; Fig. 2A). Locally interfingering with Trollhøtta metabasalts is

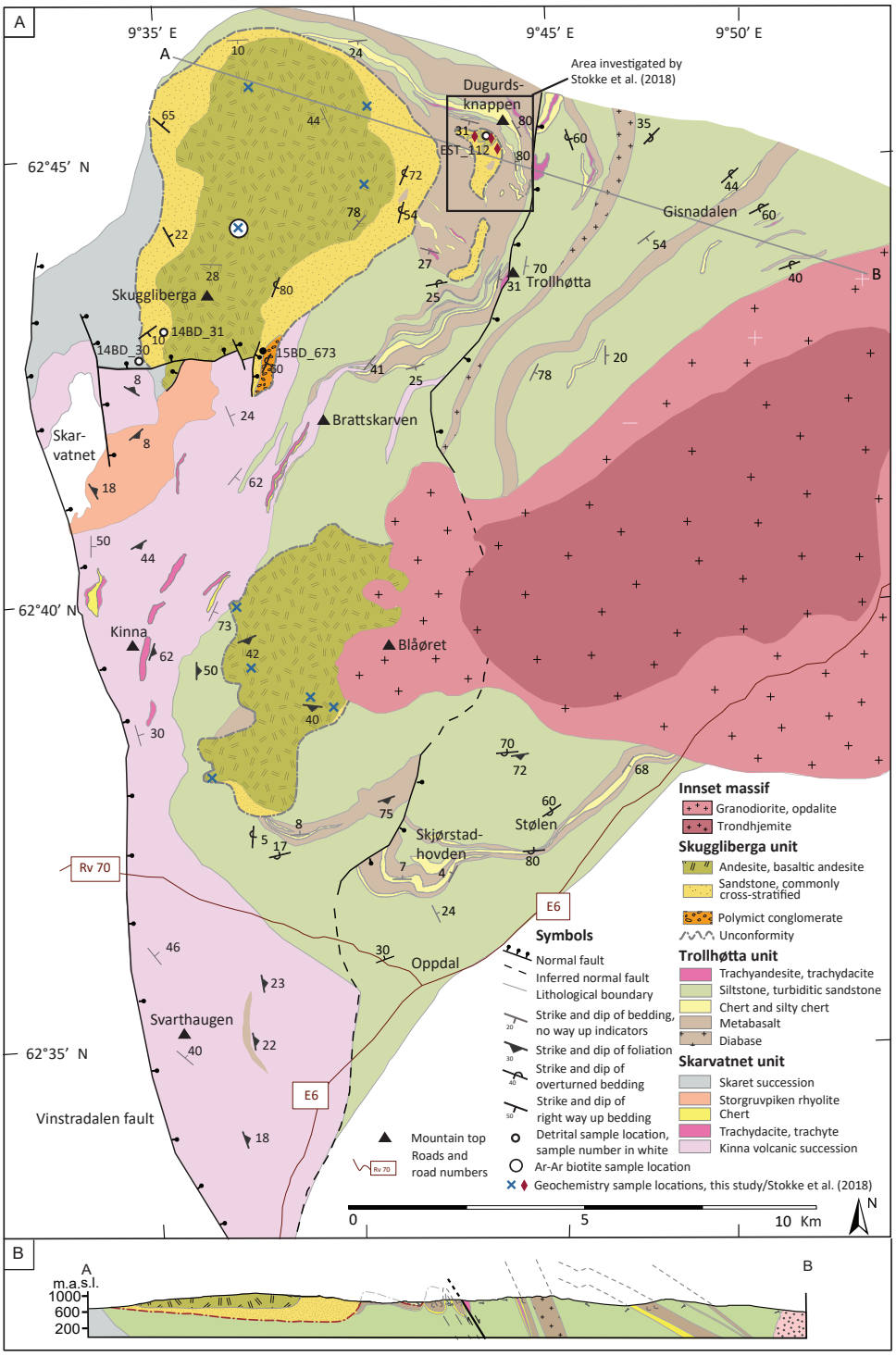

Figure 2. (A) Geological map of the Oppdal area according to our own mapping. (B) Interpretative profile through the northern part of the Skuggliberga and Trollhøtta units, modified from Stokke et al. (2018) and Dalslåen et al. (2020b).

the Kinna metavolcanic succession (Fig. 2A), which consists of 474 ± 1 Ma mafic to felsic pyroclastic deposits strongly enriched in highly incompatible elements, and which is overlain by the slightly younger (470 ± 1 Ma) Storgruvpiken metarhyolite (Dalslåen et al., 2020a, b). The Kinna and Storgruvpiken metavolcanic rocks, together with associated metasedimentary rocks of the Skaret succession, are informally assigned to the Skarvatnet unit (Fig. 2; Dalslåen et al., 2020a). The above ages indicate that the volcanosedimentary Trollhøtta unit and the Kinna and Storgruvpiken metavolcanic rocks are c. 10 Myr younger than the LVB ophiolites to the north (c. 487-480 Ma, e.g. Slagstad et al., 2014).

The mapping by Dalslåen et al. (2020b) showed that large parts of what was previously assigned to the Hovin Group, particularly in the Gisnadalen and Skjørstadhovden–Stølen areas (Fig. 2A), are turbiditic rocks intercalated with Trollhøtta metavolcanic rocks. Hence, they are integral parts of the Lower Ordovician succession and not unconformably overlying it (compare Fig. 1B with Fig. 2A). Dalslåen et al. (2020b) also presented a different interpretation of the Rohr-Torp profile (compare Fig. 1D with Fig. 2B), with no Gula-type sedimentary rocks in the studied area and with general younging of the Trollhøtta succession towards the west. This implies that the beds are partly overturned, but not totally inverted as Rohr-Torp (1972) suggested. The contact between the Støren and Hovin groups shown in the western part of Rohr-Torp's profile as being inverted and with a basal conglomerate, was identified by Stokke et al. (2018) as representing a major angular unconformity on previously folded Trollhøtta rocks, overlain by right-way-up, less deformed and cross-stratified sandstones and metavolcanic rocks. Based on near-concordant detrital zircon data, Stokke et al. (2018) interpreted these rocks to have been deposited after c. 427 Ma, which is considerably younger than the fossil-bearing Mid- to Upper Ordovician Hovin Group of the Trondheim area.

The geological map in Fig. 2A delineates the angular unconformity identified by Stokke et al. (2018) over a larger area. On this map, the rocks above the unconformity were informally termed the Skuggliberga unit by Dalslåen et al. (2020a, b), named after the main mountain northeast of lake Skarvatnet. The main aim of the current contribution is to describe the field relations, geochemical composition and age of this Skuggliberga unit in more detail.

Field observations

Our detailed mapping in the Oppdal area revealed the presence of the angular unconformity identified by Stokke et al. (2018) over a larger area, and overlying rocks were identified in two geographically separate areas N–NW of Oppdal (Fig. 2A). The northern area is the largest, covering approximately 32 km², of which 20.5 km² are volcanic rocks and 11.5 km² are sedimentary rocks. The southern area covers approximately 13 km² and consists mainly of volcanic rocks. The areas identified by Stokke et al. (2018) are smaller deposits east of the main northern area (Fig. 2A). All rocks have undergone greenschist-facies regional metamorphism, but the prefix 'meta' is omitted in the following descriptions and discussions for simplicity.

Northern area

The northern area is preserved within an asymmetric open syncline (Fig. 2A, B). In the southern part of this area, a polymictic conglomerate of c. 100 m thickness is found at the base of the succession (Fig. 2A). The 5–30 cm conglomerate clasts are generally well rounded and consist mainly of quartzite, aplitic granite, pink felsic volcanic rocks, fine-grained marble, Kinna-type vesicular volcanic rocks with abundant phenocrysts, greenstone, jasper and chert (Fig. 3A, B). The matrix consists mainly of quartz

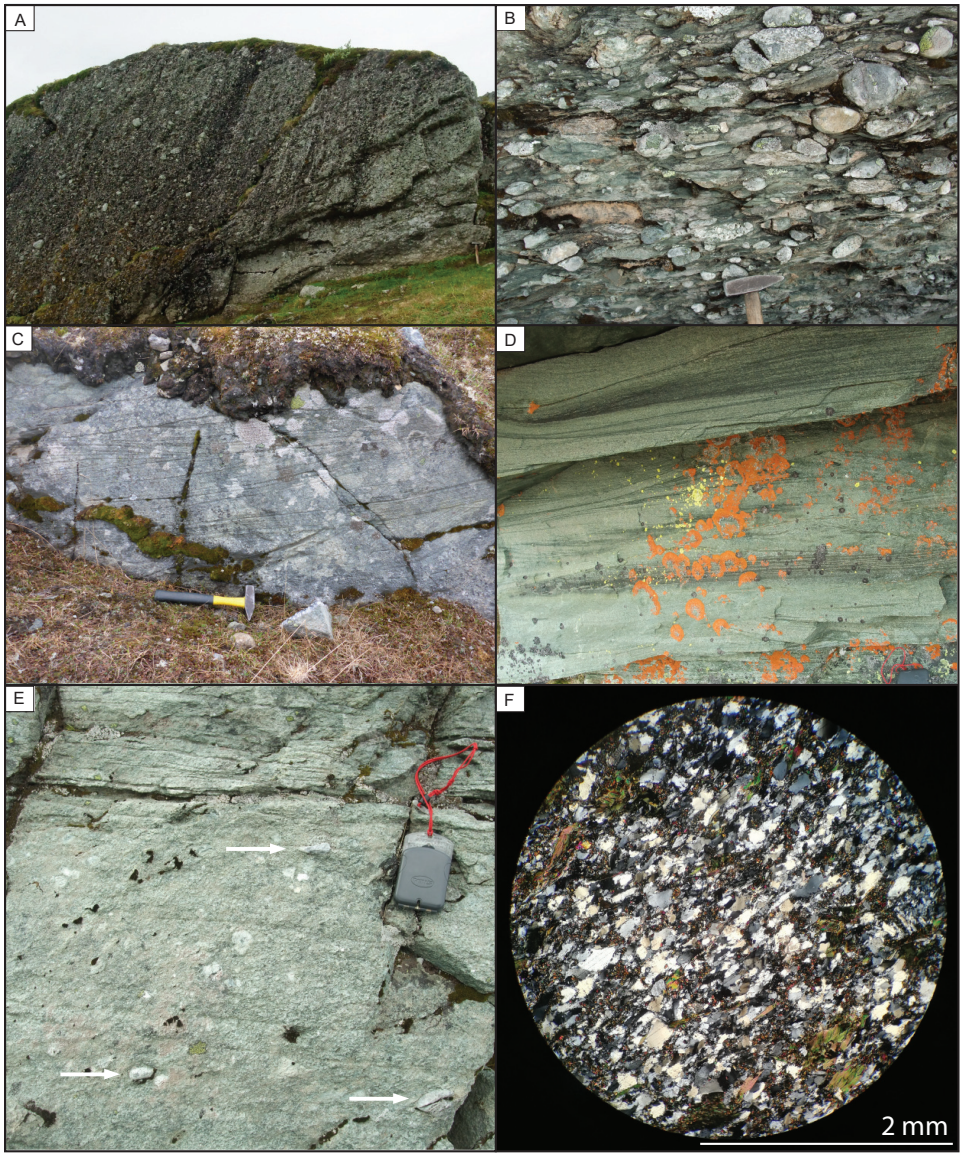

Figure 3. Field photos of the sedimentary rocks of the Skuggliberga unit, northern area. (A) Massive conglomerate, with a penetrative foliation dipping gently to the east (to the left in the picture, which is taken towards south). This foliation corresponds to foliation D3 of Stokke et al. (2018). Hammer for scale in the lower-right corner [UTM (32) 532313.6953857]. (B) Polymictic, foliated conglomerate; picture taken towards east [UTM (32) 532017.6953193]. (C) Cross-stratified sandstone [UTM(32) 529546.6954814]. (D) Cross-stratified bedded greenish sandstone, compass for scale in the lower-right corner [UTM (32) 529638.6953950]. (E) Massive sandstone with arrows pointing to scattered quartzite clasts, with thinly bedded sandstone on top [UTM (32) 532366.6954778]. (F) Photomicrograph of sample 14BD_31, the cross-stratified sandstone in Fig. 3E. Crossed polarizers.

and mica. The clasts are generally flattened and the matrix exhibits a penetrative foliation corresponding to the regional, generally ESE-dipping, tectonic foliation. The conglomerate generally fines upwards, with interbedded sandstone in its upper parts.

Except for the southernmost part, where the contact to the Skarvatnet unit is faulted, an up to c. 100 m-thick sandstone unit occurs around the entire northern area, conformably overlying the conglomerate or resting directly on the angular unconformity to the Trollhøtta and Skarvatnet units (Fig. 2A). The immature to submature sandstone is typically greenish, fine- to medium-grained and

poorly sorted. Trough cross-stratified (Fig. 3C, D) and planar-laminated beds are common in the lower part; the cross-stratifications are commonly found in the southern part of the area. Up section, the bedding becomes planar, or massive and structureless, locally with scattered quartzite clasts (Fig. 3E). The sandstone is dominated by recrystallised quartz, feldspar, metamorphic biotite, chlorite and calcite (Fig. 3F), with biotite and chlorite marking the dark bedding surfaces (Fig. 3D).

The sandstone is overlain by a light-green, fine- to medium-grained, fragment-bearing volcanic rock (Figs. 2A & 4A–D). The exposed thickness of the volcanic rock is up to 400 m, and it is apparently

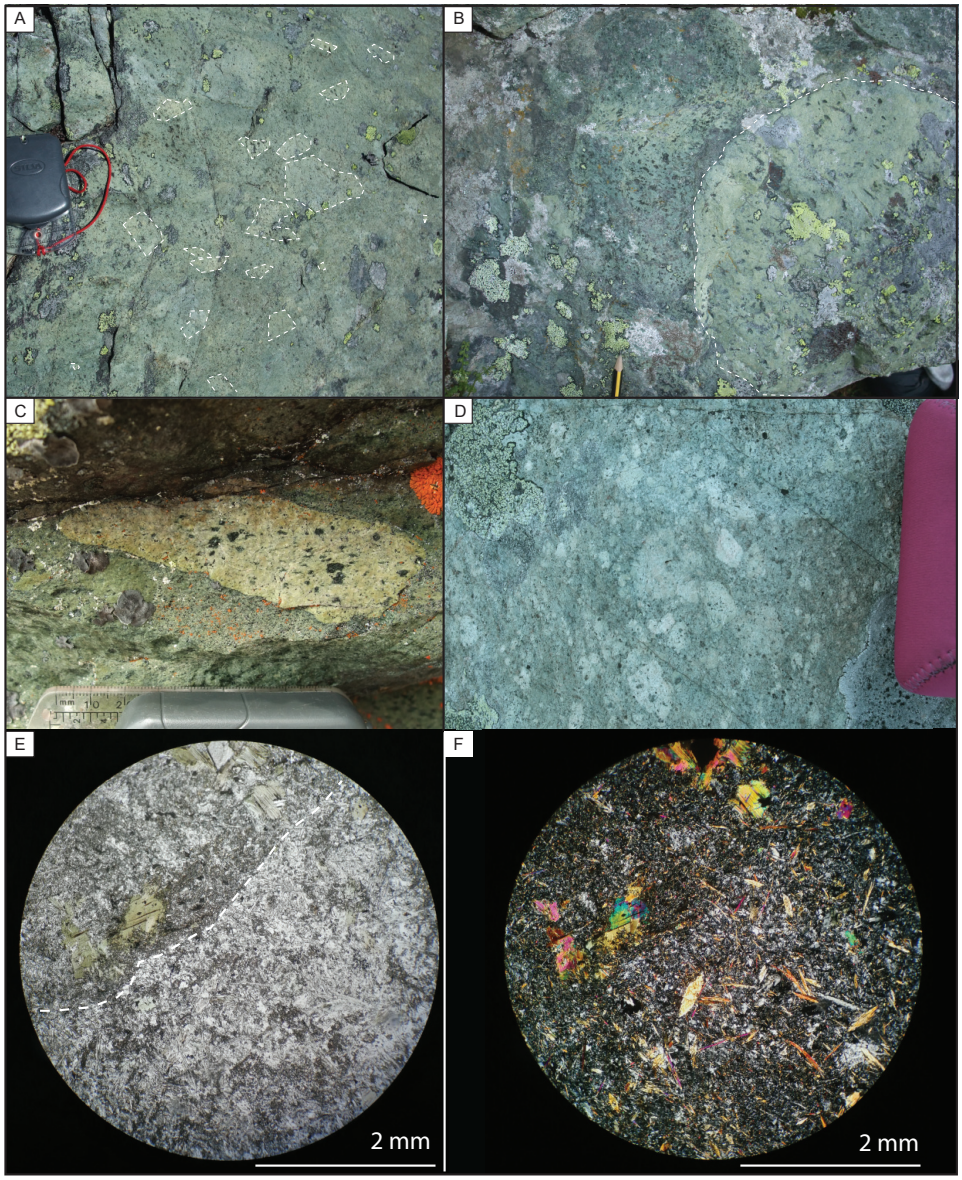

Figure 4. Field photos of the volcanic rocks of the Skuggliberga unit from the northern area. (A) Typical outcrop, where the fragments have a colour very similar to that of the matrix [UTM (32) 531625.6957167]. (B) Pale-green fragment in a similar matrix. The fragment is slightly lighter than the matrix and has larger biotite aggregates [UTM (32) 530258.6954294]. (C) Fine-grained fragment with dark hornblende/biotite aggregates, lighter coloured than the matrix [UTM (32) 530017.6955137]. (D) Small fragments in a matrix with similar colour and grain size. The pink camera case is approximately 12 cm [UTM (32) 532635.6955734]. (E) Photomicrograph of sample 15BD_152, the sample selected for Ar–Ar biotite dating. The upper left (above the stippled line) is a part of a fragment with large biotite grains, while the lower-right part is from the matrix. Plane-polarised light [UTM (32)531987.6956753]. (F) Same view as 4E, with crossed polarizers.

thickest in the northernmost part of the area. The fragments, ranging in size from a few millimetres to 70 cm, are angular to subangular and scattered or concentrated in faint beds. A few small (0.5–2 cm) fragments of pink volcanic rocks have been observed. The largest fragments are found in the northern part of the area. Other primary features are poorly preserved, but some green, sandy beds occur locally within the volcanic rock. The light-green colour of the volcanic rock is due to a high content of chlorite, epidote and zoisite. Both fragments and the matrix contain characteristic aggregates of biotite that can be up to 1 cm in diameter; individual grains are commonly subhedral or anhedral but euhedral biotite has also been observed. Biotite is commonly partly or totally chloritised. Heavily saussuritised plagioclase is common as phenocrysts and was apparently also a major constituent of the groundmass. Some euhedral phenocrysts of amphibole partly replaced by biotite have been observed; in thin-sections amphibole occurs as small, euhedral or partly altered pale-yellow or green grains. The overall mineralogy is similar in the matrix and the fragments, but the fragments are commonly lighter green and finer-grained, and generally have larger biotite grains/aggregates compared to the matrix (Fig. 4C, E, F).

Southern area

In the southern area, the contact to the underlying units is generally poorly exposed and the angular unconformity is less prominent, as the Trollhøtta unit is relatively flat-lying in this area. Massive, structureless, greenish sandstone is preserved in the southernmost part of the area, and a 3–5 m-thick bed of cross-stratified sandstone with scattered conglomerate clasts was observed in the eastern part close to the Innset intrusion (Fig. 2A). The cross-stratified sandstone contains up to 10 cm large erratic clasts of light-greenish, fine-grained volcanic rock with characteristic biotite aggregates (Fig. 5A), resembling the main Skuggliberga volcanic rock. The conglomerate beds are monomictic, consisting of the same light-greenish volcanic rocks, varying only in grain size and aggregate content (Fig. 5B). The main part of the southern area consists of a light-greenish volcanic rock similar to that of the

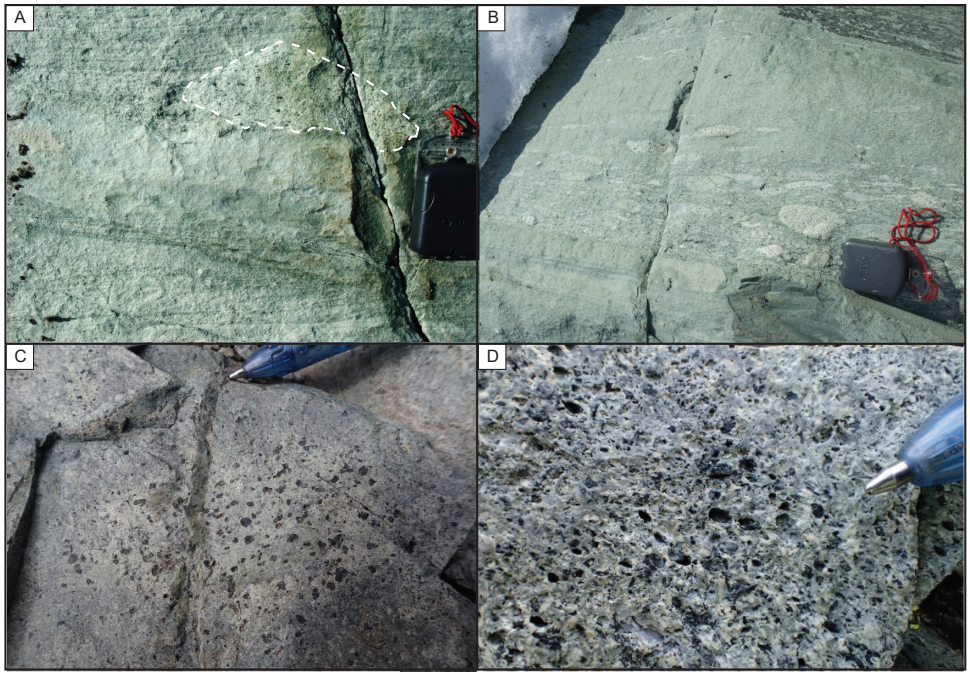

Figure 5. Field photos of sedimentary and volcanic rocks from the southern area. (A) Greenish sandstone, with a fragment of volcanic rock with characteristic aggregates of biotite outlined by the white stippled line [UTM(32) 533705.6946384]. (B) Conglomeratic bed intercalated with the sandstone in Fig. 5A, with volcanic clasts only [UTM(32) 533705.6946384]. (C) Volcanic fragment with well-preserved phenocrysts of amphibole [UTM(32)534846.6949344]. (D) Volcanic rock with phenocrysts and filled vesicles [UTM(32)534375.6948183].

northern area, but generally with fewer and smaller fragments. Small euhedral phenocrysts of feldspar are common, as well as dark aggregates of biotite and amphibole (Fig. 5C). Locally, up to 3 mm-sized, roundish, calcite-filled vesicles were observed in the clasts (Fig. 5D). Greenish, sandy beds are locally interlayered with the volcanic rocks; these are coarser-grained than the volcanic rocks but have similar colour and mineralogy. In the area north and west of the Blåøret mountain (Fig. 2A), granodiorite of the Innset massif is in direct contact with the volcanic rocks. The volcanic rocks close to the contact are contact-metamorphosed and irregularly veined by granodiorite, clearly demonstrating that the Innset pluton intruded the volcanic rocks.

Geochemistry

Methods

We analysed nine samples from the Skuggliberga volcanic rocks for major and trace elements; four samples are from the northern Skuggliberga area and five samples are from the southern area (Fig. 2A). Eight samples are from matrix or homogeneous zones without visible fragments, while one sample is from a fragment. Small fragments hardly distinguishable from the matrix due to similar colour and texture are common throughout the unit, and the matrix samples are therefore likely to contain such fragments. Three samples of Skuggliberga volcanic rocks analysed by Stokke et al., (2018) are included for comparison.

All samples were analysed at the Geological Survey of Norway, Trondheim. Major elements were analysed by X-ray fluorescence (XRF) spectrometry on glass beads fused with lithium tetraborate, and trace elements were analysed by XRF spectrometry on pressed powder beads. Rare Earth Elements (REE) and selected trace elements were analysed by Laser Ablation Inductively Coupled Plasma Mass Spectrometry (LA-ICP-MS) on the glass beads used for XRF major element analysis. Common international standards were used for all methods. The results are reported in Table 1 and in Figs. 6 & 7.

Table 1. Major and trace element analyses. Elements in italics are analysed by LA–ICP–MS, other elements are analysed by XRF. LOI – Loss on ignition.

Sample	BD14.35	BD14.36	BD15_621	BD15_1560	15BD_152	15BD_1490	BD15_1209	15BD_1411	15BD_1236
UTM (32)	532558 6959408	532909 6959050	531699 6953870	534050 6957520	531987 6956753	531653 6948549	534380 6959243	533699 6946415	533107 6946688
SiO_2 %	54.5	51.5	49.2	54.6	54.0	50.5	55.8	49.9	58.3
Al_2O_3	16.0	17.2	15.5	15.3	15.5	12.9	15.1	16.1	17.8
Fe_2O_3	7.03	7.34	8.65	7.14	7.48	7.79	6.36	8.01	6.07
TiO_2	0.74	1.36	1.16	0.60	0.87	0.75	0.573	0.999	0.73
MgO	6.16	5.27	8.77	6.61	6.60	12.3	3.04	8.28	2.33
CaO	5.92	8.15	8.16	8.39	7.81	7.63	12.2	7.13	5.81
Na_2O	3.43	3.18	3.30	2.38	3.48	2.01	2.97	3.63	3.05
K_2O	2.16	0.766	0.674	0.757	0.677	1.29	0.436	1.10	1.85
MnO	0.111	0.103	0.133	0.122	0.132	0.122	0.133	0.120	0.125
P_2O_5	0.167	0.295	0.189	0.130	0.142	0.145	0.092	0.163	0.306
LOI	3.01	2.97	3.33	2.69	2.37	3.52	2.68	2.99	2.44

Ba (ppm)	409	148	179	299	166	508	126	211	898
Co	30.3	29.6	39.5	24.4	29.6	43.5	16.2	37.8	8.3
Cr	273	334	471	278	202	799	79.0	442	22.0
Cu	44.5	19.6	20.9	15.7	20.6	<5	1120	18.4	<5
Ga	16.4	19.6	13.9	15.5	13.5	12.4	18.0	14.8	17.6
Ni	88.5	157	154	65.2	64.2	293	20.9	98.4	<5
Pb	7.9	20.4	6.5	12.1	7.8	11.7	12.1	8.4	11.9
Rb	60.1	20.2	14.9	17.7	16.9	35.7	10.4	40.1	59.8
Sc	20.3	14.6	20.9	19.5	15.0	19.9	21.9	20.4	5.9
Sn	<5	<5	<5	<5	<5	<5	<5	<5	<5
Sr	352	429	530	369	326	493	410	465	1090
V	154	185	158	141	156	151	193	177	98.8
Y	16.6	26.8	20.2	13.9	18.8	15.3	11.6	21.2	20.8
Zn	59.5	65.6	63.1	62.8	66.3	61.7	30.9	54.0	76.8
Zr	113	231	135	94.2	110	104	63.3	121	175
Nb	7.15	13.5	4.13	6.26	4.63	5.3	4.2	3.68	11
Cs	<10	<10	<10	<10	<10	<10	<10	<10	<10
Ge	N. A.	N.A.	<2	<2	<2	<2	<2	<2	2.0
Be	1.40	1.40	1.20	1.10	<1	1.1	<1	1.2	1.90
La	24.9	37.6	14.0	18.9	11.5	23.0	9.75	14.9	51.4
Ce	46.3	67.8	31.4	33.7	27.0	41.6	18.1	31.4	98.5
Pr	5.19	8.20	4.14	4.11	3.38	5.15	2.41	3.95	11.5
Nd	22.1	37	18.5	17.0	13.8	21.5	10.6	16.3	43.8
Sm	4.79	8.32	4.44	3.87	3.36	4.74	2.71	4.16	7.97
Eu	1.58	2.02	1.61	1.16	0.992	1.44	0.870	1.36	2.16
Gd	4.27	7.37	4.21	3.42	2.74	3.90	2.39	3.86	5.37
Tb	0.743	1.24	0.740	0.559	0.483	0.665	0.444	0.644	0.815
Dy	4.52	7.48	4.48	3.28	2.93	3.77	2.72	4.05	4.66
Ho	0.956	1.61	0.973	0.709	0.636	0.786	0.565	0.853	0.927
Er	2.55	4.29	2.37	1.85	1.65	2.08	1.52	2.29	2.41
Tm	0.376	0.608	0.345	0.274	0.249	0.329	0.239	0.334	0.379
Yb	2.22	4.00	2.11	1.65	1.59	1.97	1.45	2.11	2.35
Lu	0.319	0.581	0.318	0.252	0.230	0.315	0.213	0.316	0.329
Hf	3.89	7.81	3.33	2.99	2.44	3.18	1.85	3.12	4.79
Ta	0.523	0.993	0.273	0.425	0.334	0.328	0.299	0.245	0.714
W	N. A.	N.A.	0.55	0.26	0.24	0.41	<0.2	0.80	1.58
Bi	<0.5	<0.5	<0.5	<0.5	<0.5	<0.5	<0.5	<0.5	<0.5
Th	6.69	11.5	2.49	4.65	2.94	4.56	2.18	3.15	11.6
U	2.29	3.86	0.837	1.58	1.44	0.746	0.825	1.12	2.98
La_N/Lu_N	5.85	4.85	3.30	5.62	3.75	5.47	3.43	3.53	11.71

Results

All samples fall along a calc-alkaline trend in the AFM diagram (Fig. 6A). They plot as basaltic andesite or andesite in the TAS diagram (Fig. 6B), which is confirmed by the Nb/Y vs. Zr/Ti diagram (Fig. 6C, Pearce, 1996) that relies on immobile elements only. In tectonic discrimination diagrams based on immobile trace elements, such as the Th/Yb vs. Nb/Yb plot (Fig. 6D, Pearce, 2008), all samples plot within the continental arc field (Fig. 6D). In MORB-normalised multi-element plots (Fig. 7A), the samples show a marked enrichment in highly incompatible trace elements (e.g., Th ≈ 8.7–46 × N-MORB), with a negative anomaly at Nb–Ta and a peak at Pb (12.7–40 × N-MORB). Except for small negative anomalies in Zr, Ti and Y, the pattern is flat for the less incompatible elements. Chondrite-normalised REE patterns (Fig. 7B) have relatively steep slopes for the light to middle REE and more gentle slopes for the middle to heavy REE, with La_N/Lu_N ratios ranging from 3.30 to 5.85 (except one sample with a ratio of 11.71), and no significant Eu anomalies. There is no systematic difference between samples from the southern and northern deposits. The highly enriched mafic to intermediate volcanic rocks of the Kinna volcanic succession (Dalslåen et al., 2020a) and the MORB-like basalts from the Trollhøtta unit (Dalslåen et al., 2020b) are distinctly different from the Skuggliberga volcanic rocks (Figs. 6D & 7A, B).

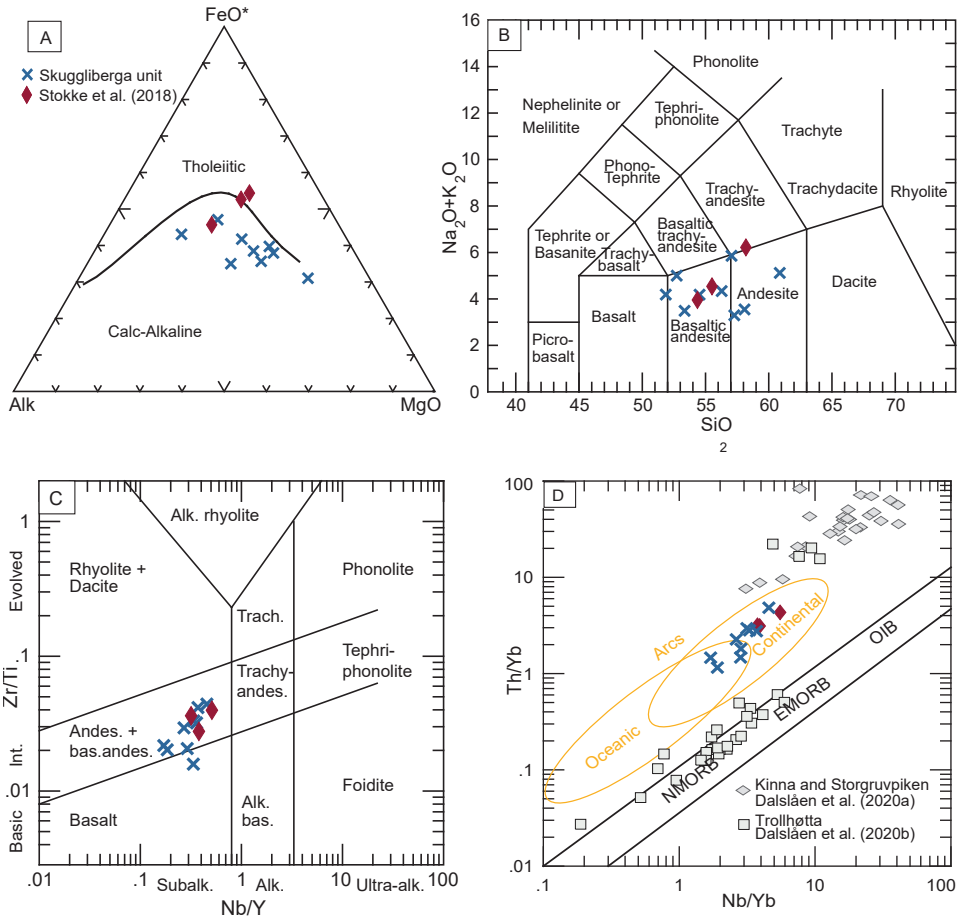

Figure 6. Discrimination diagrams for the Skuggliberga volcanic rocks; red diamonds are the volcanic rocks from Stokke et al. (2018). (A) AFM plot showing the calc-alkaline affinity. (B) TAS diagram and (C) Nb/Y vs. Zr/Ti plot (Pearce, 1996), both showing basaltic andesite and andesite compositions. (D) Nb/Yb vs. Th/Yb plot (Pearce, 2008) demonstrating continental-arc geochemical affinities. The compositional fields of Kinna and Storgruvpiken (grey diamonds; Dalslåen et al., 2020a) and Trollhøtta (grey squares, Dalslåen et al., 2020b) are shown for comparison.

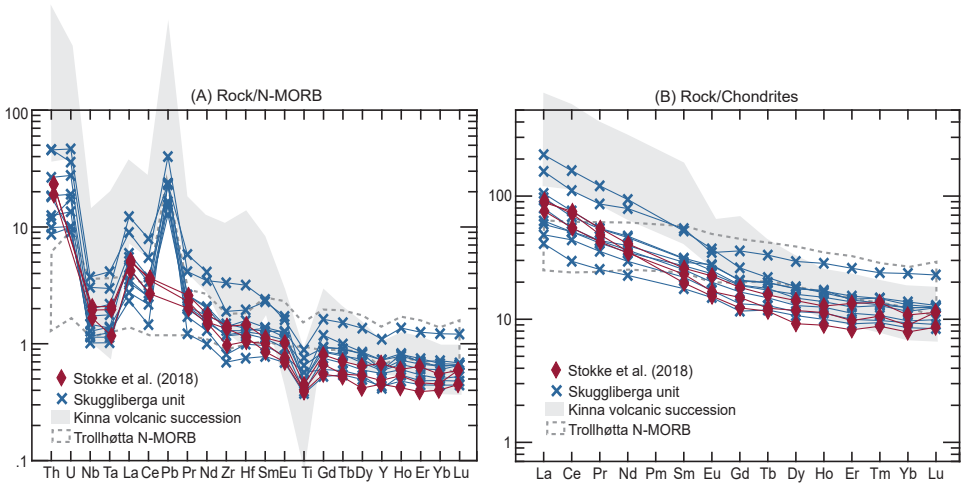

Figure 7. Multi-element plots for the Skuggliberga volcanic rocks. (A) MORB-normalised patterns; normalising values are from average N-MORB data of Gale et al. (2013). (B) Chondrite-normalised patterns; chondrite values from Sun & McDonough (1989). The patterns of the Kinna volcanic succession (Dalslåen et al., 2020a) and the MORB-like mafic rocks of the Trollhøtta unit (Dalslåen et al., 2020b) are added for comparison.

Geochronology

Several attempts were made to directly date the volcanic rocks of the Skuggliberga unit. Unfortunately, the volcanic rocks we separated (with up to 137 ppm of Zr) did not contain zircon, monazite or other heavy minerals that could have provided an age of volcanism. To obtain at least a maximum depositional age of the Skuggliberga unit, two sandstone samples were selected for detrital zircon analysis. In addition, we analysed biotite from one volcanic sample by Ar–Ar geochronology, which provides an age for the cooling following regional metamorphism.

LA-ICP-MS analysis of detrital zircon

Method

Three sandstone samples were selected for detrital zircon analysis, one from the directly underlying Skaret succession of the Skarvatnet unit (Dalslåen et al., 2020a), and two from the northern area of the Skuggliberga unit (Fig. 2A). The sample previously analysed by Stokke et al. (2018) from the small, northeastern sandstone area at Dugurdsknappen is included for comparison (Figs. 2A & 8). The samples were processed at the University of Oslo. They were crushed using standard methods and washed on a Wilfley table. A hand magnet was used to remove strongly magnetic minerals. The zircons were separated using heavy liquids with a density of 2.80 ± 0.02 g/ml. The separated grains were randomly picked, mounted in epoxy and examined with a combination of backscattered electron imaging and cathodoluminescence imaging prior to analysis. U–Pb analyses were carried out by LA-ICP-MS, using a Nu Plasma HR multicollector mass spectrometer equipped with Cetac LSX-213 G2+ laser microprobe at the Department of Geosciences, University of Oslo. U–Pb analyses follow the analytical protocols of Andersen et al. (2009). Ablation conditions were beam diameter 40 µm (aperture imaging mode) and pulse frequency 10 Hz. An in-house spreadsheet was used for data reduction.

Only analyses with less than ± 10% central discordance are included in the following descriptions and plots. For plots of the Palaeozoic population and maximum depositional age calculations, only analyses with less than ± 5% central discordance are included, as we consider data less than 5%

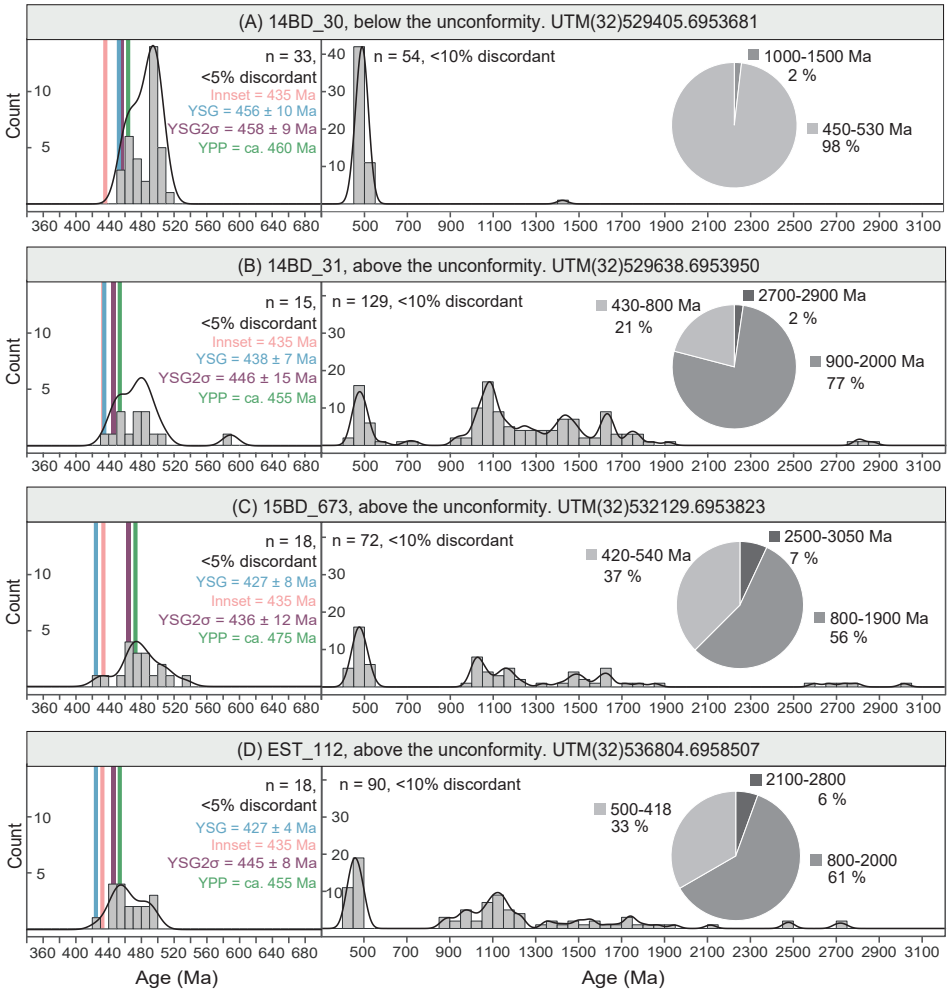

Figure 8. Detrital zircon age spectra for four sandstone samples; combined histograms and kernel density estimates (KDE). All detrital zircon U–Pb age plots are made with the 'detzrcr software package for R' (Andersen et al., 2018). Band width = 10 in the Caledonian populations, band width = 25 in the full spectra. The Caledonian populations are shown separately and represent data less than 5% discordant, all other data shown are less than 10% discordant. Thin pink bars in the Caledonian populations are the age of the Innset massif (435 Ma; Nilsen et al., 2003), blue bars represent the youngest single grain (YSG), purple bars are the calculated maximum deposition age based on the 3 youngest zircons with overlapping age at 2σ (YGC2σ), and the thin green bars are the youngest graphical peak (YPP).

discordant to be more robust for maximum depositional age calculations. For grains older than 1000 Ma the $^{207}Pb/^{206}Pb$ age is reported, while for grains younger than 1000 Ma the $^{206}Pb/^{238}U$ age is reported. 1000 Ma is chosen as a limit because only few grains are close to this age and it is preferable to avoid changing the parameters within an age fraction. All data are plotted as histograms with Kernel Density Estimates and cake plots in Fig. 8, and as upper quartile/lower quartile plots and cumulative distribution plots (Andersen et al., 2018) in Fig. 9. The full analytical dataset can be found in Electronic Supplement 1.

No common lead correction was applied to samples 14BD_31 and 15BD_673. For sample 14BD_30, a common lead correction was applied, as the majority of grains in this sample had high contents of common lead; 18 of the 54 reported analyses have been common lead-corrected following the procedure described in Andersen et al. (2009) using an in-house spreadsheet program.

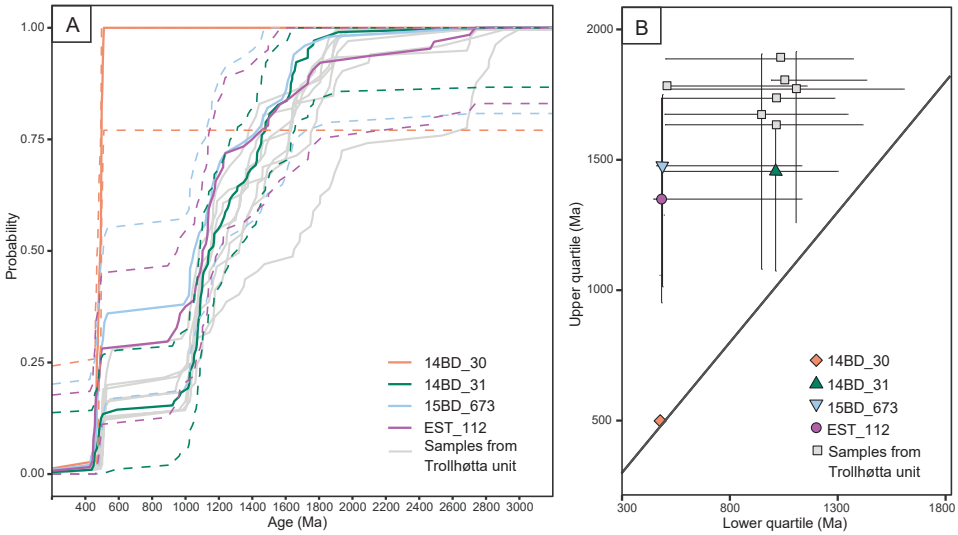

Figure 9. Detrital zircon data from sedimentary rocks of the studied area. (A) Plot of the cumulative distribution of zircon U–Pb ages (Andersen et al., 2018). Sample 14BD_30 from directly below the unconformity is clearly different from the samples above the unconformity. Samples from the Trollhøtta unit (Dalslåen et al., 2020b) are plotted in grey. Uncertainties are omitted for the Trollhøtta samples to increase readability of the diagram. (B) Upper/lower quartile plot of zircon U–Pb ages (Andersen et al., 2018), with Trollhøtta samples plotted in grey.

Detrital zircon datasets are commonly used to calculate a maximum depositional age (MDA) for the sedimentary rock in which the zircons occur. Multiple methods have been proposed for calculating a MDA, the most commonly used being the youngest single grain (YSG), the youngest grain cluster composed of three or more grains that overlap at 2σ (YGC 2σ) and the youngest graphical peak (YPP; e.g., Dickinson & Gehrels, 2009; see a summary of several methods in Coutts et al., 2019). There is no recommendation for discordance filtering included in the description of these methods (Dickinson & Gehrels, 2009), but we apply a 5% central discordance filter for our Palaeozoic age fractions used for MDA calculation.

Results

Sample 14BD_30 is a grey granule conglomerate with a biotite-rich carbonaceous matrix, belonging to the Skaret succession of the Skarvatnet unit and sampled stratigraphically directly below the unconformable contact to the northern part of the Skuggliberga unit (Dalslåen et al., 2020a; Fig. 2A). 92 grains were analysed, 54 of which were <10% discordant. Except for one grain at 1423 ± 12 Ma (- 8.3% discordant, Figs. 8A & 9), this sample has an exclusively Ordovician to Cambrian (450–530 Ma) zircon population with a major peak at c. 490 Ma (Fig. 8A). The different methods to estimate the MDA give 456 ± 10 Ma (YSG, - 0.1% discordant), 458 ± 9 Ma (YGC 2σ) and c. 460 Ma (YPP).

Sample 14BD_31 is a cross-stratified sandstone from the western part of the northern Skuggliberga unit (Fig. 2A). The sample has abundant zircon. 149 zircons were analysed, of which 129 were <10% discordant. The sample consists of 2% Archaean grains (2700–2900 Ma), 77% Neo- to Palaeoproterozoic grains (900–2000 Ma) and 21% Silurian to Cambrian grains (430–800 Ma, Figs. 8B & 9). The Cambrian–Silurian analyses are spread between 430 and 500 Ma with one grain at 580 Ma. The different methods to estimate the MDA give 438 ± 7 Ma (YSG, 2.8% discordant), 446 ± 15 Ma (YGC 2σ) and c. 455 Ma (YPP).

Sample 15BD_673 is a cross-stratified sandstone from the southeastern part of the northern Skuggliberga deposit, where it overlies the massive conglomerate (Fig. 2A). The sample has abundant zircon and 125 grains were analysed, of which 72 were <10% discordant. The sample consists of 7% Archaean grains (2500–3050 Ma), 56% Neo- to Palaeoproterozoic grains (800–1900 Ma) and 37% Silurian to Cambrian grains (430–540 Ma, Figs. 8C & 9). The different methods to estimate the MDA give 436 ± 8 Ma (YSG, 0.3% discordant), 463 ± 12 Ma (YGC 2σ) and c. 475 Ma (YPP).

Sample EST112 is a cross-stratified sandstone from the small preserved deposits east of the main, northern Skuggliberga area, and has previously been analysed for detrital zircon by Stokke et al. (2018). In order to compare the results from this sample with our new data, it is plotted in the same way as our new samples in Figs. 8D & 9. One hundred zircons were analysed, of which 91 were <10% discordant. The sample consists of 6% Palaeoproterozoic to Neoarchaean grains (2100–2800 Ma), 61% Neo- to Palaeoproterozoic grains (800–2100 Ma), and 33% Silurian to Cambrian grains (418–500 Ma). The different methods to estimate the MDA give 427 ± 4 Ma (YSG, 4% discordant), 445 ± 8 Ma (YGC 2σ) and c. 455 Ma (YPP).

Ar–Ar dating of biotite

Method

We separated biotite from a fine-grained fragment with subhedral biotite from sample 15BD_152 (Fig. 4E, F) to obtain an age of the Caledonian metamorphism in the Oppdal area. The sample was crushed and sieved to obtain 180–250 µm fractions. The finer particles were decanted in tap water and the coarser residue further ultrasonically washed in acetone and deionised water several times. The optically best biotite grains, void of any coatings and inclusions, were hand-picked under a stereomicroscope. The sample was packed in an aluminum capsule together with the PP20 fluence monitor standard along with zero-age reagent-grade K_2SO_4 and optical grade CaF_2 salts for interference corrections. We calculated J-values relative to an age of 1080.4 ± 1.1 Ma for the PP20 hornblende fluence monitor (Renne et al., 2010). The sample was irradiated at the BNC reactor (Hungary) for c. 6.5 hours, with a nominal fast neutron flux density of c. 5.5 × 10^{13} n ($cm^{-2}s^{-1}$). The interference correction factors for the production of isotopes from Ca and K are presented in Electronic Supplement 2. The rest of the analytical procedure follows Vissers et al. (2020).

Result

The degassing spectrum and inverse isochron results from sample 15BD_152 are displayed in Fig. 10 while the main results can be found in Table 2. The degassing experiment displays a flat release spectrum for 100% cumulative released ^{39}Ar from which an inverse error weighted mean of 416.3 ± 3.2 Ma was calculated. The inverse isochron result overlaps with the plateau age and the trapped $^{40}Ar/^{36}Ar$ estimate overlaps with modern air composition (Lee et al., 2006) so we use the plateau age of 416 ± 3 Ma as the best age estimate of these biotites in the following discussion.

Table 2. Main results from Ar–Ar biotite geochronology. TGA – total gas age, MSWD (P) is the mean squared weighted deviations and probability of fit.

					Spectrum					Inverse Isochron			
Sample	Material	Lat	Long	Steps (n)	%^{39}Ar	Age ± 1.96σ	MSWD (P)	TGA ± 1.96σ	K/Ca ± 1.96σ	Age ± 1.96σ	MSWD (P)	Trapped $^{40}Ar/^{36}Ar$	Spread (%)
15BD_152	Biotite	62.73979	9.625941	1-27 (27)	100	416.29 ± 3.24	0.65 (0.91)	415.12 ± 3.69	0.72 ± 2.27	417.42 ± 3.39	0.59 (0.95)	289.84 ± 11.19	90.4

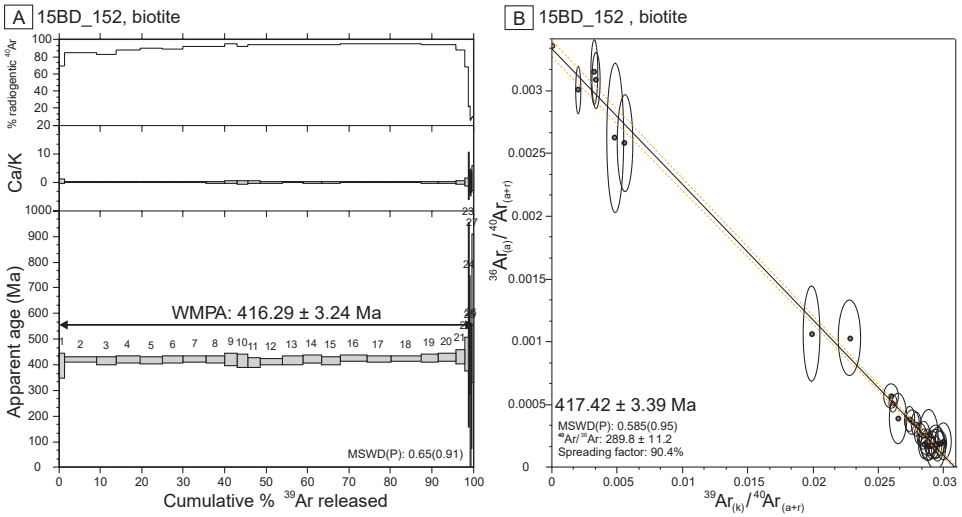

Figure 10. (A) Ar–Ar degassing spectrum. (B) Inverse isochron results for sample 15BD_152.

Discussion

Depositional environment and source of the Skuggliberga sedimentary rocks

The polymictic conglomerate in the northern area was deposited unconformably on the deformed Trollhøtta unit, and no clasts of Skuggliberga volcanic rocks are observed. This indicates that Skuggliberga volcanism was not active yet at the time of deposition of the conglomerate, and we therefore interpret it as representing the oldest deposit within the Skuggliberga unit. Many clasts within this conglomerate are from rock types present in the underlying Trollhøtta and Kinna units, and especially the presence of Kinna-type clasts is a strong indication of a significant local source. On the other hand, granite, quartzite and limestone clasts have no known source in exposed underlying units and indicate the presence of more long-travelled material. Except for a faint bedding, there are no internal structures preserved that can give unequivocal clues to the depositional environment of the conglomerate, but given the clast size, a river or beach deposit is most likely. The much thinner conglomerate beds preserved in the southern Skuggliberga area are dominated by clasts derived from Skuggliberga volcanic rocks, indicating local deposition contemporaneous with volcanism.

The cross-stratified to massive sandstones that overlie the polymictic conglomerate or are deposited directly upon Trollhøtta rocks, are immature to sub-mature and poorly sorted and have probably undergone limited transport. This indicates proximal, shallow-water deposition. Cross-stratified varieties suggest a depositional environment such as a meandering river or shallow-marine deposition above the wave base on a tidal flat. The lack of enclosing, clearly marine sediments (mudstone, limestone) indicate a fluvial setting, although a marine setting cannot be completely ruled out. The change from cross-stratified to planar-bedded and more massive, structureless sandstones up section could reflect a change in water depth or stream velocity, increased sediment input, or a combination of these.

The detrital zircon spectra from the two sandstone samples above the unconformity indicate sediment contributions from two main sources: (1) a Cambro–Ordovician source, probably derived from subduction, and arc-related Iapetus rocks equivalent to those in regionally underlying successions; and (2) an Archaean to Neoproterozoic continental source (in agreement with the character of some of the conglomerate clasts) or recycling of material derived from such a source. These age spectra contrast with those of sandstone sample 14BD_30 from directly below the unconformity, which is sourced entirely from Cambro–Ordovician source rocks in agreement with the volcanic-dominated detritus in the Skaret succession. The latter consists of a variety of chaotic volcanic-derived conglomerates with partly carbonaceous matrix, indicating deposition on unstable slopes of volcanic islands (Dalslåen et al., 2020a). The detrital zircon spectra from the Skuggliberga sandstones are comparable with the detrital zircon spectra from sandstones of the Trollhøtta unit (Fig. 9; Dalslåen et al. 2020b), but samples 15BD_673 and EST_112 (and one Trollhøtta sample) have a larger proportion of Palaeozoic zircon and plot at younger lower quartile ages compared to the Trollhøtta samples (Fig. 9B). Even though the Skuggliberga sandstones seemingly have a larger fraction of juvenile material, the detrital zircon spectra indicate input from similar sediment sources as during Trollhøtta sedimentation and/or recycling of Trollhøtta sedimentary rocks into the Skuggliberga basin.

Depositional environment and tectonic setting of the Skuggliberga volcanic rocks

Identifying the nature and depositional environment of the Skuggliberga volcanic rocks is not straightforward due to the regional metamorphic overprint and limited outcrop quality. Stokke et al. (2018) mentioned that the volcanic rocks might represent sheets within the sandstones, possibly indicating that parts of the volcanic rocks could represent shallow intrusions. However, our observations of fragment-bearing, fine-grained, massive and vesicular varieties lead us to conclude that most of the volcanic rocks probably represent primary volcanic surface deposits.

The Skuggliberga volcanic deposits are basaltic andesites and andesites (Fig. 6B), rock types that may be associated with both explosive and effusive eruptions and a wide range of depositional styles. Basaltic andesites commonly form channellised aa lava flows, which typically are 2–20 m thick with a massive core and a layer of clinker (fragmented crust of the lava flow) at the top and the bottom (e.g., Cas & Wright, 1988; Rowland & Walker, 1990). By contrast, andesites commonly form lava flows that are shorter and thicker and covered in blocky fragments; pyroclastic deposits are more common. The angular to subangular fragments in the Skuggliberga volcanic rocks and the alternation between fragment-bearing and massive parts could be interpreted both in terms of lava flows and as pyroclastic rocks. The massive, fragment-free parts could represent central parts of lava flows sandwiched between layers of fragmented and welded clinker, or the deposits could be pyroclastic rocks where the fragments are intraformational/cognate lithic fragments (e.g. Cas & Wright, 1988).

Several observations indicate that the Skuggliberga volcanic rocks represent pyroclastic deposits rather than lava flows: (1) the fragments are scattered and dispersed in the matrix, which would not be the case if the fragments had formed during autobrecciation of the outer part of a lava flow; aa and blocky lavas commonly form rubbly, fragment-supported layers at the top and base of the flow. (2) The fragments are more abundant and larger in the northern part of the northern area, while smaller, fewer clasts and local beds of greenish, probably volcanic-derived sandstone characterise the southern area. This indicates that the northern part might have been more proximal to the eruption site, while the southern part was more distal and therefore dominated by finer-grained pyroclastic or even volcaniclastic material. (3) The Skuggliberga volcanic rocks are porphyritic with phenocrysts

of biotite and amphibole, and the phenocrysts are typically larger in the fragments compared with the matrix and fragment-free parts. Such systematic variation in grain size could result from explosive eruptions with a high fragmentation rate, either during eruption or during subsequent transport, the smaller biotite and amphibole in the matrix and in the fragment-free deposits representing broken phenocrysts. This variation in phenocryst size between fragments and matrix cannot be explained in terms of autobrecciation of a lava flow. In other areas, phenocrysts are seemingly preserved in the fragment-free parts; this suggests that some eruptive phases were less violent. Unfortunately, small-scale structures are destroyed by metamorphism, which makes an interpretation of the eruptional and depositional style difficult. This is especially valid for thin-section analysis, as the fine-grained epidote overgrowths and advanced alteration of feldspars make it difficult to assess whether the varying phenocryst size is a primary magmatic feature or resulted from fragmentation during eruption and subsequent transport.

Locally observed volcanic-derived sandstones between the volcanic rocks indicate that eruption and deposition was probably episodic and occurred in a terrestrial (fluvial) or shallow-marine environment. The sand beds indicate periods of erosion and redeposition of the volcanic rocks within the volcanic succession. An episodic eruption style with a volcanic centre to the north is also supported by the volcanic fragments within the sandstone below the southern volcanic deposit; the southern sandstone must have been deposited during or after volcanic activity started in the north.

The geochemical composition of the Skuggliberga volcanic rocks is clearly different from the underlying MORB-like basaltic rocks of the Trollhøtta unit as well as the extremely enriched volcanic rocks of the Skarvatnet unit (Figs. 6D & 7; Dalslåen et al. 2020a, b). The andesitic composition and the trace element signature of the Skuggliberga volcanic rocks both suggest a volcanic arc environment; especially the negative Nb–Ta anomaly and the flat pattern from Y to Lu in MORB-normalised plots (Fig. 7A) are common features of arc-related volcanic rocks (e.g., Pearce & Peate, 1995; Hermann & Rubatto, 2009). As demonstrated by the Th/Yb vs. Nb/Yb diagram (Fig. 6D), the volcanic rocks are also akin to continental rather than oceanic arcs, making a continental arc setting most likely.

The age of the Skuggliberga unit

Stokke et al. (2018), who first described the rocks of the Skuggliberga unit, concluded with a post-427 Ma age for the cross-stratified sandstone and the volcanic rocks in the western part of the northern area (Fig. 2A), suggesting that the Skuggliberga unit might represent a hitherto unknown Silurian volcanic phase within the Scandinavian Caledonides. This age estimate was based on a MDA YGC2σ calculation, using the five youngest grains less than 10% discordant, of which four were 5–10% discordant. By using a more rigorous 5% discordance filter as in the current study, the EST112 sample from Stokke et al. (2018) gives an older MDA of 446 ± 5 Ma by the YGC2σ method.

The post-427 Ma age suggestion of Stokke et al. (2018) is in conflict with our new field observations from the southern area, where the Skuggliberga volcanic rocks were intruded by granodiorite of the Innset massif dated at 434.8 ± 0.5 Ma and 435.8 ± 0.9 Ma (Nilsen et al., 2003), indicating that the Skuggliberga unit is older than 435 Ma. MDA calculations based on <5% discordant data and using the YGC2σ and YPP approach agree with this information (Fig. 8), whereas MDA estimates based on YSG are too young (the YSG MDAs overlap in age with the Innset intrusion, Fig. 8).

A common problem with MDA calculation based on detrital zircon data, particularly in datasets where the ages of near-depositional grains and metamorphism are close, is that undetected lead loss can lead to MDA estimates younger than the true depositional age (e.g., Andersen et al., 2019; Coutts et al., 2019). Andersen et al. (2019) presented theoretical considerations and practical examples showing

that even when applying a discordance filter of 5 or 10%, the remaining near-concordant grains may have suffered undetected lead loss. Such grains can represent any combination of upper and lower intercept ages and degrees of lead loss that keeps the analysis inside the 5% or 10% discordance envelope. Processes that potentially result in lead loss in detrital zircons at a certain point after deposition include diagenetic fluids, regional metamorphism and contact metamorphism (e.g., Andersen, 2013; Andersen et al., 2019).

Following the reasoning of Andersen et al. (2019), the five <10% discordant grains used by Stokke et al. (2018) to define a MDA of 427 Ma for the Skuggliberga sandstone could represent older grains that experienced undetected lead loss at some point in time. An obvious candidate for a lead loss event might be the regional metamorphism represented by the c. 416 Ma cooling age as indicated by the Ar–Ar age of biotite. Basically, any Cambro–Ordovician (500–460 Ma) zircon affected by lead loss at 416 Ma would stay within the 5% discordance envelope due to the weak curvature of the concordia curve during this time interval. Similarly, a c. 1100 Ma zircon, which represents an age peak in our samples, could be moved to near concordia at 427 Ma by considerable lead loss at 416 Ma. We therefore consider the interpretation of a post-427 Ma age for the Skuggliberga unit as being based on a spurious detrital zircon age fraction probably caused by undetected lead loss. We consider the field observation of the Innset massif intruding the Skuggliberga volcanic rocks as more robust, demonstrating that the unit is older than 435 Ma.

The maximum age of the Skuggliberga unit is constrained by the age of the underlying deformed volcanic rocks of the Trollhøtta and Skarvatnet units, which have extrusion ages of c. 475–470 Ma (Dalslåen et al., 2020a, b). The most conservative MDA estimates (YPP) from three separate samples are still up to 15 Myr younger than the ages of the underlying volcanic units (455, 475 and 455 Ma for samples 14BD_31, 15BD_673, and EST112, respectively). However, when pooling all Palaeozoic <5% discordant analyses from the three samples, the youngest graphical peak estimate (YPP) becomes 475 Ma (Fig. 11), which corresponds to the age of the underlying volcanic units. This illustrates how sample size and chosen MDA method greatly influences the resultant MDA estimate (Coutts et al., 2019). It is noteworthy that 17 analyses are still included in histogram bins younger than the YPP (Fig. 11), and many other MDA methods based on the youngest grains therewith would deliver considerably younger MDAs. We consider it likely that those younger grains might hide undetected lead loss similar to the grains used by Stokke et al. (2018), but an origin from younger (e.g., 470–450 Ma) protosources cannot be excluded completely. In order to assess the likelihood of magmatic protosources in the age range 470–450 Ma and to constrain the most likely time of deposition for the Skuggliberga unit, a comparison with Middle Ordovician to early Silurian magmatic and sedimentary rocks elsewhere in the Scandinavian Caledonides is attempted below.

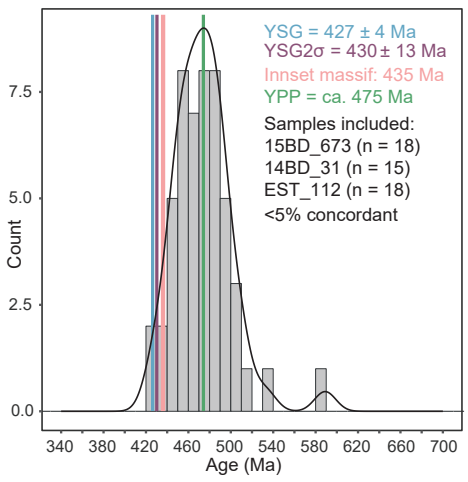

Figure 11. Pooled histogram and kernel density estimates (KDE) of all <5% discordant grains from samples 14BD_31, 15BD_673 and EST_112, showing that the youngest graphical peak is at 475 Ma corresponding to the age of the underlying volcanic rocks.

Comparison of the Skuggliberga unit with other Middle Ordovician to early Silurian rocks in the Scandinavian Caledonides

On the map of Nilsen & Wolff (1989), the northern part of the Skuggliberga unit was correlated with the Hovin Group of the TNC south of Trondheim. Originally defined as Lower and Upper Hovin Series (Vogt, 1945), the Hovin Group contains fossils of Middle and Late Ordovician age (470-445 Ma; e.g., Ryan et al., 1980; Neuman & Bruton, 1989; Neuman et al., 1997). Two major volcanic episodes have been documented within the Hovin Group: (1) the older Hølonda Porphyrites, represented by basaltic to andesitic rocks of shoshonitic affinity (e.g., Grenne & Roberts, 1998), which are associated with late Arenig/early Llanvirn (c. 467–463 Ma) fossiliferous limestone and shale (Neuman & Bruton, 1989) and (2) the younger rhyolites and rhyolitic tuffs of the Høgknippen, Hårråklett and Grimsås areas, which are associated with late Caradoc/early Ashgill (c. 453–445 Ma) fossiliferous limestones (Vogt, 1945; Ryan et al., 1980; Neuman et al., 1997). None of these two volcanic units is lithologically or geochemically similar to the Skuggliberga volcanic rocks, and limestones are totally missing in the Skuggliberga unit. A direct correlation to any part of the Hovin Group rocks farther north is therefore unlikely. However, the volcanic rocks of the Hovin Group could possibly represent protosources for detrital zircons in the age range 467–445 Ma, potentially delivering some of the <470 Ma detrital grains observed in the Skuggliberga unit.

Based on the age data provided in Stokke et al. (2018), Roberts et al. (2019) suggested that the Skuggliberga unit may correlate with the Ekne Group northeast of Trondheim (Fig. 1A). Four detrital zircon samples from the Ekne Group are dominated by Palaeozoic detrital zircons which show main peaks at 460–450 Ma, interpreted by Roberts et al. (2019) to indicate deposition in the Late Ordovician to Silurian. However, the Ekne Group is lithologically different from the Skuggliberga unit, as it is dominated by turbiditic sandstones and siltstones and does not contain volcanic rocks. The Palaeozoic-dominated detrital zircon signature of the Ekne Group is also very different from the more diverse signature of the Skuggliberga unit. Therefore, a direct correlation of the Ekne Group with the Skuggliberga unit is unlikely.

Post-470 Ma volcano-sedimentary successions are known from the Scandinavian Caledonides both south and north of the TNC. South of the TNC, the Karmøy–Bømlo–Bergen arc area (Fig. 1A) contains late Cambrian to Early Ordovician SSZ ophiolites overlain by Early Ordovician (c. 476–473 Ma) volcanic rocks (the Kattnakken and Siggjo complexes), which were deformed prior to deposition of fossiliferous Late Ordovician to early Silurian volcano-sedimentary successions (e.g., Dunning & Pedersen, 1988). The Vikafjord Group of Bømlo, deposited unconformably on deformed Siggjo volcanic rocks, consists of alluvial to shallow-marine sediments succeeded by subaerial basaltic, calc-alkaline volcanic rocks (Nordås et al., 1985). Fossils in the Vikafjord Group indicate a depositional age of c. 450–433 Ma (Nordås et al., 1985), in agreement with the possible depositional age span for the Skuggliberga unit. The similar association of fluvial to shallow-marine sedimentary and calc-alkaline volcanic rocks makes a correlation with the Skuggliberga unit reasonable. The Os Group of the Bergen arc area, resting unconformably on the Gullfjellet ophiolitic fragment, contains Late Ordovician to early Silurian fossils and comprises polymictic conglomerate overlain by shale, minor limestone and cross-stratified sandstone, but lacks volcanic rocks like those of the Vikafjord and Skuggliberga units (Ingdahl, 1989). The Late Ordovician (c. 443 Ma) Solund–Stavfjord ophiolite complex falls within the same time span (Furnes et al., 2012). It is dominated by N-MORB-type lavas with only a weak subduction influence, but arc-related, early Silurian (c. 439 Ma) mafic to felsic volcanic rocks also occur (Furnes & Lippard, 1983; Hartz et al., 2002), possibly representing time-equivalents to the Skuggliberga volcanic rocks.

North of the TNC, the Sulitjelma area (Fig. 1A) contains remnants of a marginal basin with an E-MORB type gabbro-basalt complex (Sulitjelma), overlain by the fossiliferous Late Ordovician to early Silurian Furulund Group that contains calc-alkaline (Lomivann) basaltic rocks (Boyle, 1989; Pedersen et al., 1991). This basin has been correlated with the Solund–Stavfjord basin and also represents a marginal basin that is potentially correlatable with the Skuggliberga unit in terms of age and depositional-volcanic environment. Even farther north, Late Ordovician to early Silurian turbidites and local carbonate and volcanic rocks are known from the Sagelvvatn Group (Fig. 1A; Bjørlykke & Olaussen, 1981) and from the Oksfjord Group (Fig. 1A; Lindahl et al., 2005). However, both groups contain basaltic lava flows with tholeiitic within-plate type geochemical affinities, different from the calc-alkaline nature of the Skuggliberga andesites. Finally, the Magerøy Supergroup of Late Ordovician to early Silurian age in northern Norway (Fig. 1A) was intruded—similar to the Skuggliberga unit—by a major 438 ± 1 Ma composite plutonic complex (Andersen, 1981; Corfu et al., 2006). However, the Magerøy Supergroup is composed entirely of shallow- to deep-marine turbiditic and calcareous rocks and does not contain volcanic rocks.

Middle Ordovician to early Silurian continental arc-related plutonic complexes are common from Smøla and Hitra in the south to the Helgeland Nappe Complex and correlatives farther north (Fig. 1A). Magmatic activity stretches from c. 482 Ma to c. 424 Ma and is considered to result from subduction under the Laurentian margin (Tucker et al., 2004; Barnes et al., 2007; Barnes et al., 2011; Augland et al., 2012; Slagstad & Kirkland, 2018). Like the Skuggliberga volcanic rocks, many of these complexes have arc-like geochemical signatures, e.g., the 440–445 Ma Smøla–Hitra Batholith (Gautneb & Roberts, 1989; Tucker et al., 2004), the 456 ± 2 Ma Møklevatnet monzodiorite (Meyer et al., 2003) and the 460 ± 3 Ma Follafoss tonalite (Tucker et al., 2004; Hollocher et al., 2016). They are also broadly comparable to the 460–440 Ma 'younger arc rocks' of Hollocher et al. (2016), a suite of metamorphic and deformed intrusive rocks exposed along the central Norwegian coast that were assigned to the Trondheim Nappe Complex. Given that the Skuggliberga volcanic rocks are geochemically comparable both to older and younger arc-related plutonic rocks, such a comparison does not allow further constraints on the age of the Skuggliberga unit within the 470–435 Ma time frame, but generally highlights the genetic link between the plutonic continental-arc complexes and the Skuggliberga unit. Circa 438–434 Ma bimodal mafic-felsic intrusive complexes comparable to the Innset massif can be found all along the Scandinavian Caledonides and have been interpreted to have formed in localised extensional basins at the onset of the Laurentia–Baltica collision (Nilsen et al., 2007; Slagstad & Kirkland, 2018).

The Pre-Skuggliberga orogenic event

The Skuggliberga unit has been deposited on the folded and eroded Skarvatnet and Trollhøtta units, indicating the presence of a deformation phase between the formation of the Skarvatnet and Trollhøtta units (formation age c. 475-470 Ma; Dalslåen et al., 2020a,b) and deposition of the Skuggliberga unit. This orogenic phase is represented by deformation phases D_1 and D_2 of Stokke et al. (2018), and is regionally represented by tilting and overturning of the succession towards west (Fig. 2B). Constraining the age of this deformation phase is hampered by the uncertain depositional age of the Skuggliberga unit, but assuming a depositional age of c. 450–435 Ma—by analogy with the Vikafjord Group—the deformation phase must have happened between ca. 470 and 450 Ma.

Palaeogeographically this deformation phase can be constrained by the link between the Trollhøtta–Kinna rocks and the Støren and Hølonda rocks farther north. The deformed Trollhøtta unit has been correlated with the Støren sensu stricto basaltic rocks (Stokke et al., 2018; Dalslåen et al., 2020b), and the Kinna volcanic succession has geochemical similarities with the Hølonda Porphyrites (Grenne & Roberts, 1998; Dalslåen et al., 2020a). The Hølonda Porphyrites are coeval with

deposition of limestone with a Laurentian fauna (Neuman & Bruton, 1989) placing formation of the Trollhøtta–Kinna and Støren–Hølonda systems close to the Laurentian margin. The connection to Laurentia is strengthened by the detrital zircon signature of the Trollhøtta unit (Dalslåen et al., 2020b). Dalslåen et al. (2020a) proposed that the onset of proper subduction under the Laurentian margin within the mid-Norwegian sector is marked by the voluminous arc magmatism that started at c. 460 Ma (e.g. Tucker et al., 2004). This could have caused accretion of the Trollhøtta–Kinna basin to the Laurentian margin or an associated microcontinent, causing the deformation of the rocks. Ordovician accretionary events, generally correlated with the Laurentian Taconian orogeny, are well known from the Helgeland Nappe Complex farther north (e.g., Yoshinobu et al., 2002; Roberts et al., 2002, 2007) and from the Appalachians in Newfoundland (e.g., van Staal et al., 2009), but the lack of a definite age of the Skuggliberga volcanic rocks hampers further correlation of events.

Conclusions

The Skuggliberga unit of the Oppdal area represents a distinct volcano-sedimentary unit within the southern Trondheim Nappe Complex. It was deposited unconformably upon the deformed c. 475–470 Ma Trollhøtta and Skarvatnet units and was intruded by the Innset massif at c. 435 Ma. The Skuggliberga unit consists of polymictic conglomerate and cross-stratified to massive sandstone, as well as calc-alkaline basaltic andesites and andesites. The sedimentary rocks indicate deposition in a fluvial or shallow-marine environment. The volcanic rocks most likely represent pyroclastic deposits. Detrital zircon spectra from three sandstone samples of the Skuggliberga unit are dominated by Archaean to Neoproterozoic grains, with a limited number of Palaeozoic grains. Spuriously young detrital zircon grains (<435 Ma) are probably the result of undetected lead loss of Early Palaeozoic grains caused by greenschist-facies metamorphism preceeding an Ar–Ar cooling age of c. 416 Ma. The possibility of undetected lead loss in the youngest detrital zircons means that the Palaeozoic detrital zircon grains cannot be used to constrain the maximum age of deposition any further. Comparison with other Middle Ordovician to early Silurian volcano-sedimentary units within the Scandinavian Caledonides suggests that the Skuggliberga unit has most in common with Upper Ordovician to early Silurian (ca. 450–435 Ma) units such as the Vikafjord Group of Bømlo, the Solund–Stavfjord ophiolite complex, or the Furulund Group of the Sulitjelma area. Our data imply that the unit has no direct correlative within the TNC and represents a hitherto unknown volcano-sedimentary phase within the Central Norwegian Caledonides. However, it has geochemical similarities with several continental arc-related plutonic complexes spanning the same age interval along the coastal area of central Norway, and the Skuggliberga volcanic rocks may represent an extrusive part of this magmatic arc system. Deposition of the Skuggliberga units is preceded by an orogenic phase resulting in deformation of the underlying Trollhøtta and Skarvatnet units, probably related to Taconian accretionary events along the Laurentian margin.

Acknowledgements. E. W. Stokke assisted in the field and lab, G. Fjeld Bye (UiO) prepared samples, and thin-sections have been made by S. Akhavan (UiO). Geochemical analyses have been performed by J. Schönenberger, A. E. Karlsen, Ø. Skår and T. S. Røhr at NGU. Discussions with Magnus Kristoffersen and Tom Andersen are highly appreciated. This paper is part of the Ph.D. work of B. H. Dalslåen which is funded by the University of Oslo; fieldwork and analyses are partly funded by the Geological Survey of Norway project number 353000. Constructive comments by an anonymous reviewer and editor Trond Slagstad are highly appreciated.

References

Andersen, T.B. 1981: The structure of the Magerøy Nappe, Finnmark, North Norway. *Norges geologiske undersøkelse 363*, 1–23.

Andersen, T. 2013: Age, Hf isotope and trace element signatures of detrital zircons in the Mesoproterozoic Eriksfjord sandstone, southern Greenland: are detrital zircons reliable guides to sedimentary provenance and timing of deposition? *Geological Magazine 150*, 426–440. https://doi.org/10.1017/S0016756812000623.

Andersen, T., Andersson, U.B., Graham, S., Åberg, G. & Simonsen, S.L. 2009: Granitic magmatism by melting of juvenile continental crust: new constraints on the source of Palaeoproterozoic granitoids in Fennoscandia from Hf isotopes in zircon. *Journal of the Geological Society 166*, 233–247. https://doi.org/10.1144/0016-76492007-166.

Andersen, T., Kristoffersen, M. & Elburg, M.A. 2018: Visualizing, interpreting and comparing detrital zircon age and Hf isotope data in basin analysis–a graphical approach. *Basin Research 30*, 132–147. https://doi.org/10.1111/bre.12245.

Andersen, T., Elburg, M.A. & Magwaza, B.N. 2019: Sources of bias in detrital zircon geochronology: Discordance, concealed lead loss and common lead correction. *Earth-Science Reviews 197*, 102899. https://doi.org/10.1016/j.earscirev.2019.102899.

Augland, L.E., Andresen, A., Corfu, F., Simonsen, S.L. & Andersen, T. 2012: The Beiarn nappe complex: a record of Laurentian Early Silurian arc magmatism in the Uppermost Allochthon, Scandinavian Caledonides. *Lithos 146*, 233–252. https://doi.org/10.1016/j.lithos.2012.05.016.

Barnes, C.G., Frost, C.D., Yoshinobu, A.S., McArthur, K., Barnes, M.A., Allen, C.M., Nordgulen, Ø. & Prestvik, T. 2007: Timing of sedimentation, metamorphism, and plutonism in the Helgeland Nappe Complex, north-central Norwegian Caledonides. *Geosphere 3*, 683–703. https://doi.org/10.1130/GES00138.1.

Barnes, C.G., Reid, K., Frost, C.D., Barnes, M.A., Allen, C.M. & Yoshinobu, A.S. 2011: Ordovician and Silurian magmatism in the Upper Nappe, Uppermost Allochthon, Helgeland Nappe Complex, north-central Norway. *Norwegian Journal of Geology 91*, 121–136.

Bjørlykke, A. & Olaussen, S. 1981: Silurian sediments, volcanics and mineral deposits in the Sagelvvatn area, Troms, North Norway. *Norges geologiske undersøkelse 365*, 1–38.

Boyle, A. 1989: The geochemistry of the Sulitjelma ophiolite and associated basic volcanics: tectonic impilcations. *In* Gayer, R.A. (ed.): *The Caledonide Geology of Scandinavia.* Graham & Trotman, pp. 153–163. https://doi.org/10.1007/978-94-009-2549-6_13.

Cas, R. & Wright, J.V. 1988: *Volcanic successions modern and ancient: A geological approach to processes, products and successions.* Springer Science & Business Media, 528 pp. https://doi.org/10.1007/978-94-009-3167-1.

Corfu, F., Torsvik, T., Andersen, T., Ashwal, L., Ramsay, D. & Roberts, R. 2006: Early Silurian mafic–ultramafic and granitic plutonism in contemporaneous flysch, Magerøy, northern Norway: U–Pb ages and regional significance. *Journal of the Geological Society 163,* 291–301. https://doi.org/10.1144/0016-764905-014.

Corfu, F., Andersen, T. & Gasser, D. 2014: The Scandinavian Caledonides: main features, conceptual advances and critical questions. *Geological Society, London, Special Publications 390*, 9–43. https://doi.org/10.1144/SP390.25.

Coutts, D.S., Matthews, W.A. & Hubbard, S.M. 2019: Assessment of widely used methods to derive depositional ages from detrital zircon populations. *Geoscience Frontiers 10,* 1421–1435. https://doi.org/10.1016/j.gsf.2018.11.002.

Dalslåen, B., Gasser, D., Grenne, T., Augland, L. & Corfu, F. 2020a: Ordovician shoshonitic to ultrapotassic volcanism in the central Norwegian Caledonides: The result of sediment subduction, mantle metasomatism and mantle partial melting. *Lithos 356,* 105372. https://doi.org/10.1016/j.lithos.2020.105372.

Dalslåen, B.H., Gasser, D., Grenne, T., Augland, L.E. & Andresen, A. 2020b: Early to Middle Ordovician sedimentation and bimodal volcanism at the margin of Iapetus: The Trollhøtta–Kinna basin of the Central Norwegian Caledonides. *In* Murphy, J., Strachan, R. & Quesada, C. (eds.): *Pannotia To Pangaea: Neoproterozoic and Paleozoic Orogenic Cycles in the Circum-Atlantic Region 503*, Geological Society, London, Special Publications, London, pp. 251–277. https://doi.org/10.1144/SP503-2020-37.

Dickinson, W.R. & Gehrels, G.E. 2009: Use of U–Pb ages of detrital zircons to infer maximum depositional ages of strata: a test against a Colorado Plateau Mesozoic database. *Earth and Planetary Science Letters 288*, 115–125. https://doi.org/10.1016/j.epsl.2009.09.013.

Domeier, M. 2016: A plate tectonic scenario for the Iapetus and Rheic oceans. *Gondwana Research 36*, 275–295. https://doi.org/10.1016/j.gr.2015.08.003.

Dunning, G. & Pedersen, R. 1988: U/Pb ages of ophiolites and arc-related plutons of the Norwegian Caledonides: implications for the development of Iapetus. *Contributions to Mineralogy and Petrology 98*, 13–23. https://doi.org/10.1007/BF00371904.

Furnes, H. & Lippard, S.J. 1983: Devonian lavas from Solund, West Norway - field relationships and geochemistry. *Norges Geologiske Undersøkelse Skrifter 328,* 1–15.

Furnes, H., Dilek, Y. & Pedersen, R.B. 2012: Structure, geochemistry, and tectonic evolution of trench-distal backarc oceanic crust in the western Norwegian Caledonides, Solund-Stavfjord ophiolite (Norway). *Geological Society of America Bulletin 124,* 1027–1047. https://doi.org/10.1130/B30561.1.

Gale, A., Dalton, C.A., Langmuir, C.H., Su, Y. & Schilling, J.G. 2013: The mean composition of ocean ridge basalts. *Geochemistry, Geophysics, Geosystems 14*, 489–518. https://doi.org/10.1029/2012GC004334.

Gautneb, H. & Roberts, D. 1989: Geology and petrochemistry of the Smøla–Hitra Batholith, central Norway. *Norges geologiske undersøkelse Bulletin 416,* 1–24.

Gee, D., Guezou, J., Roberts, D. & Wolff, F. 1985: The central-southern part of the Scandinavian Caledonides. *The Caledonide orogen-Scandinavia and related areas 1,* 109–133.

Gee, D.G., Fossen, H., Henriksen, N. & Higgins, A.K. 2008: From the early Paleozoic platforms of Baltica and Laurentia to the Caledonide Orogen of Scandinavia and Greenland. *Episodes 31*, 44–51. https://doi.org/10.18814/epiiugs/2008/v31i1/007.

Goldschmidt, V.M. 1916: Geologisch-Petrographische Studien im Hochgebirge des Südlischen Norwegens. IV Überschit der Eruptivgesteine im Kaledonishen Gebirge Zwischen Stavanger und Trondhjem. *Skrifter Videnskapelig-Selskap Christiania I. Mat-naturv. Kl.no. 2 2*, 140.

Grenne, T. & Roberts, D. 1998: The Hølonda Porphyrites, Norwegian Caledonides: geochemistry and tectonic setting of Early–Mid-Ordovician shoshonitic volcanism. *Journal of the Geological Society 155*, 131–142. https://doi.org/10.1144/gsjgs.155.1.0131.

Hartz, E.H., Martin, M.W., Andresen, A. & Andersen, T.B. 2002: Volcanic rocks in the Devonian Solund Basin, Western Norway: large landslides of Silurian (439 Ma) rhyolites. *Journal of the Geological Society 159*, 121–128. https://doi.org/10.1144/0016-764901-063.

Hermann, J. & Rubatto, D. 2009: Accessory phase control on the trace element signature of sediment melts in subduction zones. Chemical Geology 265, 512–526. https://doi.org/10.1016/j.chemgeo.2009.05.018.

Hollocher, K., Robinson, P., Seaman, K. & Walsh, E. 2016: Ordovician–early Silurian intrusive rocks in the northwest part of the Upper Allochthon, mid-Norway: Plutons of an Iapetan volcanic arc complex. *American Journal of Science 316*, 925–980. https://doi.org/10.2475/10.2016.01

Holmsen, P. 1955: Trekk av Opdalsfeltets geologi. *Norsk Geologisk Tidsskrift 35*, 135–150.

Ingdahl, S. 1989: The Upper Ordovician-Lower Silurian rocks in the Os area, Major Bergen Arc, Western Norway. *Norsk Geologisk Tidsskrift 69,* 163–175.

Krill, A.G. 1980: Tectonics of the Oppdal area, central Norway. *Geologiska Föreningen i Stockholm Förhandlingar 102*, 523-530. https://doi.org/10.1080/11035898009454505.

Krill, A.G. 1985: Relationships between the Western Gneiss Region and the Trondheim Region : Stockwerk-tectonics reconsiderd. *In* Gee, D. & Sturt, B. (eds.): *The Caledonide Orogen - Scandinavia and Related Areas*, John Wiley & Sons Ltd, pp. 475–483.

Lee, J.-Y., Marti, K., Severinghaus, J.P., Kawamura, K., Yoo, H.-S., Lee, J.B. & Kim, J.S. 2006: A redetermination of the isotopic abundances of atmospheric Ar. *Geochimica et Cosmochimica Acta 70*, 4507–4512. https://doi.org/10.1016/j.gca.2006.06.1563.

Lindahl, I., Stevens, B.P. & Zwaan, K.B. 2005: The geology of the Vaddas area, Troms: a key to our understanding of the Upper Allochthon in the Caledonides of northern Norway. *Norges Geologiske undersøkelse Bulletin 445*, 5–43.

Meyer, G., Grenne, T. & Pedersen, R. 2003: Age and tectonic setting of the Nesåa Batholith: implications for Ordovician arc development in the Caledonides of Central Norway. *Geological Magazine 140,* 573–594. https://doi.org/10.1017/S0016756803008069.

Neuman, R. & Bruton, D. 1989: Brachiopods and trilobites from the Ordovician Lower Hovin Group (Arenig/Llanvirn), Hølonda area, Trondheim region, Norway: new and revised taxa and paleogeographic interpretation. *Norges geologiske undersøkelse Bulletin 414*, 49–89.

Neuman, R.B., Pojeta Jr, J. & Bruton, D.L. 1997: Fossils from the Ordovician" Upper Hovin Group" (Caradoc-Ashgill), Trondheim Region, Norway. *Norges geologiske undersøkelse Bulletin 432*, 25–58.

Nilsen, O. & Wolff, F.C. 1989: Røros og Sveg. Berggrunnskart Røros og Sveg, scale 1:250000, *Norges Geologiske Undersøkelse.*

Nilsen, O., Sundvoll, B., Roberts, D. & Corfu, F. 2003: U-Pb geochronology and geochemistry of trondhjemites and a norite pluton from the SW Trondheim Region, Central Norwegian Caledonides. *Norges Geologiske Undersøkelse Bulletin 441*, 5–16.

Nilsen, O., Corfu, F. & Roberts 2007: Silurian gabbro-diorite-trondhjemite plutons in the Trondheim Nappe Complex, Caledonides, Norway; petrology and U-Pb geochronology. *Norwegian Journal of Geology 87*, 329-342.

Nordås, J., Amaliksen, K., Brekke, H., Suthern, R., Furnes, H., Sturt, B., Robins, B. & Gee, D. 1985: Lithostratigraphy and petrochemistry of Caledonian rocks on Bømlo, SW Norway. *In* Gee, D.G. & Sturt, B.A. (eds.): *The Caledonide Orogen—Scandinavia and Related Areas*, John Wiley & Sons Ltd, New York, pp. 679–692.

Pearce, J.A. 1996: A user's guide to basalt discrimination diagrams. *In* Wyman, D.A. (ed.): *Trace element geochemistry of volcanic rocks: applications for massive sulphide exploration*, Geological Association of Canada, Short Course Notes 12, pp. 79–113.

Pearce, J.A. 2008: Geochemical fingerprinting of oceanic basalts with applications to ophiolite classification and the search for Archean oceanic crust. *Lithos 100*, 14–48. https://doi.org/10.1016/j.lithos.2007.06.016.

Pearce, J.A. & Peate, D.W. 1995: Tectonic implications of the composition of volcanic arc magmas. *Annual review of Earth and planetary sciences 23,* 251–285. https://doi.org/10.1146/annurev.ea.23.050195.001343.

Pedersen, R.B. & Dunning, G.R. 1997: Evolution of arc crust and relations between contrasting sources: U-Pb (age), Nd and Sr isotope systematics of the ophiolitic terrain of SW Norway. *Contributions to Mineralogy and Petrology 128*, 1–15. https://doi.org/10.1007/s004100050289.

Pedersen, R., Furnes, H. & Dunning, G. 1991: A U/Pb age for the Sulitjelma Gabbro, North Norway: further evidence for the development of a Caledonian marginal basin in Ashgill-Llandovery time. *Geologic Magazine 128,* 141–153. https://doi.org/10.1017/S0016756800018331.

Pedersen, R., Bruton, D. & Furnes, H. 1992: Ordovician faunas, island arcs and ophiolites in the Scan-dinavian Caledonides. *Terra Nova 4*, 217–222. https://doi.org/10.1111/j.1365-3121.1992.tb00475.x.

Renne, P.R., Mundil, R., Balco, G., Min, K. & Ludwig, K.R. 2010: Joint determination of 40K decay constants and 40Ar*/40K for the Fish Canyon sanidine standard, and improved accuracy for 40Ar/39Ar geochronology. *Geochimica et Cosmochimica Acta 74,* 5349–5367. https://doi.org/10.1016/j.gca.2010.06.017.

Roberts, D., Melezhik, V. & Heldal, T. 2002: Carbonate formations and early NW-diected thrusting in the highest allochthons of the Norwegian Caledonides. *Journal of the Geological Society of London 159,* 117-120. https://doi.org/10.1144/0016-764901-128.

Roberts, D., Nordgulen, O. & Melezhik, V. 2007: The Uppermost Allochthon in the Scandinavian Caledonides: From a Laurentian ancestry through Taconian orogeny to Scandian crustal growth on Baltica. *In* Hatcher Jr., R.D., Carlson, M.P., McBride, J.H. & Martinez Catalan, J.R. (eds.): *4-D Framework of Continental Crust*, Geological Society of America Memoir 200, pp. 357–377. https://doi.org/10.1130/2007.1200(18).

Roberts, D., Morton, A. & Frei, D. 2019: A Silurian age for the metasedimentary rocks of the Ekne Group, Trøndelag, Mid-Norwegian Caledonides: and inferences for a peri-Laurentian provenance. *Norwegian Journal of Geology 99*, 583–595. https://doi.org/10.17850/njg99-4-3.

Rohr-Torp, E. 1972: A major inversion of the western part of the Trondheim nappe. *Norwegian Journal of Geology 52,* 453–458.

Rohr-Torp, E. 1974: Contact metamorphism around the Innset massif. *Norwegian Journal of Geology 54*, 13–33.

Rowland, S.K. & Walker, G.P. 1990: Pahoehoe and aa in Hawaii: volumetric flow rate controls the lava structure. *Bulletin of Volcanology 52*, 615–628. https://doi.org/10.1007/BF00301212.

Ryan, P.D., Williams, D. & Skevington, D. 1980: Revised interpretation of the Ordovician stratigraphy of Sør Trøndelag, and its implications for the evolution of the Scandinavian Calcdonides. *In* Wones, D. & Blackburn, W. (eds.): *The Caledonides in the USA" : I.G.C.P.project 27: Caledonide orogen*, Virginia Polytechnic Institute, pp. 99–104.

Slagstad, T. & Kirkland, C.L. 2018: Timing of collision initiation and location of the Scandian orogenic suture in the Scandinavian Caledonides. *Terra Nova 30,* 179–188. https://doi.org/10.1111/ter.12324.

Slagstad, T., Pin, C., Roberts, D., Kirkland, C.L., Grenne, T., Dunning, G., Sauer, S. & Andersen, T. 2014: Tectonomagmatic evolution of the Early Ordovician suprasubduction-zone ophiolites of the Trondheim Region, Mid-Norwegian Caledonides. *Geological Society, London, Special Publications 390,* 541–561. https://doi.org/10.1144/SP390.11.

Stokke, E.W., Gasser, D., Dalslåen, B.H. & Grenne, T. 2018: Tectonic evolution of syn-to late-orogenic sedimentary–volcanic basins in the central Norwegian Caledonides. *Journal of the Geological Society 175*, 605–618. https://doi.org/10.1144/jgs2017-091.

Sun, S.-S. & McDonough, W.-S. 1989: Chemical and isotopic systematics of oceanic basalts: implications for mantle composition and processes. *Geological Society, London, Special Publications 42*, 313–345. https://doi.org/10.1144/GSL.SP.1989.042.01.19.

Tucker, R.D., Robinson, P., Solli, A., Gee, D.G., Thorsnes, T., Krogh, T.E., Nordgulen, Ø. & Bickford, M. 2004: Thrusting and extension in the Scandian hinterland, Norway: New U-Pb ages and tectonostratigraphic evidence. *American Journal of Science 304*, 477–532. https://doi.org/10.2475/ajs.304.6.477.

van Staal, C.R., Whalen, J.B., Valverde-Vaquero, P., Zagorevski, A. & Rogers, N. 2009: Pre-Carboniferous, episodic accretion-related, orogenesis along the Laurentian margin of the northern Appalachians. *Geological Society, London, Special Publications 327*, 271–316. https://doi.org/10.1144/SP327.13.

Vissers, R.L., Ganerød, M., Pennock, G.M. & van Hinsbergen, D.J. 2020: Eocene seismogenic reactivation of a Jurassic ductile shear zone at Cap de Creus, Pyrenees, NE Spain. *Journal of Structural Geology 134,* 103994. https://doi.org/10.1016/j.jsg.2020.103994.

Vogt, T. 1945: The geology of part of the Hølonda-Horg district, a type area in the Trondheim region. *Norwegian Journal of Geology 25*, 449–528.

Wilson, J.T. 1966: Did the Atlantic close and then re-open? *Nature 211*, 676–681. https://doi.org/10.1038/211676a0.

Yoshinobu, A.S., Barnes, C.G., Nordgulen, Ø., Prestvik, T., Fanning, M. & Pedersen, R. 2002: Ordovician magmatism, deformation, and exhumation in the Caledonides of central Norway: An orphan of the Taconic orogeny? *Geology 30*, 883–886. https://doi.org/10.1130/0091-7613(2002)030<0883:OMDAEI>2.0.CO;2.

Supplementary material A: Stokke et al., 2018

Stokke, E. W., Gasser, D., Dalslåen, B. H. and Grenne, T., 2018, *Tectonic evolution of syn-to late-orogenic sedimentary–volcanic basins in the central Norwegian Caledonides.*

Published in Journal of the Geological Society, v. 175, no. 4, p. 605-618.

Supplementary material B: Detrital zircon data from the Trollhøtta unit (Paper II)

This is the LA-ICP-MS detrital zircon analytical data for the results published in Dalslåen, B.H., Gasser, D., Grenne, T., Augland, L.E. and Andresen, A., 2020. **Early to Middle Ordovician sedimentation and bimodal volcanism at the margin of Iapetus: The Trollhøtta–Kinna basin of the Central Norwegian Caledonides.** *In*: Murphy, J.B., Strachan, R. & Quesada, C. (eds) *Pannotia to Pangaea: Neoproterozoic and Paleozoic Orogenic Cycles in the Circum-Atlantic Region.* Geological Society, London, Special Publications, 503. https://doi.org/10.1144/SP503-2020-37

The data are also available for download from https://doi.org/10.6084/m9.figshare.c.4990752

Supplementary material C: Detrital zircon data from the Skuggliberga unit (Paper III)

This is the LA-ICP-MS detrital zircon analytical data for the results published in Dalslåen, B.H., Gasser, D., Grenne, T., Ganerød, M. and Andresen, A. **The Skuggliberga unit of the Oppdal area, central Scandinavian Caledonides: calc-alkaline andesitic pyroclastic volcanism in a fluvial to shallow marine basin following mid-Ordovician tectonism.** Accepted for publication in Norwegian Journal of Geology.

The dataset will also be available for download from https://njg.geologi.no/

		ppm						*Ratios*
sample	name	U	^{206}Pb	$^{206}Pb_c$(%)	206/204	$^{207}Pb/^{206}Pb^*$	1SE	$^{207}Pb/^{235}U^*$
14BD_3(	14_30_93	1836	143.7	1.10E+00	1410	0.05654	0.00039	0.62319
14BD_3(	14_30_62	1439	105.1	0.00E+00	47745	0.05669	0.00021	0.62549
14BD_3(	14_30_95	733	52.9	8.40E-01	2138	0.05592	0.00068	0.57659
14BD_3(	14_30_120	373	29.2	0.00E+00	16905	0.05686	0.00042	0.6358
14BD_3(	14_30_69	1171	92.9	0.00E+00	21976	0.05701	0.00034	0.64494
14BD_3(	14_30_121	285	22	0.00E+00	9139	0.05676	0.00043	0.62581
14BD_3(	14_30_112	346	26.9	0.00E+00	11920	0.05675	0.00043	0.62315
14BD_3(	14_30_116	405	31.6	0.00E+00	14538	0.057	0.00042	0.63489
14BD_3(	14_30_48	610	45.9	1.00E+00	1503	0.05728	0.00055	0.65122
14BD_3(	14_30_40	668	49	0.00E+00	35055	0.05684	0.00022	0.62318
14BD_3(	14_30_98	502	39.9	0.00E+00	12249	0.05706	0.0004	0.6325
14BD_3(	14_30_38	742	52.6	0.00E+00	28464	0.05661	0.0003	0.59961
14BD_3(	14_30_106	186	14.1	0.00E+00	6385	0.05668	0.00043	0.60379
14BD_3(	14_30_18	209	14.4	0.00E+00	6987	0.05611	0.00032	0.56731
14BD_3(	14_30_81	1693	130.1	2.10E-01	7935	0.05699	0.00038	0.62132
14BD_3(	14_30_54	755	56.1	8.30E-01	1716	0.05715	0.00037	0.63071
14BD_3(	14_30_41	685	50.7	2.50E-01	10862	0.05709	0.00033	0.62652
14BD_3(	14_30_94	447	33.2	0.00E+00	13517	0.05681	0.00038	0.60729
14BD_3(	14_30_26	676	47.9	0.00E+00	24795	0.05632	0.00024	0.576
14BD_3(	14_30_75	1847	146.5	8.80E-01	20558	0.05744	0.00193	0.6
14BD_3(	14_30_80	460	33.6	0.00E+00	13977	0.05667	0.00037	0.59557
14BD_3(	14_30_31	297	20.9	0.00E+00	48493	0.05662	0.00026	0.58888
14BD_3(	14_30_21	317	22.3	0.00E+00	17691	0.05661	0.00026	0.58607
14BD_3(	14_30_25	251	17.6	0.00E+00	6973	0.05672	0.00029	0.58916
14BD_3(	14_30_36	157	10.9	0.00E+00	4809	0.05652	0.00029	0.57792
14BD_3(	14_30_39	1001	74.6	1.60E+00	939	0.05748	0.00118	0.63582
14BD_3(	Plot_data	1001	74.6	1.60E+00	939	0.05748	0.00118	0.63582
14BD_3(	14_30_74	1786	139.2	1.90E+00	964	0.05754	0.00175	0.6368
14BD_3(	14_30_35	199	13.7	0.00E+00	67538	0.05655	0.0003	0.5753
14BD_3(	14_30_115	266	20.5	0.00E+00	6026	0.05745	0.00044	0.62678
14BD_3(	14_30_42	180	12.5	0.00E+00	6172	0.05713	0.00028	0.60486
14BD_3(	14_30_65	2730	210.1	2.20E+00	1122	0.05725	0.00296	0.61228
14BD_3(	14_30_60	255	17	0.00E+00	7770	0.05671	0.00026	0.57825
14BD_3(	14_30_16	1029	74.8	0.00E+00	30860	0.05743	0.00023	0.61463
14BD_3(	14_30_59	732	52	0.00E+00	13781	0.05747	0.00025	0.61637
14BD_3(	14_30_32	730	54	0.00E+00	83376	0.05787	0.00024	0.63542
14BD_3(	14_30_97	260	20.1	0.00E+00	8413	0.05768	0.00042	0.6236
14BD_3(	14_30_100	274	21	0.00E+00	67923	0.05787	0.00042	0.62127
14BD_3(	14_30_17	161	34.4	0.00E+00	14607	0.08987	0.0006	2.80449
14BD_3(	14_30_43	306	21.7	1.60E+00	1053	0.05758	0.00031	0.60415
14BD_3(	14_30_49	497	37.8	3.90E+00	1997	0.05846	0.00306	0.65197
14BD_3(	14_30_47	563	43.4	0.00E+00	10897	0.0592	0.00025	0.69366
14BD_3(	14_30_57	694	49.8	1.30E+00	1399	0.0578	0.00049	0.61359
14BD_3(	14_30_19	163	11.2	0.00E+00	12433	0.05735	0.00033	0.58326
14BD_3(	14_30_37	899	64.1	3.40E-01	3645	0.05792	0.00038	0.61328
14BD_3(	14_30_67	1702	133.5	0.00E+00	43785	0.05626	0.00033	0.62959
14BD_3(	14_30_63	1246	90.2	0.00E+00	1489044	0.05611	0.00021	0.61385
14BD_3(	14_30_76	1436	112.4	1.10E+00	1274	0.05634	0.00038	0.6

				Discordance		*Ages*					
1SE	$^{206}Pb/^{238}U^{*}$	1SE	Rho	Central	Minim	207/206	1σ	207/235	1σ	206/238	1σ
0.01234	0.079934	0.00149	0.939	4.8	.	474	15	492	8	496	9
0.00964	0.080018	0.0012	0.972	3.6	.	480	8	493	6	496	7
0.01269	0.074782	0.00137	0.832	3.6	.	449	26	462	8	465	8
0.01112	0.081096	0.00128	0.904	3.5	.	486	16	500	7	503	8
0.01113	0.082046	0.00133	0.938	3.4	.	492	12	505	7	508	8
0.01064	0.079969	0.00122	0.897	3	.	482	16	493	7	496	7
0.01001	0.07964	0.00113	0.883	2.6	.	482	16	492	6	494	7
0.01067	0.080789	0.00122	0.897	2	.	491	17	499	7	501	7
0.00981	0.08246	0.00096	0.771	1.8	.	502	20	509	6	511	6
0.01029	0.079512	0.00128	0.973	1.7	.	485	8	492	6	493	8
0.00969	0.080396	0.0011	0.889	1	.	494	15	498	6	498	7
0.0097	0.076819	0.00118	0.946	0.2	.	476	11	477	6	477	7
0.00958	0.077253	0.00108	0.879	0.1	.	479	16	480	6	480	6
0.01352	0.073331	0.0017	0.972	-0.1	.	457	12	456	9	456	10
0.01202	0.079072	0.00144	0.940	-0.1	.	491	14	491	8	491	9
0.01143	0.080037	0.00135	0.934	-0.2	.	497	14	497	7	496	8
0.0098	0.079591	0.00116	0.93	-0.3	.	495	12	494	6	494	7
0.01148	0.077524	0.00137	0.937	-0.6	.	484	14	482	7	481	8
0.01477	0.074175	0.00188	0.986	-0.8	.	465	9	462	10	461	11
0.02468	0.081384	0.00149	0.477	-0.8	.	508	72	505	15	504	9
0.01076	0.076221	0.00128	0.932	-1.1	.	479	14	474	7	474	8
0.01448	0.075434	0.00182	0.983	-1.7	.	477	10	470	9	469	11
0.01409	0.075091	0.00177	0.981	-2.1	.	476	10	468	9	467	11
0.01453	0.07534	0.00182	0.978	-2.6	.	481	11	470	9	468	11
0.0145	0.074158	0.00182	0.979	-2.6	.	473	11	463	9	461	11
0.01572	0.080225	0.0011	0.552	-2.6	.	510	43	500	10	497	7
0.01572	0.080225	0.0011	0.552	-2.6	.	510	43	500	10	497	7
0.02382	0.080273	0.00174	0.579	-2.9	.	512	65	500	15	498	10
0.01493	0.073778	0.00188	0.979	-3.3	.	474	11	461	10	459	11
0.01018	0.079122	0.00113	0.882	-3.7	.	509	16	494	6	491	7
0.00748	0.076787	0.00087	0.921	-4.1	.	497	10	480	5	477	5
0.03381	0.077567	0.0015	0.351	-4.1	.	501	109	485	21	482	9
0.0074	0.073951	0.00089	0.935	-4.4	.	480	10	463	5	460	5
0.01554	0.077625	0.00194	0.988	-5.3	-1.4	508	8	486	10	482	12
0.0085	0.077786	0.00102	0.947	-5.4	-1	510	10	488	5	483	6
0.01005	0.079639	0.00122	0.965	-6.1	-2	525	9	499	6	494	7
0.00968	0.07841	0.00107	0.881	-6.2	.	518	16	492	6	487	6
0.00946	0.07786	0.00104	0.878	-8.2	-1.5	525	16	491	6	483	6
0.07976	0.226339	0.00626	0.972	-8.3	-5.5	1423	12	1357	21	1315	33
0.00844	0.076098	0.00098	0.923	-8.3	-3.1	514	11	480	5	473	6
0.03566	0.080887	0.00127	0.287	-8.7	.	547	109	510	22	501	8
0.00995	0.084986	0.00116	0.954	-8.8	-5.1	574	9	535	6	526	7
0.0099	0.076993	0.00106	0.85	-8.8	-1	522	18	486	6	478	6
0.01383	0.073763	0.0017	0.971	-9.5	-3.8	505	12	467	9	459	10
0.01643	0.0768	0.002	0.969	-9.8	-3.5	527	14	486	10	477	12
0.01076	0.081158	0.0013	0.940	9	2.1	463	13	496	7	503	8
0.0093	0.079349	0.00117	0.970	8.1	3.1	457	8	486	6	492	7
0.01201	0.08047	0.00145	0.935	7.4	.	466	15	493	8	499	9

		ppm						*Ratios*
sample	name	U	^{206}Pb	$^{206}Pb_c$(%)	206/204	$^{207}Pb/^{206}Pb^*$	1SE	$^{207}Pb/^{235}U^*$
14BD_3(	14_30_64	864	64.4	5.00E-01	3918	0.05657	0.00031	0.63679
14BD_3(	14_30_109	390	30.7	0.00E+00	14351	0.05656	0.00041	0.6
14BD_3(	14_30_66	1362	108.1	1.50E+00	941	0.05673	0.0006	0.63871
14BD_3(	14_30_111	427	33.3	0.00E+00	53724	0.05649	0.00042	0.62343
14BD_3(	14_30_79	1816	143.9	1.00E+00	1442	0.05677	0.00038	0.6391
14BD_3(	14_30_110	291	22.5	0.00E+00	11920	0.05641	0.00041	0.6158
14BD_3(	14_30_77	1242	99.3	0.00E+00	38728	0.05604	0.00033	0.63968
14BD_3(	14_30_68	1534	121	0.00E+00	52314	0.05606	0.00033	0.63001
14BD_3(	14_30_78	2039	160.7	0.00E+00	54026	0.05614	0.00033	0.62886
14BD_3(	14_30_23	623	39.4	0.00E+00	15916	0.05638	0.00024	0.52103
14BD_3(	14_30_86	1383	112.7	0.00E+00	7270	0.05993	0.00049	0.67137
14BD_3(	14_30_101	312	24.2	0.00E+00	8719	0.05944	0.00044	0.6
14BD_3(	14_30_108	448	35.7	0.00E+00	4668	0.06025	0.00049	0.67701
14BD_3(	14_30_56	331	30.3	0.00E+00	897	0.07214	0.00062	0.99525
14BD_3(	14_30_99	1324	93.8	0.00E+00	1619	0.06436	0.0005	0.63463
14BD_3(	14_30_123	339	26.5	0.00E+00	1669	0.06755	0.00063	0.75603
14BD_3(	14_30_58	1014	86.1	0.00E+00	916	0.07194	0.00093	0.92133
14BD_3(	14_30_119	174	13.9	0.00E+00	1718	0.0695	0.00113	0.79189
14BD_3(	14_30_87	1271	105.2	0.00E+00	1050	0.07007	0.00085	0.80161
14BD_3(	14_30_53	647	48.4	0.00E+00	773	0.07419	0.00107	0.82583
14BD_3(	14_30_27	967	70.6	0.00E+00	795	0.07363	0.00073	0.77919
14BD_3(	14_30_73	1655	133.6	0.00E+00	689	0.07716	0.00109	0.88486
14BD_3(	14_30_24	455	33.3	0.00E+00	698	0.07678	0.00085	0.8
14BD_3(	14_30_107	384	31.2	0.00E+00	626	0.08072	0.00125	0.92332
14BD_3(	14_30_55	468	34.9	0.00E+00	513	0.08194	0.00052	0.9
14BD_3(	14_30_118	158	13.7	0.00E+00	575	0.09228	0.00289	1.1373
14BD_3(	14_30_71	1554	160.6	0.00E+00	411	0.10927	0.00636	1.65454
14BD_3(	14_30_28	546	40.7	0.00E+00	402	0.09021	0.0009	0.98753
14BD_3(	14_30_70	2097	167.4	0.00E+00	367	0.09275	0.00119	1.05467
14BD_3(	14_30_33	737	59.2	0.00E+00	478	0.10069	0.00447	1.2
14BD_3(	14_30_34	590	43.2	0.00E+00	327	0.09683	0.00151	1.03922
14BD_3(	14_30_29	1090	90.2	0.00E+00	254	0.10963	0.00208	1.3286
14BD_3(	14_30_117	466	40.4	0.00E+00	234	0.11885	0.00401	1.4558
14BD_3(	14_30_61	582	45.8	0.00E+00	219	0.11992	0.00226	1.4288
14BD_3(	14_30_72	1279	107.5	0.00E+00	212	0.12148	0.00262	1.45804
14BD_3(	14_30_44	381	32	0.00E+00	175	0.13163	0.00215	1.64237
14BD_3(	14_30_105	683	55	0.00E+00	200	0.12345	0.00276	1.38587
14BD_3(	14_30_102	1187	100	0.00E+00	186	0.13162	0.00347	1.54422
14BD_3(	14_30_50	507	41.2	0.00E+00	136	0.15558	0.00293	1.88002
14BD_3(	14_30_46	440	39.2	0.00E+00	100	0.19243	0.00465	2.6
14BD_3(	14_30_122	138	14.9	0.00E+00	80	0.23642	0.00877	3.63352
14BD_3(	14_30_103	763	110.3	0.00E+00	40	0.42049	0.01981	8.78955
14BD_3(	14_30_104	478	51.9	0.00E+00	67	0.26633	0.01066	4.07248
14BD_3(	14_30_30	599	53.6	0.00E+00	87	0.21921	0.00813	2.84644

				Discordance				*Ages*			
1SE	$^{206}Pb/^{238}U^{*}$	1SE	Rho	Central	Minim	207/206	1σ	207/235	1σ	206/238	1σ
0.00945	0.081639	0.00113	0.929	6.8	0.6	475	12	500	6	506	7
0.00989	0.080682	0.00112	0.886	5.6	.	475	15	496	6	500	7
0.01302	0.08166	0.00142	0.855	5.4	.	481	22	502	8	506	8
0.01004	0.08004	0.00114	0.887	5.4	.	472	16	492	6	496	7
0.01206	0.08165	0.00144	0.936	5	.	483	14	502	7	506	9
0.00979	0.079173	0.00112	0.89	5	.	469	15	487	6	491	7
0.01126	0.082787	0.00137	0.942	13.5	6	454	13	502	7	513	8
0.01106	0.0815	0.00135	0.942	11.5	4.2	455	13	496	7	505	8
0.01142	0.081246	0.0014	0.946	10.4	3.1	458	13	495	7	504	8
0.01393	0.067031	0.00177	0.988	-10.8	-6.5	467	9	426	9	418	11
0.01367	0.081247	0.00152	0.917	-16.9	-11	601	18	522	8	504	9
0.0099	0.078685	0.00106	0.874	-16.9	-11	583	16	505	6	488	6
0.01102	0.08149	0.00115	0.867	-18.3	-13	613	17	525	7	505	7
0.02509	0.100062	0.00237	0.939	-39.7	-37	990	17	701	13	615	14
0.01102	0.071521	0.00111	0.894	-42.3	-39	753	15	499	7	445	7
0.01373	0.081168	0.00127	0.859	-42.8	-39	855	18	572	8	503	8
0.01803	0.092889	0.00137	0.753	-43.7	-40	984	25	663	10	573	8
0.01812	0.082632	0.00133	0.701	-45.7	-41	914	34	592	10	512	8
0.01573	0.082972	0.00128	0.785	-46.6	-43	930	25	598	9	514	8
0.01907	0.080731	0.00146	0.781	-54.2	-51	1047	28	611	11	500	9
0.02179	0.07675	0.00201	0.936	-55.8	-53	1031	19	585	12	477	12
0.02053	0.08317	0.00153	0.794	-56.4	-53	1125	27	644	11	515	9
0.02227	0.07825	0.00192	0.912	-58.6	-56	1116	21	613	12	486	11
0.01945	0.082957	0.00119	0.679	-60	-57	1215	29	664	10	514	7
0.01616	0.080376	0.00134	0.935	-62.2	-61	1244	12	656	9	498	8
0.0405	0.089388	0.00152	0.479	-65.2	-61	1473	60	771	19	552	9
0.11734	0.109821	0.00445	0.571	-65.6	-59	1787	101	991	45	672	26
0.02683	0.079398	0.00201	0.93	-68	-67	1430	19	697	14	493	12
0.02215	0.082473	0.00137	0.79	-68.1	-67	1483	23	731	11	511	8
0.06105	0.085666	0.0022	0.501	-70.4	-66	1637	81	796	28	530	13
0.0318	0.077835	0.00205	0.859	-71.7	-70	1564	29	724	16	483	12
0.0434	0.087896	0.00234	0.815	-72.6	-71	1793	34	858	19	543	14
0.0545	0.088837	0.00144	0.434	-74.7	-72	1939	61	912	23	549	9
0.03565	0.086413	0.00141	0.654	-75.6	-74	1955	32	901	15	534	8
0.04049	0.087051	0.00152	0.628	-75.8	-74	1978	36	913	17	538	9
0.03661	0.090496	0.00137	0.680	-76.8	-76	2120	27	987	14	558	8
0.04	0.081419	0.00149	0.634	-77.7	-76	2007	39	883	17	505	9
0.04644	0.085094	0.00123	0.481	-78.1	-77	2120	43	948	19	526	7
0.04836	0.087639	0.00153	0.68	-80.7	-80	2408	31	1074	17	542	9
0.07355	0.097624	0.00145	0.524	-81.8	-81	2763	38	1298	21	600	9
0.16981	0.111464	0.00317	0.608	-81.9	-81	3096	57	1557	37	681	18
0.54751	0.151602	0.00618	0.654	-82.3	-81	3984	69	2316	57	910	35
0.18498	0.110902	0.00238	0.473	-83.3	-82	3285	59	1649	37	678	14
0.1357	0.094175	0.00282	0.628	-83.9	-83	2975	58	1368	36	580	17

		ppm						*Ratios*
sample	name	U	^{206}Pb	$^{206}Pb_c$(%)	206/204	$^{207}Pb/^{206}Pb^*$	1SE	$^{207}Pb/^{235}U^*$
15BD_67	15BD_673_75	181	14	0.00E+00	4800	0.05584	0.00055	0.57806
15BD_67	15BD_673_41	188	15.2	0.00E+00	7759	0.05561	0.00039	0.56031
15BD_67	15BD_673_143	769	69.1	0.00E+00	23043	0.05633	0.00027	0.60401
15BD_67	15BD_673_57	64	21.6	0.00E+00	4899	0.09882	0.00055	3.99065
15BD_67	15BD_673_62	35	23.2	0.00E+00	7296	0.18912	0.00142	14.29164
15BD_67	15BD_673_72	520	115	0.00E+00	37745	0.07896	0.00081	2.24764
15BD_67	15BD_673_4	520	119.8	0.00E+00	68484	0.07837	0.00034	2.19664
15BD_67	15BD_673_45	25	9.1	0.00E+00	6797	0.10505	0.00063	4.56029
15BD_67	15BD_673_85	228	17.6	0.00E+00	5124	0.05608	0.00056	0.58327
15BD_67	15BD_673_109	706	173.2	0.00E+00	51882	0.08175	0.00036	2.43426
15BD_67	15BD_673_79	210	42.9	0.00E+00	109849	0.07692	0.0008	2.04418
15BD_67	15BD_673_53	175	34.5	0.00E+00	13188	0.07344	0.00036	1.77048
15BD_67	15BD_673_24	126	42.4	0.00E+00	17964	0.10036	0.00051	4.0
15BD_67	15BD_673_35	254	49.9	0.00E+00	13309	0.07336	0.00035	1.76069
15BD_67	15BD_673_84	254	19.6	0.00E+00	5862	0.05638	0.00057	0.6
15BD_67	15BD_673_156	64	5.1	0.00E+00	1702	0.05556	0.00045	0.5367
15BD_67	15BD_673_90	1047	85.5	0.00E+00	19529	0.05704	0.00056	0.6265
15BD_67	15BD_673_36	137	28.3	0.00E+00	9112	0.0755	0.00037	1.90452
15BD_67	15BD_673_3	354	70.2	0.00E+00	26469	0.07397	0.00032	1.78747
15BD_67	15BD_673_167	190	13.6	0.00E+00	5765	0.05646	0.00031	0.6
15BD_67	15BD_673_32	239	62.6	0.00E+00	18453	0.08579	0.0004	2.71808
15BD_67	15BD_673_22	207	57.6	0.00E+00	17600	0.08913	0.00042	2.98377
15BD_67	15BD_673_111	91	7.9	0.00E+00	3057	0.05673	0.00039	0.60377
15BD_67	15BD_673_67	189	41.5	0.00E+00	31977	0.08042	0.00084	2.26761
15BD_67	15BD_673_131	1034	93.2	0.00E+00	23379	0.05701	0.00026	0.61899
15BD_67	15BD_673_98	49	13.1	0.00E+00	4365	0.09195	0.00109	3.21377
15BD_67	15BD_673_149	510	119.3	0.00E+00	51872	0.07971	0.00042	2.20916
15BD_67	15BD_673_103	118	34.6	0.00E+00	13312	0.0931	0.00045	3.30135
15BD_67	15BD_673_129	230	43.4	0.00E+00	15595	0.07244	0.00033	1.65427
15BD_67	15BD_673_10	88	28.4	0.00E+00	6217	0.09935	0.00049	3.8156
15BD_67	15BD_673_120	908	84	0.00E+00	36547	0.05761	0.00024	0.64728
15BD_67	15BD_673_136	119	23.5	0.00E+00	8834	0.07435	0.00039	1.77654
15BD_67	15BD_673_164	106	19.5	0.00E+00	12078	0.07764	0.00041	2.01965
15BD_67	15BD_673_89	845	74.6	0.00E+00	10795	0.05839	0.00059	0.69368
15BD_67	15BD_673_133	87	7.4	0.00E+00	2577	0.05666	0.00034	0.5874
15BD_67	15BD_673_69	100	19.7	0.00E+00	15134	0.07714	0.00083	1.9735
15BD_67	15BD_673_21	59	11.2	0.00E+00	6451	0.07348	0.00043	1.70018
15BD_67	15BD_673_115	115	32.1	0.00E+00	8673	0.09122	0.00041	3.08071
15BD_67	15BD_673_86	130	10.4	0.00E+00	5298	0.05732	0.00068	0.62045
15BD_67	15BD_673_124	197	63.6	0.00E+00	27360	0.10138	0.00049	3.9372
15BD_67	15BD_673_68	95	34.1	0.00E+00	10416	0.11339	0.00139	5.03011
15BD_67	15BD_673_56	91	27.9	0.00E+00	8047	0.09756	0.00058	3.59744
15BD_67	15BD_673_150	169	37	0.00E+00	14268	0.07842	0.00041	2.0466
15BD_67	15BD_673_157	109	8.6	0.00E+00	4240	0.05579	0.00039	0.52645
15BD_67	15BD_673_153	175	15.3	0.00E+00	8802	0.0571	0.00032	0.60241
15BD_67	15BD_673_139	52	10.2	0.00E+00	144142	0.07496	0.00046	1.78223
15BD_67	15BD_673_152	118	22.4	0.00E+00	6851	0.0732	0.0004	1.65429
15BD_67	15BD_673_74	591	50.3	0.00E+00	6503	0.05806	0.00055	0.7

				Discordance		*Ages*					
1SE	$^{206}Pb/^{238}U^{*}$	1SE	Rho	Central	Minim	207/206	1σ	207/235	1σ	206/238	1σ
0.00841	0.075081	0.0008	0.735	4.8	.	446	22	463	5	467	5
0.00815	0.073078	0.00093	0.878	4.2	.	437	15	452	5	455	6
0.01234	0.077774	0.00155	0.972	3.9	.	465	10	480	8	483	9
0.07264	0.292881	0.00508	0.953	3.8	.	1602	10	1632	15	1656	25
0.40437	0.54807	0.01495	0.964	3.7	.	2735	13	2769	27	2817	62
0.03697	0.206456	0.00265	0.78	3.6	.	1171	20	1196	12	1210	14
0.03044	0.203295	0.00268	0.951	3.5	0.3	1156	8	1180	10	1193	14
0.0878	0.314835	0.00577	0.951	3.3	.	1715	10	1742	16	1764	28
0.00871	0.075434	0.00084	0.745	3	.	455	21	467	6	469	5
0.04402	0.215965	0.00379	0.970	1.9	.	1240	8	1253	13	1261	20
0.03284	0.192752	0.00237	0.765	1.7	.	1119	20	1130	11	1136	13
0.02779	0.174842	0.00261	0.950	1.3	.	1026	10	1035	10	1039	14
0.06617	0.290873	0.00455	0.952	1.1	.	1631	9	1639	13	1646	23
0.0262	0.174069	0.00246	0.948	1.1	.	1024	9	1031	10	1034	13
0.00937	0.075445	0.00093	0.774	0.3	.	467	21	469	6	469	6
0.01132	0.070053	0.00136	0.922	0.3	.	435	17	436	7	436	8
0.01042	0.079655	0.00107	0.806	0.2	.	493	20	494	7	494	6
0.02821	0.18295	0.00256	0.945	0.1	.	1082	10	1083	10	1083	14
0.02433	0.175255	0.00226	0.949	0	.	1041	9	1041	9	1041	12
0.00827	0.075746	0.00098	0.921	0	.	471	12	471	5	471	6
0.04346	0.229787	0.00351	0.956	0	.	1333	9	1333	12	1333	18
0.04432	0.242807	0.00342	0.949	-0.4	.	1407	9	1403	11	1401	18
0.00967	0.077186	0.00111	0.901	-0.4	.	481	16	480	6	479	7
0.03814	0.204507	0.00269	0.782	-0.7	.	1207	20	1202	12	1199	14
0.01158	0.078741	0.00143	0.970	-0.7	.	492	9	489	7	489	9
0.06013	0.253493	0.00367	0.775	-0.8	.	1466	22	1460	14	1456	19
0.04756	0.201012	0.0042	0.970	-0.8	.	1190	10	1184	15	1181	23
0.06003	0.257173	0.00451	0.964	-1.1	.	1490	9	1481	14	1475	23
0.02929	0.165616	0.00283	0.966	-1.1	.	998	9	991	11	988	16
0.05853	0.27854	0.00404	0.946	-2	.	1612	9	1596	12	1584	20
0.01044	0.081482	0.00127	0.967	-2.1	.	515	9	507	6	505	8
0.03313	0.173299	0.0031	0.960	-2.1	.	1051	10	1037	12	1030	17
0.03073	0.188671	0.00269	0.937	-2.2	.	1138	10	1122	10	1114	15
0.01124	0.086165	0.0011	0.784	-2.2	.	544	21	535	7	533	6
0.00994	0.07519	0.00119	0.935	-2.4	.	478	12	469	6	467	7
0.03368	0.185541	0.00245	0.774	-2.7	.	1125	22	1107	12	1097	13
0.02715	0.167821	0.0025	0.931	-2.8	.	1027	12	1009	10	1000	14
0.05643	0.244946	0.00435	0.969	-3	-1	1451	9	1428	14	1412	23
0.01046	0.078506	0.00095	0.715	-3.4	.	504	25	490	7	487	6
0.07888	0.281676	0.00548	0.97	-3.4	-1.5	1649	9	1621	16	1600	28
0.10495	0.321728	0.00543	0.810	-3.5	.	1854	21	1824	18	1798	27
0.06428	0.267444	0.00451	0.943	-3.6	-1.1	1578	11	1549	14	1528	23
0.04349	0.189288	0.0039	0.970	-3.8	-1.1	1157	10	1131	14	1118	21
0.0107	0.068444	0.0013	0.938	-4	.	444	16	429	7	427	8
0.01204	0.076521	0.00147	0.960	-4.2	.	495	12	479	8	475	9
0.03597	0.172435	0.00332	0.954	-4.3	-1	1067	12	1039	13	1026	18
0.03423	0.163905	0.00327	0.965	-4.3	-1.3	1020	11	991	13	978	18
0.00956	0.082196	0.0009	0.754	-4.5	.	532	20	513	6	509	5

		ppm						*Ratios*
sample	name	U	^{206}Pb	$^{206}Pb_c$(%)	206/204	$^{207}Pb/^{206}Pb^*$	1SE	$^{207}Pb/^{235}U^*$
15BD_67	15BD_673_125	211	67.2	0.00E+00	24404	0.1007	0.00049	3.8
15BD_67	15BD_673_50	569	53	0.00E+00	14132	0.05663	0.00026	0.65662
15BD_67	15BD_673_77	782	61.5	0.00E+00	16617	0.05558	0.00053	0.58262
15BD_67	15BD_673_14	137	11.3	0.00E+00	8351	0.05547	0.00032	0.57251
15BD_67	15BD_673_55	106	34.1	0.00E+00	9399	0.09288	0.0005	3.59086
15BD_67	15BD_673_51	68	14.1	0.00E+00	5699	0.07301	0.00048	1.85269
15BD_67	15BD_673_13	163	14.4	0.00E+00	4232	0.05621	0.00033	0.61665
15BD_67	15BD_673_93	438	99.2	0.00E+00	60486	0.07906	0.00085	2.33761
15BD_67	15BD_673_97	301	25.2	0.00E+00	9247	0.05671	0.00059	0.64322
15BD_67	15BD_673_66	866	74.9	0.00E+00	34912	0.05696	0.00052	0.65121
15BD_67	15BD_673_119	95	17.4	0.00E+00	7239	0.07315	0.00037	1.62865
15BD_67	15BD_673_135	111	8.9	0.00E+00	4487	0.05644	0.00037	0.55442
15BD_67	15BD_673_155	1207	101.2	0.00E+00	27162	0.0567	0.00028	0.56498
15BD_67	15BD_673_123	149	89.4	0.00E+00	27710	0.19598	0.00143	13.65744
15BD_67	15BD_673_132	218	39.5	0.00E+00	15040	0.07293	0.00036	1.59236
15BD_67	15BD_673_147	270	23.7	0.00E+00	4944	0.05745	0.00029	0.60495
15BD_67	15BD_673_38	346	64.8	0.00E+00	17456	0.07483	0.00037	1.71922
15BD_67	15BD_673_101	270	84.4	0.00E+00	32006	0.10894	0.00136	4.40234
15BD_67	15BD_673_106	31	19.9	0.00E+00	7218	0.22473	0.00175	17.01333
15BD_67	15BD_673_146	138	39.3	0.00E+00	13792	0.09454	0.00051	3.18877
15BD_67	15BD_673_145	138	39.3	0.00E+00	13792	0.09454	0.00051	3.18877
15BD_67	15BD_673_82	131	70.4	0.00E+00	29342	0.18137	0.00313	11.67029
15BD_67	15BD_673_142	172	13.8	0.00E+00	5363	0.05672	0.00035	0.54971
15BD_67	15BD_673_166	109	50.7	0.00E+00	29669	0.1741	0.0013	10.73423
15BD_67	15BD_673_83	181	53.1	0.00E+00	24356	0.10536	0.00126	3.96283
15BD_67	15BD_673_118	267	23	0.00E+00	25365	0.05798	0.0003	0.60859
15BD_67	15BD_673_134	313	24.2	0.00E+00	8973	0.05696	0.0003	0.53795
15BD_67	15BD_673_137	295	23.5	0.00E+00	6347	0.0573	0.00028	0.55605
15BD_67	15BD_673_138	230	68.7	0.00E+00	13965	0.106	0.00058	3.78686
15BD_67	15BD_673_70	163	32	0.00E+00	1509	0.08402	0.00111	2.13825
15BD_67	15BD_673_46	246	22.9	0.00E+00	5407	0.06049	0.00033	0.6992
15BD_67	15BD_673_2	415	123.1	0.00E+00	45024	0.10692	0.00052	3.79143
15BD_67	15BD_673_58	293	25.6	0.00E+00	10073	0.0597	0.00044	0.65228
15BD_67	15BD_673_44	215	32.6	0.00E+00	9166	0.07204	0.00037	1.34987
15BD_67	15BD_673_95	160	41.1	0.00E+00	15332	0.10315	0.00127	3.46385
15BD_67	15BD_673_33	289	47	0.00E+00	12030	0.07503	0.00038	1.50606
15BD_67	15BD_673_42	279	60.9	0.00E+00	17483	0.08864	0.00044	2.35945
15BD_67	15BD_673_122	263	28.3	0.00E+00	10742	0.06438	0.0004	0.86041
15BD_67	15BD_673_11	372	34.9	0.00E+00	11320	0.06189	0.0003	0.72064
15BD_67	15BD_673_91	478	56.3	0.00E+00	13445	0.06884	0.00072	1.08038
15BD_67	15BD_673_78	281	85.6	0.00E+00	19060	0.12442	0.00165	4.79616
15BD_67	15BD_673_20	211	45.5	0.00E+00	11101	0.09246	0.00061	2.45681
15BD_67	15BD_673_128	27	2.3	0.00E+00	1501	0.06029	0.00072	0.61846
15BD_67	15BD_673_99	160	12.5	0.00E+00	4175	0.06099	0.00122	0.64902
15BD_67	15BD_673_59	123	31.1	0.00E+00	578046	0.10417	0.00062	3.19565
15BD_67	15BD_673_126	692	55.5	0.00E+00	4981	0.05958	0.00033	0.57983
15BD_67	15BD_673_30	200	15.9	0.00E+00	5306	0.05996	0.00038	0.59636
15BD_67	15BD_673_92	456	33.9	0.00E+00	4620	0.06055	0.00066	0.61363

				Discordance				*Ages*			
1SE	$^{206}Pb/^{238}U^{*}$	1SE	Rho	Central	Minim	207/206	1σ	207/235	1σ	206/238	1σ
0.07767	0.275967	0.00543	0.971	-4.5	-2.6	1637	9	1599	16	1571	27
0.01089	0.084088	0.00134	0.959	9.4	3.5	477	10	513	7	520	8
0.01048	0.076029	0.00116	0.850	8.8	.	436	21	466	7	472	7
0.0072	0.074852	0.00084	0.892	8.2	1.6	431	12	460	5	465	5
0.06411	0.280394	0.00477	0.953	8.2	3.9	1485	10	1548	14	1593	24
0.0305	0.184044	0.00278	0.917	8	3.6	1014	12	1064	11	1089	15
0.00779	0.079569	0.00089	0.883	7.4	1	461	13	488	5	494	5
0.04078	0.214444	0.00295	0.79	7.4	2.4	1174	21	1224	12	1252	16
0.01047	0.082262	0.00104	0.773	6.4	.	480	22	504	6	510	6
0.0104	0.082916	0.00108	0.818	5	.	490	20	509	6	514	6
0.02676	0.161482	0.00253	0.952	-5.6	-2.8	1018	10	981	10	965	14
0.00987	0.07125	0.00118	0.93	-5.7	.	470	13	448	6	444	7
0.01208	0.072263	0.0015	0.973	-6.5	-1.3	480	10	455	8	450	9
0.40431	0.505424	0.0145	0.969	-6.8	-4.8	2793	12	2726	28	2637	62
0.02857	0.158355	0.00273	0.961	-6.8	-4.1	1012	9	967	11	948	15
0.01325	0.07637	0.00163	0.973	-7	-2	509	11	480	8	474	10
0.026	0.166635	0.00238	0.944	-7.1	-4.5	1064	10	1016	10	994	13
0.08829	0.293098	0.0046	0.783	-7.9	-4	1782	22	1713	17	1657	23
0.5219	0.549071	0.01629	0.967	-7.9	-5.8	3015	13	2936	29	2821	68
0.07014	0.244639	0.00522	0.97	-7.9	-5.8	1519	10	1454	17	1411	27
0.07014	0.244639	0.00522	0.970	-7.9	-5.8	1519	10	1454	17	1411	27
0.3125	0.466687	0.00956	0.765	-8.9	-4.6	2665	27	2578	25	2469	42
0.0102	0.070292	0.00123	0.943	-9.2	-2.8	481	13	445	7	438	7
0.26855	0.447177	0.01068	0.955	-9.9	-7.8	2597	12	2500	23	2383	48
0.07686	0.272795	0.00416	0.787	-10.8	-7.1	1721	21	1627	16	1555	21
0.01061	0.076127	0.00127	0.954	-11	-6.2	529	11	483	7	473	8
0.00917	0.068494	0.00111	0.951	-13.3	-8.2	490	11	437	6	427	7
0.00955	0.070377	0.00116	0.960	-13.3	-8.8	503	10	449	6	438	7
0.08446	0.259097	0.0056	0.970	-15.9	-14	1732	10	1590	18	1485	29
0.03818	0.184568	0.00221	0.672	-16.9	-13	1293	25	1161	12	1092	12
0.01064	0.083827	0.00119	0.935	-17.2	-13	621	11	538	6	519	7
0.06216	0.257183	0.00403	0.955	-17.4	-16	1748	8	1591	13	1475	21
0.01036	0.079247	0.00112	0.887	-17.7	-12	593	16	510	6	492	7
0.02282	0.135906	0.00219	0.952	-17.9	-15	987	10	868	10	821	12
0.06557	0.243548	0.0035	0.760	-18.3	-15	1682	22	1519	15	1405	18
0.02643	0.145586	0.00245	0.957	-19.3	-17	1069	10	933	11	876	14
0.0377	0.193049	0.00293	0.95	-20.2	-18	1396	9	1230	11	1138	16
0.01718	0.096925	0.00184	0.951	-21.9	-18	754	13	630	9	596	11
0.00907	0.084442	0.00098	0.922	-23	-20	670	10	551	5	523	6
0.02036	0.113822	0.00178	0.830	-23.5	-19	894	20	744	10	695	10
0.09357	0.279581	0.004	0.734	-24.1	-21	2021	23	1784	16	1589	20
0.05545	0.192706	0.00416	0.957	-25.2	-23	1477	13	1259	16	1136	22
0.01237	0.074396	0.00119	0.802	-25.6	-18	614	25	489	8	463	7
0.01512	0.077174	0.00092	0.514	-25.9	-12	639	41	508	9	479	6
0.05858	0.222501	0.00386	0.946	-26.2	-25	1700	11	1456	14	1295	20
0.0112	0.07058	0.00131	0.958	-26.2	-22	588	12	464	7	440	8
0.00911	0.072131	0.001	0.91	-26.3	-22	602	13	475	6	449	6
0.01033	0.073499	0.00095	0.766	-27.6	-21	623	22	486	6	457	6

		ppm						*Ratios*
sample	name	U	^{206}Pb	$^{206}Pb_c$(%)	206/204	$^{207}Pb/^{206}Pb^*$	1SE	$^{207}Pb/^{235}U^*$
15BD_67	15BD_673_15	153	12.7	0.00E+00	3050	0.06142	0.00061	0.6
15BD_67	15BD_673_121	189	37.4	0.00E+00	11197	0.09174	0.0005	2.24602
15BD_67	15BD_673_107	402	32.8	0.00E+00	4386	0.06187	0.00072	0.6237
15BD_67	15BD_673_5	276	24	0.00E+00	3757	0.06344	0.0009	0.68742
15BD_67	15BD_673_27	332	38.8	0.00E+00	4962	0.0709	0.00039	1.02553
15BD_67	15BD_673_130	141	11.2	0.00E+00	4506	0.06162	0.00047	0.59948
15BD_67	15BD_673_94	446	51.4	0.00E+00	7204	0.07462	0.00097	1.18705
15BD_67	15BD_673_18	321	25.2	0.00E+00	5850	0.06194	0.00044	0.60406
15BD_67	15BD_673_65	208	29.5	0.00E+00	5059	0.07944	0.00082	1.40199
15BD_67	15BD_673_105	200	26.5	0.00E+00	11723	0.07694	0.00059	1.27039
15BD_67	15BD_673_87	466	103.4	0.00E+00	14223	0.11504	0.00182	3.36821
15BD_67	15BD_673_26	129	26.2	0.00E+00	6913	0.10462	0.00101	2.72463
15BD_67	15BD_673_1	485	92.9	0.00E+00	4610	0.09882	0.00051	2.30104
15BD_67	15BD_673_31	516	64.1	0.00E+00	1445	0.07605	0.00039	1.16401
15BD_67	15BD_673_23	448	64.3	0.00E+00	1047	0.08345	0.00085	1.49043
15BD_67	15BD_673_43	497	78.5	0.00E+00	12912	0.08842	0.0005	1.72159
15BD_67	15BD_673_17	16	2	0.00E+00	847	0.08271	0.00414	1.41949
15BD_67	15BD_673_144	256	20.1	0.00E+00	1426	0.06525	0.00054	0.62061
15BD_67	15BD_673_88	302	40.3	0.00E+00	1495	0.0897	0.00115	1.60317
15BD_67	15BD_673_148	430	36.6	0.00E+00	3291	0.06807	0.0004	0.6964
15BD_67	15BD_673_47	102	26.3	0.00E+00	13381	0.16262	0.00157	5.23726
15BD_67	15BD_673_40	125	32.3	0.00E+00	6967	0.16972	0.00193	5.56115
15BD_67	15BD_673_116	525	68.6	0.00E+00	12031	0.09191	0.00053	1.5
15BD_67	15BD_673_108	116	9.9	0.00E+00	1546	0.07698	0.00152	0.82253
15BD_67	15BD_673_61	35	3	0.00E+00	794	0.05513	0.00067	0.59806
15BD_67	15BD_673_160	192	14	0.00E+00	4544	0.06	0.00051	0.6353
15BD_67	15BD_673_163	232	25.1	0.00E+00	10539	0.06976	0.00037	1.09722
15BD_67	15BD_673_165	232	33.3	0.00E+00	10630	0.07984	0.00044	1.6478
15BD_67	15BD_673_168	1154	85.3	0.00E+00	4117	0.05979	0.00027	0.64468
14BD_31	14BD_31_127	701	51.7	0.00E+00	17835	0.05627	0.0005	0.60573
14BD_31	14BD_31_43	394	74	0.00E+00	79518	0.0765	0.00041	2.07431
14BD_31	14BD_31_91	603	110.2	0.00E+00	44761	0.07428	0.00066	1.89091
14BD_31	14BD_31_42	122	23.3	0.00E+00	10932	0.07751	0.00043	2.14222
14BD_31	14BD_31_66	156	24.5	0.00E+00	13820	0.07494	0.00034	1.93818
14BD_31	14BD_31_86	540	41.2	0.00E+00	26643	0.05632	0.00047	0.60317
14BD_31	14BD_31_5	333	61	0.00E+00	19144	0.07577	0.00037	1.98914
14BD_31	14BD_31_137	494	91.8	0.00E+00	28348	0.07508	0.00033	1.9354
14BD_31	14BD_31_134	816	65.2	0.00E+00	35517	0.05696	0.00023	0.64143
14BD_31	14BD_31_13	317	62.8	0.00E+00	27810	0.07871	0.00039	2.21828
14BD_31	14BD_31_9	322	58	0.00E+00	26600	0.07526	0.00036	1.9
14BD_31	14BD_31_88	226	15.5	0.00E+00	6592	0.05535	0.00049	0.53611
14BD_31	14BD_31_162	302	23.3	0.00E+00	9272	0.05673	0.00028	0.6225
14BD_31	14BD_31_142	410	30.7	0.00E+00	13028	0.05632	0.00026	0.59557
14BD_31	14BD_31_169	289	55.8	0.00E+00	72250	0.07703	0.00036	2.07225
14BD_31	14BD_31_84	1147	268.7	0.00E+00	227123	0.08484	0.00079	2.70677
14BD_31	14BD_31_54	141	22.3	0.00E+00	9718	0.07582	0.00035	1.96824
14BD_31	14BD_31_114	466	32.6	0.00E+00	57669	0.05589	0.00049	0.56648

				Discordance				*Ages*			
1SE	$^{206}Pb/^{238}U^{*}$	1SE	Rho	Central	Minim	207/206	1σ	207/235	1σ	206/238	1σ
0.00966	0.074819	0.00087	0.759	-29.9	-25	654	20	498	6	465	5
0.0442	0.17757	0.00336	0.961	-30.2	-29	1462	10	1196	14	1054	18
0.01165	0.073117	0.00107	0.783	-33.2	-27	670	24	492	7	455	6
0.01245	0.078592	0.00088	0.619	-33.8	-27	723	29	531	7	488	5
0.01589	0.1049	0.00152	0.936	-34.3	-32	955	11	717	8	643	9
0.01062	0.070561	0.00113	0.902	-34.6	-31	661	15	477	7	440	7
0.02788	0.115375	0.00226	0.833	-35.3	-31	1058	25	795	13	704	13
0.00953	0.070729	0.001	0.895	-35.6	-32	672	14	480	6	441	6
0.03212	0.127994	0.00262	0.892	-36.5	-33	1183	20	890	14	776	15
0.02379	0.119756	0.00204	0.911	-36.9	-34	1120	15	833	11	729	12
0.07191	0.212342	0.00304	0.671	-37.3	-34	1881	27	1497	17	1241	16
0.09192	0.188891	0.00611	0.958	-37.7	-35	1708	17	1335	25	1115	33
0.03875	0.168872	0.00271	0.952	-40.1	-39	1602	9	1213	12	1006	15
0.02502	0.111003	0.00232	0.971	-40.1	-38	1096	10	784	12	679	13
0.03201	0.129536	0.00245	0.879	-41	-38	1280	20	926	13	785	14
0.03351	0.141215	0.00263	0.957	-41.4	-40	1392	11	1017	13	852	15
0.08814	0.12447	0.00458	0.592	-42.5	-29	1262	94	897	37	756	26
0.01244	0.068987	0.00126	0.912	-46.5	-43	782	17	490	8	430	8
0.03039	0.129625	0.00181	0.736	-47.4	-45	1419	23	971	12	786	10
0.01369	0.074198	0.00139	0.954	-48.7	-47	871	12	537	8	461	8
0.18332	0.233582	0.00786	0.961	-50.3	-49	2483	16	1859	30	1353	41
0.18482	0.23765	0.00742	0.940	-51.1	-49	2555	18	1910	29	1374	39
0.03484	0.116634	0.00267	0.969	-54.3	-53	1465	10	921	14	711	15
0.02041	0.077491	0.00117	0.608	-59.2	-56	1121	38	609	11	481	7
0.01167	0.078673	0.0012	0.782	17.5	4.5	418	27	476	7	488	7
0.00984	0.076788	0.00099	0.833	-21.8	-16	604	18	499	6	477	6
0.02001	0.114075	0.00199	0.957	-25.7	-23	921	11	752	10	696	12
0.02784	0.149685	0.00239	0.946	-26.4	-24	1193	10	989	11	899	13
0.00958	0.078205	0.00111	0.951	-19.3	-16	596	10	505	6	485	7
0.01261	0.078077	0.00147	0.903	4.9	.	463	20	481	8	485	9
0.03496	0.196659	0.00314	0.947	4.8	0.8	1108	11	1140	12	1157	17
0.04058	0.184618	0.0036	0.909	4.5	.	1049	17	1078	14	1092	20
0.036	0.200445	0.00318	0.944	4.2	0.2	1134	11	1163	12	1178	17
0.03654	0.18758	0.00343	0.971	4.2	.	1067	9	1094	13	1108	19
0.01157	0.077675	0.00134	0.9	3.8	.	465	18	479	7	482	8
0.03026	0.190406	0.00274	0.946	3.5	.	1089	9	1112	10	1124	15
0.02007	0.18695	0.00176	0.908	3.5	0.8	1071	9	1093	7	1105	10
0.00563	0.081673	0.00063	0.883	3.4	.	490	9	503	3	506	4
0.03682	0.204406	0.00324	0.955	3.2	.	1165	10	1187	12	1199	17
0.0291	0.186815	0.00266	0.947	2.9	.	1076	9	1095	10	1104	14
0.0104	0.070251	0.00121	0.889	2.8	.	426	20	436	7	438	7
0.00614	0.079582	0.00068	0.864	2.7	.	481	11	491	4	494	4
0.00567	0.0767	0.00064	0.877	2.6	.	465	10	474	4	476	4
0.02371	0.195122	0.00204	0.915	2.6	.	1122	9	1140	8	1149	11
0.06151	0.231399	0.0048	0.913	2.5	.	1312	17	1330	17	1342	25
0.03618	0.188278	0.00335	0.968	2.2	.	1090	9	1105	12	1112	18
0.01147	0.073514	0.00134	0.900	2.2	.	448	19	456	7	457	8

		ppm						*Ratios*
sample	name	U	^{206}Pb	$^{206}Pb_c$(%)	206/204	$^{207}Pb/^{206}Pb^*$	1SE	$^{207}Pb/^{235}U^*$
14BD_3:	14BD_31_187	550	39.1	0.00E+00	13029	0.05578	0.00027	0.55929
14BD_3:	14BD_31_74	524	39.3	0.00E+00	14962	0.05626	0.00047	0.58727
14BD_3:	14BD_31_101	211	61.1	0.00E+00	19923	0.09903	0.001	3.93381
14BD_3:	14BD_31_106	62	10.9	0.00E+00	10145	0.0743	0.0007	1.84446
14BD_3:	14BD_31_148	238	57.9	0.00E+00	21771	0.08763	0.0004	2.92152
14BD_3:	14BD_31_79	471	35.8	0.00E+00	15276	0.05653	0.00048	0.603
14BD_3:	14BD_31_178	202	34.8	0.00E+00	15585	0.07342	0.00035	1.77278
14BD_3:	14BD_31_70	681	119.9	0.00E+00	64194	0.07344	0.00066	1.77318
14BD_3:	14BD_31_100	236	43.2	0.00E+00	12500	0.07567	0.0007	1.9444
14BD_3:	14BD_31_180	222	38.2	0.00E+00	11435	0.07339	0.00035	1.76922
14BD_3:	14BD_31_173	288	21.1	0.00E+00	6371	0.05637	0.00029	0.59006
14BD_3:	14BD_31_51	70	11.1	0.00E+00	8140	0.07621	0.00038	1.97628
14BD_3:	14BD_31_177	586	190.9	0.00E+00	101608	0.10815	0.00055	4.75245
14BD_3:	14BD_31_94	222	42.9	0.00E+00	14707	0.07771	0.00071	2.09046
14BD_3:	14BD_31_111	192	32.3	0.00E+00	12516	0.0733	0.00068	1.75153
14BD_3:	14BD_31_141	160	25.6	0.00E+00	8792	0.07086	0.00036	1.57104
14BD_3:	14BD_31_153	152	27.6	0.00E+00	13488	0.07512	0.00037	1.8903
14BD_3:	14BD_31_50	93	14.3	0.00E+00	15988	0.07568	0.00034	1.93152
14BD_3:	14BD_31_147	345	109.1	0.00E+00	73572	0.10604	0.00052	4.53762
14BD_3:	14BD_31_76	239	42.2	0.00E+00	324693	0.07392	0.00067	1.8
14BD_3:	14BD_31_129	357	65.7	0.00E+00	38493	0.07568	0.00033	1.9
14BD_3:	14BD_31_17	548	138.5	0.00E+00	60452	0.09256	0.00048	3.29667
14BD_3:	14BD_31_31	120	26	0.00E+00	13561	0.08468	0.00045	2.6312
14BD_3:	14BD_31_167	297	61.1	0.00E+00	32397	0.08056	0.00036	2.30027
14BD_3:	14BD_31_47	191	39.7	0.00E+00	14350	0.08286	0.00046	2.48223
14BD_3:	14BD_31_2	223	16.5	0.00E+00	6904	0.05694	0.00032	0.61954
14BD_3:	14BD_31_99	166	30.6	0.00E+00	11556	0.07635	0.00071	1.96661
14BD_3:	14BD_31_87	468	159.9	0.00E+00	48389	0.11276	0.00121	5.14585
14BD_3:	14BD_31_92	95	20.2	0.00E+00	8843	0.08168	0.00077	2.37983
14BD_3:	14BD_31_44	109	26.3	0.00E+00	9743	0.0908	0.00051	3.13029
14BD_3:	14BD_31_80	367	89.2	0.00E+00	38151	0.08836	0.00085	2.9193
14BD_3:	14BD_31_83	222	46.9	0.00E+00	17548	0.08144	0.00075	2.35188
14BD_3:	14BD_31_103	206	41.1	0.00E+00	22791	0.07989	0.00075	2.22798
14BD_3:	14BD_31_133	224	47	0.00E+00	21339	0.08144	0.00036	2.35097
14BD_3:	14BD_31_152	315	79.9	0.00E+00	35356	0.0913	0.00044	3.1626
14BD_3:	14BD_31_37	210	44.1	0.00E+00	20040	0.08358	0.00045	2.51952
14BD_3:	14BD_31_123	144	25.8	0.00E+00	14987	0.07625	0.00075	1.94564
14BD_3:	14BD_31_150	175	26.6	0.00E+00	11690	0.07002	0.00034	1.48469
14BD_3:	14BD_31_32	250	69.9	0.00E+00	32185	0.10037	0.00056	3.94861
14BD_3:	14BD_31_38	181	45.4	0.00E+00	18573	0.09353	0.00051	3.34544
14BD_3:	14BD_31_68	498	99.9	0.00E+00	45211	0.07898	0.00072	2.1507
14BD_3:	14BD_31_158	205	60.3	0.00E+00	27018	0.10163	0.00049	4.0604
14BD_3:	14BD_31_89	141	40.7	0.00E+00	15160	0.09966	0.001	3.9
14BD_3:	14BD_31_117	93	16.6	0.00E+00	8679	0.07616	0.00075	1.92938
14BD_3:	14BD_31_120	228	63.7	0.00E+00	24595	0.10033	0.00104	3.93395
14BD_3:	14BD_31_185	108	31.2	0.00E+00	16533	0.10084	0.00053	3.97799
14BD_3:	14BD_31_104	146	42.3	0.00E+00	14422	0.10184	0.00104	4.06583
14BD_3:	14BD_31_21	116	32.5	0.00E+00	66025	0.10079	0.00056	3.96555

				Discordance		*Ages*					
1SE	$^{206}Pb/^{238}U^{*}$	1SE	Rho	Central	Minim	207/206	1σ	207/235	1σ	206/238	1σ
0.00712	0.072727	0.00086	0.923	2.1	.	443	10	451	5	453	5
0.0111	0.075708	0.00128	0.896	1.8	.	463	19	469	7	470	8
0.09823	0.288113	0.00658	0.914	1.8	.	1606	18	1621	20	1632	33
0.04018	0.180052	0.00354	0.902	1.8	.	1050	18	1061	14	1067	19
0.03159	0.241793	0.00237	0.906	1.7	.	1374	9	1388	8	1396	12
0.01156	0.077363	0.00133	0.895	1.6	.	473	19	479	7	480	8
0.02041	0.175129	0.00184	0.913	1.6	.	1025	9	1036	7	1040	10
0.03716	0.175118	0.00332	0.905	1.5	.	1026	17	1036	14	1040	18
0.04276	0.186356	0.00372	0.908	1.5	.	1086	18	1097	15	1102	20
0.019	0.174838	0.00168	0.893	1.5	.	1025	10	1034	7	1039	9
0.00604	0.075923	0.00068	0.868	1.1	.	467	11	471	4	472	4
0.0371	0.188081	0.00341	0.964	1	.	1101	10	1107	13	1111	18
0.06553	0.3187	0.00408	0.929	1	.	1769	9	1777	12	1783	20
0.04583	0.195095	0.00389	0.908	0.9	.	1140	17	1146	15	1149	21
0.03828	0.173313	0.00343	0.904	0.9	.	1022	18	1028	14	1030	19
0.01548	0.160792	0.00136	0.859	0.9	.	953	10	959	6	961	8
0.02014	0.182512	0.00172	0.884	0.9	.	1072	10	1078	7	1081	9
0.03552	0.185105	0.0033	0.969	0.8	.	1087	9	1092	12	1095	18
0.05516	0.310368	0.00345	0.915	0.7	.	1732	8	1738	10	1743	17
0.03774	0.175859	0.00334	0.902	0.5	.	1039	18	1043	14	1044	18
0.01845	0.184235	0.00157	0.889	0.4	.	1087	9	1089	6	1090	9
0.05763	0.258316	0.00432	0.955	0.2	.	1479	9	1480	14	1481	22
0.0446	0.22537	0.00363	0.95	0.2	.	1308	10	1309	12	1310	19
0.02416	0.207098	0.00196	0.903	0.2	.	1211	9	1212	7	1213	10
0.04304	0.217262	0.00357	0.946	0.1	.	1266	11	1267	13	1267	19
0.00866	0.078907	0.00101	0.917	0	.	489	12	490	5	490	6
0.04291	0.186807	0.00368	0.903	0	.	1104	18	1104	15	1104	20
0.13944	0.330967	0.00824	0.919	-0.1	.	1844	19	1844	23	1843	40
0.05367	0.211311	0.00432	0.907	-0.2	.	1238	18	1237	16	1236	23
0.05624	0.250021	0.00427	0.950	-0.3	.	1443	10	1440	14	1439	22
0.0686	0.239609	0.00513	0.912	-0.5	.	1390	18	1387	18	1385	27
0.05214	0.20945	0.00423	0.911	-0.6	.	1232	17	1228	16	1226	23
0.04996	0.20226	0.00412	0.907	-0.6	.	1194	18	1190	16	1187	22
0.02395	0.209375	0.00192	0.9	-0.6	.	1232	9	1228	7	1225	10
0.0366	0.251242	0.00264	0.909	-0.6	.	1453	9	1448	9	1445	14
0.04319	0.218624	0.00356	0.950	-0.7	.	1283	10	1278	12	1275	19
0.04554	0.185069	0.00393	0.908	-0.7	.	1102	18	1097	16	1095	21
0.01494	0.15378	0.00136	0.879	-0.8	.	929	9	924	6	922	8
0.07305	0.285324	0.00504	0.954	-0.9	.	1631	10	1624	15	1618	25
0.06018	0.259431	0.00445	0.952	-0.9	.	1499	10	1492	14	1487	23
0.04674	0.197496	0.0039	0.909	-0.9	.	1172	17	1165	15	1162	21
0.04768	0.289772	0.0031	0.91	-0.9	.	1654	9	1646	10	1640	15
0.09583	0.282526	0.00637	0.913	-1	.	1618	19	1610	20	1604	32
0.04325	0.183735	0.00371	0.900	-1.2	.	1099	19	1091	15	1087	20
0.10048	0.284371	0.00663	0.913	-1.2	.	1630	19	1621	21	1613	33
0.05071	0.28612	0.00333	0.912	-1.2	.	1640	9	1630	10	1622	17
0.10242	0.289549	0.00666	0.914	-1.3	.	1658	18	1647	21	1639	33
0.07202	0.285345	0.00493	0.951	-1.4	.	1639	10	1627	15	1618	25

		ppm						*Ratios*
sample	name	U	^{206}Pb	$^{206}Pb_c$(%)	206/204	$^{207}Pb/^{206}Pb^*$	1SE	$^{207}Pb/^{235}U^*$
14BD_3:	14BD_31_23	336	52.2	0.00E+00	15260	0.07202	0.00035	1.61709
14BD_3:	14BD_31_118	147	38.8	0.00E+00	22123	0.09629	0.00098	3.56375
14BD_3:	14BD_31_151	257	62.6	0.00E+00	39133	0.08974	0.00042	3.00387
14BD_3:	14BD_31_160	163	31.7	0.00E+00	18166	0.0789	0.00038	2.12953
14BD_3:	14BD_31_48	43	6.3	0.00E+00	6054	0.07478	0.00047	1.81471
14BD_3:	14BD_31_69	262	50.4	0.00E+00	18839	0.07773	0.0007	2.03555
14BD_3:	14BD_31_108	284	19.9	0.00E+00	7778	0.0562	0.00051	0.56341
14BD_3:	14BD_31_126	72	20.3	0.00E+00	8014	0.10212	0.0011	4.07121
14BD_3:	14BD_31_12	308	62.6	0.00E+00	67711	0.08267	0.00056	2.41541
14BD_3:	14BD_31_41	21	3.5	0.00E+00	2711	0.07511	0.00051	1.83241
14BD_3:	14BD_31_61	125	9.7	0.00E+00	25758	0.05992	0.00031	0.78998
14BD_3:	14BD_31_183	127	29.1	0.00E+00	21404	0.08728	0.00047	2.78109
14BD_3:	14BD_31_130	167	31.4	0.00E+00	53250	0.07754	0.00037	2.01138
14BD_3:	14BD_31_135	133	23.6	0.00E+00	10649	0.07528	0.00036	1.84243
14BD_3:	14BD_31_181	35	6.3	0.00E+00	3939	0.07615	0.00053	1.90578
14BD_3:	14BD_31_52	21	2.9	0.00E+00	1725	0.07305	0.0005	1.67752
14BD_3:	14BD_31_149	171	59.1	0.00E+00	33661	0.11734	0.0006	5.45617
14BD_3:	14BD_31_3	68	12.8	0.00E+00	4664	0.079	0.00044	2.11096
14BD_3:	14BD_31_75	249	76.9	0.00E+00	81830	0.1061	0.00109	4.38554
14BD_3:	14BD_31_166	175	53.2	0.00E+00	31569	0.10608	0.00055	4.38367
14BD_3:	14BD_31_161	27	4.2	0.00E+00	2067	0.07111	0.00057	1.52643
14BD_3:	14BD_31_119	128	8.7	0.00E+00	3269	0.05628	0.00054	0.55958
14BD_3:	14BD_31_138	105	26	0.00E+00	11549	0.09151	0.00044	3.0921
14BD_3:	14BD_31_73	139	39.7	0.00E+00	18477	0.10023	0.00102	3.83
14BD_3:	14BD_31_140	127	30.4	0.00E+00	24550	0.09006	0.00042	2.96601
14BD_3:	14BD_31_163	104	17.6	0.00E+00	8176	0.07442	0.0004	1.75563
14BD_3:	14BD_31_16	62	15.3	0.00E+00	7677	0.09378	0.00055	3.27145
14BD_3:	14BD_31_4	46	10	0.00E+00	4705	0.08645	0.00051	2.66845
14BD_3:	14BD_31_45	408	94	0.00E+00	25506	0.09022	0.00052	2.97042
14BD_3:	14BD_31_59	151	26.3	0.00E+00	26047	0.08232	0.00048	2.3
14BD_3:	14BD_31_188	177	43.6	0.00E+00	33865	0.0925	0.00047	3.15398
14BD_3:	14BD_31_124	859	255.7	0.00E+00	64382	0.1079	0.00115	4.49371
14BD_3:	14BD_31_10	124	20.8	0.00E+00	10245	0.0754	0.00042	1.81532
14BD_3:	14BD_31_116	41	10.4	0.00E+00	4805	0.09508	0.00103	3.35328
14BD_3:	14BD_31_172	66	16.3	0.00E+00	15040	0.09262	0.0005	3.14784
14BD_3:	14BD_31_40	403	219.6	0.00E+00	151587	0.19844	0.00164	14.26021
14BD_3:	14BD_31_144	137	32.4	0.00E+00	16992	0.09013	0.00047	2.93906
14BD_3:	14BD_31_176	819	66.1	0.00E+00	48238	0.05651	0.00025	0.64536
14BD_3:	14BD_31_107	473	33.3	0.00E+00	14954	0.05527	0.00048	0.55802
14BD_3:	14BD_31_182	452	35.7	0.00E+00	22352	0.05649	0.00028	0.63584
14BD_3:	14BD_31_34	413	78.7	0.00E+00	36528	0.07601	0.00038	2.08481
14BD_3:	14BD_31_14	590	45.4	0.00E+00	30558	0.05666	0.00027	0.64186
14BD_3:	14BD_31_95	1015	73.1	0.00E+00	36145	0.05553	0.00046	0.56735
14BD_3:	14BD_31_115	1065	191.9	0.00E+00	60387	0.07386	0.00068	1.88868
14BD_3:	14BD_31_1	644	110.9	0.00E+00	54800	0.07271	0.00034	1.7883
14BD_3:	14BD_31_30	319	24.7	0.00E+00	15471	0.05681	0.00029	0.64315
14BD_3:	14BD_31_131	1031	251.5	0.00E+00	91755	0.09139	0.00041	3.02988
14BD_3:	14BD_31_8	141	31.6	0.00E+00	68048	0.08882	0.00047	2.82043

				Discordance		*Ages*					
1SE	$^{206}Pb/^{238}U^{*}$	1SE	Rho	Central	Minim	207/206	1σ	207/235	1σ	206/238	1σ
0.02514	0.162857	0.0024	0.949	-1.5	.	986	10	977	10	973	13
0.08855	0.268417	0.00608	0.911	-1.5	.	1554	18	1541	20	1533	31
0.03362	0.242781	0.00246	0.907	-1.5	.	1420	9	1409	9	1401	13
0.02249	0.195763	0.00183	0.887	-1.6	.	1170	9	1158	7	1153	10
0.03346	0.175999	0.00305	0.939	-1.8	.	1063	13	1051	12	1045	17
0.04402	0.18994	0.00373	0.908	-1.8	.	1140	18	1127	15	1121	20
0.01117	0.072709	0.00128	0.889	-1.8	.	460	19	454	7	452	8
0.1054	0.289133	0.0068	0.909	-1.8	.	1663	19	1649	21	1637	34
0.04336	0.211914	0.00352	0.926	-1.9	.	1261	13	1247	13	1239	19
0.03308	0.176938	0.00296	0.926	-2.1	.	1071	13	1057	12	1050	16
0.01449	0.095622	0.00168	0.96	-2.1	.	601	11	591	8	589	10
0.0363	0.231096	0.00275	0.912	-2.1	.	1367	10	1350	10	1340	14
0.02001	0.18813	0.00165	0.879	-2.3	.	1135	9	1119	7	1111	9
0.01833	0.177511	0.00155	0.876	-2.3	.	1076	9	1061	7	1053	8
0.02406	0.181519	0.00191	0.832	-2.3	.	1099	13	1083	8	1075	10
0.03139	0.166553	0.0029	0.931	-2.4	.	1015	14	1000	12	993	16
0.06979	0.337251	0.00395	0.915	-2.6	-0.7	1916	9	1894	11	1873	19
0.03251	0.193798	0.00278	0.932	-2.8	.	1172	11	1152	11	1142	15
0.11217	0.299792	0.00702	0.915	-2.8	.	1733	18	1710	21	1690	35
0.05368	0.299718	0.00333	0.906	-2.8	-0.9	1733	9	1709	10	1690	17
0.01964	0.155688	0.00157	0.784	-3.1	.	961	16	941	8	933	9
0.01167	0.072117	0.00133	0.887	-3.2	.	463	21	451	8	449	8
0.03291	0.245056	0.00233	0.895	-3.4	-1.4	1457	9	1431	8	1413	12
0.09443	0.277143	0.00622	0.910	-3.6	.	1628	18	1599	20	1577	31
0.03217	0.238854	0.00233	0.900	-3.6	-1.6	1427	9	1399	8	1381	12
0.01872	0.171094	0.00157	0.860	-3.6	-0.8	1053	11	1029	7	1018	9
0.05654	0.253003	0.00411	0.940	-3.7	-1.2	1504	11	1474	13	1454	21
0.04387	0.223878	0.00344	0.933	-3.8	-1.1	1348	11	1320	12	1302	18
0.05415	0.238791	0.00413	0.950	-3.9	-1.4	1430	10	1400	14	1380	22
0.04661	0.20626	0.00393	0.956	-3.9	-1.1	1253	12	1225	14	1209	21
0.0371	0.247304	0.00262	0.902	-4	-1.9	1478	9	1446	9	1425	14
0.11759	0.302044	0.00721	0.913	-4.1	.	1764	18	1730	22	1701	36
0.02758	0.174623	0.00247	0.93	-4.2	-1.2	1079	11	1051	10	1038	14
0.08618	0.255794	0.00597	0.907	-4.5	-0.1	1530	19	1494	20	1468	31
0.03615	0.246506	0.0025	0.883	-4.5	-2.3	1480	10	1444	9	1420	13
0.40394	0.521187	0.01412	0.957	-4.7	-2.4	2813	12	2767	27	2704	60
0.03956	0.236496	0.00294	0.923	-4.7	-2.4	1428	9	1392	10	1368	15
0.0076	0.082827	0.0009	0.926	8.9	3.8	472	10	506	5	513	5
0.01101	0.07323	0.0013	0.898	8	.	423	19	450	7	456	8
0.00638	0.081636	0.00072	0.874	7.5	2.4	472	11	500	4	506	4
0.03405	0.198918	0.00309	0.951	7.4	3.4	1095	10	1144	11	1170	17
0.00899	0.082154	0.00108	0.94	6.6	1.2	478	10	503	6	509	6
0.01108	0.074099	0.00131	0.905	6.5	.	434	18	456	7	461	8
0.04267	0.18547	0.00383	0.914	6.2	0.3	1038	17	1077	15	1097	21
0.02824	0.17837	0.00269	0.955	5.6	1.8	1006	9	1041	10	1058	15
0.0101	0.082107	0.00122	0.946	5.3	.	484	11	504	6	509	7
0.03743	0.240458	0.00277	0.932	-5	-3.1	1455	8	1415	9	1389	14
0.04616	0.230292	0.00357	0.947	-5.1	-2.8	1400	10	1361	12	1336	19

		ppm						*Ratios*
sample	name	U	^{206}Pb	$^{206}Pb_c$(%)	206/204	$^{207}Pb/^{206}Pb^*$	1SE	$^{207}Pb/^{235}U^*$
14BD_3:	14BD_31_20	105	7.4	0.00E+00	4025	0.05694	0.00035	0.58793
14BD_3:	14BD_31_174	40	8.5	0.00E+00	3756	0.08467	0.00054	2.48918
14BD_3:	14BD_31_15	60	4.9	0.00E+00	1565	0.05881	0.00054	0.69646
14BD_3:	14BD_31_157	62	4.6	0.00E+00	2136	0.05738	0.00037	0.61156
14BD_3:	14BD_31_65	98	22	0.00E+00	9162	0.09839	0.00052	3.58796
14BD_3:	14BD_31_56	43	11.3	0.00E+00	4943	0.10889	0.00056	4.49756
14BD_3:	14BD_31_132	74	19.8	0.00E+00	8604	0.09916	0.00051	3.61551
14BD_3:	14BD_31_121	38	19.8	0.00E+00	7257	0.19656	0.00307	13.73084
14BD_3:	14BD_31_90	205	24.3	0.00E+00	7268	0.0656	0.00059	1.09459
14BD_3:	14BD_31_46	127	28.7	0.00E+00	17649	0.1004	0.00042	3.65641
14BD_3:	14BD_31_146	172	39.2	0.00E+00	19753	0.09	0.00043	2.81594
14BD_3:	14BD_31_63	285	26.6	0.00E+00	22685	0.06455	0.00028	1.01687
14BD_3:	14BD_31_33	278	59.3	0.00E+00	39434	0.08894	0.00047	2.70954
14BD_3:	14BD_31_128	57	31.1	0.00E+00	12694	0.20535	0.00152	14.38138
14BD_3:	14BD_31_25	148	10.9	0.00E+00	4043	0.05823	0.00041	0.63234
14BD_3:	14BD_31_155	54	13	0.00E+00	5078	0.09647	0.00053	3.21573
14BD_3:	14BD_31_143	267	138.7	0.00E+00	63016	0.20259	0.00163	13.70659
14BD_3:	14BD_31_110	86	40.9	0.00E+00	16790	0.19259	0.00297	12.37031
14BD_3:	14BD_31_64	487	102	0.00E+00	45397	0.09842	0.00045	3.29743
14BD_3:	14BD_31_55	310	122	0.00E+00	216936	0.17053	0.00102	9.93016
14BD_3:	14BD_31_159	66	33.1	0.00E+00	13918	0.2008	0.00149	13.21949
14BD_3:	14BD_31_35	127	26.2	0.00E+00	8655	0.09031	0.00061	2.66521
14BD_3:	14BD_31_98	342	32.5	0.00E+00	26305	0.06294	0.00065	0.85905
14BD_3:	14BD_31_96	290	133.3	0.00E+00	47150	0.18768	0.00281	11.42576
14BD_3:	14BD_31_122	314	67.7	0.00E+00	28554	0.09436	0.00096	2.8899
14BD_3:	14BD_31_58	469	183.4	0.00E+00	191310	0.18075	0.00116	10.53128
14BD_3:	14BD_31_102	21	8.1	0.00E+00	3284	0.17085	0.00247	9.03296
14BD_3:	14BD_31_36	135	31	0.00E+00	22049	0.1054	0.00062	3.46983
14BD_3:	14BD_31_39	162	63.5	0.00E+00	261559	0.17892	0.00144	9.55194
14BD_3:	14BD_31_67	241	40.4	0.00E+00	12020	0.08379	0.00079	1.92182
14BD_3:	14BD_31_28	121	16.7	0.00E+00	8075	0.07974	0.00064	1.61496
14BD_3:	14BD_31_186	242	42.5	0.00E+00	19187	0.08949	0.00045	2.18993
14BD_3:	14BD_31_136	378	132.3	0.00E+00	74102	0.16672	0.00106	7.8
14BD_3:	14BD_31_184	578	70.8	0.00E+00	21965	0.08401	0.00072	1.47224
14BD_3:	14BD_31_171	165	16.3	0.00E+00	6063	0.07655	0.00075	1.08448

				Discordance				*Ages*			
1SE	$^{206}Pb/^{238}U^{*}$	1SE	Rho	Central	Minim	207/206	1σ	207/235	1σ	206/238	1σ
0.00845	0.074881	0.00098	0.907	-5.1	.	489	13	470	5	465	6
0.03207	0.213225	0.00238	0.868	-5.2	-2.4	1308	12	1269	9	1246	13
0.01561	0.085888	0.00175	0.912	-5.4	.	560	19	537	9	531	10
0.00653	0.077297	0.00066	0.802	-5.4	.	506	14	485	4	480	4
0.084	0.264483	0.00604	0.975	-5.7	-3.6	1594	10	1547	19	1513	31
0.10002	0.299569	0.00648	0.973	-5.9	-4	1781	10	1731	18	1689	32
0.0405	0.264449	0.00263	0.889	-6.7	-4.8	1608	9	1553	9	1513	13
0.50011	0.506632	0.01667	0.903	-6.8	-2.4	2798	25	2731	34	2642	71
0.02264	0.12101	0.00226	0.901	-7.7	-1.8	794	18	751	11	736	13
0.07465	0.26414	0.00528	0.979	-8.3	-6.7	1631	7	1562	16	1511	27
0.03022	0.226919	0.00218	0.894	-8.3	-6.4	1426	9	1360	8	1318	11
0.0176	0.114259	0.00192	0.968	-8.6	-5.7	760	9	712	9	697	11
0.04587	0.220945	0.00355	0.95	-9.1	-6.9	1403	10	1331	13	1287	19
0.24169	0.507921	0.00766	0.898	-9.4	-7.4	2869	12	2775	16	2648	33
0.00964	0.078758	0.00107	0.888	-9.6	-3.4	538	14	498	6	489	6
0.03698	0.241771	0.00244	0.879	-11.5	-9.5	1557	10	1461	9	1396	13
0.25881	0.490685	0.00838	0.904	-11.6	-9.5	2847	13	2730	18	2574	36
0.43306	0.46584	0.01464	0.897	-13	-9	2764	24	2633	33	2465	64
0.06858	0.24299	0.00493	0.976	-13.4	-12	1594	9	1480	16	1402	26
0.28503	0.422343	0.01186	0.978	-13.5	-12	2563	10	2428	26	2271	54
0.21895	0.477479	0.00708	0.895	-13.5	-12	2833	11	2695	16	2516	31
0.04945	0.214048	0.0037	0.931	-14	-11	1432	12	1319	14	1250	20
0.01925	0.098996	0.00197	0.889	-14.5	-7.6	706	21	630	11	609	12
0.37996	0.441546	0.01311	0.893	-16	-12	2722	24	2559	31	2358	59
0.06911	0.222134	0.00481	0.905	-16.2	-13	1515	19	1379	18	1293	25
0.30635	0.422578	0.01199	0.975	-17.3	-16	2660	11	2483	27	2272	54
0.32728	0.38346	0.01274	0.917	-21.6	-18	2566	23	2341	33	2092	59
0.06404	0.238765	0.00418	0.948	-22	-20	1721	10	1520	15	1380	22
0.25112	0.387198	0.00969	0.952	-23.6	-22	2643	12	2393	24	2110	45
0.04086	0.166358	0.00317	0.895	-24.8	-21	1288	17	1089	14	992	18
0.03522	0.146895	0.00298	0.931	-27.6	-25	1190	15	976	14	884	17
0.02863	0.177483	0.00214	0.922	-27.7	-26	1415	9	1178	9	1053	12
0.10767	0.340047	0.00416	0.887	-29.1	-28	2525	11	2210	12	1887	20
0.02439	0.127102	0.0018	0.856	-42.8	-41	1293	16	919	10	771	10
0.01903	0.102748	0.00149	0.828	-45.3	-43	1110	19	746	9	630	9